Guide to Instruments and Methods of Observation

Volume II – Measurement of Cryospheric Variables

2024 edition

WEATHER CLIMATE WATER

WORLD
METEOROLOGICAL
ORGANIZATION

WMO-No. 8

Guide to Instruments and Methods of Observation

Volume II – Measurement of Cryospheric Variables

2024 edition

WORLD
METEOROLOGICAL
ORGANIZATION

WMO-No. 8

EDITORIAL NOTE

METEOTERM, the WMO terminology database, may be consulted at https://wmo.int/wmo-community/meteoterm.

Readers who copy hyperlinks by selecting them in the text should be aware that additional spaces may appear immediately following http://, https://, ftp://, mailto:, and after slashes (/), dashes (-), periods (.) and unbroken sequences of characters (letters and numbers). These spaces should be removed from the pasted URL. The correct URL is displayed when hovering over the link or when clicking on the link and then copying it from the browser.

WMO-No. 8

Chair, Publications Board
World Meteorological Organization (WMO)
7 bis, avenue de la Paix
P.O. Box 2300
CH-1211 Geneva 2, Switzerland

Tel.: +41 (0) 22 730 84 03
Email: publications@wmo.int

ISBN 978-92-63-10008-5

CONTENTS

Page

FOREWORD

WMO Guides describe the practices and procedures that Members are invited to follow or implement in establishing and conducting their arrangements for compliance with the WMO Technical Regulations.

One longstanding publication in this series is the *Guide to Instruments and Methods of Observation* (WMO-No. 8), which was first published in 1950. The Guide is the authoritative reference for all matters related to instrumentation and methods of observation in the context of the WMO Integrated Global Observing System (WIGOS). Uniform, traceable and high-quality observational data represent an essential input for most WMO applications, such as climate monitoring, numerical weather prediction, nowcasting and severe weather forecasting, all of which facilitate the improvement of the well-being of societies around the world.

The main purpose of the Guide is to provide guidance on the most effective practices and procedures for undertaking meteorological, hydrological and related environmental measurements and observations in order to meet specific requirements for different application areas. It also provides information on the capabilities of instruments and systems that are regularly used to perform such observations. The theoretical basis of the techniques and observational methods is outlined in the text and supported by references and further reading for additional background information and details.

The continuous evolution and standardization of measurement and observational practices and the rapid development of new measurement techniques and technologies have led to the evolution of the Guide into a significantly larger publication that constitutes a fundamental and essential source of information. Beginning with the 2018 edition, the Guide has been separated into "volumes" that can be updated and published independently.

The outline of the current guide is:

Volume I – Measurement of Meteorological Variables

Volume II – Measurement of Cryospheric Variables

Volume III – Observing Systems

Volume IV – Space-based Observations

Volume V – Quality Assurance and Management of Observing Systems

This 2024 edition of Volume II was approved by the WMO Commission for Observation, Infrastructure and Information Systems (INFCOM) at its third session (INFCOM-3). In comparison to the 2023 edition of Volume II, this edition includes updates to Chapter 1 – General, and a new Chapter 4 – Measurement of permafrost.

On behalf of WMO, I would like to express my sincere gratitude to Global Cryosphere Watch community experts and to the INFCOM Standing Committee on Measurements, Instrumentation and Traceability and its Editorial Board, whose tremendous efforts have enabled the publication of this new edition.

(Prof. Celeste Saulo)
Secretary-General

CHAPTER 1. GENERAL

This chapter was authored by:

Charles Fierz, WSL Institute for Snow and Avalanche Research SLF (Switzerland)

1.1 OBSERVATION OF THE CRYOSPHERE

The cryosphere refers to the component of the Earth system that contains ice, including solid precipitation, snow, glaciers and ice caps, ice sheets, ice shelves, icebergs, sea ice, lake ice, river ice, permafrost, and seasonally frozen ground, or even "dry" material in the case of permafrost. The cryosphere includes elements on or beneath the Earth's surface or that are measured at the surface in the case of solid precipitation. It therefore excludes ice clouds (see *Technical Regulations – Basic Documents No. 2: General Meteorological Standards and Recommended Practices* (WMO-No. 49), Volume I).

The above definition is in very close agreement with the definition of the Intergovernmental Panel on Climate Change (Matthews et al., 2021). The cryosphere is global, existing not just in the Arctic, Antarctic and mountain regions, but at various latitudes in approximately one hundred countries. It provides some of the most useful indicators of climate change, yet is one the most under-sampled parts of the Earth system. Improved cryospheric monitoring and integration of such monitoring is essential to fully assess, predict and adapt to climate variability and change.

1.2 OBSERVING SYSTEMS OF THE CRYOSPHERE

WMO, in cooperation with other national and international bodies and organizations, and using its global observing and telecommunication capability, is in a position to provide an integrated, authoritative, continuing assessment of the cryosphere – the Global Cryosphere Watch (GCW). The GCW surface observation network is considered as the cryospheric component of the WMO Integrated Global Observing System (WIGOS), contributing to the Global Climate Observing System (GCOS) and the Global Earth Observation System of Systems (GEOSS). The Global Cryosphere Watch facilitates the establishment of high-latitude and alpine meteorological stations with co-located measurements of key cryospheric variables, thus enhancing GCOS and its Global Terrestrial Networks for glaciers, permafrost and hydrology.

1.3 GENERAL SITING AND EXPOSURE REQUIREMENTS FOR A STATION MEASURING CRYOSPHERIC VARIABLES

The characteristics of the measurement site should be captured in the station metadata. Important siting details include, but may not be limited to, surface type (mineral soil or organic layers, vegetation type, ice, etc.), prevailing wind direction, site layout and, more important, exposure to both wind and solar radiation. The measurement area should be representative of the surrounding landscape. At alpine stations, measurements on areas with higher exposure than the surrounding landscape should be avoided to guard against unrepresentative measurements.

Finally, siting should take into consideration accessibility and permanence, which will ultimately impact the continuity of the record. For automated measurements, the source of available power and communications may also be a consideration for siting.

1.4 MEASUREMENT STANDARDS AND BEST PRACTICES

To ensure high quality and consistent observations, measurements of cryospheric variables at GCW stations will be made in accordance with accepted standards. Many measurement standards have been compiled by GCW and other networks, though the compilation is not exhaustive for several cryospheric measurements. An initial inventory of existing documents describing measurement practices, or in some cases best practices for processing the observations, can be found on the legacy GCW website.

Some cryosphere networks have their own standards. It will be a major effort for GCW to establish standards in agreement with the existing ones as well as with guidelines for observations of single cryospheric variables, some of which are routinely used. Thus GCW measurement standards will draw on existing ones. New ones will be added as necessary, which will be reviewed by the scientific community, modified as needed, and maintained in the present Guide, which is the GCW standard document for measurements and best practices related to the cryosphere.

The Global Cryosphere Watch established a list of required, desired and optional variables for each component of the cryosphere as tabulated below. Many of these variables are already included in the WIGOS Metadata Representation (WMDR) with their notation given in Tables 1.1–1.11. Moreover, whenever possible, the variables match corresponding products of the GCOS Essential Climate Variables (ECV). Currently, required variables are listed only for meteorological surface measurements at CryoNet stations, and only measurements of desired[1] cryospheric variables are described in the present Guide. The desired measurements of cryospheric variables may become required at a later stage.

1.4.1 Snow

There is no global, coordinated monitoring of snow on the ground yet. This is due to the fact that network requirements differ from one application to the next: avalanche warning, meteorological observations, snow, hydrology, and so forth. Guidance on best practices can thus be found in various manuals pertaining to each of these applications, often coinciding. Moreover, best practices that work in an alpine region may not work in extreme conditions such as those found in East Antarctica, where, for example, snow depth is much more difficult to define unequivocally.

Standard best practices for snow measurements are found in the present Volume, Chapter 2. They draw on standards such as those set out, for example, in the *Guide to Hydrological Practices* (WMO-No. 168), *Snow Cover Measurements and Areal Assessment of Precipitation and Soil Moisture* (Sevruk, 1992) or the *International Classification for Seasonal Snow on the Ground* (ICSSG). The ICSSG has existed since 1954 and covers many but not all aspects of snow monitoring as well as measurements and observations of snow properties. A working group of the International Association of Cryospheric Sciences (IACS) revised the ICSSG, which is available online (Fierz et al., 2009).

However, as the number of regular and continuous manual observations diminishes worldwide, there is an urgent need to improve our ability to measure automatically snow on the ground and to validate those measurements against manual observations. Important steps in that direction were the WMO Solid Precipitation Intercomparison Experiment (SPICE) (Nitu et al., 2018) as well as the establishment of the WMO-INFCOM Measurement Lead Centre "Snow Monitoring Competence Centre – Davos (SMCC)". Again, requirements vary depending on the application. While an avalanche forecaster will not be too concerned about an error of ±5 cm in the depth of snowfall, road maintenance may be needed as soon as a road is covered by 1 cm of snow.

[1] Desired cryospheric variable is a qualitative term used to describe those variables measured using widely accepted methods, which are documented, for example, in Chapter 2 of the present Volume. These are variables commonly observed in the framework of operational and research activities. Optional cryospheric variables, by contrast, are those for which observing methods and measuring instruments are still at the experimental or emerging stage and have not been widely documented and validated.

Table 1.1. List of required, desired and optional snow variables

Measurement designation	*WMDR notation*	*Variable*	*Timescale*				
			hourly	*daily*	*weekly*	*monthly*	*yearly*
Required		None yet					
Desired	629	Snow depth	A (S, G, SI, LRI, IS, P)	M (S, P)	M (SI, LRI)[a]		M (G, IS)
	631	Water equivalent of snow cover	A (S)		M (S)[a]		M (S, G, IS)[b]
	12007	Presence of snow		M (S)			
Optional	627	Depth of snowfall		M (S)			
	12008	Water equivalent of snowfall		M (S)			
	628	Snow cover extent	A (S, SI, LRI)		M (SI, LRI)[a]		
	630	Snow surface state					
		Snow albedo	A		M (SI, LRI)[a]		
		Snow-surface temperature	A (S, SI)		M (SI, LRI)[a]		
		Snow temperature	A (S)		M (S)[a]		
		Snow density			M (S)[a]		
		Liquid water content			M (S)[a]		
		Drifting and blowing snow	A (S)	M (S)			
		Specific surface area		M (S)	M (S)[a]		M (IS)

Key:

A:	automatic	LRI:	lake and river ice	G:	glaciers	S:	snow
M:	manual	P:	permafrost	IS:	ice sheets	SI:	sea ice

Notes:
[a] Once every two weeks
[b] Seasonal

1.4.2 Glaciers

The Global Terrestrial Network for Glaciers (GTN-G) is the framework for the internationally coordinated monitoring of glaciers in support of the United Nations Framework Convention on Climate Change (UNFCCC). This GCOS network is jointly run by the World Glacier Monitoring Service (WGMS) of the International Association of Cryospheric Sciences (IACS), the United States National Snow and Ice Data Center (NSIDC) and the Global Land Ice Measurements from Space initiative (GLIMS).

Beside detailed (index) in situ measurements of mass balance, glacier inventories contain basic information on physiographic properties of glaciers, including glacier boundaries and surface topography. Efforts are also made to compile standardized data on glacier thickness measurements.

In 2015, WGMS designed the Global Glacier Change Bulletin (GGCB) series with the aim of providing an integrative assessment of worldwide and regional glacier changes at two-year intervals. The basic data can be found on the official websites of the above-mentioned organizations.

Standard best practices for glacier measurements are found in the present Volume, Chapter 3. They draw on standards such as those set out, for example, in *Glacier Mass-balance Measurements: A Manual for Field and Office Work* (Østrem and Brugman, 1991) and *A Manual for Monitoring the Mass Balance of Mountain Glaciers* (Kaser et al., 2003).

Table 1.2. List of required, desired and optional glacier variables

Measurement designation	*WMDR notation*	*Variable*	*Timescale*				
			hourly	*daily*	*weekly*	*monthly*	*yearly*
Required		None yet					
Desired	12011	Surface accumulation at a point	A				M[a]
	12012	Surface ablation at a point	A				M
	12010	Glacier-wide mass balance					M
	12009	Glacier mass balance at a point	A				M
	12013	Glacier area					M[b]
Optional		Glacier-wide surface accumulation					M
		Glacier-wide surface ablation					M
		Basal ablation at a point	A				M
		Glacier thickness at a point					M[b]
	612	Glacier topography				A	
		Glacier volume					M[b]
		Glacial runoff	A				
		Calving flux at a point					A/M
	611	Glacier motion		A			M
		Ice/firn temperature profile at a point	A				

Key:
A: automatic M: manual

Notes:
[a] Seasonal
[b] Multi-year

1.4.3 **Permafrost**

Changes in permafrost temperature frequently reflect changes in surface climate over time, and therefore they serve as a useful indicator of climate change. The Global Terrestrial Network for Permafrost (GTN-P) was set up by the International Permafrost Association (IPA) to organize and manage a global network of permafrost observatories for detecting, monitoring and predicting climate change. Existing local networks focus on monitoring the key thermal state parameters permafrost temperature and active layer depth. The Global Terrestrial Network for Permafrost provides access to these data. In addition, rock glacier velocity is a new product of the ECV Permafrost, and global monitoring of permafrost extent is suggested in the GCOS Implementation Plan (GCOS-244).

Standard best practices for permafrost measurements are found in the present Volume, Chapter 4. They draw on standards such as those set out, for example, in *Measurement Recommendations and Guidelines for the Global Terrestrial Network for Permafrost (GTN-P)* (Streletskiy et al., 2022).

Table 1.3. List of required, desired and optional permafrost variables

Measurement designation	*WMDR notation*	*Variable*	*Timescale*				
			hourly	*daily*	*weekly*	*monthly*	*yearly*
Required		None yet					
Desired	12014	Permafrost temperature	A				
	12015	Active layer thickness		A			M
	12283	Rock glacier velocity					M[a]
Optional		Rock glacier discharge	M				
		Rock glacier spring temperature	M				
		Seasonal frost heave/subsidence					M
		Surface elevation change					M[b]
		Ground-ice volume					M
		Coastal retreat					M
	12277	Soil moisture		A		M	

Key:
A: automatic M: manual

Notes:
[a] Half-yearly
[b] Multi-year

1.4.4 Seasonally frozen ground

For soil temperature measurements we currently refer to Chapter 2, Volume I of the present Guide.

Table 1.4. List of required and desired variables for seasonally frozen ground

Measurement designation	*WMDR notation*	*Variable*	*Timescale*				
			hourly	*daily*	*weekly*	*monthly*	*yearly*
Required		None yet					
Desired	596	Soil temperature	A				

Key:
A: automatic

1.4.5 Sea ice

Sea ice, as well as ice-covered lakes and rivers, and icebergs affect large regions of economic, environmental and social importance.

Information on sea-ice conditions is provided by the national ice services conducting continuous monitoring of sea ice, lake and river ice as well as icebergs. Other bodies involved in this monitoring include the International Ice Patrol as well as the research community on hemispheric, circumpolar and regional scales. For operational purposes many ice properties are displayed as two-dimensional (2D) parameters (polygons) in ice charts. However, it is evident that satellite remote sensing is the primary source of data for sea-ice monitoring, though not all of the key parameters can be observed with sufficient accuracy by space-borne measurement devices. In situ, coastal, shipborne and airborne measurements are a vital complementary, and sometimes primary, source of information. These initiatives, especially shipborne and airborne measurement, are largely taken in support of scientific research.

Standard observation procedures for sea ice will be included in the present Volume as a further chapter. They will draw on standards such as those set out, for example, in *Sea-ice Information and Services* (WMO-No. 574), the Antarctic Sea Ice Processes and Climate (ASPeCt) sea-ice observation protocol and the Arctic Shipborne Sea Ice Standardization Tool (ASSIST), and have proven crucial to the successful uptake of the data. Recently, efforts have been initiated to unify the Antarctic and Arctic observing protocols.

Table 1.5. List of required, desired and optional sea-ice variables

Measurement designation	*WMDR notation*	*Variable*	*Timescale*				
			hourly	*daily*	*weekly*	*monthly*	*yearly*
Required		None yet					
Desired	406	Sea-ice thickness	A		M[a]		
		Sea-ice freeboard	A		M[a]		
		Sea-ice melting stage			M		
		Sea-ice class (pack or fast ice)		M			
Desired – applicable for pack ice	407	Sea-ice type		M			
		Form of ice (floe size)			M		
Optional		Sea-ice openings (leads, polynyas, cracks)		A			
		Sea-ice velocity	A	M			
		Sea-ice deformation (divergence/convergence)	A	M			
		Sea-ice ridge cover (concentration and height of ice ridges)	A	M			
		Sea-ice draft			M[a]		
		Sea-ice salinity profile (vertical)			M[a]		
		Sea-ice stratigraphy			M[a]		
		Surface temperature (surface–air interface)	A				
		Sea-ice temperature profile (vertical)	A		M[a]		
Satellite-based (non in situ)		Sea-ice concentration		A/M			

Key:
A: automatic M: manual

Note:
[a] Once every two weeks

1.4.6 Ice sheets

Table 1.6. List of required, desired and optional ice sheet variables

Measurement designation	*WMDR notation*	*Variable*	*Timescale*				
			hourly	*daily*	*weekly*	*monthly*	*yearly*
Required		None yet					
Desired		Surface accumulation at a point		A			
		Surface ablation at a point		A			
		Surface mass balance at a point		A			M
Optional	613	Ice sheet topography				A	
		Ice sheet thickness at a point					M[a]
		Ice velocity at a point				A	
		Ice/firn temperature profile (point)	A				

Key:
A: automatic M: manual

Note:
[a] Multi-year

1.4.7 Ice shelves

Table 1.7. List of required and desired ice shelf variables

Measurement designation	*WMDR notation*	*Variable*	*Timescale*				
			hourly	*daily*	*weekly*	*monthly*	*yearly*
Required		None yet					
Desired		Basal ablation					A/M
		Ice velocity		A			M

Key:
A: automatic M: manual

1.4.8 **Icebergs**

Icebergs largely occur in the Arctic Ocean and adjacent seas, as far south as Newfoundland and Labrador, and in the Southern Ocean. Iceberg monitoring is a crucial safety issue for travelling and offshore ventures in polar seas, and provides input for climatological analysis, such as assessing mass loss of the glacial ice sheets.

Iceberg monitoring is largely based on remotely-sensed imagery. Nevertheless, iceberg observations form part of several in situ observation programmes, including ship-based observation (see Jacka and Giles, 2007; Romanov et al., 2011).

In situ iceberg observations for both the Arctic and Antarctic include basic observations of the position, size and distribution density, as well as motion, shape and draft.

Table 1.8. List of required, desired and optional iceberg variables

Measurement designation	*WMDR notation*	*Variable*	*Timescale*				
			hourly	*daily*	*weekly*	*monthly*	*yearly*
Required		None yet					
Desired		Iceberg position			M		
		Iceberg form and size			M		
		Iceberg concentration (distance)			M		
Optional		Iceberg motion		A/M			
		Iceberg height (above water)		A/M			
		Iceberg width and length (at waterline)		A/M			
		Iceberg draft			A[a]		
		Underwater 3D form			A[a]		

Key:
A: automatic M: manual

Note:
[a] Once every two weeks

1.4.9 Lake ice

Table 1.9. List of required, desired and optional lake-ice variables

Measurement designation	*WMDR notation*	*Variable*	*Timescale*				
			hourly	*daily*	*weekly*	*monthly*	*yearly*
Required		None yet					
Desired		Ice thickness	A		M[a]		
		Ice concentration		A/M			
		Ice class (pack or fast ice)		M			
		Ice type (level/rafted/ridged and floe descriptor)		M			
		Form of ice (floe size)			M		
		Stage of ice development			M		
		Ice phenomena dates of freeze-up, fast-ice formation/breakout, melt onset, break-up)			A/M		M
		Ice melting stage		M			
Optional		Areal extent of floating/grounded ice			M		
		Ice-surface temperature	A				
		Ice openings (leads, polynyas, cracks)		A			
		Ice velocity	A	M			
		Ice deformation (divergence/convergence)	A	M			
		Ice ridge height	A	M			
		Ice ridge cover (concentration of ice ridges)	A	M			
		Ice stratigraphy			M[a]		
		Ice temperature profile (vertical)	A		M[a]		

Key:
A: automatic M: manual

Note:
[a] Once every two weeks

1.4.10 **River ice**

Table 1.10. List of required, desired and optional river-ice variables

Measurement designation	*WMDR notation*	*Variable*	*Timescale*				
			hourly	*daily*	*weekly*	*monthly*	*yearly*
Required		None yet					
Desired		Ice thickness	A		M[a]		
		Ice concentration		A/M			
		Ice class (pack or fast ice)		M			
		Ice type (level/rafted/ridged and floe descriptor)		M			
		Form of ice (floe size)			M		
		Stage of ice development			M		
		Ice phenomena (dates of freeze-up, fast-ice formation/breakout, melt onset, break-up)			A/M		M
		Ice melting stage		M			
		River-ice jams and dams		M			
		Flooding extent caused by jams and dams		M			
		River icings (*Aufeis*)		M			
		Maximum level		M			
Optional		Areal extent of floating/grounded ice			M		
		Ice-surface temperature	A				
		Ice openings (leads, polynyas, cracks)		A			
		Ice deformation (divergence/convergence)	A	M			
		Ice ridge height	A	M			
		Ice ridge cover (concentration of ice ridges)	A	M			
		Ice stratigraphy			M[a]		
		Ice temperature profile (vertical)	A		M[a]		

Key:
A: automatic M: manual

Note:
[a] Once every two weeks

1.4.11 Surface meteorology (at CryoNet stations)

For surface meteorology measurements we refer to Chapters 2–8, Volume I of the present Guide.

Table 1.11. List of required, desired and optional surface meteorology variables

Measurement designation	*WMDR notation*	*Variable*	*Timescale*				
			hourly	*daily*	*weekly*	*monthly*	*yearly*
Required	224	Air temperature (at specified distance from the reference surface)	A				
	12249	Relative humidity (with respect to water)	A				
	12006	Horizontal wind speed (at specified distance from the reference surface)	A				
	12005	Horizontal wind direction (at specified distance from the reference surface)	A				
Desired	216	Atmospheric pressure	A				
	573	Downward short-wave irradiance	A				
	574	Upward short-wave irradiance	A				
Optional	566	Downward long-wave irradiance	A				
	567	Upward long-wave irradiance	A				
	210	Amount of precipitation	A				

Key:
A: automatic

1.5 UNCERTAINTY OF MEASUREMENTS

Establishing best practices, guidelines and standards for cryospheric measurements entails consideration of data uncertainty, homogeneity and interoperability, and compatibility of observations from all GCW constituent observing and monitoring systems and of derived cryospheric products.

Additionally, instrument intercomparison campaigns will regularly be conducted to determine and compare performance characteristics of instruments under field conditions and to link readings of different instruments.

The term "standard" and other similar terms denote the various instruments, methods and scales used to establish the uncertainty of measurements. A nomenclature for standards of measurement is given in the *International Vocabulary of Metrology – Basic and General Concepts and Associated Terms (VIM)* developed by the Joint Committee for Guides in Metrology (BIPM et al., 2012).

REFERENCES

Bureau International des Poids et Mesures (BIPM); International Electrotechnical Commission (IEC); International Federation of Clinical Chemistry and Laboratory Medicine (IFCC) et al. *International Vocabulary of Metrology – Basic and General Concepts and Associated Terms (VIM)*, 3rd ed.; JCGM 200:2012; Joint Committee for Guides in Metrology (JCGM): Paris, 2012. http://www.bipm.org/en/publications/guides/vim.html.

Fierz, C.; Armstrong, R. L.; Durand, Y. et al. *The International Classification for Seasonal Snow on the Ground*; IHP-VII Technical Documents in Hydrology No. 83; IACS Contribution No 1; UNESCO-IHP: Paris, 2009. https://cryosphericsciences.org/publications/snow-classification.

Global Climate Observing System (GCOS). *The 2022 GCOS Implementation Plan* (GCOS-244/Global Ocean Observing System (GOOS)-272); World Meteorological Organization (WMO): Geneva, 2022.

Jacka, T. H.; Giles, A. B. Antarctic Iceberg Distribution and Dissolution from Ship-Based Observations. *Journal of Glaciology* **2007**, *53* (182), 341–356. https://doi.org/10.3189/002214307783258521.

Kaser, G., Fountain, A.; Jansson, P. *A Manual for Monitoring the Mass Balance of Mountain Glaciers*; Technical Documents in Hydrology No. 59; United Nations Educational, Scientific and Cultural Organization International Hydrological Programme (UNESCO-IHP), Paris, 2003. https://unesdoc.unesco.org/ark:/48223/pf0000129593.

Matthews, J. B. R.; Möller, V.; van Diemen, R. et al. Annex VII: Glossary. *In Climate Change 2021: The Physical Science Basis. Working Group I Contribution to the Sixth Assessment Report of the Intergovernmental Panel on Climate Change.* Masson-Delmotte, V.; Zhai, P.; Pirani, A. et al. Eds.; Cambridge University Press: Cambridge, United Kingdom and New York, USA, 2021. https://doi.org/10.1017/9781009157896.022.

Nitu, R.; Roulet, Y.-A.; Wolff, M. et al. *WMO Solid Precipitation Intercomparison Experiment (SPICE) (2012–2015)* (Instruments and Observing Methods (IOM) Report No. 131); World Meteorological Organization (WMO): Geneva, 2018.

Østrem G.; Brugman, M. *Glacier Mass-balance Measurements: A Manual for Field and Office Work*; NHRI Science Report No. 4; Norwegian Water Resources and Energy Administration, Oslo, and National Hydrology Research Institute, Saskatoon, Canada, 1991. https://wgms.ch/downloads/Oestrem_Brugman_GlacierMassBalanceMeasurements_1991.pdf.

Romanov, Y. A.; Romanova, N. A.; Romanov, P. Shape and Size of Antarctic Icebergs Derived from Ship Observation Data. *Antarctic Science* **2012**, *24* (1), 77–87. https://doi.org/10.1017/S0954102011000538.

Sevruk, B., Ed. *Snow Cover Measurements and Areal Assessment of Precipitation and Soil Moisture* (WMO-No. 749); Operational Hydrology Report No. 35; World Meteorological Organization (WMO): Geneva, 1992.

Streletskiy, D.; Noetzli, J.; Smith, S. L. et al. *Measurement Recommendations and Guidelines for the Global Terrestrial Network for Permafrost (GTN-P)*; Zenodo, 2022. https://doi.org/10.5281/zenodo.5973079.

World Meteorological Organization (WMO). *Guide to Hydrological Practices* (WMO-No. 168), Volume I. Geneva, 2008.

World Meteorological Organization (WMO). *Technical Regulations – Basic Documents No. 2: General Meteorological Standards and Recommended Practices* (WMO-No. 49), Volume I. Geneva, 2023.

World Meteorological Organization (WMO). *Sea-ice Information and Services* (WMO-No. 574). Geneva, 2024.

CHAPTER 2. MEASUREMENT OF SNOW

2.1 GENERAL

This chapter describes some of the most common snow measurement methods, provides guidance on the procedures and best practices for setting up a snow monitoring network, and indicates the common sources of error in measuring snow on the ground (where "ground" or "base surface" could refer to any reference surface below the top of the snow cover, for example, soil, glacier and sea ice). The information provided is for both manual and automated measurements (where applicable), with the exception of measurement of precipitation, which is described as a meteorological variable in Volume I, Chapter 6 of this Guide. Snow measurements included here are snow depth (HS, for height of snow), snow thickness (DS), water equivalent of snow cover (SWE), depth of snowfall (HN, for height of new snow), presence of snow on the ground (PSG).

2.1.1 Definitions, units and scales

The snow cover is, in general, the accumulation of snow on the base surface, and in particular, the areal extent of snow-covered ground (NSIDC, 2018); this term should be used in conjunction with the climatologic relevance of snow on the ground. For the definition of shallow versus deep snow cover in this chapter, we define shallow snow cover as having a depth of 50 cm or less.

The snowpack is the accumulation of snow at a given site and time; this term should be used in conjunction with the physical and mechanical properties of snow on the ground.

The base surface is taken as the interface at the bottom of the snow cover or snowpack: it is the ground surface in case of soil, or the surface of another component of the cryosphere such as the surface of sea ice. On glaciers, it is either the ice surface within the ablation zone or the previous year's hardened summer surface in the accumulation zone (see the present Guide, Volume II, Chapter 3, 3.7.1).

A snow layer results from intermittent precipitation, the action of wind and the continuous metamorphism of snow. Distinct layers of snow build up the snowpack and each such stratigraphic layer differs from the adjacent layers above and below in at least one of the following characteristics: microstructure or density, which together define the snow type; snow hardness; liquid water content; salinity; chemistry; isotopic content; or impurities, which all describe the state of this type of snow. Thus, at any one time, the type and state of the snow forming a layer have to be defined because its physical, chemical and mechanical properties depend on them (Fierz et al., 2009). It should be borne in mind that a snow layer cannot be classified with a single parameter such as grain shape.

Snow depth (HS) is defined as the vertical distance from the snow surface to a stated reference level and must be reported in centimetres (cm), rounded to the nearest centimetre. In most cases the reference level corresponds to the base surface; on ice sheets it may refer to a depth recorded at some fixed time. Snow thickness (DS) – the perpendicular distance from the snow surface to a stated reference level – is related to HS through the slope angle φ as follows:

$$DS = HS \cdot (\cos\varphi) \tag{2.1}$$

The slope angle is the acute angle measured from the horizontal plane of the slope (see Figure 2.1). Conversely, HS can be calculated from DS as follows:

$$HS = DS \cdot (\cos\varphi)^{-1} \tag{2.2}$$

Unless otherwise specified, a snow-depth measurement refers to a measurement at a single location at a given time.

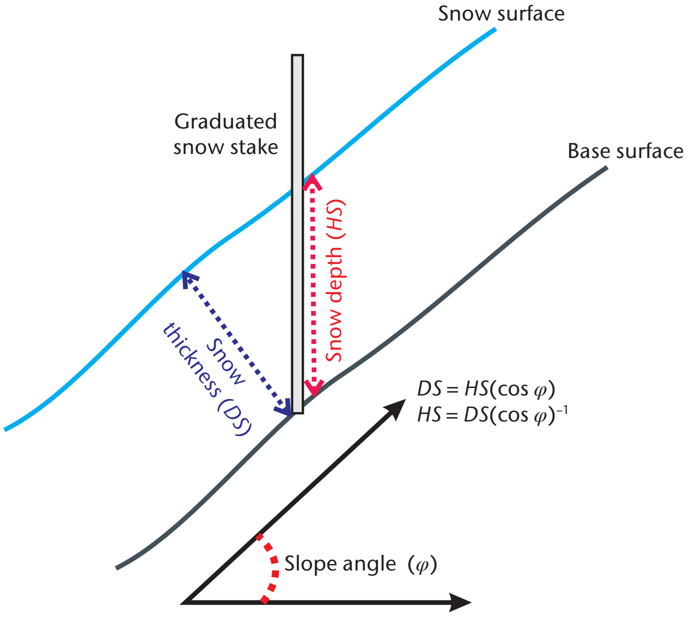

Figure 2.1. Relationship between *HS* and *DS* on a slope

Water equivalent of snow cover (*SWE*) is the vertical depth of water that would be obtained if the snow cover melted completely, which equates to the snow-cover mass per unit area. It is expressed either in mm w.e. or in kg m^{-2}, where the addition of w.e. to the length unit is strongly recommended. Water equivalent of snow cover is the product of the snow height in metres and the depth-averaged bulk density of the snow cover in kilograms per cubic metre (Goodison et al., 1981, p. 224). It can represent the snow cover over a given region or a confined snow sample in a specific area. The reported resolution of *SWE* is to be 1 mm w.e. or 1 kg m^{-2}.

Snow properties define the physical, mechanical and chemical properties of a snow layer (see 2.1.1 above for the definition of snow layer). These can include density, grain size and shape, hardness, liquid water content, salinity, impurity and isotopic content. Snow properties are traditionally observed layer by layer. Some modern instruments, however, already record continuous profiles of many snow properties.

Depth of snowfall (*HN*) is the vertical depth in centimetres of freshly fallen snow that has accumulated on the base surface or on a snow board during a specific period, usually of 24 hours. When reporting *HN* for observation periods other than for 24 hours, the period must be added in parentheses to the symbol (for example, an 8-hour measurement will be expressed as *HN*(8h)). The depth of snowfall is reported in centimetres and rounded to the nearest centimetre. As with *HS*, the perpendicular measurement of snowfall, *DN*, is related to *HN* via the slope angle φ.

Presence of snow on the ground (*PSG*) is a binary observation of the presence of snow cover at the measurement location. The measurement location is of the scale of the instrument compound and is generally about 50 m x 50 m but not less than 10 m x 10 m.

2.2 SITING AND EXPOSURE

The characteristics of the measurement site should be captured in the station metadata. Important siting details for snow measurements to be listed in the metadata include, but may not be limited to, slope, aspect, surface type (mineral soil or organic layers, vegetation type, ice, etc.), prevailing wind direction, site layout and exposure (including distance to surrounding wind barriers). Generally, the ideal site for measuring snow is a flat, wind-sheltered area, where the snow cover and the base surface are relatively homogenous. However, the measurement area should be representative of the surrounding landscape. For example, if the surrounding landscape is open (such as a flat plain with no significant barriers to wind) *HS* or *SWE* measurements should not be made inside an unrepresentative sheltered area. The exception to this is the measurement of the depth of snowfall which should, if possible, be made in a sheltered location to minimize the impact of wind. For forested sites, a measurement location within a clearing is preferred. In alpine regions, a flat area large enough to make a representative measurement without encountering edge effects should be chosen, while basins, slopes and ridges should be avoided. Alpine sites in particular should be sheltered from the prevailing wind and clear of large rocks. At alpine stations, measurements in areas with higher exposure than the surrounding landscape should be avoided, as the exposure may cause unrepresentative seasonal melting rates and yield unrepresentative measurements.

For the manual point measurement of *HS* or *SWE*, a measurement field should be established prior to the snow season. An optimal field is a 10 m x 10 m area that can remain relatively undisturbed over the course of the winter (that is, sufficiently distant from walking paths or instruments that may require servicing over the winter, so that instrument servicing will not affect the snow measurement area). Prior knowledge of the snow-depth distribution in the measurement area helps in choosing spatially representative point measurements. Caution is required so that obstructions or variability in exposure do not result in preferential accumulation or scouring due to drifting snow or in preferential melt due to exposure. Measurements should be carried out away from obstacles, at a distance at least twice the obstacle height, but a site assessment is required to ensure that this spacing is adequate, taking into consideration exposure (and shading) and dominant wind direction during the winter season.

Siting considerations for an automated *HS* or *SWE* instrument should be the same as for the siting of a point measurement, even though the measurement principle of automated *SWE* instruments provides more spatial integration. It is recognized that for automated instruments it might be difficult to arrange that the distance between the instrument and an obstacle is at least twice the height of the obstacle, due to the proximity of the instrument mounting structure, so exceptions need to be made. As with *HS*, unless the measurement area is very homogenous, the point *SWE* measurement will likely not be representative of the surrounding landscape. Consequently, an extensive survey of *HS* and *SWE* is recommended at least once per season (see 2.3.1.2 and 2.4.1.2), timed to coincide with maximum accumulation, to assess the spatial representativeness of the point measurement. Since the spatial variability in the bulk density of the snow cover is generally much lower than the snow cover depth (Dickinson and Whitely, 1972), the variability can often be assessed with a *HS* survey alone.

The measurement of *HN* should be carried out where the new snow falling on the measurement area is representative of the surrounding area. This is best done in a sheltered location where wind effects will be minimal and where the snow is allowed to fall undisturbed. As with the measurement of precipitation, the surrounding obstacles should be at a sufficient distance (roughly twice the height of the obstacle) so as not to interfere with the measurement.

Fixed snow-depth transects, also known as stake farms, should be sited, using the same criteria as point measurements, at a sufficient distance from instruments, obstructions and walking paths to minimize disturbance, without jeopardizing the observer's ability to read the stakes. The transect will necessarily be closer to the path that the observer will use to make the measurements, while avoiding disturbance of the measurement area as much as possible.

Finally, siting should take into consideration accessibility and permanence, which will ultimately affect the continuity of the record. For automated measurements, the source of available power and communications may also be a consideration for siting.

2.3 SNOW DEPTH

2.3.1 Manual measurements of snow depth

2.3.1.1 *Measurement techniques*

Graduated devices

Manual *HS* measurements are made with a sturdy ruler, stake (see Figure 2.2, left and centre) or extendible graduated rod (see Figure 2.2, right). Measurements may consist of an observation at a single point, or of many points in a transect. Unlike a point measurement, the observation of multiple snow depths in a transect enables the observer to assess the spatial variability at the observation site. The measurement instrument can be permanently fixed to the ground (stake) or manually inserted at the observation point (rod) before each measurement.

Snow-depth measurements at remote sites with deep snow cover can be made using vertical snow stakes with horizontal cross arms at fixed intervals, which can be viewed from long distances (see Figure 2.3).

Photometry

At unstaffed sites, a viable alternative to visually observed snow stakes is scheduled automated photometry (for example, a web camera) which allows the snow stakes to be photographed and the snow depth manually interpreted from the images (see Figure 2.4). Snow depths can either be retrieved in real time or later from the saved images.

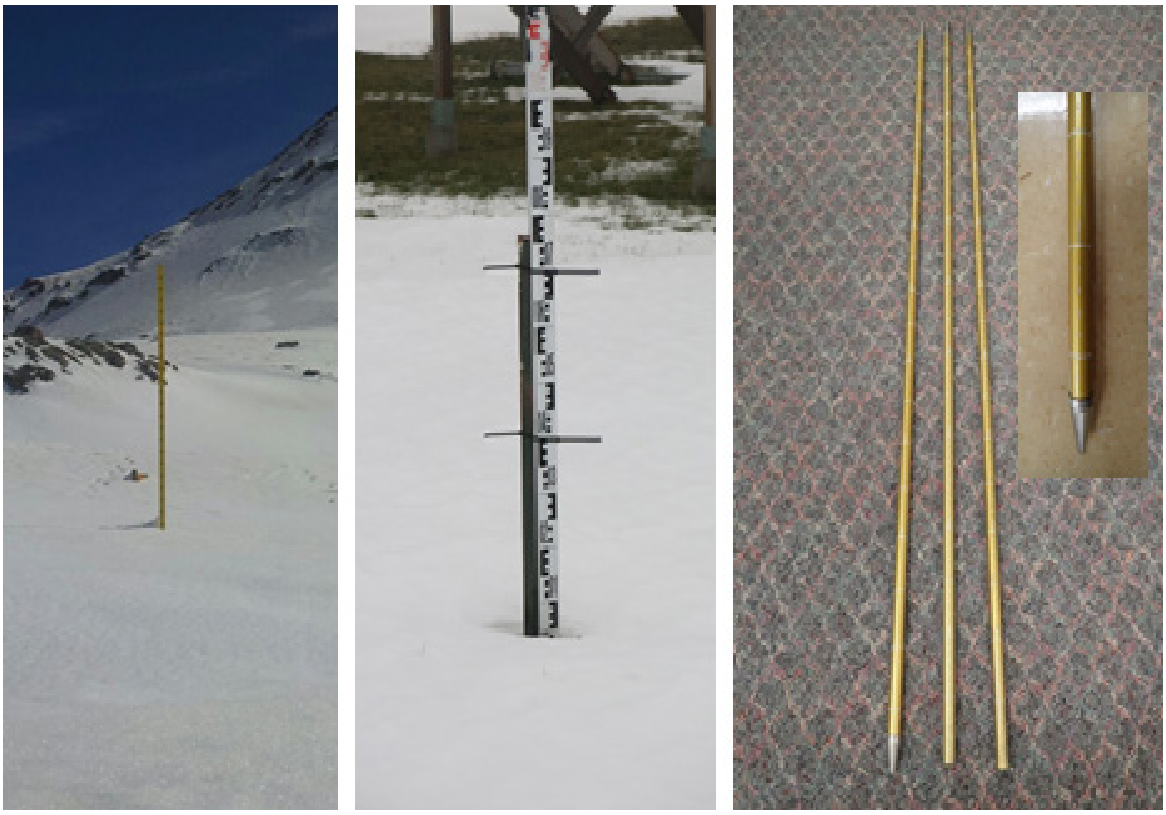

Figure 2.2. Graduated snow stakes in deep alpine snow cover (left, Pyrenees, Spain; photo courtesy of the Spanish State Meteorological Agency) and in shallow snow cover (centre, southern Ontario, Canada; photo courtesy of Environment and Climate Change Canada (ECCC)). An extendable 1 cm graduated snow rod (right, photo courtesy of ECCC)

Figure 2.3. Vertical snow stake with horizontal cross arms (left, photo courtesy of the WSL Institute for Snow and Avalanche Research SLF, Davos, Switzerland) and colour coded bands (right, photo courtesy of the Spanish State Meteorological Agency)

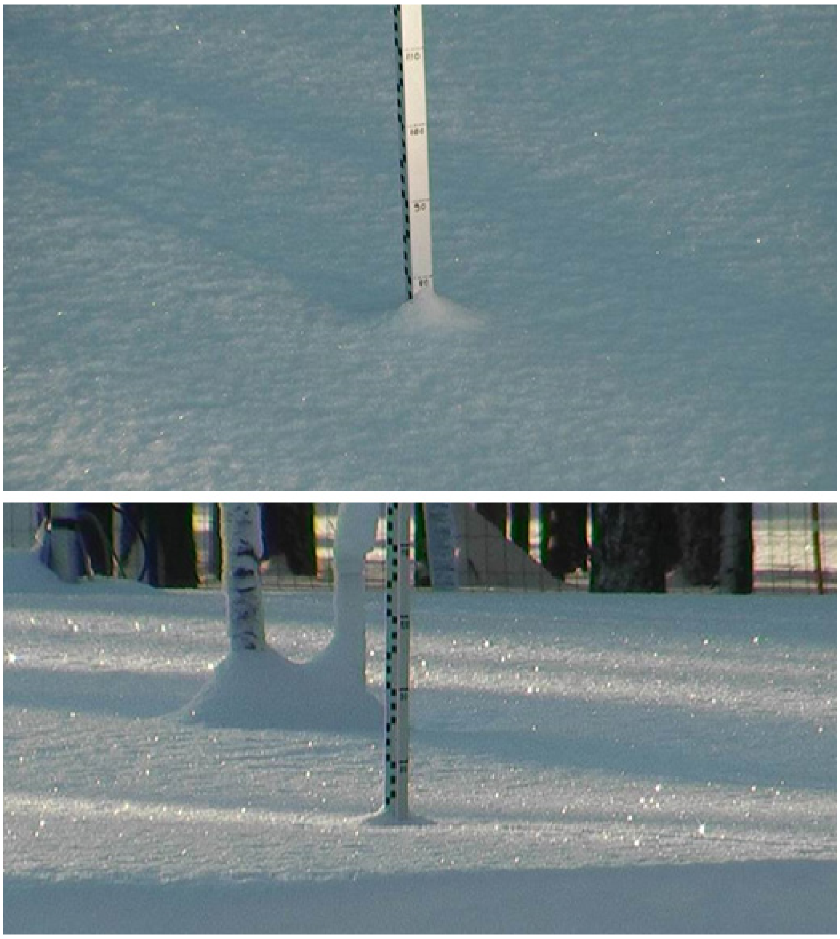

Figure 2.4. A snow stake photographed by a web camera at an elevated grazing angle to the stake (Sodankylä, Finland, photo courtesy of the Finnish Meteorological Institute)

Electronic probe

Another option, especially for surveys in shallow snow cover, is the use of a recording snow-depth probe equipped with a GNSS antenna (see Figure 2.5; Sturm and Holmgren, 2018). The probe is manually inserted into the snowpack until it contacts the base surface, and the snow depth is then electronically measured and stored for subsequent data retrieval and analysis.

Ground penetrating radar

Ground penetrating radars (GPRs) are used to determine snow depth at a point or over large distances and along gridded snow courses. In general, a lightweight sled containing the instrumentation is pulled over the snow cover (Lundberg et al., 2010; Griessinger et al., 2018). It is also becoming common practice on glaciers and the method is further detailed in the present Guide, Volume II, Chapter 3, 3.7.1. The data analysis for GPR can be either done manually or automated.

Figure 2.5. Recording snow-depth probe equipped with a GNSS antenna (Canadian Arctic, photo courtesy of Environment and Climate Change Canada)

2.3.1.2 *Measurement procedures and best practices*

Measurement device

The measurement device for manual *HS* measurement should be a graduated stake (fixed measurement) or a graduated ruler or rod (non-fixed measurement) with the graduation in centimetres. The choice of measurement device may depend both on the permanency of the installation and on the nature of the snowpack being measured. Regardless of permanency, the location of the measurement should be the same for each measurement, as outlined below.

For permanent (fixed) or semi-permanent (that is seasonally fixed) point installations, the recommended measurement device is a fixed snow stake (see Figure 2.2, left) with highly visible graduations such that it can be read at a distance. The snow stake should be vertical and firmly anchored to the ground in concrete or with pegs. If the installation is seasonal, it is important that the stake is placed at the exact same location each year. Use of Differential Global Positioning Systems (DGPSs) is preferred; otherwise, orientation with landmarks is the next option. The material of the stake should have a relatively low thermal conductivity and low heat-storage capacity (such as wood or fiberglass) and painted white (high albedo) to minimize melting around the stake. If the stake is to be photographed in low-light conditions, graduations in reflective material may increase visibility. Low-light photography of a snow stake may require specialized camera equipment with infrared capability or an external light source (for example LED) to improve the quality of the photographs. The angle between the camera and the snow stake should be as low as practical to minimize interpretation of the snow line against the stake. Attention should be paid to the orientation of the camera with respect to direct sunlight and shadowing.

For manual *HS* measurements, where permanent stakes are not installed (that is non-fixed), a ruler (for example, an aluminium or wooden metre stick) can be inserted into the snowpack down to the ground surface. For measuring deep and/or dense snowpacks or snowpacks with ice layers, the use of a snow rod is recommended such that it can be rammed through the snow until the pointed end comes into contact with the surface, with the rod extensions added as required for deep snowpacks. A rod, unlike a ruler, will not flex when inserted into deep or dense snow cover.

For spatially distributed *HS* measurements, the length and number of stakes in the transect line will be determined by the snow variability at the study site. Generally, a transect line will consist of 5 to 10 stakes installed 5 to 10 metres apart. According to Neumann et al. (2006), the minimum length of a transect can be determined by assessing the change in the coefficient of variation (CV) with increasing transect length, where CV is defined as the ratio of the standard deviation to the sample mean expressed as a percentage. A constant CV indicates that the transect line has captured the local variability. López-Moreno et al. (2011) indicate that for plot size measurements (that is 10 m x 10 m) the error can be minimized by obtaining 5 to 10 samples with measurement spacing of at least 2 m.

Measurement protocols

Snow stakes are to be observed from a sufficient distance so as not to disturb the snow near the stake. Observations are to be made parallel to the snow surface. This can be accomplished with the observer viewing the graduations on the stake from a vantage point close to the surface of the snowpack. It is recommended that the observations be made from approximately the same observation point each time, especially if there is more than one observer. This observation point should be identified prior to the measurement season. Some interpolation by the observer may be required when there is a mound, a well or an uneven distribution of snow around the snow stake at the time of observation, so that a mean *HS* across the face of the snow stake is reported (see Figure 2.6). Snow depth, stake number (if more than one) and time of observation should be recorded along with any relevant present weather information such as the occurrence and intensity of precipitation during the observation. If multiple stakes in a transect line are averaged,

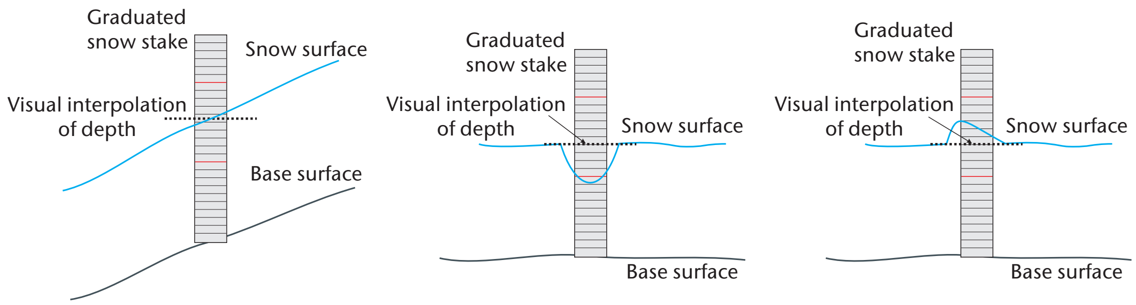

Figure 2.6. Cross section of a fixed snow stake illustrating how to interpolate and observe uneven HS across the face of the stake due to a sloping snow surface (left), welling (middle) and mounding (right).

the reported average should be rounded to the nearest centimetre. If more than 50% of the measurement field is bare (see 2.7), a snow height of 0 cm is entered into the logbook, even if there is still some snow at the stake itself.

For a non-fixed snow-depth observation, the same principles as above apply. The observation should be made in the same location each time, bearing in mind that some adjustment in the location may be required to sample undisturbed snow. The observer should walk on the same path for each observation, reaching as far as possible off of the path to measure undisturbed snow. The ruler or rod is inserted firmly into the snowpack to penetrate any layers of dense snow or ice. The observer must ensure that the device reaches the base surface but caution is required not to penetrate soft soil or organic layers (over-probing) and thus overestimate HS. The observer should have prior knowledge of the nature of the surface below the snow and should use his/her own judgement. On inclined surfaces, the rod (or avalanche probe) should be inserted vertically into the snowpack down to the base surface. A clinometer may be used to ensure that the measurement is made at the correct inclination. The measurement or estimate of the slope angle (φ) should be included in the metadata for the measurement. These techniques also apply to snow-depth transects measured with an electronic probe. Note that an electronic probe will likely have a flat basket (see Figure 2.5) which rests on top of the snow surface during the measurement. The potential for an overestimate exists when the incline is steep and the basket is not flush with the surface. This should be noted in the metadata for the measurement along with an estimate of the error.

Photometry

When snow stakes are observed via photometry, the camera should be at the lowest grazing angle practical from the snow surface near the stake. The observer should use their best judgement to interpret the mean level of the snow against the snow stake, considering the viewing angle. It is recognized that this can be difficult, especially in low-light conditions, increasing the uncertainty of a photometric measurement as compared to a visual measurement. If automated retrieval methods are used, they should be compared extensively to manual retrievals and quality controlled appropriately.

2.3.1.3 ***Sources of error***

Sources of error in manual HS measurements include observer's errors when reading or recording the measurement, or in finding the base surface with a snow rod (in non-fixed measurements), frost heave of fixed stakes, poor siting and misinterpretation of photographed HS due to the observation angle. Many errors in manual measurements result from misinterpretation of a HS reading or from incorrect entry in a log book. These can be minimized by following measurement procedures. With due care and observer experience, many of these sources of error can be minimized. Errors in measurements of this type can usually be removed through data quality control processes (range and jump checks).

A measurement error can occur when an observer misjudges the location of the base surface with a snow ruler or rod. In deep snowpacks, an observer may mistakenly interpret a deep ice layer as being the base surface since it may be difficult to penetrate with the snow rod; this will result in an underestimate of *HS*. Alternatively, a soft organic layer will also be difficult to interpret as the base surface, and this will result in over-probing and an overestimate of *HS*. These errors can be avoided by having prior knowledge of the base surface conditions and through the observer's experience. They do not occur with fixed snow-depth measurements. The magnitude of such errors, depending on the nature of the snowpack and the base surface, could range from a few centimetres to tens of centimetres.

In fixed transects, errors in *HS* observations can occur if the frost changes the height of the snow stake relative to the ground, resulting in an underestimate of *HS*. Generally, such errors will have a magnitude of a few centimetres at most.

Poor siting of a snow-depth measurement (see 2.2), whether using a single stake or a multi-point transect, could result in large errors, the magnitude of which depends on the site mean and variability but could potentially be as high or higher than the mean, with relative errors increasing with decreasing snow depth. A poorly sited snow-depth measurement could result in the stake being located within a snow drift or scoured area. This can be minimized by siting snow stakes in areas where the snow depth is known to be relatively homogenous, usually in sheltered locations. If this is not possible and the observer believes the stake to be non-representative, the observation should be replaced with spatially distributed non-fixed observations, noting this where appropriate in the site metadata.

Errors in interpretation of both visually observed and photographed stakes, especially if the viewing angle is high and the snow around the stake is uneven (mounding, welling or sloping), can be as large as a few centimetres, but such errors can usually be minimized with experience and following best practices for stake observations.

2.3.2 Automated measurements of snow depth

2.3.2.1 *Measurement techniques*

Automated *HS* measurements can be made with instruments using either sonic or optical (laser) technology. Both sonic and optical devices measure the distance to a target (that is, the snowpack, the base surface or a target flush with the base surface), rather than the distance from the base surface to the top of the snow cover. Although other automated techniques exist, these two types of instruments are the most widely available and the most commonly used.

Sonic instruments

Sonic instruments transmit an ultrasonic pulse towards the target and listen for a return echo from that target. Correcting for the speed of sound with concurrently measured air temperature, the distance to the target is calculated as follows:

$$\text{Distance to target} = \text{Instrument reading} \cdot \sqrt{\frac{T_{air}}{273.15}} \tag{2.3}$$

where T_{air} is measured in kelvin, assuming that the raw instrument reading is correct for the speed of sound at 0 °C.

By subtracting the measured distance to the target from a previously derived distance to the snow-free base surface (zero depth distance), *HS* can be derived:

$$HS = \text{Zero depth distance} - \text{Distance to target} \tag{2.4}$$

Sonic instruments usually measure the distance to the highest obstacle within the automated instrument's response area. The response area is a conical footprint, the radius of which depends on the height of the instrument above the target (see, for example, Figure 2.7).

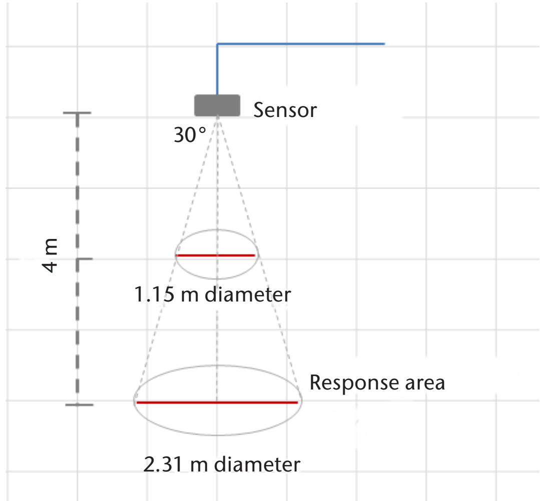

Figure 2.7. Conceptual diagram of a typical sonic instrument and its response area

Optical instruments

An optical or laser instrument emits a modulated beam of light in the visible spectrum and determines the distance to a target by comparing the phase information from the reflected beam. Unlike sonic instruments, the response area of a laser instrument is quite small (<5 mm radius at a distance of 4 m), and the speed of light is not affected by temperature. Optical instruments usually can output a signal strength measurement which can be useful for optically determining the presence of snow beneath the instrument. It is strongly recommended to use a laser beam classified safe for the eyes (maximum power class 2).

2.3.2.2 ***Measurement procedures and best practices***

Choice of automated instruments

The choice between an automated sonic or laser instrument mainly depends on both the requirements for measurement uncertainty and the availability of power. Laser instruments have a higher degree of precision (~0.1 cm) than sonic instruments (~2 cm), but require more power for operation and may not be suitable for measurements at remote sites where power consumption is a concern. Heated sonic or laser instruments should be considered for climates where snow or frost accumulation on the instrument has the potential to impede its function (see Figure 2.11), bearing in mind that such functions require more power. Automated snow-depth instruments should be purchased from a reputable supplier and be proven to work within the manufacturer's specifications to provide a data uncertainty of not more than ±2 cm, but preferably not more than ±1 cm. Proper installation, use and maintenance as prescribed in this chapter and in the instrument manual will help the instrument to achieve the manufacturer's specified uncertainty.

Installation height

Automated instruments need to be installed at a sufficient height above the maximum anticipated snowpack. The minimum and maximum height above the target should be checked with the instrument manufacturer. As an example, some sonic instruments require at least a 1 m clearance between the instrument and the target. In some networks, the peak snow depth can vary substantially from station to station, so it is not important that all of the instruments in the network be installed at the same height.

Mounting structure

The mounting structure needs to be solidly built so as to prevent instrument movement (for example, due to wind), while minimizing interference with the accumulation and ablation of snow beneath the instrument. Steel mounting beams and vertical poles secured with concrete are recommended (see Figure 2.8). The mounting arm of a sonic instrument needs to extend the instrument out horizontally from the vertical mounting pole such that the target area is minimally influenced by the mount (see Figure 2.8, left). At locations that receive heavy snowfall in low wind conditions, it is advisable that the horizontal mounting beam be mounted at a 30° to 45° angle (see Figure 2.8, middle) to prevent snow from collecting on the beam, potentially influencing the measurement of snow depth in the target area. Laser instruments need to be mounted at an angle (for example 10° to 20°) large enough so that the targeted point is sufficiently distant from the mounting structure to minimize interference from the vertical mounting pole (see Figure 2.8, right).

In alpine regions, where the instrument is necessarily installed at greater height above the ground, the structure may have to be more substantial to solidly support the instrument and prevent vibrations due to wind. An example of this structure is shown in Figure 2.9. Note that the response area of the instrument also increases with the instrument's distance from the target (see Figure 2.7).

Surface target

It is recommended that snow depth be measured on a level surface but, if this is not possible due to sloping terrain, the measurement should be made perpendicular to the sloping surface such that the instrument measures DS rather than HS. For sonic instruments, this is done by adjusting the angle of the instrument mount so that the instrument itself is perpendicular to the surface. Since laser instruments point towards a target at an angle, the depth of snow on a sloping surface can be calculated geometrically (see 2.1.1).

Surface preparation prior to snowfall is required to minimize instrument noise and erroneous data due to interference from surface vegetation or other obstacles within the response area of the instrument. An adequately prepared target area will increase the instrument's capability to detect the first accumulations of snow occurring on the bare surface. Because sonic instruments have a much larger response area than laser instruments, surface preparation is generally more

Figure 2.8. Automated sonic snow-depth instrument with steel mounting beam and pole secured with concrete (left), angled mounting beam to reduce collection of snow (middle), and laser instrument mounted at an angle away from the vertical mounting pole (right) (Sodankylä, Finland, photos courtesy of the Finnish Meteorological Institute).

Figure 2.9. Sonic snow-depth instrument (Spanish Pyrenees, photo courtesy of the Spanish State Meteorological Agency)

important. Sonic instruments require a stable, flat surface for the clean reflection of the sonic pulse, keeping in mind that the sonic measurement will usually be made from the tallest obstacle in the response area.

A high-quality measurement can be achieved by either siting the instrument over closely mown grass (or an otherwise flat and bare natural surface, such as under the instrument in Figure 2.9) or by using an artificial target similar to that shown in Figure 2.8, made of artificial turf. An acceptable maintenance-free option is the use of a plastic surface such as the perforated and textured target construction shown in Figure 2.10, which has been shown to have thermal properties similar to natural ground. It is advantageous if the artificial target has optical properties (which could impact the radiation budget) and texture (which could influence snow deposition or scouring) similar to the natural surroundings.

It is recommended that the zero snow-depth distance between the instrument and the surface be verified prior to, and immediately following an accumulation season to determine the instrument offset before accumulation and to check whether this offset has changed over the course of the season. The relative distance between the instrument and the target may change due to settling (positive change in relative distance) or frost heaving (negative change in the relative distance) and will impact the calculated HS in equation 2.4. Changes in the zero snow-depth distance between the beginning and the end of the winter season should be noted in the site metadata as these changes affect the measurement uncertainty. Small changes in the zero snow-depth distance during the measurement season will reduce the measurement reliability for shallow snow depths (for example, 0 to 2 cm) which requires the relative distance between the instrument and the target to remain unchanged under all conditions.

Figure 2.10. Perforated and textured grey plastic target during construction. The panels measuring approximately 1.2 m x 1.2 m are installed on a wooden frame (photo courtesy of Environment and Climate Change Canada).

Minimizing vegetation and vegetation growth in the target area will prevent misinterpretation of growing vegetation as a change in snow depth and will, therefore, improve data quality. This is more significant in regions where snow depth is shallow or ephemeral and the uncertainty of the shallow measurements is more important.

Data quality control

The quality of data from automated instruments can be improved through frequent (for example, more than once per minute) measurements over a period of time short enough not to incur significant changes in *HS* (for example, 5 minutes), with the value reported for the period being the median of those high-frequency measurements. This reduces the impact of signal noise on the reported value. In addition to this, other quality control procedures are advisable. These should include a maximum and minimum (site specific) range check for *HS* measurement, where the maximum value should be ~20% higher than the maximum expected *HS* and the minimum value should be 0 minus 2x the manufacturer's stated instrument uncertainty. A minimum range check value of less than 0 allows for variability in the zero snow-depth distance to be around the instrument's stated uncertainty without flagging the data as out of range. A step change check should also be used to ensure that changes in *HS* from one measurement to the next are within a physically realistic range for the site. Note that the zero depth distance should be verified at the end of each winter and the offset adjusted if necessary. Drift in the zero depth distance, caused by relative changes in height of the target surface and the instrument, is a source of measurement uncertainty. If the timing and magnitude of the drift can be identified, the observation can easily be adjusted, but often zero depth distance drift will be a non-linear process occurring between the start and end of the snow season, making the data difficult to adjust. Change in the zero depth distance should be noted in the metadata.

2.3.2.3 *Sources of error*

The sources of error in automated snow-depth measurements include instrument malfunction, inadequate or improperly installed mounting structure, zero depth drift, incorrect sonic temperature correction, accumulation of frost or snow on the instrument hindering the measurement, and inconsistencies in the target area due to rapid melt or rain.

For automated point measurements, inconsistencies under the instrument can be minimized by an artificial surface target, especially during the season of active vegetation growth and at the beginning of the accumulation period. Inconsistencies due to rapid melt (that is, large variations in depth across the target area, especially in deep snow covers) are difficult to prevent or correct, but they can be identified through the use of daily photometry of the target area.

Instrument malfunctions can be minimized through proper and routine maintenance as suggested by the manufacturer. Instrument failures can also be a result of power supply, wiring, or data logger (operation or programming) issues.

Improper instrument installation could lead to unwanted motion during windy conditions resulting in erroneous or uncertain measurements due to changes in the relative distance between the instrument and the surface target.

Zero snow-depth drift could potentially produce small but incremental errors in measured HS that are difficult to assess or to adjust during the winter season. This impact should be assessed annually at the end of each seasonal ablation, and the zero snow-depth distance should be updated before the beginning of the next accumulation season. If an artificial target is used, settling is most likely to occur during the first accumulation season (due to the disturbed ground followed by the weight of the snowpack on the target) although frost heave of the target could occur during any winter season. An incorrect zero depth offset in the instrument, data logger or during post-processing will result in the reporting of erroneous snow depths.

Potentially large errors can result from erroneous air temperature measurements when used for correcting sonic distances. This may be due to a faulty instrument or may be the result of radiative heating of unshielded or poorly shielded temperature instruments. Good radiation shields (for example, a white reflective construction with well-ventilated louvers to allow air to pass freely through) along with quality assurance of the temperature data used for the sonic correction can minimize these errors. If possible, the temperature measurements should be made in the aspirated radiation shield to reduce radiation errors. Generally, errors associated with the height of the instrument in relation to the temperature profile between the instrument and the target are small, even with the temperature instrument installed at the same height as the snow-depth instrument rather than closer to the average distance to the target.

Lastly, errors in automated HS measurements could result from the accumulation of frost or snow on the instrument (see Figure 2.11). Some instruments have heating capability to minimize this problem and should be used where required. Heating of the mounting beams with heat tape and the use of angled mounting beams (see Figure 2.8, middle) may also help prevent snow and frost build-up around the instrument.

2.4 WATER EQUIVALENT OF SNOW COVER

2.4.1 Manual measurements of water equivalent of snow cover

2.4.1.1 *Measurement techniques*

There is a large variety of manual measurement techniques for SWE. Measurement techniques will vary depending on snowpack depth and conditions. The following sections try to capture those techniques and some of the factors that determine them. Only direct measurement methods are presented. Active or passive radiative absorption methods are excluded here as many of these techniques have been automated and are discussed in subsequent sections.

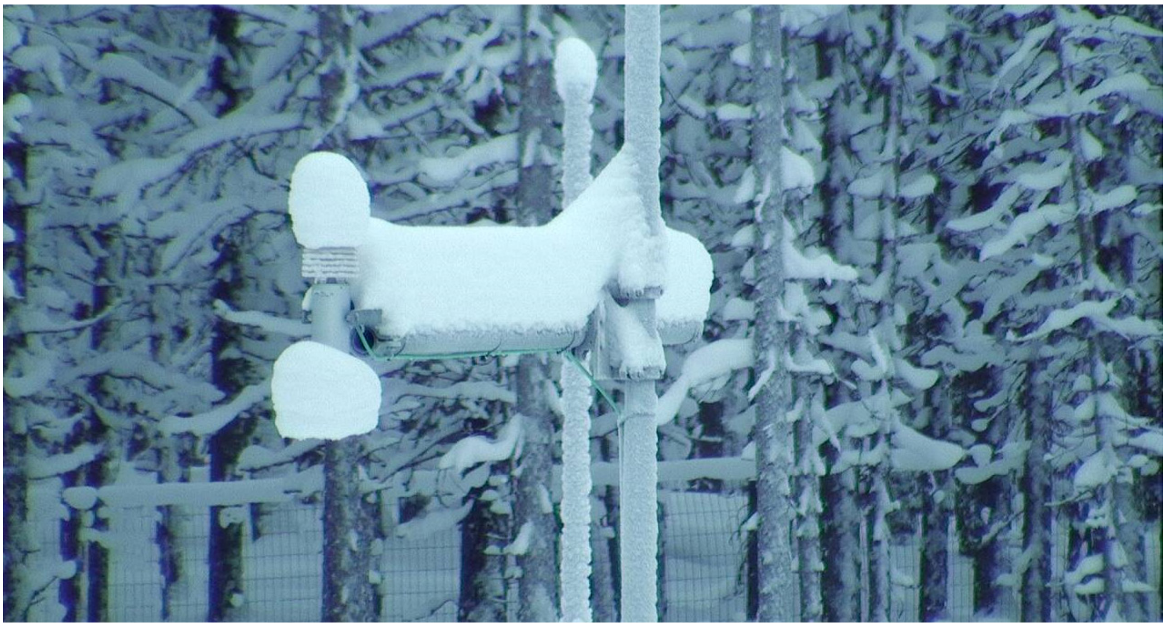

Figure 2.11. Unheated snow-depth instrument and mounting structure collecting snow in a low wind environment (photo courtesy of the Finnish Meteorological Institute)

Generally, all direct measurement techniques involve a gravimetric snow sampler which collects a known (or calculable) volume of snow from which the snow density can be derived. Techniques range from the use of a small volumetric sampler (for example, 1 000 cm^3) in a snow pit (see Figure 2.12, left) to a 10-point snow course using a snow tube (see Figure 2.12, right). There is a large variety of volumetric samplers and snow tubes in use and their choice largely depends on the nature of the snowpack being sampled. Many of these samplers are listed and discussed in Farnes et al. (1983) and Haberkorn (2019), while only a few are discussed in this chapter in the context of measuring various snowpack regimes. On glaciers, coring augers are widely used to measure SWE. For details on using coring augers see the present Guide, Volume II, Chapter 3, 3.7.1.

There is not a standard volumetric sampler for making SWE measurements; some samplers work better in certain snow conditions than others. These are described further in 2.4.1.2. The discussion here focuses on two general SWE measurement techniques: snow pits and snow courses, with their respective advantages and disadvantages.

SWE measurements in snow pits

Snow pits (see Figure 2.13) involve manually digging a hole in the snowpack down to the reference surface such that an undisturbed face of the snowpack is exposed. Snow pits are a useful technique for observing the stratigraphy of the snow, especially for deeper snowpacks. These gravimetric observations of SWE are generally performed weekly, biweekly or seasonally, depending on their purpose. The measurement technique is destructive in that a large pit is usually necessary, so it must be dug in a different location each time. A sampler of a known volume (typically 10^{-4} to ~$4 \cdot 10^{-3}$ m^3) is inserted into the snow and a sample of a known thickness L (m) is extracted (either of each snow layer or layer thickness independent) and weighed (see Figure 2.12, left). Snow density ρ_s of the sample (kg m^{-3}) is then obtained as:

$$\rho_s = \frac{m_{sample}}{V_{sample}} \quad (2.5)$$

Figure 2.12. A 55 cm-high volumetric sampler being weighed with a spring scale (left, photo courtesy of the WSL Institute for Snow and Avalanche Research SLF, Davos, Switzerland) and a tube snow sampler (right, courtesy of Environment and Climate Change Canada)

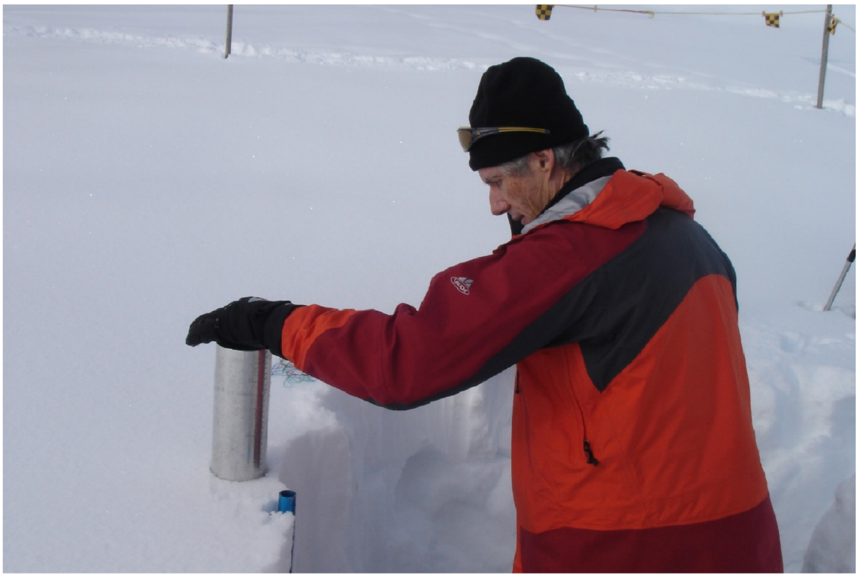

Figure 2.13. Sampling the top layer in a snow pit with an ETH-cylinder sampler (photo courtesy of the WSL Institute for Snow and Avalanche Research SLF, Davos, Switzerland)

Where m_{sample} is the mass of the sample (kg) and V_{sample} is the sample volume (m^3) which often corresponds to the volume of the sampler. The water equivalent WE of the sample is then determined by:

$$WE = L \cdot \rho_s \tag{2.6}$$

Taking several samples seamlessly from the snow surface down to the reference surface, SWE will then be the sum of the water equivalent of each sample.

SWE measurements on snow courses

Observation of SWE on a snow course is generally carried out with a tube snow sampler (see Figure 2.12, right) in a multi-point transect, usually consisting of 5 to 10 measurement locations spaced 30 m apart. There is a variety of snow tubes but the sampling principles are much the same. The snow tube is inserted into the snowpack (see Figure 2.14) to the ground surface, using tube extensions where required, and a snow core is extracted. The volume of that core is calculated from the depth of the core in the tube, knowing the sampler radius. The sample is then either weighed with a snow-tube cradle and spring balance or bagged and weighed with a scale. Some spring balances are calibrated to directly provide the SWE measurement in mm w.e. or kg m^{-2} (after subtracting the weight of the tube), or density can be calculated manually as follows:

$$\rho_s = \frac{m_{sample}}{\left(\pi R^2 \cdot L\right)} \tag{2.7}$$

where R is the inside radius of the snow-tube cutter (m), L is the depth of the snow sample measured with the snow tube (m), and m_{sample} is the mass of the sample (kg) with the weight of the tube or the sample bag (if the sample is collected in a bag rather than weighed in the tube) removed.

SWE is then calculated according to:

$$SWE = L \cdot \rho_s \tag{2.8}$$

The advantage of snow-course sampling over snow-pit sampling is in the relative speed of the snow-tube sampling technique and the minimal disturbance of the snowpack allowing for repeated measurements very close to each other over the course of the winter season.

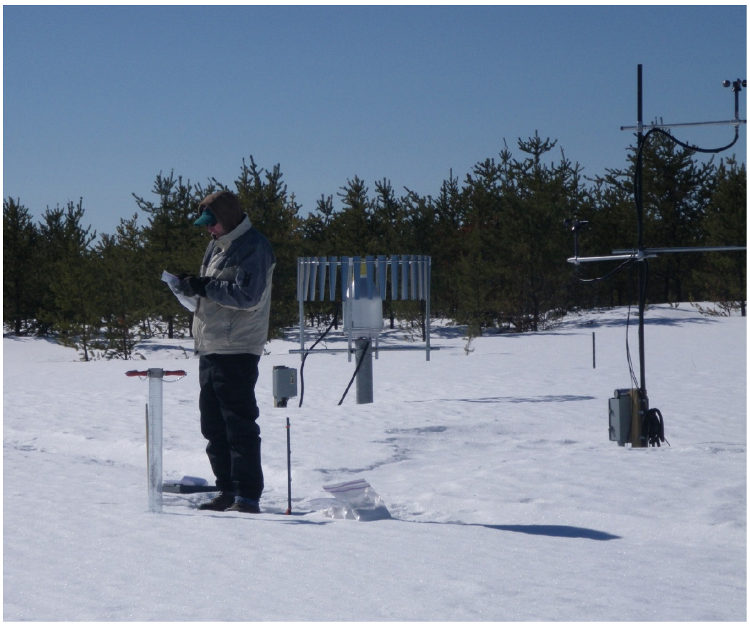

Figure 2.14. Sampling with a snow tube (photo courtesy of Environment and Climate Change Canada)

The disadvantage as compared to snow pits is the inability of the observer to determine whether the snow sample is being collected intact, especially in complex snow covers with non-cohesive layers or ice lenses. Some of these difficulties are discussed in 2.4.1.2.

On a snow course, a technique called double sampling is usually employed, where multiple snow depths (usually 10 to 15, depending on the snow cover variability) are obtained using a ruler or rod between SWE samples (see 2.3). The areal SWE is then calculated with equation 2.8, using the average density from the 5 or 10 snow-tube samples and the average HS measured with the ruler or rod. This technique has been shown to improve the areal estimation of SWE and to reduce the variance of the measurement, in comparison with SWE sampling in the snow course without multiple HS measurements (Rovansek et al., 1993), provided that the snow depths are obtained with minimal error.

2.4.1.2 ***Measurement procedures and best practices***

Measurement techniques and devices

The two options for manually sampling SWE are a snow course with a snow tube sampler, and a snow pit with integration of small volumetric samples. A snow course and snow tube should be used where SWE is less spatially homogenous, hence the need for increased spatial sampling. A snow course and snow tube will, therefore, create less disturbance of the snow cover and enable faster multi-point sampling. Site variability can be estimated using a snow-depth transect, as discussed in 2.3.1.2; a coefficient of variation greater than 10% would suggest the need for multiple point samples on a snow course rather than a snow pit. The disadvantage of a snow course with a snow tube sampler is increased uncertainty in the measurement. Where the snow cover is more homogenous, a single snow pit can be used to assess SWE by integrating multiple small volumetric samples from the surface of the snow to the surface of the ground. These are more labour intensive and require more time and disturbance of the snowpack but are generally more accurate. The measurement protocols are detailed below.

Measurement protocols for snow pits

Manual SWE measurements are often conducted by measuring the density of the snowpack in incremental steps, starting at the surface of the snow in the snow pit and continuing until the base has been reached. The procedure requires a graduated cylinder, a spring scale, a sharpened thin metal plate (approximately 20 cm x 20 cm) and a tool such as a crystal card, scraper or spatula to cut out the samples from the surrounding snow. The maximum height of a layer is determined by the length of the cylinder. A conceptual diagram of the process is shown in Figure 2.15.

Choosing a snow pit location:

(a) A snow pit should be in a flat location where the pit can be excavated without disturbing other measurements at the site;

(b) Depending on the frequency of pit measurements, more room may be required for future pit excavations, so keep this in mind when locating the first and subsequent pits;

(c) Choose a location for the snow pits before snow accumulation starts so that the base surface is clear of rocks or other debris.

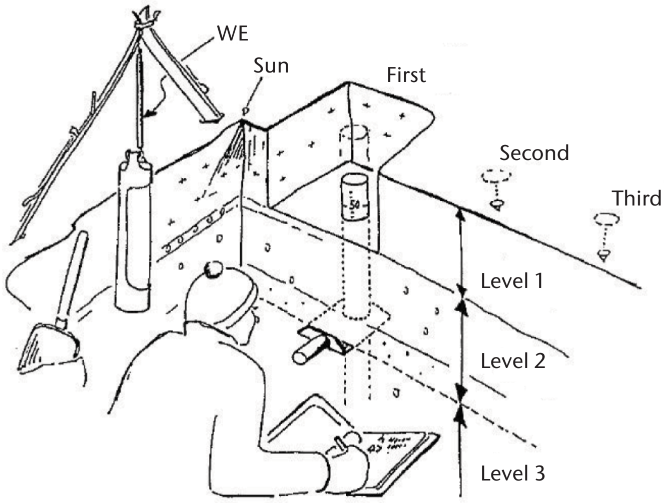

Figure 2.15. Conceptual diagram of *SWE* observation using a snow pit (photo courtesy of G. Kappenberger, WSL Institute for Snow and Avalanche Research SLF, Davos, Switzerland)

Making the measurements:

(a) At the location chosen for the snow pit measurement, dig a pit to expose the face of the snow pack that does not incur direct sunlight. This will help to prevent the face from warming in the sun and will help to avoid snow sticking in the sampler;

(b) The samples for the measurement of *SWE* are taken vertically and continuously starting from the surface of the snowpack. Insert the metal plate horizontally into the exposed face at a depth slightly less than the cylinder length;

(c) Insert the cylinder, which should have sharpened edges at one end, vertically down to the plate and record the corresponding sample height as shown on the graduations on the cylinder;

(d) Cut the sample out of the exposed face using a crystal card, scraper or spatula, being careful not to drop loose snow out of the sampler before it is weighed;

(e) The sample is either weighed with a spring scale hung in a convenient location, as shown in Figure 2.12 (left), or it can be bagged, labelled and weighed on a bench scale at a later time;

(f) It is recommended to resample each level a short distance away from the first sample (see Figure 2.15). It is important that this distance is not too great in order to decrease the uncertainty related to spatial variability. The mean height and weight of the repeated measurements determine the sample volume and mass, which is then used to calculate the density and finally the *SWE* for each layer. If the height or weight of the repeated measurements differs by more than 5%, the measurement should be repeated a third time;

(g) To sample the next incremental level, clear the remaining snow away from the metal plate and reinsert it near the bottom of the next level. Repeat the sampling procedure until the base surface is reached;

(h) Finally, the *SWE* of the whole snowpack is calculated by adding up the water equivalents of each sampled layer. Be aware that the sum of the layer thicknesses is often smaller than the measured *HS* due to uneven ground and the thickness of the metal plate.

Measurement protocols for snow course surveys

The following general procedure should be used to measure *SWE* on a snow course using a snow tube. The double sampling technique is described here.

A snow course should be established before the beginning of the snow accumulation season, although prior knowledge of local snow cover variability would be useful (see 2.2). Sampling locations where large rocks, logs, underbrush or drainage channels could impede the measurement should be avoided.

To set up a snow course:

(a) Select a site and determine the length of the course and the number of samples required to capture the spatial variability at the site. A 10-point course, with measurement points spaced 30 m apart, will have a baseline of 270 m. A 5-point course will have a 120 m baseline but should be extended if the site experiences high spatial variability;

(b) Establish the starting point of the course with a marker (stake or post) that will be visible well above the maximum *HS*. It is suggested that the stake or post be painted with a highly visible colour and marked clearly with a number;

(c) With a measuring tape, measure the 30 m distance to the next survey point and install the next marked stake or post. Continue like this to the end of the snow course, numbering the stakes sequentially. Obstacles such as tree stumps or ditches that may impact the snow cover should be avoided;

(d) For metadata purposes, draw a diagram of the snow course including direction of course, distance between marker stakes, slope, vegetation cover and obstacles.

Making the measurements:

(a) Measurements on the first snow course should start on the first snow survey date when the depth of the snow at the site exceeds 5 cm, and should continue according to schedule until two or more points of the 5-point course, or four or more points on the 10-point course, are snow free. A typical measurement schedule is weekly or biweekly;

(b) Sampling on a snow course should be completed early in the day when air temperatures are cooler and the snowpack is dry. A cold tube should be used to avoid snow sticking to the inside of the tube. If the tube has been stored in a warm location, lay it in the snow to allow the tube to cool off before starting the survey. Wear gloves to avoid transferring heat to the tube during the survey. Note the time of the start of the snow-course sampling;

(c) Starting with the first marked stake on the course and continuing sequentially to the last marked stake, make a bulk density sample with the tube in an undisturbed location within 1.5 m of the stake, avoiding previously sampled locations and minimizing disturbance of the area that may affect subsequent measurements. Consecutive samples can be made at a prescribed incremental distance from the marked stake to avoid sampling in previously disturbed snow. A field diagram of the sampling locations is recommended, especially if there is more than one observer at the site;

(d) Before each sample, inspect the tube to make sure that it is free of snow and soil, and beware of the sharp teeth on the cutter;

(e) Insert the snow tube vertically, cutter first, into the surface of the snow. Gently rotate the tube so that the cutter drills into the snow until it reaches the base surface (prior knowledge of *HS* can assist in this assessment). Use of excessive pressure will cause the tube to plough through the snow and push material away from the tube instead of collecting it. If resistance is encountered due to ice layers, rotate the tube more aggressively clockwise using the handles, and apply increasing vertical pressure on the tube to allow the cutter to penetrate the ice layer and continue through the remaining snowpack. Hesitation during sampling should be avoided if possible. The efficiency and quality of the sample will be increased by keeping the cutter teeth as sharp as possible and resharpening the teeth with a file or sharpening stone following contact with rocks or hard surfaces;

(f) When you are confident that the cutter has reached the base surface, note the depth of the snowpack observed on the tube graduations in the data form. When sampling a deep snowpack (that is deeper than the length of the snow tube), add segments onto the tube to reach the required depth. Note the depth of the core sample in the tube, and record this information in the data form. If the depth of the core in the tube is less than 80% of the depth of the undisturbed snow, the core has likely collapsed beneath the cutter and has been spilled out of the tube or has not been captured by the cutter. In this case, you will have to take another sample;

(g) Applying increasing pressure, turn the tube at least twice clockwise so that the cutter bites into the surface beneath the snowpack. Ideally, the cutter should penetrate the surface approximately 2 cm such that an adequate soil plug can hold the snow sample in the tube during extraction from the snowpack. If the surface is too hard for the cutter to extract a plug, you will need to dig down to the surface along the tube so that a shovel or plate can be carefully inserted under the tube to hold the sample during extraction (this is generally only practical in shallow snow cover);

(h) With a soil plug in the cutter, the tube can then be carefully extracted from the snowpack with the sample intact;

(i) With a small tool, such as a flat screwdriver or small knife, remove the plug from the cutter, carefully working around the sharp teeth. If the plug has ice or large crystals clinging to it, scrape or remove these carefully, returning as much ice or snow back into the tube (or the sample collection bag);

(j) If the sample is to be weighed with a spring scale and cradle, point the tube lengthwise into the wind (or find a sheltered location), place the tube in the cradle and attach the cradle to the spring scale. The scale may be hung on a structure, such as a sturdy tree branch, to increase the stability and decrease the uncertainty of the weight measurement. Gently bounce the scale to make sure that it is not sticking, observe the weight (which includes the tube) on the scale and note it in the data form. Dump the sample from the handle end of the tube and ensure that the tube is empty and clear of snow and debris. The empty tube is then weighed again using the cradle and spring scale to record the tare weight, which is noted in the data form and removed from the total weight to derive that of the snow sample;

(k) If the sample is to be bagged and weighed at a later stage using a bench scale, empty the contents of the tube into a water-tight sealable bag from the handle end of the tube. The bag should be marked with the measurement location. An empty bag can be used to determine the tare weight prior to weighing the sample on the scale. The scale should be calibrated (for example, ±1%) and of a precision appropriate to the weight of the sample. The calibration of the scale should be confirmed seasonally with a calibration weight. Medium-quality postal or food scales are generally accurate and portable enough for this purpose;

(l) Between bulk density sample markers, use a snow rod to obtain at least 10 equally spaced snow-depth measurements, and record these in the data form.

It is recognized that the sampling procedure and choice of sampler will vary with snow conditions. Observers may choose to use sampling equipment that is historically used in their national observation programmes, which may be adapted to the snow conditions being sampled. This is acceptable, although it is preferable that observers use equipment that has been characterized in previous intercomparison exercises (for example, Farnes et al., 1983).

For shallow snowpacks (≤50 cm) and snowpacks with ice layers or depth hoar, it is recommended to use a snow tube with a larger (>20 cm^2) cutter area that is, however, small enough to ensure that a soil plug can be extracted from the surface. Larger cutter areas will be less prone to plugging with ice or dense snow and less likely to induce the collapse of non-cohesive layers under the cutter. However, the observer needs to pay particular attention to the length of the extracted core to ensure that the entire sample has been captured. For densified snowpacks or snowpacks with ice lenses, sharp cutter teeth are required to reduce sampling errors. In deeper snowpacks, a smaller diameter cutter (for example the Federal 11.2 cm^2 cutter and tube, Figure 2.16) may be used as it will be easier to insert into the deeper snow. It should be borne in mind, however, that smaller diameter cutters tend to overestimate *SWE* and that a correction (see Farnes et al., 1983) should be applied.

In deep alpine snowpacks where one or more tube extensions may be required, it might be more difficult for the observer to determine whether the snow tube cutter has come into contact with the surface. Prior information about the total *HS* at the marked snow stake (that is, via a snow rod or avalanche probe) is useful as a reference for the depth measurement obtained from the tube graduations. In such circumstances, and where snow cover characteristics are relatively homogenous, a single snow pit *SWE* measurement may be the preferred technique.

2.4.1.3 ***Sources of error***

Snow pits (*SWE* integrated from volume samples)

Since the sampling with cylinders involves repeated measurements through the entire snowpack, the probability of a misreading or incorrect transcription of a reading is greater than with one snow tube measurement. The plate used to separate the different measurement levels should be thin and sharp in order to minimize the impact on the applied snow layer. Where a thick ice layer is above a loose snow layer, the measurement should not be taken too close to the pit wall. Moreover, the cylinder should be drilled rather than pushed into the snow to minimize the probability of loose snow falling off the pit wall instead of entering the cylinder, resulting

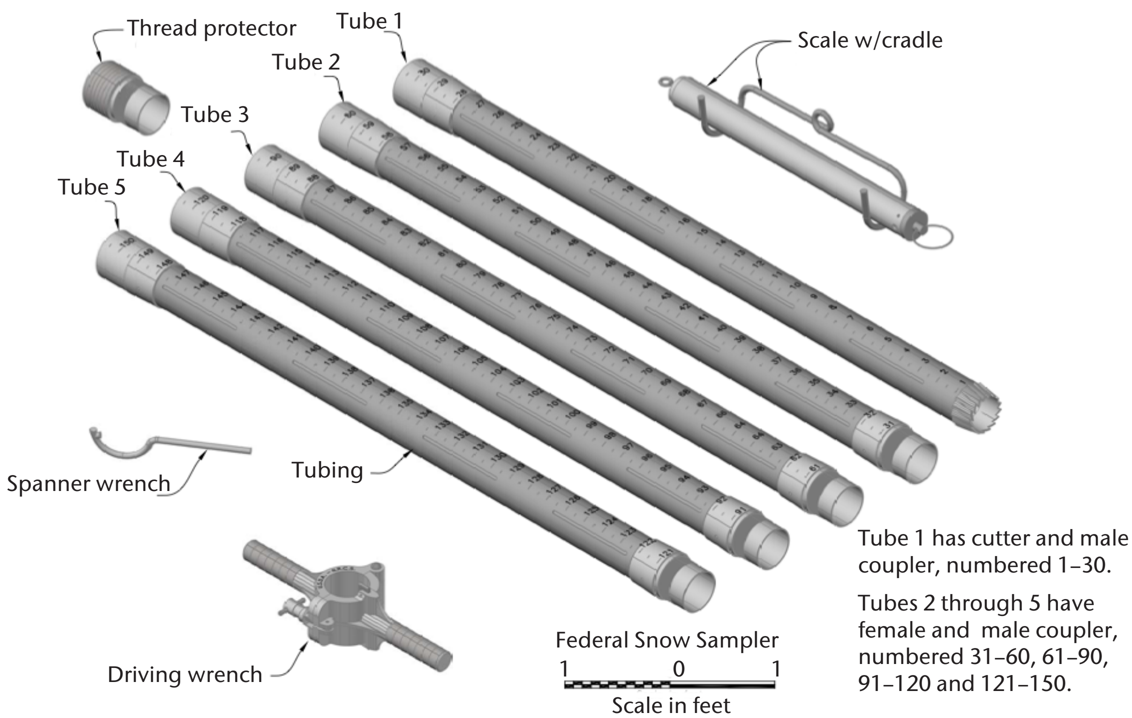

Figure 2.16. A Federal Snow Sampler (drawing by Kristi Yasumiishi, National Resources Conservation Service, United States Department of Agriculture)

in an underestimate of the sample. Proper emptying and cleaning of the cylinder after each measurement is also important to avoid biasing the next sample. This can be more easily achieved with larger diameter cylinders.

Snow course (with snow tubes)

When sampling with a snow tube, the snow is largely undisturbed except for the small area around the sample. However, this method does not allow the observer to check how the tube is penetrating through the snow or to determine whether the cutter has come into contact with the surface. It is impossible for the observer to determine if the cutter becomes plugged with dense snow or ice or if layers of loosely packed crystals are collapsing beneath the cutter, therefore biasing the density sample. The observer is also unable to visually determine if the cutter is biting into the surface of the ground to obtain a sufficient soil plug to prevent spillage from the tube as the core is extracted from the snowpack. These errors are exacerbated by a snowpack with ice layers, basal ice and layers of non-cohesive crystals. The experience of the observer also plays an important role in reducing potential errors.

The design and specification of the snow tube and cutter also influence sampling errors and bias. Many commonly used snow tubes and cutters were compared to a reference in Farnes et al. (1983) and Haberkorn (2019). To summarize, the authors showed that when compared with an integrated sample from a snow pit using a Glacier sampling tube (81.9 cm^2), errors were generally greater for smaller diameter tubes than for larger ones. For example, the standard Federal sampler (11.2 cm^2 cutter, Figure 2.16) was shown to overestimate SWE by up to 12% as a result of the design of the cutter teeth which acted to force extra snow into the tube as the tube was inserted into the snowpack. Also, smaller diameter cutters (down to 20 cm^2) were more prone to plugging as they encountered ice lenses, and more likely to induce the collapse of non-cohesive layers under the cutter, resulting in an underestimate of total SWE. The trade off with size is the ability of larger diameter cutters to cut a sufficient soil plug for the sample to be held in the tube during extraction, thus avoiding use of a shovel or plate to retain the tube, which would cause increased disturbance of the snowpack. A cutter with sharpened teeth will help to reduce these errors. Farnes et al. (1983) showed that the ideal cutter area was about 30 cm^2, demonstrated by a low error percentage of the ESC30 sampler, which ranged from a 5% overestimate to a 2% underestimate.

New snow or wet snow can also increase sampling errors, especially if the observer is collecting core samples to be weighed later rather than using a spring balance and tube cradle. Depending on temperature, new and wet snow will tend to stick in the tube and this will result in an underestimate of the SWE which could exceed 10%.

The material of the sampling tube could also help reduce errors. The sample depth can be more easily read with clear plastic tubes than with slotted aluminium tubes, thus reducing the potential for reporting errors. It is also much easier to see if a snow core has collapsed when it can be observed through a transparent tube. Although tubes made from a clear plastic material are easier to use and lighter to carry, they are not as durable as aluminium tubes, especially in the cold.

2.4.2 Automated measurements of water equivalent of snow cover

2.4.2.1 *Measurement techniques*

There are several techniques for the automated measurement of SWE. The most common are weighing mechanisms (snow pillows and snow scales) and passive radiation (gamma) instruments. Other devices, such as GPS (Jacobson, 2010; Koch et al., 2014) and cosmic ray instruments (Gottardi et al., 2012; Sigouin and Si, 2016) are also available and the reader is referred to the current literature for more information.

Snow pillows

This is probably the most common method for the automated measurement of *SWE*. Snow pillows have been in use since the 1960s (Beaumont, 1965) and consist of an antifreeze-filled synthetic rubber or stainless steel bladder with an approximate diameter of 3 m. The antifreeze fluid usually consists of a mixture of methyl alcohol and water or a methanol-glycol-water solution; since methanol is a toxic substance, it should be handled with care (see Volume I, 6.3.2, of the present Guide). The pillow is installed level with the surface of the ground so as not to affect the accumulation of snow on the surface (see Figure 2.17, left). The hydrostatic pressure in the bladder increases with the weight of the overlying snowpack and is measured either with a float device, which is pushed up a vertical standpipe, or a pressure transducer. The calibrated readings of either instrument are then converted to mm w.e. The typical measurement frequency is hourly with resolutions as high as 1 mm w.e. (Beaumont, 1965) and expected uncertainty of 6%–12% (Palmer, 1986). To prevent damage to the equipment and to preserve the snow cover in its natural condition, it is recommended that the site be fenced and the fluid-filled bladder protected against animal damage. Under normal conditions, snow pillows can be used for 10 years or more but there are environmental concerns because of the toxicity of the bladder contents.

Snow scales

Snow scales (see Figure 2.17, right) are becoming more common as a replacement for snow pillows. The measurement principle is similar in that the instrument measures the weight of the snowpack on top of it, converting the weight to an *SWE* estimate. However, the weight is measured with an electronic load cell, eliminating the need for a fluid-filled bladder. Snow scales have a typical measurement area of 6 m^2 to 10 m^2 and although the typical measurement frequency is 1 hour the instruments have the capability of measuring at higher frequencies. The measurement resolution is typically less than 1 mm w.e. but the expected uncertainty is 10%.

Figure 2.17. Operational snow pillow site (left, photo courtesy of the United States Department of Agriculture), and snow scale (right) with the central panel being the sensing element (photo courtesy of the WSL Institute for Snow and Avalanche Research SLF, Davos, Switzerland)

Passive gamma radiation instruments

Passive gamma radiation instruments (see Figure 2.18) work on the principle that the natural breakdown of potassium or thallium in the soil produces a background level of gamma radiation which is attenuated by the water in the snowpack. The instrument, mounted above the surface, compares gamma radiation measurements of snow on the ground with measurements obtained over bare soil, and calculates the attenuation due to the presence of snow. The attenuation is then related to SWE. The instrument typically reports an SWE value every 6 hours with a resolution of 1 mm w.e and expected uncertainty of 5% to 30% (Smith et al., 2017). The response area is related to the height of the instrument (~40 m^2 at 2 m above the snow surface). Instruments require a pre-snowpack soil moisture calibration so that the attenuation due to soil moisture can be accounted for in the retrieval of SWE.

2.4.2.2 *Measurement procedures and best practices*

Choice of automated instruments

The choice of automated instruments should depend on site conditions, the required temporal measurement resolution, installation considerations and environmental concerns. Passive gamma radiation instruments should be used if the instrument needs to be installed over the surface without disturbing the substrate, or to measure an existing snowpack. However, these instruments require long (more than 6 hour) integration periods which limit their temporal resolution and increase the measurement uncertainty. Passive gamma radiation instruments also have a maximum SWE depth measurement capability which should be taken into account if the measurement is to be made in deep alpine snowpacks (greater than ~600 mm w.e.). The user should also be aware that passive gamma instruments may interpret near-surface soil moisture as SWE, therefore overestimating the total SWE in the snowpack (Smith et al., 2017). Snow scales

Figure 2.18. Passive gamma radiation SWE instrument (photo courtesy of the Finnish Meteorological Institute)

are the preferred option for measuring *SWE* at temporal resolutions of 6 hours or less, but they require more substantial surface preparation before installation. The user must also consider the potential for the system to "bridge" in some snowpack conditions (snow with freeze and thaw cycles, wind-swept regions, etc.). While snow pillows have capabilities similar to those of snow scales, their use should be avoided due to increased maintenance concerns and potential environmental hazards resulting from animal damage and leakage of the antifreeze fluid from the rubber bladder. The desired uncertainty of an automated *SWE* measurement should be ±5 mm w.e.

Installation height

Snow scales (and pillows) are to be installed flush with the surface, to prevent adverse edge effects. Passive gamma radiation instruments need to be installed at the height recommended by the manufacturer but generally 2 m above the maximum *HS*, noting that the height above the snow affects the radius of the instrument response area.

Mounting structure

Gamma radiation instruments are generally not affected by disturbances to the mounting structure, which should, nevertheless, be designed and installed so as to minimize the preferential accumulation of snow inside the response area of the instrument. This applies also to snow scales and pillows, even though they are not installed above the surface. The mounting structure should be as simple as possible yet sturdy enough to securely support the instrument.

Data quality control

As with *HS*, the first level of data quality control should be a range check for reasonable (site dependent) values between zero (or close to zero to allow for a small amount of instrument drift) and the maximum possible *SWE* for the site. An appropriate data filter should also be used to check for unreasonable step changes in the hourly (or daily) *SWE* values, taking into consideration maximum accumulation and ablation rates and wind redistribution. As noted above, changes in *SWE* can be linked to changes in *HS* using a co-located instrument. The snow-depth instrument will help to identify the snow-free period (that is the period when the *SWE* instrument should also read zero) and bridging occurrences on weighing instruments (that is extended periods of increasing *HS* without a corresponding increase in *SWE*).

2.4.2.3 ***Sources of error***

Errors in automated measurements can occur due to non-environmental issues such as instrument malfunction and incorrect instrument calibration (or calibration drift). Errors can also be the result of circumstances related to the measurement environment such as bridging of weight-based measurements or changes in mid-season soil moisture levels under a gamma radiation instrument. Non-environmental errors are more easily identified through quality control procedures (that is min/max filtering) than environmental errors, which tend to be more subtle and less easily detected in the absence of manual sampling.

Under- and over-measurements are a common issue with weight-based *SWE* measurements. It is generally caused by freeze–thaw cycles and snowpack settling, which ultimately leads to a disconnect between the weighing mechanism and the overlying snowpack, and the error could theoretically be as high as 100%. The occurrence of measurement errors is most easily identified by periodic manual *SWE* measurements near the instrument, but often this is not possible. An indication of under-measurement is an increase in *HS* (over several days or weeks) without a corresponding increase in instrument-measured *SWE*. This is most easily detected by co-locating an automated *HS* instrument with the *SWE* instrument. However, even a co-located snow depth sensor may not guarantee a reliable method for identifying those errors, especially when there is possibility of rain events or when under- or over-measurements are subtle.

Errors in automated *SWE* weight-based measurements, especially with snow scales, can be caused by the instrument either settling into the substrate (for example, sand) in which it is installed, or heaving out of the ground due to freezing and thawing of the substrate (for example, soil with a high clay and water content). Settling would decrease the pressure on the load cell and result in an underestimation of *SWE* while heaving would increase the pressure on the load cell, thereby leading to an overestimation of *SWE*. Both conditions are difficult to assess during the accumulation period but may be identified by observing changes in the height of the instrument relative to the surface (which ideally should be zero) as soon as the instrument is free of snow. The magnitude of these errors is difficult to predict but they are likely to be small in comparison to bridging errors discussed above.

Gamma radiation instruments are influenced by the amount of soil moisture present when the soil freezes and are sensitive to mid-season changes in soil moisture. Generally, the instruments should be calibrated annually with a gravimetric soil moisture measurement made just before the soil freezes. However, this is usually not possible as often the first seasonal snow accumulation will occur on non-frozen soil. It is estimated that *SWE* errors are approximately 10 mm w.e. for each 0.10 change in gravimetric water content (Smith et al., 2017). Monitoring the change in soil moisture prior to the ground freezing may assist in identifying these errors, which could potentially persist throughout the accumulation period.

2.5 SNOW PROPERTIES

Snowpack observations require a large enough snow pit to allow for multiple observations in addition to measurements of *SWE* (see 2.4). The pit face on which the snow is to be observed should be in the shade, vertical and smooth. On inclined terrain, the shaded observation face should be parallel to the fall line, which is the natural downhill course of a slope.

Characterizing a distinct layer of snow requires more than simply classifying the observed grain shapes. Additional properties such as snow density also need to be recorded to give as accurate as possible a description of the snow type and its state. Appendix C.2: Snowpack observations in Fierz et al. (2009) contains guidelines on how this is best achieved, with examples shown in either graphical or tabular form.

2.6 DEPTH OF SNOWFALL

Currently, there are no accepted automated techniques for measuring *HN*. The main reason for this is that *HN* is to be measured as the accumulation on a snow-free surface while suitable automated snow-depth instruments would generally be used to measure incremental depth increases on an existing snow cover. If there was snow on the ground before the measurement, it would be incorrect to calculate *HN* as the difference between two consecutive measurements of *HS*, since lying snow settles and may suffer ablation, resulting in an underestimation of *HN*. Therefore, only manual techniques are described here.

2.6.1 Manual measurements of depth of snowfall

2.6.1.1 *Measurement techniques*

The depth of snowfall is measured with a graduated device, such as a ruler, at a defined temporal interval (the most common interval being 24 hours). Snow is allowed to accumulate undisturbed on an artificial surface (for example, a snowboard; see Figure 2.19) for the prescribed measurement interval, then a ruler is inserted vertically into the accumulated snow to obtain a depth measurement. After the observation, the artificial surface is cleared of snow and placed on top of the existing snowpack in preparation for the next observation period.

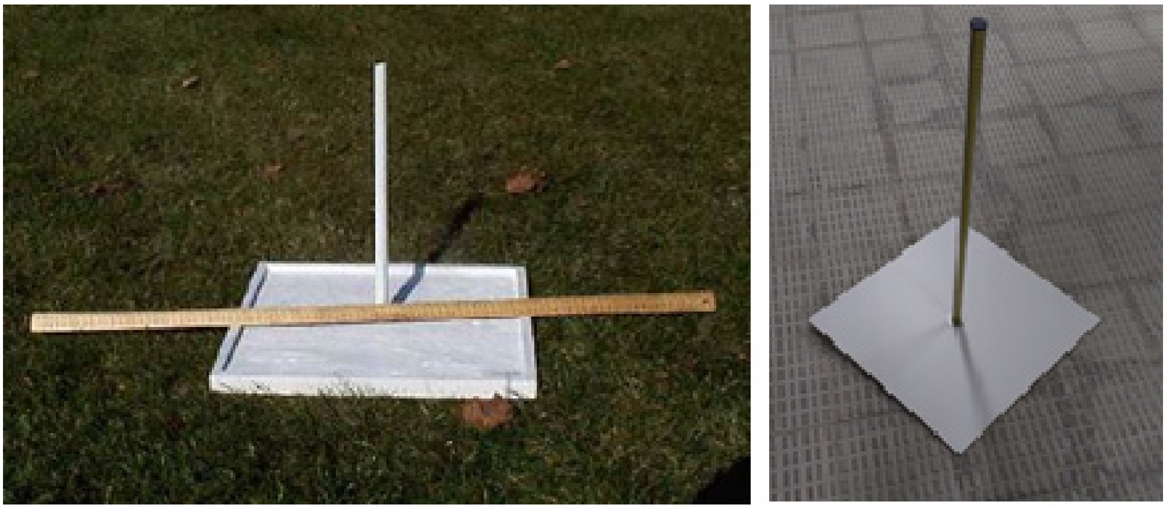

Figure 2.19. Examples of snowboards used for measuring *HN*. The board on the left is called a Weaverboard and is used for new snow observations in Canada (photo courtesy of Environment and Climate Change Canada). The board on the right, which has a graduated rod in the centre, is used by the Spanish State Meteorological Agency.

Another method for measuring *HN* consists in using a cylindrical container, such as a rain gauge, of sufficient diameter (at least 20 cm) and depth to prevent snow from blowing out. The snow can thus be collected uncompressed in the container and can be measured with a ruler to estimate depth. However, a cylinder mounted high enough above the surface to prevent catch of blowing snow is also subject to wind-induced bias. A shield around the collector may reduce but not eliminate this bias.

Some work has been done on automated techniques to estimate *HN* (Fischer, 2011) but this has proven difficult to gauge without guidance from an observer due to factors such as drifting and melting.

2.6.1.2 ***Measurement procedures and best practices***

The depth of snowfall should be measured using a snowboard made of plywood (2 cm thick or less) with dimensions (length and width) between 40 cm and 60 cm. The snowboard should be painted white or covered in white felt to prevent the board from becoming warmer than the snow surface during the day. The snowboard should be placed directly on the bare ground prior to the accumulation of snow. See 2.2 for siting and exposure considerations.

Snow is to be allowed to collect undisturbed on the snowboard during the observation period. Observations are to be made at the same time each day. The observer should measure *HN* on the board using a ruler to the nearest 0.5 cm. The depth of snowfall may have to be measured in several locations on the board if the snow is not evenly distributed, in which case an average depth should be reported. After the depth has been measured and recorded, the board should be swept clear and placed on top of the existing snow cover for the next accumulation period. If the snow cover on the board is less than 50% or too thin to be measurable (less than 0.5 cm), the observer should record “trace” as the observation. Surface hoarfrost on the snowboard should not be considered as new snow and should be cleared off at the time of the observation.

In the event of wind redistribution or melting, the observer will be required to exercise judgement when interpreting *HN*. If wind has swept some or all of the snow from the snowboard, the observer should estimate what would have fallen on the board in the absence of wind. The observer can make this estimate taking into account what can be observed in the vicinity of the board, and considering both the presence of drifts and shallow areas. With inhomogeneous depths of snowfall due to wind redistribution, observers should make multiple measurements until satisfied with their approximation of the mean. If melting has occurred during the accumulation period, the observer should make an estimate of what the depth of snowfall would have been had no melting occurred. In either event, the observer shall make a note regarding melting or blowing snow such that the observation is known to be an estimate rather than a ruler measurement. If snow is found on the board, but the observer is confident that no snowfall has occurred since the last observation period (for example, in the event of drifting snow), the observer should note that *HN* is zero.

2.6.1.3 *Sources of error*

The main source of error in *HN* measurements is the estimate of depth in the presence of either wind redistribution or melting, and it could largely depend on the experience of the observer. The magnitude of these errors is difficult to assess but could be as much as 100%. Errors due to wind can be reduced by proper siting and minimizing the exposure of the snowboard. Errors due to melting can be minimized by not exposing the snowboard directly to the sun. The uncertainty of the measurement can also be heavily influenced by the timing of the measurement. Especially during warm spells, observations an hour earlier or later may make a difference of several centimetres.

Small errors (<0.5 cm) can occur as a result of misreading the depth measurement on the ruler, especially at an angle to the snow surface. This can be minimized by reading the ruler graduations at an angle as close to perpendicular with the surface as possible.

2.7 PRESENCE OF SNOW ON THE GROUND

This observation is usually done in situ by an observer although semi-automated or automated techniques such as photometry can be used.

2.7.1 Manual measurements of presence of snow on the ground

2.7.1.1 *Measurement techniques*

The manual measurement of *PSG* generally consists of a visual assessment of whether or not the field of view of the measurement site is more or less than 50% covered with snow of any depth.

Photometry techniques for measuring the presence of snow are identical to visual measurements except that the interpretation of coverage is done via a photograph or live video feed rather than in person. Automated techniques for extracting this information from photographs are evolving, but as they are not widely used, they are not discussed here.

2.7.1.2 *Measurement procedures and best practices*

Firstly, the area in which *PSG* is to be assessed needs to be defined. This should be the area in which meteorological and cryospheric measurements are being made and should not be limited to the area surrounding the snow stake. The field of view of this area is defined in 2.1.1.

At the same time each day, the field of view of the measurement site should be observed visually or photographed, and the percentage of snow cover assessed. If the snow cover fraction is larger than 50%, the site should report the presence of snow. If the snow cover fraction is less than 50%, the site should report no presence of snow. This observation is independent of the point *HS* measurement, although the opposite is not true.

2.7.1.3 *Sources of error*

The main source of error in this observation is the observer’s interpretation of the snow cover fraction, especially as it approaches 50%. A misinterpretation might affect the timing of snow-free report for the site by several days.

REFERENCES AND FURTHER READING

Beaumont, R. T. Mt. Hood Pressure Pillow Snow Gage. *Journal of Applied Meteorology and Climatology* **1965**, *4* (5), 626–631. https://doi.org/10.1175/1520-0450(1965)004<0626:MHPPSG>2.0.CO;2.

Dickinson, W.T, and H.R Whiteley. A sampling Scheme for Shallow Snowpacks. *Bulletin of the International Association of Hydrological Sciences* **1972**, *17* (3), 246–258. https://doi.org/10.1080/02626667209493832.

Farnes, P. E.; Goodison B. E.; Peterson N. R. et al. *Final Report: Metrication of Manual Snow Sampling Equipment*; Western Snow Conference: Spokane, WA, 1983.

Fierz, C.; Armstrong, R. L.; Durand, Y. et al. *The International Classification for Seasonal Snow on the* Ground; IHP-VII Technical Documents in Hydrology No. 83, IACS Contribution No. 1; International Hydrological Programme of the United Nations Educational, Scientific and Cultural Organization (UNESCO-IHP): Paris, 2009. https://cryosphericsciences.org/publications/snow-classification/.

Fischer, A. P. The Measurement Factors in Estimating Snowfall Derived from Snow Cover Surfaces Using Acoustic Snow Depth Sensors. *Journal of Applied Meteorology and Climatology* **2011**, *50* (3), 681–699. https://doi.org/10.1175/2010JAMC2408.1.

Global Cryosphere Watch. *Cryosphere Glossary* web page. http://globalcryospherewatch.org/reference/glossary.php.

Goodison, B. E.; Ferguson, H. L.; McKay, G. A. Measurement and Data Analysis. In *Handbook of Snow*, Reprint; Gray, D. M.; Male, D. H., Eds.; 191–274; Blackburn Press: Caldwell, NJ, 1981.

Gottardi, F.; Obled, C.; Gailhard, J. et al. Statistical Reanalysis of Precipitation Fields Based on Ground Network Data and Weather Patterns: Application over French Mountains. *Journal of Hydrology* **2012**, *432–433*, 154–167. https://doi.org/10.1016/j.jhydrol.2012.02.014.

Griessinger, N.; Mohr, F.; Jonas, T. Measuring Snow Ablation Rates in Alpine Terrain with a Mobile Multioffset Ground-penetrating Radar System. *Hydrological Processes* **2018**, *32* (21), 3272–3282. https://doi.org/10.1002/hyp.13259.

Haberkorn, A., Ed. *European Snow Booklet: An inventory of Snow Measurements in Europe*; EnviDat: 2019. https://doi.org/10.16904/envidat.59.

Jacobson, M. D. Inferring Snow Water Equivalent for a Snow-Covered Ground Reflector Using GPS Multipath Signals. *Remote Sensing* **2010**, *2* (10), 2426–2441. https://doi.org/10.3390/rs2102426.

Johnson, J. B.; Marks, D. The Detection and Correction of Snow Water Equivalent Pressure Sensor Errors. *Hydrological Processes* **2004**, *18* (18), 3513–3525. https://doi.org/10.1002/hyp.5795.

Koch, F.; Prasch, M.; Schmid, L. et al. Measuring Snow Liquid Water Content with Low-Cost GPS Receivers. *Sensors* **2014**, *14* (11), 20975–20999. https://doi.org/10.3390/s141120975.

López-Moreno, J. I.; Fassnacht, S. R.; Beguería, S. et al. Variability of Snow Depth at the Plot Scale: Implications for Mean Depth Estimation and Sampling Strategies. *The Cryosphere* **2011**, *5* (3), 617–629. https://doi.org/10.5194/tc-5-617-2011.

Lundberg, A.; Granlund, N.; Gustafsson, D. Towards Automated 'Ground Truth' Snow Measurements – A Review of Operational and New Measurement Methods for Sweden, Norway, and Finland. *Hydrological Processes* **2010**, *24* (14), 1955–1970. https://doi.org/10.1002/hyp.7658.

National Snow and Ice Data Center (NSIDC). *Cryosphere Glossary* web page. https://nsidc.org/learn/cryosphere-glossary.

Neumann, N. N.; Derksen, C.; Smith, C.; Goodison, B. Characterizing Local Scale Snow Cover Using Point Measurements during the Winter Season. *Atmosphere-Ocean* **2006**, *44* (3), 257–269. https://doi.org/10.3137/ao.440304.

Palmer, P. L. Estimating Snow Course Water Equivalent from SNOTEL Pillow Telemetry: An Analysis of Accuracy. In *Proceedings of the 54th Western Snow Conference*, Phoenix, AZ, 15–17 April 1986; Western Snow Conference: 1986; 81–86.

Rovansek, R. J.; Kane, D. L.; Hinzman, L. D. Improving Estimates of Snowpack Water Equivalent Using Double Sampling. In *Proceedings of the 61st Western Snow Conference*, Quebec City, 9–11 June 1993; Western Snow Conference: 1993; 157–163.

Sigouin, M. J. P.; Si, B. C. Calibration of a Non-Invasive Cosmic-Ray Probe for Wide Area Snow Water Equivalent Measurement. *The Cryosphere* **2016**, *10* (3), 1181–1190. https://doi.org/10.5194/tc-10-1181-2016.

Smith, C. D.; Kontu, A.; Laffin, R.; Pomeroy, J. W. An Assessment of Two Automated Snow Water Equivalent Instruments during the WMO Solid Precipitation Intercomparison Experiment. *The Cryosphere* **2017**, *11* (1), 101–116. https://doi.org/10.5194/tc-11-101-2017.

Sturm, M.; Holmgren, J.; Liston, G. E. A Seasonal Snow Cover Classification System for Local to Global Applications. *Journal of Climate* **1995**, *8* (5), 1261–1283. https://doi.org/10.1175/1520-0442(1995)008<1261:ASSCCS>2.0.CO;2.

Sturm, M.; Holmgren, J. An Automatic Snow Depth Probe for Field Validation Campaigns. *Water Resources Research* **2018**, *54* (11), 9695–9701. https://doi.org/10.1029/2018WR023559.

World Meteorological Organization (WMO). *Guide to Hydrological Practices* (WMO-No. 168), Volume I. Geneva, 2008.

CHAPTER 3. MEASUREMENT OF GLACIERS

3.1 GENERAL

3.1.1 Summary

This chapter describes state-of-the-art methods used in measurements of glaciers and their changes in response to climatic forcing. Following up on previous guidelines that describe terminology and methodology in glaciological measurements and monitoring, it focuses on the classical measurements of glaciological mass balance, glacier front variations and glacier thickness. Many of the methods developed during the 20th century are still in active use (stake and pit methods for mass balance, distance measurements for glacier front variation). In recent decades, however, new technologies such as ground penetrating radar (GPR), global navigation satellite systems (GNSSs), airborne and spaceborne laser scanning, a range of new optical and radar satellite sensors, uncrewed aerial vehicles (UAVs) and automated ablation measurements have opened up new opportunities for researchers and professionals. Progress has also been made in observational technology, data analysis and processing. Various modelling approaches are also used to interpolate measurements and to further evaluate the data.

In the 21st century, a transformation is likely to occur towards more automated, real-time glaciological observations supported by satellite monitoring and modelling. Nevertheless, it is clear that field-based measurements will remain an important pillar of monitoring efforts as they allow seamless continuity of long-term data series. Furthermore, localized mass-balance measurements are unlikely to be fully replaced by automated and remotely applied methods. This chapter does not aim to provide a manual for all the newly emerging technologies nor to describe in detail the methodology behind new datasets and approaches. Rather, it focuses on the field techniques and mentions remote-sensing platforms and techniques needed by researchers for measuring glacier mass balance, front variation and ice thickness (such as deriving glacier outlines or digital terrain models). Not all glaciological variables are covered in this chapter (for example, ice velocity, ice temperature), nor are techniques to study glacial hydrology or ice avalanches. Ice core studies are not covered here, either.

Recommendations:

– **Data archiving and metadata:** Data collected in the field should be archived with proper metadata and submitted to data repositories such as Global Land Ice Measurements from Space (GLIMS) (for example, glacier outlines, snowlines, flowlines) and the World Glacier Monitoring Service (WGMS) (ice thickness, glacier front variation, glaciological and geodetic mass balance, special events). It is recommended that the researchers refer to published guidelines (such as GLIMS, 2022; WGMS, 2019) prior to data analysis so that relevant metadata are included to facilitate their usage.

– **Combination of different methods to reduce uncertainties:** Considerable potential lies in the combination of different observational methods to reduce uncertainties and to increase the consistency of the final results. This pertains for example to the frequent validation of in-situ mass-balance records with geodetic ice-volume changes or the homogenization of long-term length change records with aerial or satellite imagery.

– **Increase consistency and foster knowledge transfer:** Standardization of glacier monitoring products is crucial to increase the consistency and comparability of data sets at the global scale. Adherence to common protocols as well as regular exchange between national monitoring programmes are recommended to foster knowledge transfer.

3.1.2 Introduction

Glaciers form in regions of the world where winter or wet-season snowfall survives summer melt. Their changes in response to climate variations have been monitored on the ground for more than 100 years. Over recent decades, the coverage and detail of airborne and spaceborne observations have been steadily increasing, allowing glacier monitoring on a global scale. Existing observational time series from long-term field measurements combined with remote-sensing data provide the foundation for our understanding of glacier response to climate change.

Changes in glacier length, extent and volume occur in response to changes in air temperature and precipitation, on timescales ranging from years to millennia.

These changes have local, regional and global effects ranging from changes to water availability for agriculture to rising global sea levels. In addition, human lives and societal infrastructure are impacted by glacier-related hazards. Accordingly, modelling the mass balance and future evolution of glaciers from local to global scales is an active research area, making use of field and remote-sensing data for calibration and validation purposes. This calls for standardization of best practices in glacier measurements and data treatment.

The main focus of this chapter is on field methods to determine glacier mass balance.

Introductory sections cover glacier inventory data (outlines, areas, volumes) and measurements of glacier front variations. The text is partly based on previously published manuals and guidelines that describe the terminology and methodology used in glaciological measurements and monitoring, in particular:

– Østrem and Brugman (1991): A comprehensive manual for scientists conducting mass-balance measurements on glaciers, including also sections on meteorological and hydrological observations.

– Kaser et al. (2003): A manual on mass balance work, with focus on methods and safety during measurements on high-mountain glaciers.

– Cogley et al. (2011): The comprehensive *Glossary of Glacier Mass Balance and Related Terms*, including definitions of the variables used.

Since glaciers are fed by snowfall, repeated reference is made to methods used in measurements of snow on the ground (Fierz et al. 2009; and Chapter 2 of Volume II of the present Guide).

3.1.3 Definition

Glacier. A perennial mass of ice, and possibly firn and snow, originating on the land surface by the recrystallization of snow or other forms of solid precipitation and showing evidence of past or present flow (Cogley et al., 2011).

This definition is physically based and is at the base of that used in remote-sensing studies aiming to delineate the outlines of individual glaciers (see Section 3.3.2). It is stressed that neither of these definitions is intended to be used in any sort of legal context.

In daily language, the term *glacier* often refers not only to the various types of glaciers but also to ice caps (a dome-shaped ice body with radial flow) and to icefields (an ice mass on a plateau from which several valley glaciers emerge). This convention will be followed in this chapter, in accordance with recent recommendations (IPCC, 2021; Cogley et al., 2011).

In mass-balance studies, glaciers are delineated by outlines across which mass transfer of ice is zero. If mass transfer occurs (for example, at the grounding line of a calving glacier), the ice discharge must be included as a component of the mass balance. On ice caps, separate ice-flow basins can be delineated by determining the direction of the driving stress from surface elevation models. In practice, however, this is often implemented by deriving a flow direction grid from a digital elevation model (DEM) and calculating hydrological basins from watershed analysis.

3.1.4 Glaciers around the world

Glaciers are found in all regions of the world when climate conditions permit. Accordingly, their distribution on the Earth's surface is not uniform due to widely varying climatic and topographic conditions. Glaciers form where snow deposited during winter (or during periods of high accumulation) does not melt entirely during the summer season (or dry season). Air temperature is the main control on the existence of glaciers, which thus are mainly present in the polar and subpolar regions or at high elevations. Topographic conditions and precipitation (snowfall) levels must be sufficient for ice masses to form through transformation of snow to ice and for it to be sustained. When a critical thickness is attained, the accumulated mass starts to deform and flow under its own weight, transporting part of the mass to lower elevations where the ice melts. Past climatic conditions have caused a much larger extent of ice masses than at present. As an example, 25% of the Earth's land surface was covered with ice sheets and glaciers during the Last Glacial Maximum (LGM), whereas global ice cover is presently around 10% (Ruddiman, 2014).

Today, more than 200 000 glaciers are known to exist on Earth outside of the polar ice sheets, covering a total area of 705 000 km^2 (RGI Consortium, 2017) and an estimated volume of 158 000 km^3 (Farinotti et al., 2019). This excludes the two large ice sheets in Antarctica and Greenland but includes glaciers and ice caps in the periphery of the Greenland Ice Sheet.

3.1.5 Variables used in mass-balance observations

The *WIGOS Metadata Standard* (WMO-No. 1192)[1] prepared by WMO incorporates the key variables listed in Table 3.1, which are essential for the determination of long-term glacier mass balance from point measurements. Point measurements of accumulation and ablation allow calculation of point mass balance. Multiplication of interpolated point mass-balance values with the known areas of elevation bands covered by a glacier yields glacier-wide mass balance (glaciological method). Mass balance is typically reported in m or mm water equivalent (w.e.), and the definition of water equivalent of snow cover (SWE) is therefore included in the table. See detailed discussion of SWE determination in Chapter 2, 2.4 of Volume II of the present Guide.

The *geodetic method* for determination of glacier mass balance by repeated mapping of the glacier surface and related subtraction yields mass-balance volume change over a stated period of time. The volume change has to be converted to mass change using appropriate assumptions about the densities of ice and snow. See further description of this method in Section 3.9.2.

3.2 GLACIER INVENTORIES AND CLASSIFICATION SCHEMES

3.2.1 Glacier inventories

The first efforts to create a worldwide inventory of glaciers were initiated during the International Hydrological Decade, declared by the United Nations Educational, Scientific and Cultural Organization (UNESCO) for the period 1965–1974. This effort resulted in the World Glacier Inventory, which was published in 1989 by WGMS. WGMS continues the collection and publication of standardized information about ongoing glacier fluctuations, that is, changes in glacier length, volume, and mass since 1986. The United States of America (US) National Snow and Ice Data Center (NSIDC), founded in 1982, also has archived data on glaciers, for example, the World Glacier Inventory (WGI).[2] In 1995, the GLIMS initiative was launched,

1 WIGOS = WMO Integrated Global Observing System
2 https://nsidc.org/data/g01130

Table 3.1. Key measured/derived variables in mass-balance studies on glaciers. All variables except SWE are listed in the *WIGOS Metadata Standard*.

GLACIERS		
Variable	*Definition*	*WMDR notation (WMO Code Registry)*[a]
Surface accumulation at a point	The mass added to the glacier at a point on its surface expressed over a stated period of time.[b]	12011
Surface ablation at a point	The mass removed from the glacier at a point on its surface expressed over a stated period of time.[b]	12012
Glacier mass balance at a point	The sum of all processes adding and removing mass from the glacier at a point on its surface, expressed over a stated period of time.	12009
Glacier area	Area enclosed by the projection of the glacier outline onto the surface of an ellipsoid approximating the surface of the Earth or onto a planar horizontal approximation to that ellipsoid. The glacier area excludes nunataks but includes debris-covered parts of the glacier. The glacier outline separates the glacier from unglacierized terrain and from contiguous glaciers.	12013
Glacier-wide mass balance	The result of all processes adding and removing mass from the glacier at its surface, expressed over a stated period of time and integrated over the entire glacier (or basin) area.[c]	12010
Water equivalent of snow cover (SWE)	The vertical depth of water that would result if the snow cover melted completely, which equals the snow-cover mass per unit area. The SWE is the product of the snow depth in metres and the depth-averaged bulk snow density in kg m^{-3}. SWE can be expressed in mm w.e. or in kg m^{-2} (1 000 mm w.e. equals 1 000 kg m^{-2}).	631 See the present volume, Chapter 2, 2.1.1

Notes:
a WMO Codes Registry: wmdr/_ObservedVariableTerrestrial
b On a (typical) mid- to high-latitude glacier, accumulation will dominate in winter and ablation during summer. Both processes will, however, usually occur during both winter and summer. Thus, the winter balance will be the net result of mass added and lost throughout the winter and the summer balance likewise.
c Unless otherwise stated, glacier mass balance refers to surface mass balance and does not include basal or internal melting but includes refreezing in snow and firn.

under which regional investigators contribute glacier outlines[3] to a global database for open and free redistribution. A further initiative started in 2011, the so-called Randolph Glacier Inventory (RGI), which has compiled and updated a globally complete inventory of glacier coverage (Pfeffer et al., 2014; RGI Consortium, 2017). Between 2020 and 2023, an International Association of Cryospheric Sciences (IACS) Working Group aims to maintain and further develop the RGI. The Global Terrestrial Network for Glaciers (GTN-G), established in 2009 and operated jointly by WGMS, NSIDC and GLIMS, oversees the management and upgrading of glacier monitoring as part of a global observation strategy under the auspices of the United Nations and IACS.

3.2.2 Characterizing glaciers

Glaciers can be described by a list of parameters outlining their geographical and topographical characteristics, as summarized in Table 3.2. As is evident from the table, slightly different conventions are used by WGMS, GLIMS and NSIDC. The differences largely follow from the historical development and the different purposes of the inventories.

[3] https://www.glims.org/

Table 3.2. Parameters characterizing glaciers

Country or territory[a] Country or territory in which the glacier is located. If a country code is required, the 2-letter ISO 3166 code can be used: (https://www.iso.org/iso-3166-country-codes.html)
Identification – glacier number[a,b,c] WGMS Identifier: Attribute A3 is a 5-digit numeric code. The GLIMS ID is of the form: GnnnnnnEmmmmm[N|S] and gives latitude and longitude to 3 decimal places. See explanations in Section 3.3.2. RGI Identifier: A 14-character identifier of the form RGIvv-rr.nnnnn, where vv is the version number, rr is the first-order region number and nnnnn is an arbitrary identifying code that is unique within the region.
Glacier name[a,b,c] WGMS: Attribute A2 GLIMS: If an official name of the main glacier is available, it should be provided. RGI: Name of the glacier, or the WGI or WGI-XF ID code (modified after Müller et al., 1978) if available. The names of individual tributaries or outlet glaciers should also be listed, when appropriate. Abbreviations are allowed for very long names. The spelling of the name should be in the Latin alphabet. In some cases, glaciers may be unnamed and will only carry a catalog number but may later be named, or a name that has been in use by local inhabitants is discovered. In such cases this field should allow for an alternative name to be included.
Location – geographical entity, mountain range or group[a] WGMS: Attributes A8 and A9 Refers to a known geographical entity, typically a mountain range, which gives a rough idea of the location of the glacier. Examples: Western Alps, southern Norway, Andean Range, Tien Shan, Himalayas, Alaska. Examples of more specific locations: Rhone basin, Jotunheimen, Brooks Range.
Coordinates[a,b,c] **– centrally located point near the equilibrium line** The coordinates should describe the location of a central point within the glacier outline as accurately as possible. A suitable point is in the central parts of the main stream of ice. The latitude and longitude of this point should be given in decimal degrees, with a minimum precision of 4 decimal places. The coordinate point can be created automatically from the glacier outline in geographical information system (GIS) software. The location will change when the perimeter changes.
Date[a,b,c] WGMS: Attributes B11, C8, C10, D14, D16, E6, E7, E8, F4 The WGMS attributes refer to dates of surveying, front variation measurements, mass-balance measurements, reference dates and dates of special events. When glacier outlines are submitted to GLIMS or RGI, the date of acquisition (day, month and year) should be included with the submission. Special care is required when multitemporal data are used in the same region.
Surface area[a,b,c] WGMS: Attributes D7, E15, E17 (and additional attributes on area change accuracy) The *surface area* of a glacier is a key parameter, used in mass-balance modelling and other studies, including assessments of global glacier changes. The area can be calculated directly in GIS software. It is important that glacier area be measured in an appropriate metric projection. The value should be recorded in square kilometers with at least two but preferably three digits after the decimal point.
Length[a,b,c] WGMS: Attributes B9, B10 The *maximum length* of a glacier is defined as the length of the longest flowline of the whole glacier. The *mean length* is the average of the lengths of each tributary along its longest flowline to the glacier snout. It is recommended that initially only the maximum length be determined as this reduces the workload considerably. The mean length could be added in a later step. For ice caps, the above method for determining maximum length applies to each outlet glacier and ice-flow basin. The longest and shortest width of the ice cap may be more relevant information in some cases and these parameters are readily determined from maps or in GIS.
Elevation (max, min, mean, median)[a,b,c] WGMS: Attributes B6, B7, B8 It is recommended that these parameters are determined from a digital terrain model (DTM) of the glacier or ice-flow basin (using the GLIMS ID or WGMS number as an identifier). The *mean elevation* is equal to the sum of all elevation values of individual DTM cells divided by the number of cells within the glacier boundaries. The *median elevation* is the elevation which divides the glacier surface area such that 50% of the area is above and 50% is below this elevation. WGMS Attribute EEE8 is the elevation of a mass-balance measurement point.

Country or territory[a] Country or territory in which the glacier is located. If a country code is required, the 2-letter ISO 3166 code can be used: (https://www.iso.org/iso-3166-country-codes.html)
Hypsography[b,c] The area-elevation distribution of a glacier or ice cap can be calculated from a glacier DTM. It is recommended to compute the total area in each 100 m interval (or a narrower elevation band for smaller glaciers).
Orientation[a,b,c] WGMS: Attributes A13, A14 The *orientation* (aspect) of the down-glacier direction can be calculated from DTMs as the mean orientation of all DTM cells that are covered by the glacier. The orientation can be calculated separately for the accumulation and ablation regions.
Mean slope[b,c] The *mean slope* is a good proxy for other parameters, like mean thickness. It can be calculated as the mean slope of all DTM cells covering the glacier.

Notes:

a WGMS parameters. These parameters (attributes), as used for WGI, are outlined in the WGMS Attribute Description (2019), available at www.wgms.ch.

b GLIMS parameters. The basic GLIMS parameters are given in Paul et al. (2009, 2010), who provide a detailed description of the basic glacier parameters as defined by the GLIMS consortium and scripts for parameter calculation.

c RGI parameters. RGI data fields are described by the RGI Consortium (2017).

3.2.3 Glacier classification

A morphological glacier classification scheme was introduced in 1970 by a Working Group of the International Commission on Snow and Ice/International Association of Scientific Hydrology (ICSI/IASH), the forerunner of IACS (Müller et al., 1970), and subsequently adopted and updated by WGMS. The GLIMS glacier classification system builds on these earlier schemes and takes into account specific glacier features encountered in different parts of the world, including the polar regions (Rau et al., 2005). It uses nine digits to characterize the glacier type, form, frontal characteristics, longitudinal profile, source region tongue activity and moraine characteristics. This classification scheme is not widely used anymore and is thus not reproduced here, but Figures 3.1(a)–(h) display examples of different glacier types, classified according to the above-mentioned schemes and located in various mountain/highland regions.

3.2.4 Selecting glaciers for measurement

The following points should be considered when selecting glaciers to be included in a network for long-term mass balance or length change monitoring and to conduct related glaciological fieldwork. The description is partly based on Kaser et al. (2003).

Area. A glacier or ice cap selected for a mass-balance programme will ideally yield results that are representative for the regional mass balance. In inventory studies glaciers are often defined by a lower size limit of 0.01 km^2 (see, for example, Paul et al., 2020), but many glaciers of such small size might experience drastic changes in surface area and volume in response to local climate effects. For mountain glaciers the ideal area for mass-balance studies is 1–10 km^2, allowing traversing on foot or by skis. Ice caps and ice fields range in size between 10 and 50 000 km^2 and a ground-based mass-balance programme on most ice masses in that size range will have to rely on helicopters, snowmobiles or other motorized vehicles.

Altitude range. The altitude span should be representative for the glacierized region and should allow the detection of variability in the equilibrium line altitude (ELA).

Catchment area. For ice caps, a precise survey of surface topography (and bedrock topography, if available) should be used to delineate the ice-flow basins that should be monitored. The selection of mountain glaciers confined within separate cirques or valleys should aim to limit the complexity of accounting for other sources of snow accumulation than precipitation (such as avalanches from surrounding steep rock walls).

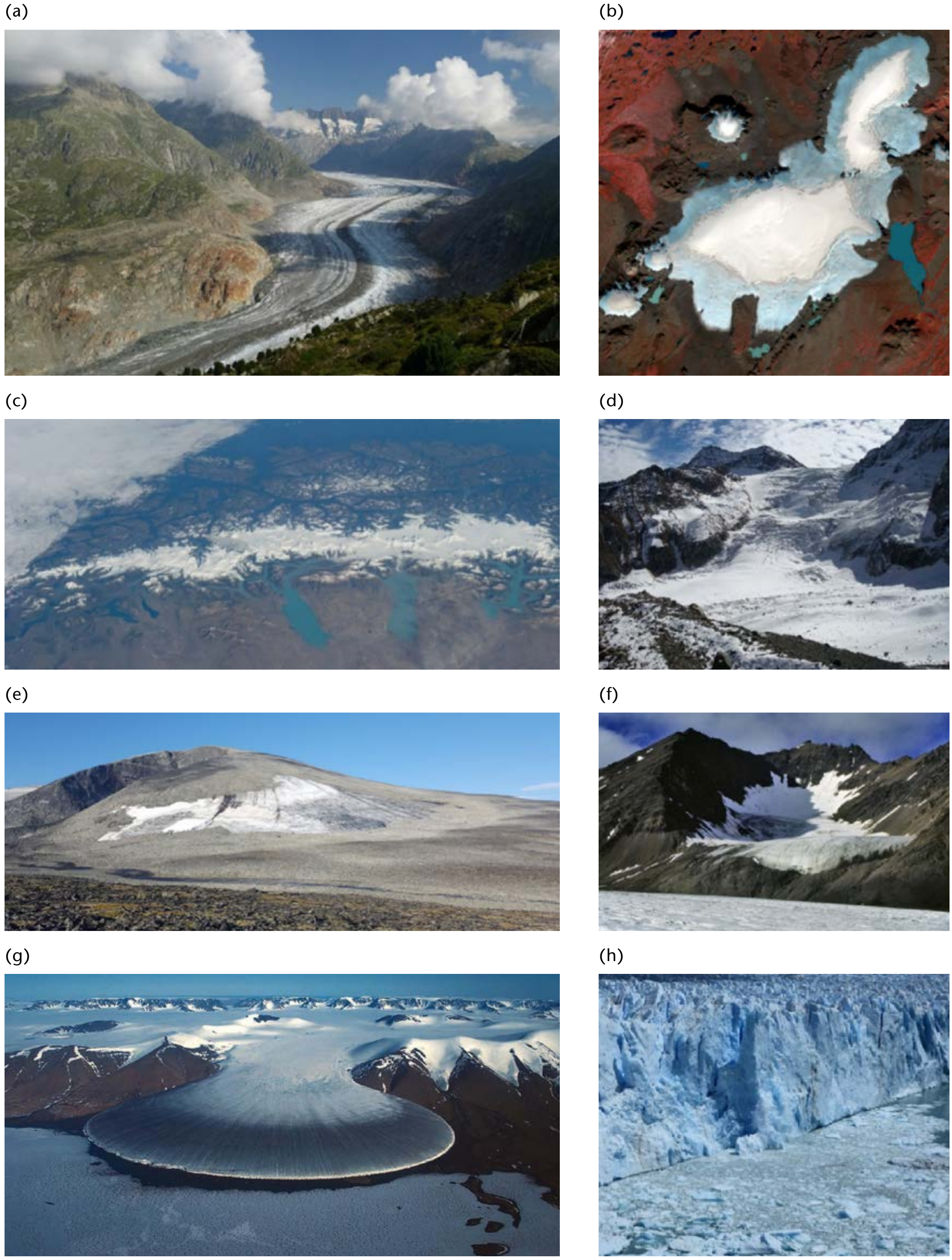

Figure 3.1. Different glacier types: (a) valley glacier (Grosser Aletschgletscher, Switzerland); (b) ice cap (Langjökull, Iceland); (c) icefield (South Patagonian Ice Field); (d) mountain glacier (Kolahoi Glacier, India); (e) ice patch (Juvfonne, Jotunheimen, Norway); (f) cirque glacier (unnamed glacier, Svalbard); (g) piedmont glacier (Elephant Foot Glacier, north-eastern Greenland); (h) calving glacier (Perito Moreno Glacier, Argentina).

Source: (a) Matthias Huss; (b) SENTINEL-2, European Space Agency (ESA); (c) National Aeronautics and Space Administration (NASA) (www.antarcticglaciers.org); (d) Thorsteinn Thorsteinsson; (f) © Glaciers online, M. Hambrey; (g) www.wikimapia.org

Geometry. Fieldwork and analysis will be simpler if the accumulation area and the ablation area are well defined and not complex in shape.

Frontal ablation. If calving into lakes or the ocean or break-off by ice avalanches at the snout play a significant role in the glacier's mass budget, this component needs to be accounted for in the mass-balance assessment.

Glacier surges. Surging glaciers are not ideal for long-term mass-balance studies because of extensive mass distribution occurring during surges, which in most cases changes the relative amounts of ice in the accumulation and ablation areas. This complicates mass-balance calculations.

Debris cover. Fieldwork on debris-covered glaciers can be challenging, since debris cover complicates the installation and maintenance of stake networks and the interpretation of glacier–climate interactions. In mountain ranges where debris-covered glaciers are common, they should be included in mass-balance programmes so that a representative sample of glaciers is being monitored.

Surface. Glaciers with smooth surfaces are easiest and safest for travel and mass-balance measurements. Crevassed areas should be avoided to the extent possible. Fixed routes of travel on the glacier can be established using a Global Positioning System (GPS) device to avoid travelling in crevassed areas. This reduces the risk of accidents when traversing the snow-covered glacier.

Accessibility. Access should be as easy as possible to facilitate regular fieldwork, minimize risks and allow a quick retreat in case of emergencies.

Safety issues. Personnel conducting measurements on glaciers need to have proper training in glacier travel and rescue operations. This should involve the use of ropes, harnesses, ice screws and ice axes as well as general mountaineering experience (Figure 3.2). Training should be offered on a regular basis and self-training should be encouraged. Access to documentation

Figure 3.2. Safe travel on glaciers. The risks of traveling on glaciers can be minimized by proper training in the use of safety equipment and by maintaining knowledge of local conditions. Roping up is essential when a freshly fallen layer of snow covers crevasses and possibly moulins.

Source: Solveig H. Winsvold

describing equipment, methods and skills needed for glaciological fieldwork is essential (see example in the appendix). In addition, documentation should be available on access routes to each glacier in the measurement programme and dangers present there (crevasses, avalanches).

Data availability. When selecting glaciers for long-term monitoring, sites with available data from previous measurements (glaciological and meteorological variables, remotely-sensed data) should be favoured.

3.3 OUTLINES AND AREAS OF GLACIERS

3.3.1 Introduction

Trigonometric surveying of glacier outlines and mapping of their surface elevation was initiated in the nineteenth century (Bauder et al., 2007). Photogrammetric methods improved the accuracy of surface elevation contours, and many glacierized regions of the world were mapped by aerial photography during the first half of the twentieth century (Hattersley-Smith, 1966). Barometric surveys and GPS measurements have been used extensively to determine surface profiles on glaciers and ice caps (Björnsson, 1988; Björnsson and Pálsson, 2020). Data from airborne and spaceborne radar systems (synthetic aperture radar (SAR) and interferometric SAR (InSAR) techniques) are now routinely used to create DTMs, often referred to as digital elevation models (DEMs) of glacier surface topography. Multispectral sensors (such as those on the Pléiades, ASTER and SPOT satellites) allow mapping of glacier surfaces with an accuracy of 0.5–2 m in the vertical (see, for example, Berthier et al., 2014) and airborne light detection and ranging (lidar) technology is now commonly used to map glacier surface elevations with a vertical accuracy better than 1 m on grids with a horizontal resolution of 5 × 5 m or better (Geist et al., 2005; Jóhannesson et al., 2013). The US Government's Arctic DEM project has recently produced a high-resolution (2 × 2 m) DEM of the entire Arctic region (north of 60°N), including its glaciers, ice caps and the Greenland ice sheet, using optical images from the WorldView satellites.[4] Plans have been developed to create repeat DEMs by that same project, which also covers the rest of the world's glaciers and Antarctica.

3.3.2 Generating glacier outlines

To calculate the mass balance of a glacier, its area and hence its outlines must be known. Glacier area is defined as the spatial distribution of perennial ice at a certain point in time, typically measured in km^2 (see Table 3.3). For smaller glaciers and ice caps it is common practice to manually digitize the glacier outlines from georeferenced aerial photographs or satellite imagery (orthophotos) or using lidar intensity values (see, for example, Paul et al., 2002; Fischer et al., 2014; Andreassen et al., 2020; Linsbauer et al., 2021; see Figure 3.3).

For larger glaciers or regions it is recommended to use automatic or semi-automatic methods from optical sensors (Paul et al., 2009; Racoviteanu et al., 2009). The following description is mainly based on Raup and Khalsa (2010).

Definition. In remote-sensing studies aiming to delineate the outlines of individual glaciers, the following definition of a glacier has been used:

> A glacier or perennial snow mass consists of a body of ice and snow that is observed at the end of the melt season, or, in the case of tropical glaciers, after transient snow melts. This includes, at a minimum, all tributaries and connected feeders that contribute ice to the main glacier, plus all debris-covered parts of it. Excluded is all exposed ground, including nunataks. An ice shelf shall be considered as a separate ice mass.

---

4 https://www.pgc.umn.edu/data/arcticdem/

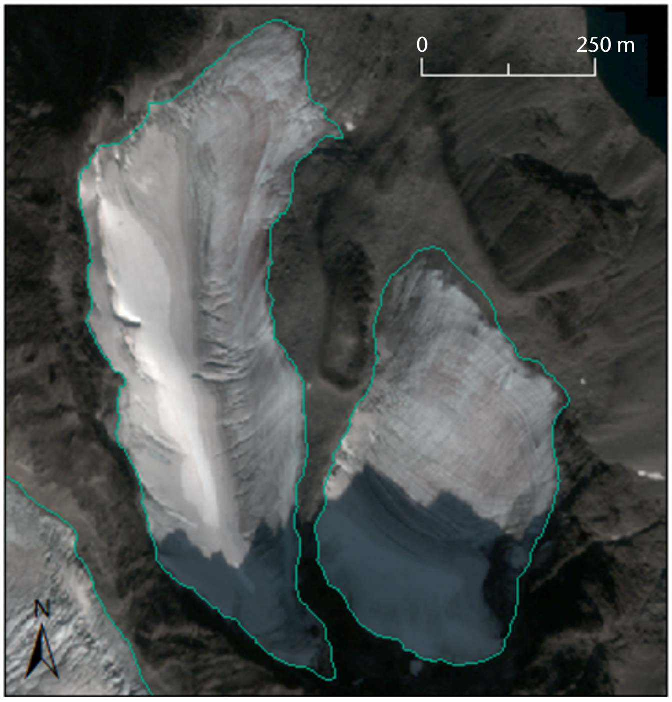

Figure 3.3. Glacier outlines can be digitized manually from orthophotos or be derived semi-automatically from satellite data. Here, outlines of two small glaciers in Jotunheimen, southern Norway, are digitized manually from a Pléiades image having 2 m resolution.

Source: © National Centre for Space Studies (France) 2019, Distribution Airbus DS. Figure modified from Andreassen et al. (2022), Journal of Glaciology

Table 3.3. IDs for a hypothetical glacier in the European Alps, as given in four glacier inventories

Glacier name	*WGMS ID*	*WGI ID*[a]	*GLIMS ID*	*RGI ID*
Alphanumeric; up to 60 characters	Numeric code	Alphanumeric; 12 characters	Alphanumeric; 14 characters	Alphanumeric; 14 characters
GLACIER	2222	CH4012506003	G007880E45990N	RGI40-11.02789

Note:
a https://nsidc.org/data/g01130

It is stressed that neither this definition nor the one in Section 3.1.3 are intended to be used in any sort of legal context.

Glacier ID. Each glacier in the WGMS, WGI, GLIMS and RGI databases is assigned an identification number (Table 3.3). Glaciers can also have national IDs or other forms of local IDs.

WGMS ID: A numeric identifier.

WGI ID: A 12-character unique glacier identifier combining a 2-character political unit, 1-digit continent code, 4-character drainage code, 2-digit free position code and 3-digit local glacier code.

GLIMS ID: A 14-character identifier of the form: *GnnnnnnEmmmmm[N|S]*. Here, [N|S] means either North or South and nnnnnn is the decimal longitude to three decimal places in the range [000000,359999]. The number mmmmm, the decimal latitude to three decimal places, has the range [00000,90000]. It is recommended to select a location in the upper part of the ablation area of the glacier.

RGI ID: A 14-character identifier of the form RGI*vv*-*rr.nnnnn*, where *vv* is the version number, *rr* is the first-order region number and *nnnnn* is an arbitrary identifying code that is unique within the region. In general, the identifying code of each glacier, *nnnnn*, should not be expected to be the same in different RGI versions.

Note – if registered with WMO, a glacier would receive a dedicated WIGOS Station Identifier (WSI).

Tools and imagery. GIS tools and software are used to manually or semi-automatically/automatically delineate glacier outlines from maps, orthorectified aerial images, DTMs or satellite imagery. Satellite platforms providing freely available raw data for glacier mapping include Landsat (since 1972), ASTER (since 1999) and Sentinel-2 (since 2015). Automated methods for deriving glacier outlines have been developed by many researchers (for example, Paul et al., 2002) along with methods to derive the uncertainty.

Criteria for glacier outlines. Using the remote sensing definition given above, certain criteria are applied to determine which features should be included as part of a certain glacier.

The outline of a glacier should include:

- Ice bodies above the bergschrund (at the glacier head)
- Tributary glaciers flowing into the glacier
- Stagnant ice masses in contact with the glacier
- Debris-covered parts connected with the glacier

The outline should not include steep rock walls from which avalanches contribute snow accumulation to the glacier, nor areas covered by seasonal snow. An ice body detached from the glacier may contribute mass to the glacier through ice avalanches and it should be left to the analyst to decide whether it should be considered part of the glacier or not (Raup and Khalsa, 2010).

An ice cap or an ice field may contain several different ice-flow basins that form a continuous ice mass but do not exchange any ice between them. Such an ice mass can either be considered a single unit, or several units when the divides separating different basins can be determined.

A persistent problem in the mapping of many glacier outlines is the presence of seasonal snow along glacier margins, due to accumulation or deposits of blown snow (snowdrifts) or avalanche snow and incomplete snow depletion at the time of image acquisition. Images from the end of the ablation period (or dry period) should therefore be used for the mapping of glaciers with such lateral snowfields, and they should be disconnected from the main glacier (but identified) if they cannot be avoided.

GLIMS distinguishes between *ice shelves* – ice downstream of the grounding zone of two or more glaciers that is floating on ocean water – and *ice tongues* – floating ice extending from a single glacier. Ice shelves are considered as separate features whereas ice tongues are included with the glacier to which they are attached.

Polygons, segments and category attributes (see Raup and Khalsa, 2010). The glacier outline is in the form of a *polygon* that circumscribes the entire glacier. Features internal to the glaciers like nunataks are excluded using polygon "holes" or by producing outlines around them and labeling them separately. Snow lines,[5] flowlines and glacial lakes can also be included.

Within GLIMS, the same GLIMS glacier ID is assigned to all polygons and segments associated with a particular glacier, that is, glacier outlines, centrelines and internal rock outlines.

---

[5] The snow line on a glacier is defined as the line separating snow from ice or firn at any time *t* (Cogley et al., 2011).

Minimum size of a glacier. Satellite sensors and orthophotos available today allow very small ice bodies to be mapped (Fischer et al., 2014). The minimum size that can be studied will vary depending on the sensor being used (image resolution), the quality of the imagery (snow depletion) and the purpose of the study. Paul et al. (2016) recommend a size of 0.01 km^2 as the minimum area for a glacier when using satellite sensors operating at 15–30 m spatial resolution. Leigh et al. (2019) point out that the minimum threshold can be lower when high-resolution imagery (<1 m) is used for mapping. However, ice masses smaller than 0.01 km^2 might not be (flowing) glaciers but ice patches (see Figure. 3.1.(e)) and could be marked accordingly in the attribute table.

Uncertainty. The GLIMS glacier database allows the assignment of two uncertainty values for each outline of a glacier, the (i) global and the (ii) local uncertainty (Paul et al., 2009). Whereas (i) can be obtained from the metadata of the (satellite) image used, (ii) depends on glacier and image characteristics.

The uncertainty of outline delineation is higher for glaciers with debris cover or in shadow and for ice divides in flat accumulation areas. As a first step, it is recommended that a fixed accuracy value be applied (for example, the size of one or two image pixels) to all glaciers, to be improved on later whenever possible (Paul et al., 2009).

In one study comparing glacier areas generated manually by different analysts, relative area differences amounting to 3%–6% were found (Paul et al., 2013). When comparing the results of manual and automated generation of glacier outlines, several authors (for example, Paul et al., 2013; Andreassen et al., 2022) have found good agreement between the two methods (differences typically in the range of 1%–5%). Automatic analysis is better at detecting the smallest glaciers and at considering all rock outcrops, which manual analysts tend to leave out or overlook. On the other hand, manual corrections of automatic classifications may be needed to correctly delineate glaciers under debris cover or in shadow, and remove wrongly classified water bodies, snow fields, sea ice or ice on water.

Image selection. When possible, analysis of imagery from different years is recommended to separate seasonal snow from perennial snow or glaciers and to select the best possible images. In cases when glaciers are invisible due to local clouds, shadows or missing data (for example, striping of Landsat 7 images acquired after May 2000), it is also possible to add the missing parts from other images, maybe acquired under worse conditions.

3.4 THICKNESS AND VOLUME OF GLACIERS

3.4.1 Radio-echo sounding to determine glacier thickness

Mass-balance data essentially reflect changes in the volume of glaciers and ice caps and thus a one-time determination of the total volume of a glacier being studied is desirable. Accurate determination of glacier volumes requires measurement of their surface areas and surveying of their thicknesses by radio-echo sounding, using equipment towed by vehicles (Björnsson and Pálsson, 2020), portable systems (for example, Mingo and Flowers, 2010) or airborne instruments (Lindbäck et al., 2018). Radar systems can also be used to trace internal reflectors within glaciers, investigate the nature of the ice–bed interface and detect subglacial and englacial water bodies (Plewes and Hubbard, 2001; Magnússon et al., 2021a).

The technique of radio-echo sounding in ice relies on the transmission and detection of electromagnetic waves at frequencies between 1 and 1 000 MHz. Frequencies in the range 2–10 MHz are suitable for sounding in temperate ice, whereas higher frequencies are applied on cold (polar) ice. Propagation of the radar signal is controlled by the relative electrical permittivity (ε_r) and the electrical conductivity (σ) of the ice (Plewes and Hubbard, 2001). Both parameters are affected by the presence of water and impurities. Permittivity can further be affected by anisotropy in the ice and by ice temperature changes.

The set-up of a typical radio-echo sounding experiment for use on temperate ice is shown in Figure 3.4. A snowmobile or some other vehicle tows two sledges, which are connected with a rope. The transmitter is placed on one sledge, the receiver on the other, and both are fitted with antennas. The simplest type of antenna, the dipole, is indicated in Figure 3.5. An oscillating electric current in the dipole generates the transmitted electromagnetic wave which is reflected by the bedrock (or by internal features in the ice). The receiver detects both the reflected wave and the direct wave transmitted along the surface.

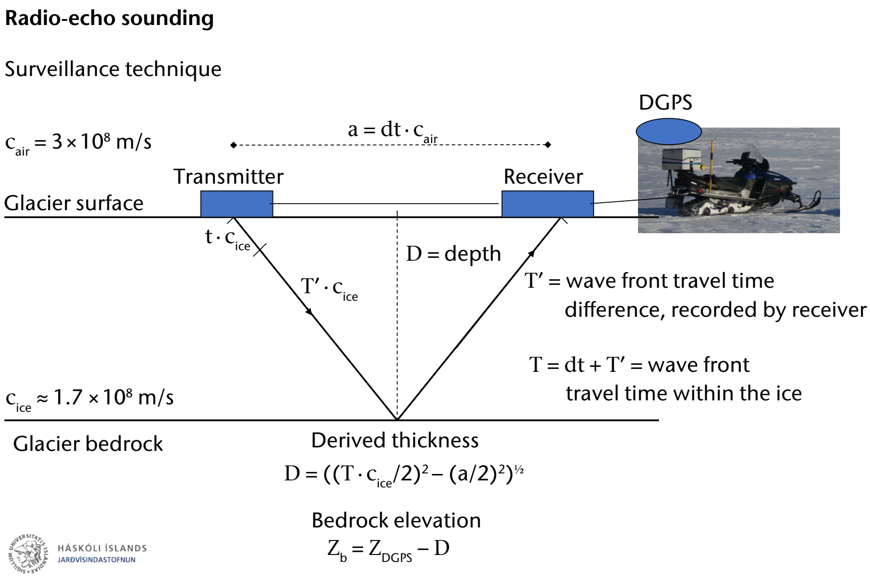

Figure 3.4. A radio-echo sounding system consists of two main components: (1) the transmitter, and (2) the receiver. The transmitter sends out a brief burst of radio waves of a specific frequency. The receiver detects the radio waves from the transmitter and any waves that have bounced, or been reflected off, nearby surfaces. The receiver records the amount of time between the arrival of the transmitted wave and any reflected waves as well as the strength of the waves (measured as an AC voltage).

Source: Figure adapted from: Eyjólfur Magnússon, University of Iceland

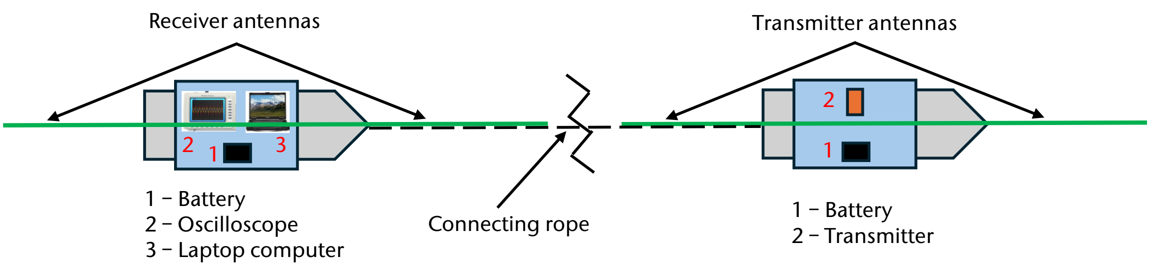

Figure 3.5. Field set-up of a radio-echo sounding system. The transmitter with antennas is placed on the front sledge. The receiver and data logging computer are placed on the rear sledge. The sledges are connected with a rope and their distance is kept constant during measurement. Typical antenna length is 10 m for systems used on temperate glaciers. On glaciers that cannot be accessed by motorized vehicles, the sledges can be hand pulled. It is also possible to tow the two sledges side by side, keeping a certain minimum distance that depends on the system configuration.

For the simplest case of a point measurement with stationary receiver and transmitter, both placed at practically the same point on the glacier surface, and assuming further that a reflection from the bed originates from directly below the antennae:

$$D = 0.5 \cdot \nu_{ice} \cdot t \tag{3.1}$$

where D is the ice thickness, ν_{ice} is the velocity of the electromagnetic wave in ice and t is the two-way travel time between the surface and the bed.

For the more general case, the wave travels between the transmitter and the receiver as indicated in Figure 3.4. In this case the vertical depth is determined as follows:

$$D = \left[\left(\nu_{ice} \cdot t/2 \right)^2 - \left(\alpha/2 \right)^2 \right]^{1/2} \tag{3.2}$$

where t is the travel time between the transmitter and receiver for the wave reflected from the bottom and α is the distance along the surface between the transmitter and the receiver. See further explanations in Figure 3.4.

A differential GNSS – often referred to as Global Positioning System (GPS) – receiver recording the position of the sounding profiles is placed on the receiver sledge and/or on the snowmobile, allowing exact determination of the location of the midpoint between the transmitter and receiver at any time.

Field operations. If the intention is to produce a high-resolution map of the bedrock topography beneath a glacier or ice cap, a sufficiently dense grid of profiles must be laid out. A horizontal spacing of 1 km between profiles is common, but denser networks are desirable for glaciers smaller than ~100 km^2. During sounding, traces should be recorded less than one-quarter wavelength apart to maximize resolution. A *trace* is a recording of the response to a single pulse of electromagnetic energy passing from the transmitter to the bedrock and back to the receiver. As an example, a 5 MHz radio-echo sounding system produces a wavelength of $\lambda = c/\nu = 1.69 \cdot 10^8$ m s^{-1}/5 $\cdot$ 10^6 s^{-1} = 34 m, and thus traces should be recorded less than 8.5 m apart in that case. For accurate determination of the glacier thickness, the topography of the glacier surface must be known. This is achieved by differential GNSS profiling concurrent with the echo sounding. Since electromagnetic wave velocities vary between different glaciers due to varying thermal regimes, water content, debris and impurity concentrations and anisotropy, it is recommended to calibrate the thickness determined by the radio-echo sounding against other data (preferably direct borehole measurements), thereby determining the electromagnetic wave velocity for the glacier being investigated. A correction because of higher electromagnetic wave velocity in snow and firn overlying glacier ice should be applied when radio-echo sounding is carried out in the accumulation areas of glaciers and ice caps. Table 3.4 summarizes key data related to radio-echo sounding on glaciers.

Table 3.4. Technical specifications for radio-echo sounding systems on polar and temperate glaciers and ice caps

Technical specification	*Cold ice*	*Temperate ice*
Electromagnetic wave velocity in ice	1.53–1.72 × 10^8 m/s	1.69 × 10^8 m/s
Frequency range	30–800 MHz	2–10 MHz
Wavelength range	0.2–5.7 m	17–85 m
Dipole antenna length	0.2–1.6 m	5–20 m
Peak power	500–3 000 W	1 250–8 000 W
Bandwidth	1–40 MHz	0.1–10 MHz
Maximum ice thickness	4 800 m	1 500 m
Vertical resolution	2.5–60 m	<10 m
Surface positioning accuracy	< 1 m	< 1 m

Source: Plewes and Hubbard (2001), Table 3; Björnsson and Pálsson (2020)

Data processing. The graphic depiction of radio-echo sounding data involves plotting the travel time (y-axis) for each trace against location on the sounding profile (x-axis).

The following data reduction steps were adapted from recommendations published by https://www.stolaf.edu/other/cegsic/background/:

(i) Organizing and cleaning of field data. This involves orienting profiles in the same direction and assigning surface coordinates to each trace.

(ii) Performing static and elevation corrections.

(iii) Band-pass filtering of data to eliminate low- and high-frequency noise.

(iv) Along-track migration (in two dimensions). The receiver can record echoes that do not originate directly below the radio-echo sounding system, thus data must be adjusted to better determine the positions of the reflectors.

(v) Interpreting and plotting the bed surface.

3.4.2 Determination of bedrock topography and glacier volume

The first two-dimensional (2D) migration is applied across the dominant topography. On a valley glacier, the dominant topography is normally the valley itself, so profiles should be recorded in the cross-glacier direction (Welch et al., 1998). On an ice cap with complex bedrock topography, previous knowledge or inferences regarding subglacial landscapes should guide the direction in which profiles are laid out (Magnússon et al., 2021b). 2D migration assumes that (1) all reflecting surfaces are located along the profiles (that is, no reflections are recorded from surfaces to either side of the profile) and (2) all apparent reflector slopes used in migration are in the direction of the profile (Welch et al., 1998). These assumptions are rarely met, and thus a three-dimensional (3D) survey is necessary to resolve complex bedrock topography. This is achieved by recording closely-spaced radio-echo sounding profiles and using fully-3D migration routines to accommodate reflections from any location. Two-pass 2D migration can also be used (Claerbout, 1985; Yilmaz, 1987). A profile spacing of 20 m was used in targeted surveys on Worthington Glacier, Alaska (Welch et al., 1998), and on Mýrdalsjökull ice cap, Iceland (Magnússon et al., 2021b).

To convert two-way travel times of reflections to depths, the appropriate EM-wave velocity in ice (Table 3.4) is used. The bedrock reflectors are then digitized to create a map of the glacier bed. Reflectors can be exported as a list of coordinates (x,y,z) in the appropriate geographic coordinate system. Cross-point statistics should be evaluated and data should be reviewed if any elevation mismatch in excess of 5 m is obtained.

The final product is a bedrock DEM obtained with Kriging interpolation of the radio-echo sounding data. Manual control of the resulting DEM is often necessary, to fill data gaps and to reduce artefacts due to shortcomings of 2D migrated radio-echo sounding data or due to Kriging interpolation. The resolution of the final bed-surface DEM depends on the profile spacing.

A map displaying glacier thickness can then be calculated by differencing the DEMs of the glacier surface and the glacier bed. Results should be compared with depths measured in boreholes reaching the bed, if drilling has taken place on the glacier. The total volume of the glacier or ice cap at the time of surveying is then obtained by summation over the entire DEM area.

3.4.3 Measurement error and uncertainties

The error in glacier-thickness measurements using pulsed radar systems stems from (i) the error in the thickness measured at a given point, and (ii) the error in thickness determination associated with the uncertainty in horizontal positioning (Lapazaran et al., 2016).

The error resulting from the first source (the measurement of thickness at a point), depends on the error in the radio-wave velocity, and the error involved in determining the bed reflection and hence the two-way travel time. The radio-wave velocity is higher in snow and firn than in ice, and thus the depth-averaged radio-wave velocity varies between the accumulation and ablation areas, due to variation in snow/firn thickness, density, water content and air content. It is, however, common practice to use a constant value for the velocity (Table 3.4), and the error is typically taken to be 1%–5% (Lapazaran et al., 2016). Errors in the determination of the two-way travel time can stem from difficulties in selecting the correct bed reflector from several possible ones, or from misinterpretation of an internal layer (such as ash layers) in the ice as bedrock. In addition, scattering from subglacial or englacial water bodies or water inclusions can prevent proper reflection from the bed, introducing error in the thickness determination. Moreover, in radio-echo sounding on valley glaciers, reflections from valley sides (out-of-plane reflections) can present problems for travel-time determination. Comparison of depths determined at crossing points of two or more sounding profiles helps to check consistency of the data and detect errors.

The uncertainty of horizontal positioning determination is on the order of a few centimetres if the positioning is obtained by differential GPS, and thus the error resulting from this source (positioning uncertainty) can be assumed to be negligible. However, this only applies if the distance between the midpoint between transmitter and receiver and the differential GPS on the towing vehicle can be kept fixed. For the configuration shown in Figure 3.4 (see Magnússon et al., 2021b), a horizontal accuracy in the midpoint position of <3 m is estimated.

The error in glacier volume determination from radio-echo sounding stems from the errors mentioned above and from the uncertainty in determining the glacier boundary and hence the glacier area (Martín-Español et al., 2016). Boundary errors can be due to debris cover or snow patches, and due to uncertainty in determining the exact positions of ice divides and calving fronts. Most importantly, however, the uncertainty in ice volume determination from ice thickness measurements depends on the coverage of profiles, and therefore the spatial extrapolation of ice-thickness over the entire ice body. As glacier ice thickness is often inhomogenous and only a certain number of direct measurements can be performed due to accessibility and other logistical limitations, extrapolation can lead to significant uncertainties in total estimated ice volume (see, for example, Andreassen et al., 2015; Grab et al., 2021).

3.4.4 **Global-scale compilation of ice-thickness measurements**

In 2014, the international Glacier Thickness Database (GlaThiDa) was launched by WGMS, with the support of IACS, as an effort towards assessing the total volume of the world's glaciers (Gärtner-Roer et al., 2014). In the first version, the focus was on gathering glacier mean and maximum thickness estimates from published literature. Versions 2 and 3 contain additional data on thickness measurements from glaciers on all continents, submitted in response to calls for data (Welty et al., 2020). The data submitted are derived from boreholes, seismic soundings, radar measurements and other geophysical studies. Archived versions of GlaThiDa are available from WGMS (https://gitlab.com/wgms/glathida). It is recommended that scientists prepare their final ice-thickness point data using the same attribute fields as in GlaThiDa to simplify data submissions for later versions of GlaThiDa.

Ice-thickness data are valuable for calibrating and validating ice-thickness models (see, for example, Ramsankaran et al., 2018; Helfricht et al., 2019; Zorzut et al., 2020). Such models based on local thickness observations have become indispensable today to provide homogenous data sets for large-scale studies to investigate glacier dynamics and water resources (e.g. Lutz et al., 2014; Hock et al., 2019). The IACS working group on ice thickness estimation (2014–2019) performed intercomparison experiments on ice-thickness modelling validated with ice-thickness data (Farinotti et al., 2017) and provided an estimate for the ice thickness distribution of all glaciers in the world (Farinotti et al., 2019).

3.5 MEASUREMENTS OF GLACIER FRONT VARIATIONS AND LENGTH

3.5.1 Background

Measurements of changes in glacier front position have a long tradition in glacier monitoring, with many records starting at the end of the 19th century or early in the 20th century (Forel, 1895; Rekstad, 1902; Eythórsson, 1949). These front variations should preferably be measured in a direction that represents a central flowline along the glacier. This will reflect changes in the length of the glacier along a given flowline or centreline. The front-position records are therefore commonly referred to as length change records (see, for example, Purdie et al., 2014; Zemp et al., 2015; WGMS, 2019). Glacier length fluctuations are natural indicators of past climate change (see, for example, Leclercq et al., 2014) and can be used to extract a climate signal (Oerlemans, 2005). Glacier front position and length change measurements are considered a key variable in global glacier monitoring strategies (see, for example, Gärtner-Roer and Bast 2019). Length change series have been reconstructed over several centuries using drawings, paintings and photographs (Nussbaumer et al., 2011). Historical maps and end moraine positions can also be used to constrain changes in glacier length (see, for example, Weber et al., 2019; Hannesdóttir et al., 2020). Monitoring of a number of glaciers in an area is useful for filtering the influence of different glacier dynamics and geometries, and local meteorological conditions. Glacier front fluctuations and length change can also be derived from georeferenced aerial photos (orthophotos) or satellite data. The growing number of high-resolution satellite sensors with higher spatial and temporal resolution, such as Sentinel-2 (10 m) or Pléiades (0.5–2 m), makes it possible to measure all glaciers within a particular region. However, classical in situ front fluctuation data are still key to understanding past glacier fluctuations and to keeping methodological consistency.

3.5.2 Front variation measurements – field data

The front variation (in metres) is derived from annual or multi-annual measurements of the distance between the glacier terminus and fixed reference points such as cairns, painted rocks or bolts (Figure 3.6). The distances are preferably measured in the direction of the flowline (or parallel to it) and normal to the glacier perimeter. The line of measurement is given as a fixed direction (using an analogue or digital compass) or marked in the field using arrows,

(a) (b)

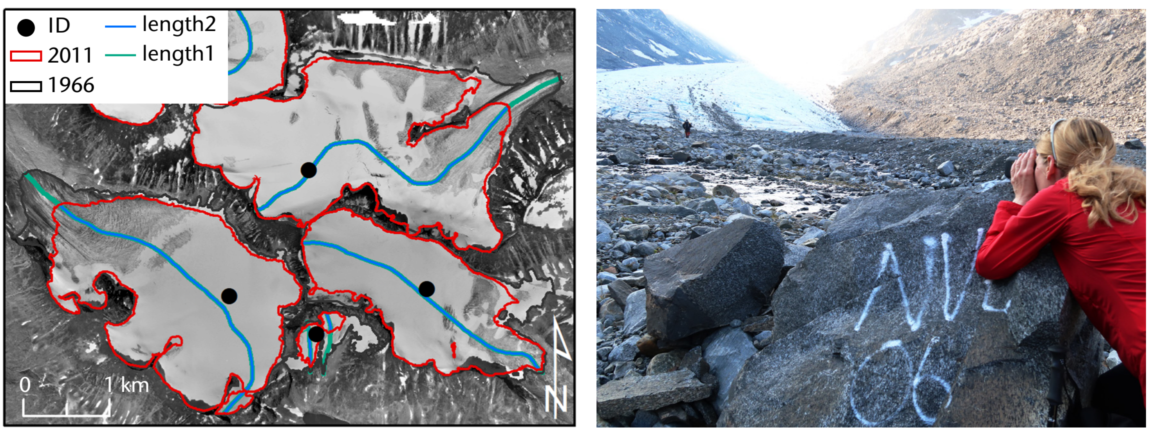

Figure 3.6. (a) Measurement of the front position of Hellstugubreen in Norway. The labeled boulder is the reference point. (b) Digitized glacier outlines in Jotunheimen, Norway. Outlines are from orthophotos taken in 1966 and 2011. The background is the 1966 orthophoto. Length1 and length2 are flowlines used to calculate the length change from maps. Glacier IDs are from the Norwegian inventory.

Source: (a) Jostein Aasen. (b) Figure from Andreassen et al. (2020); reproduced with permission from the Journal of Glaciology paint or additional cairns. One or more points along the glacier front are measured, and the observations are usually carried out at the end of the ablation season every year. Traditionally, the distance has been measured with a measuring tape providing accuracy within 2 m; nowadays a laser (electronic) distance meter is often used providing a measurement accuracy within 1 m. Differential GNSS measurement can also be used to record the position of a single point at a glacier front, or even the entire front, with accurate positioning (<10 cm). However, this should only be done when walking along the terminus is safe and easy. UAVs (drones) can also be used to generate orthoimages to map glacier outlines.

The accuracy of front-position measurements depends on the accessibility, which may become limited due to advance or retreat. In general, glaciers have different response times because of different slope, length and mass-balance gradients (see, for example, Zekollari et al., 2020). Glacier retreat can also be enhanced significantly when the glacier is calving into a proglacial lake, and such situations complicate measurements of front positions.

Glacier front-position measurements must sometimes be discontinued if the glacier terminus changes so that accurate measurements are no longer possible. This has been the case for several glaciers in Norway, in Iceland and in Switzerland (see, for example, Andreassen et al., 2020; Sigurðsson, 1998). Examples include retreat of the glacier front into terrain that is inaccessible or unsafe (for example due to quicksand or due to retreat up a very steep slope), or where debris cover makes the exact determination of the glacier boundary difficult.

Observations from maps and orthophotos can be used to prolong front variation records, fill in data gaps and homogenize/calibrate the series (see, for example, Andreassen et al., 2020; GLAMOS, 2020; Kurzböck and Huss, 2021). Glacier outlines from historical maps and orthophotos can be used together with automatically generated flowlines to extract the length changes. Often such flowlines need to be modified due to emerging nunataks or changes in the terminus form (Figure 3.6).

3.5.3 **Front variation and length change reporting**

Front variation and length change measurements are collected by WGMS and published in the series Global Glacier Change Bulletin (see, for example, WGMS, 2021). Reconstructed glacier front variations can also be submitted using standardized forms (Zemp et al., 2011). Details on data submission are given in the WGMS Attribute Description (2019). Figure 3.7 shows the front variations of seven glaciers on five continents displayed as cumulative length changes. The length of the records varies between 65 and 140 years.

3.5.4 **Length change from other sources**

In addition to orthophotos from aerial imagery, satellite data can be used for extracting frontal variation and length changes. Length changes are then typically calculated along one or several flowlines that can be manually digitized or automatically generated (see, for example, Kienholz et al., 2014; Maussion et al., 2020). A challenge with flowline methods is that the changes can be uneven along the terminus, and results will vary depending on the position of the flowlines. The so-called "box method" defines a box along the terminus with a gate perpendicular to the centreline of the glacier (Moon and Joughin, 2008; McNabb and Hock, 2014). Rapid developments in the field of remote sensing and machine learning are leading to new techniques for assessing change over the full terminus, in particular for marine-terminating glaciers (see, for example, Zhang et al., 2021).

Several studies have analyzed length change data based on data from multitemporal satellite inventories (for example, Fischer et al., 2014, Winsvold et al., 2014, Paul et al., 2020). Earlier studies showed that Landsat data of 30 m resolution are in good agreement with field data, apart from glacier tongues in cast shadow (Paul et al., 2011). However, in contrast to field observations, an accurate annual signal cannot be obtained with the 15–30 m resolution of optical satellites such as ASTER and Landsat. Because of the rapid retreat of many glaciers during the twenty-first century, new enhanced satellite sensors with higher spatial resolution often allow determination

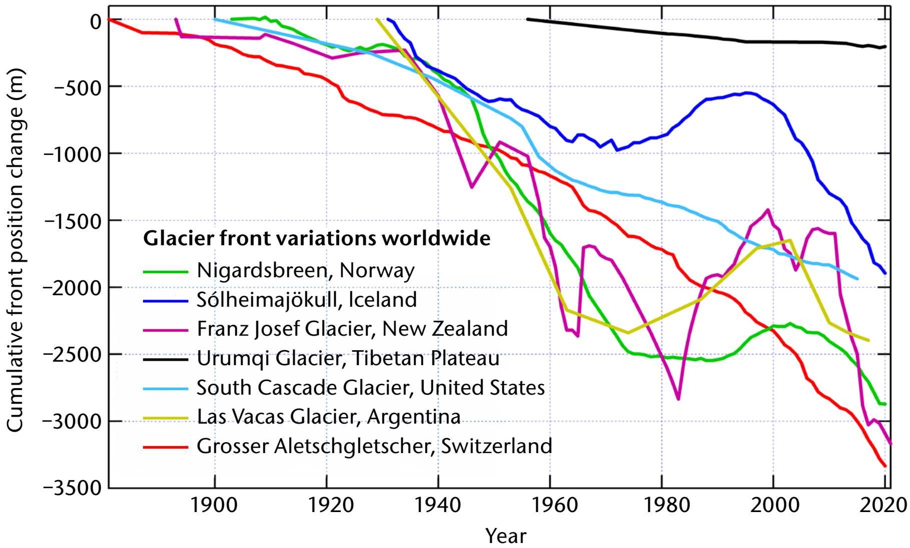

Figure 3.7. Observed cumulative length change since the beginning of the front variation measurements at: Grosser Aletschgletscher (starting in 1881), Franz Josef Glacier (1894), South Cascade Glacier (1900), Nigardsbreen (1907), Las Vacas Glacier (1929), Sólheimajökull (1932) and Urumqi Glacier (1956). All glacier fronts are in retreat, but in some cases retreat is interrupted by advances due to cooling periods, increased precipitation or surges.

Source: Data from WGMS (2021) with updates

of year-to-year changes in glacier length. Future sensors with higher resolution and free of charge imagery will enhance the possibility for more frequent and accurate measurements of glacier length changes using satellite data.

3.5.5 Uncertainty

Uncertainties in front variation and length change measurements involve the accuracy of the measurement itself and the representativeness of the points or lines used for the measurements. Front variation measurements in the field have an accuracy of within 1 m using a laser distance meter and within 10 cm using differential GNSS. For length change obtained from other sources it will depend on the spatial resolution of the image or sensor and the accuracy of the georeferencing. For both field data and remotely-sensed data an uneven terminus can result in highly variable results depending on the chosen line of sight or flowline. Front variation series should be regularly homogenized and recalibrated if needed using orthophotos and maps.

3.6 MASS BALANCE TERMINOLOGY AND REPORTING SYSTEMS

Standardized systems for mass balance terminology were described in "Mass-Balance Terms" (1969), Müller et al. (1970), Mayo et al. (1972) and Østrem and Brugman (1991). Definitions of key terms are given in Section 3.6.1 below, based on those synthesized from earlier work by Cogley et al. (2011). Note that definitions of key variables included in the WMO-WIGOS system have already been given in Section 3.1.5. The most important systems for reporting mass balance are outlined in Section 3.6.2.

3.6.1 Mass balance terminology

Accumulation (c). Includes all processes that increase the mass of a glacier (Figure 3.8). The main process of accumulation is snowfall. Accumulation also includes deposition of hoar, freezing rain, solid precipitation in forms other than snow, gain of windborne snow, avalanching and basal accumulation (often beneath floating ice). Moreover, internal accumulation can occur by refreezing of meltwater within the snowpack.

Ablation (a). Includes all processes that remove mass from a glacier (Figure 3.8). The main processes are melting and calving, but sublimation, loss of snow by wind transport and avalanching are significant on some glaciers. Ablation typically does not include basal or internal melting unless otherwise stated.

Accumulation zone. The part of the glacier or ice cap where accumulation exceeds ablation in magnitude, that is, where the cumulative mass balance relative to the start of the mass-balance year is positive (Figures 3.8 and 3.9). References to the *accumulation zone* indicate its extent at the end of the mass-balance year. The extent of the *accumulation zone* can vary strongly from year to year. The term *accumulation area* has the same meaning.

Ablation zone. The part of the glacier or ice cap where ablation exceeds accumulation in magnitude, that is, where the cumulative mass balance relative to the start of the mass-balance year is negative (Figures 3.8 and 3.9). References to the *ablation zone* indicate its extent at the end of the mass-balance year. The extent of the *ablation zone* can vary strongly from year to year. The term *ablation area* has the same meaning.

Equilibrium line. The boundary separating the accumulation zone from the ablation zone (Figures 3.8 and 3.9). At the equilibrium line the surface mass balance is zero at the end of a mass-balance year.

Equilibrium line altitude (ELA). The spatially averaged altitude of the equilibrium line.

Accumulation area ratio (AAR). The ratio, often expressed as a percentage, of the area of the accumulation zone to the area of the glacier (ice cap).

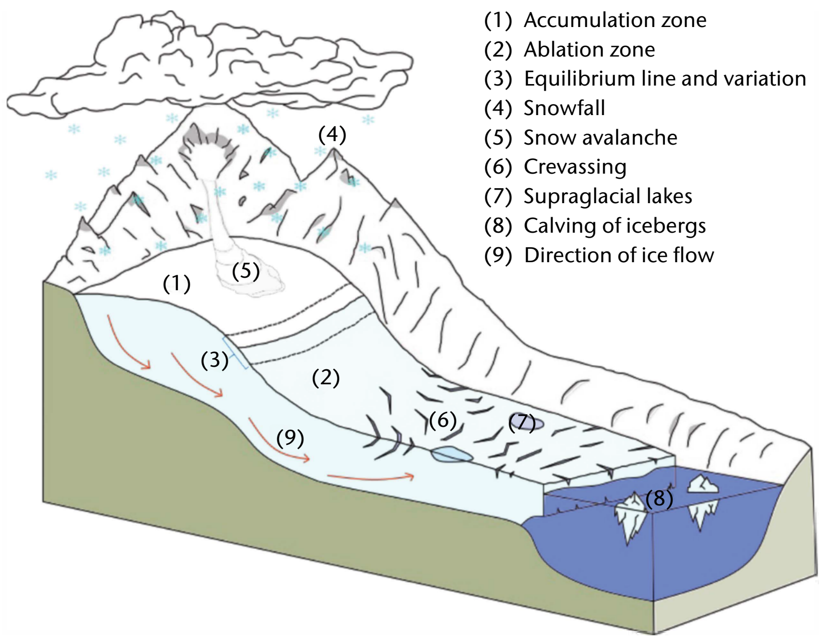

Figure 3.8. Schematic diagram showing the zones on a glacier, the equilibrium line and main mechanisms of mass gain and mass loss

Accumulation season. A time span extending from a seasonal minimum of glacier mass to a seasonal maximum (Figure 3.10). The accumulation season is the same as the winter season on most glaciers, which are of winter accumulation type. Special cases include glaciers of summer accumulation type and year-round ablation type, and glaciers that have more than one accumulation season during the year.

Ablation season. The time span extending from a seasonal maximum of glacier mass to a seasonal minimum (Figure 3.10). The ablation season is the same as the summer season on most glaciers, which are of the winter accumulation type. Special cases include glaciers of summer accumulation type and year-round ablation type, and glaciers that have more than one ablation season during the year.

Winter (mass) balance at a point (b_w). Represents the snow accumulation that will be left at the end of winter, but not the total accumulation because part of the snow may have been removed by sublimation, evaporation, wind scouring and melt events.

Summer (mass) balance at a point (b_s). Represents the mass loss between spring and autumn observations, consisting of (i) melting of snow and glacier ice in the ablation zone, and (ii) mass loss from the winter layer within the accumulation zone. For glaciers terminating in the ocean or in proglacial lakes, *calving* represents the component of ablation consisting of the breaking off of ice from the glacier margin into the lake or sea water, producing icebergs, or onto land in the case of dry calving.

Annual mass balance of a point (b_a). The change in balance during one mass-balance year, which can be expressed as the algebraic sum of winter balance and summer balance:

$$b_a = b_w + b_s \tag{3.3}$$

The annual mass balance may be positive or negative depending on conditions in the particular balance year. All values are given in metres of water equivalent (m w.e.).

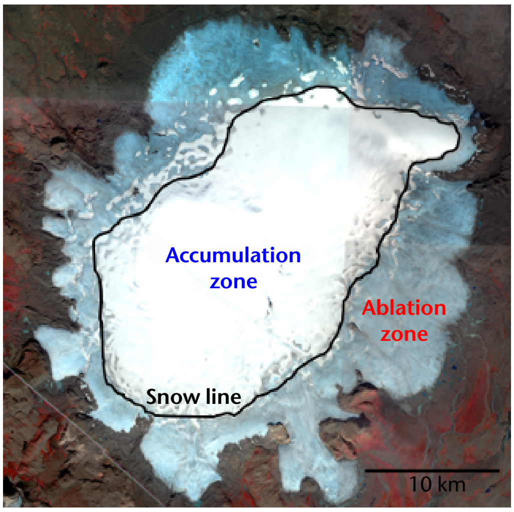

Figure 3.9. SENTINEL-2 image of the 810 km² Hofsjökull ice cap, Iceland, taken at the end of summer 2019. In the ablation zone, winter snow cover has gradually melted away during summer, exposing glacier ice below. The *snow line* delineates the lower boundary of the snow-covered area at any time. For the case shown here the *equilibrium line* coincides with the position of the snow line at the end of the melting season. Its altitude (ELA) varies with climatic conditions. Hofsjökull altitude span: 650–1 790 m, ELA = 1 300 ± 200 m.

Source: ESA (Copernicus Sentinel data 2019)

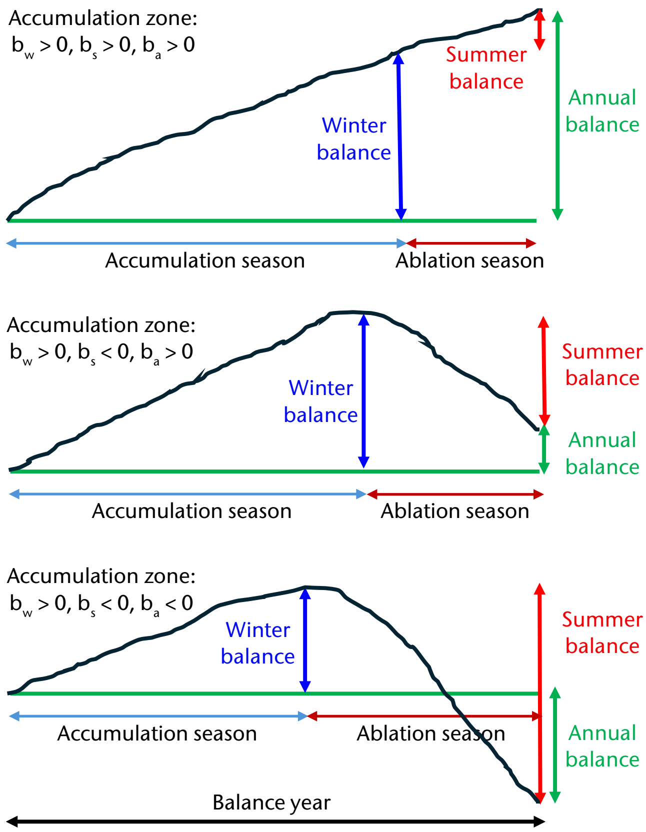

Figure 3.10. Schematic mass-balance diagrams for three locations at different elevations on a glacier. Top: At the highest elevations the summer balance can be positive and mass is added throughout the year. Middle: Typical situation for much of the accumulation zone with positive winter balance, negative summer balance and positive annual balance. Bottom: Less winter snowfall and much more summer melting lead to negative annual balance in the ablation zone. In this diagram, winter balance is stratigraphically defined for the middle and bottom examples (going from minimum to maximum mass), but arbitrarily for the top example. The balance year, as depicted, refers to the fixed-date system (see descriptions of reporting systems in Section 3.6.2). Note that the relative lengths of the accumulation and ablation seasons change with elevation on the glacier.

For the entire area of a glacier or ice cap (or a specific ice-flow basin), capital letters are used to designate mass balance:

B_w = winter balance

B_s = summer balance

B_a (or B_n) = annual balance (or net balance)

3.6.2 Mass-balance reporting systems

Typical cumulative mass-balance change throughout the glaciological year at a single point on a glacier is depicted in Figure 3.11. The most commonly used reporting systems are outlined below.

Stratigraphic system. In this system, determination of mass balance is based on the identification of successive annual minima, and for seasonal balances annual maxima as well, in the mass of the glacier/ice cap. The duration of the mass-balance year varies in this system. In practice, it is difficult to apply the stratigraphic system because field measurements are typically conducted only twice a year and the exact dates of annual minima and maxima are not known in advance. Moreover, maxima and minima may not occur at the same time at all elevations on a glacier or ice cap.

Fixed-date system. In this system the annual balance is calculated between fixed dates each year, typically 1 October in northern hemisphere settings. Other dates will obviously apply in the southern hemisphere and in high-mountain areas near the equator. If the autumn survey is made earlier or later than 1 October, mass-balance models should be employed to correct for melting and/or snow precipitation that may have occurred between 1 October and the date of the field measurement. Whereas the fixed-date system allows consistent comparison between individual years and individual glaciers, corrections to the actual measurements are always required, leading to increased uncertainty. The approach used should be documented and be reproducible.

Floating-date system. In this system the dates of the surveys determine the mass-balance year and the accumulation and ablation seasons. The winter balance, as measured during the spring field survey, equals the total water equivalent of all snow deposited at the measurement site since the previous year's autumn expedition. Snow that may have fallen before that survey is counted as a positive contribution to the previous year's summer balance, and likewise for snow that falls before the end of the current mass-balance year in this system.

Combined system. This system normally combines the stratigraphic system with either the fixed-date system or the floating-date system (Mayo et al., 1972). For example, the successive mass-balance minima indicated in Figure 3.11 can usually be inferred from stratigraphic observations if visits are made shortly after the occurrence of the stratigraphic minima. Most often, the users of this system include snow that has been deposited prior to the autumn visit with the winter balance of the following winter, but do not attempt to correct the seasonal balances for the snow that may be deposited after the spring visit.

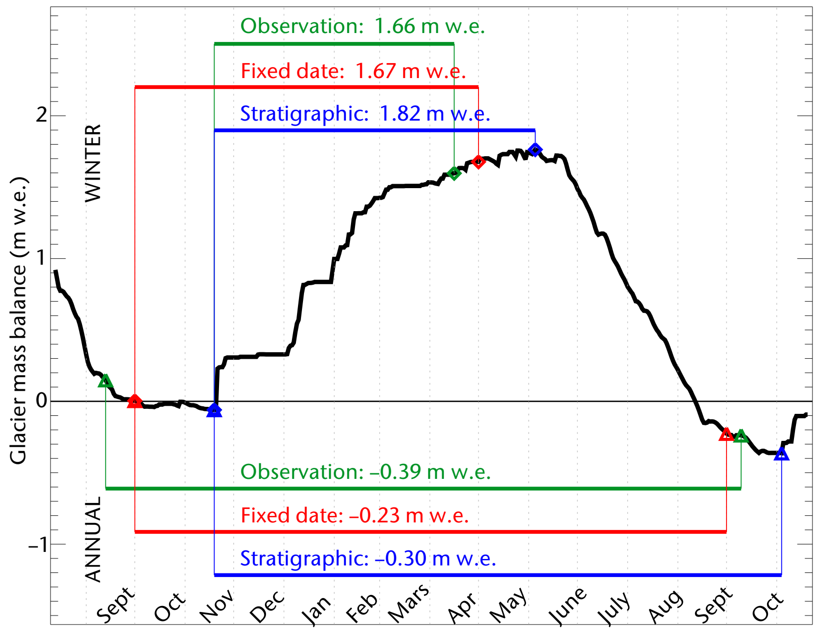

Figure 3.11. Cumulative glacier-wide mass balance over one year for a glacier in the Swiss Alps based on modelling constrained with seasonal observations. The duration of the observation period in the floating-date system, in the fixed-date system (hydrological year) and in the stratigraphic system is indicated both for the entire year and the winter period, and corresponding mass balances are given. Note that the start of the winter observation period is defined stratigraphically as measurements were based on snow probing down to the last summer's horizon, thus referring to the combined system (Mayo et al., 1972).

For a detailed treatment of the different reporting systems and variables used to calculate winter, summer and net mass balance in each case see pages 129–140 and 149–152 in Østrem and Brugman (1991), and the discussion of time systems for mass-balance measurements in Cogley et al. (2011).

3.7 SURFACE ACCUMULATION MEASUREMENTS

In this section, *snow depth* refers to the thickness of the layer of snow deposited on the surface of a glacier, usually at the end of winter, often at fixed locations where ablation stakes are placed every year. In the accumulation zone, the *summer surface* forms the base of the winter layer, which is deposited on top of older annual layers that have turned into firn. In the ablation zone, the winter layer covers glacier ice. The surface accumulation at a point location (stake location), that is, the water equivalent of the snow accumulated over the winter, is determined as the product of snow depth and bulk density of the snow accumulation at that location. The basic methods for measurement of these two quantities are described in the present Volume, Chapter 2. There, definitions and more detailed descriptions are given as well as discussions on sources of errors. The description in this section refer to measurement procedures on glaciers.

3.7.1 Manual measurements of snow depth and density on glaciers

Measuring snow depth with a graduated device (see Chapter 2, 2.4 of Volume II of the present Guide). A graduated device (snow probe) is pushed vertically through the snow layer until the *base surface or reference level* is detected. On glaciers, the *base surface or reference level* is either the ice surface (within the ablation zone) or the previous year's hardened summer surface (in the accumulation zone). Care must be taken when measuring snow depth because ice layers up to several cm in thickness may be present in the snow, due to warm spells that have caused surface melting. Best practice is to probe close to a site with known snow depth, such as a snow pit or the location of a core with a positively identified summer surface, to get a feeling for the local snowpack. Then, spatial variability can be defined using the probe based on the known local snow depth.

Snow depth on glaciers can be highly variable, even within short distances, because deposition is greatly affected by topography and wind. To represent spatial variability of snow depth at one particular stake location, snow depth should be measured at 5–10 locations in a 20 × 20 m area surrounding the stake (Østrem and Brugman, 1991). In addition, snow depth probing along the flow direction of a glacier and perpendicular to it will yield information on the snow deposition pattern on the glacier. This allows for corrections if snow depth at stake locations turns out not to be fully representative for the glacier. The probing density per unit area should be determined for each glacier based on local conditions and logistical constraints.

Measurements in snow pits. The digging and sampling of snow pits on snow-covered ground to determine SWE is described in Chapter 2, 2.4 of Volume II of the present Guide. On glaciers, sampling in snow pits can be useful to obtain accurate determination of snow depth and bulk snow density and hence of surface accumulation. The pit should be dug not more than 10 m from the ablation stake location and density measurements should be done as soon as possible after digging. The digging of snow pits deeper than 2 m, however, is very time consuming.

Snow core drilling. Coring augers are widely used to penetrate the winter snow layer at selected locations on glaciers and ice caps (Talalay, 2016; Figure 3.12). Mostly, augers connected with extensions are used, but small versions of ice core drills, connected to a wire that is wound onto a winch, can also be used. The length, diameter and mass of each core piece is measured, yielding its density and water equivalent. Summation then gives the point accumulation above the previous year's summer surface (accumulation zone) or above the glacier ice (ablation zone). The uppermost part (typically 20–50 cm) of the snowpack is often loose, and will degrade as the core is pushed out of the coring tube. This problem is circumvented by sampling the loose top layer with a cylinder in a shallow pit, using methods described in the present Volume, Chapter 2, 2.4.1. This sampling is done as close to the drill hole as possible. After each coring run,

(a) (b)

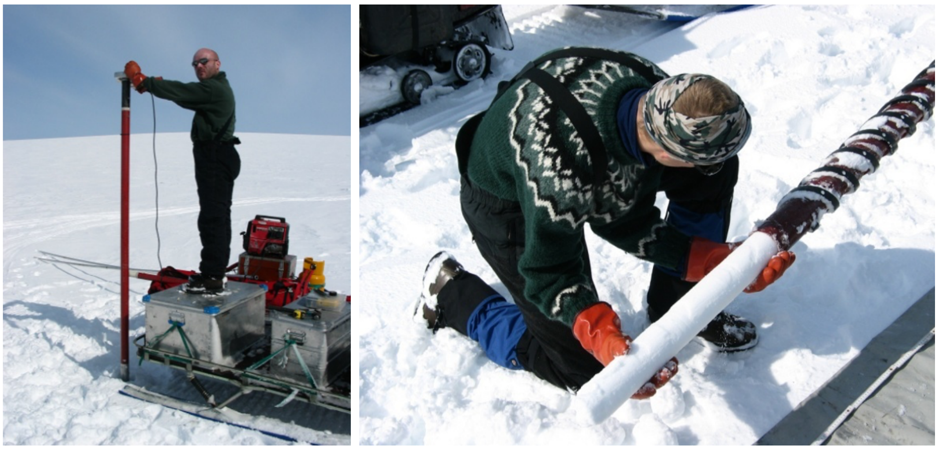

Figure 3.12.(a) Drilling a snow core through the winter layer. The drill is powered by a threading machine. (b) Removing a core from the drill. Under optimum conditions, cores 1 m long are obtained in each drilling run.

Source: Thorsteinn Thorsteinsson

the depth of the borehole should be measured with a graduated tape measure and compared with the total core length at that depth. This allows correction of the core length in case a core piece has been lost. The density of a lost core piece can be estimated from the densities of pieces immediately above and below.

Determining the depth of the *summer surface* (Figure 3.13) and hence of the winter layer involves studying the core stratigraphy to look for a transition from fine-grained winter snow to relatively coarse-grained firn that underwent densification and metamorphism during the previous summer. An ice layer formed by melting and refreezing is sometimes present at the summer surface and windblown dust from nearby deserts and mountain sides is often a clear indicator of the end of summer, even on large ice caps. Within dry snow, depth hoar layers formed by sublimation and growth of coarse crystals may indicate a summer surface. In case a mass-balance stake is present at the measurement site, the last summer's surface layer can also be marked with ochre or sawdust spread out on the previous year's surface at a defined distance from the stake. This layer can be easily detected in a snow pit or a snow core (Figure 3.14). The latter method allows unambiguous determination of the depth of the winter layer and clearly defines the period of the sampling. This approach is especially useful in high-elevation accumulation areas, and in regions with reduced seasonality, where the summer surface can be difficult to detect.

The water equivalent of the winter accumulation is obtained by adding the water equivalent of each core piece between the spring surface and the previous year's summer surface. The calculation of the winter balance depends on which time system is used (Section 3.6).

Determining accumulation from crevasse stratigraphy. In particular climatological settings with a clear seasonality, several annual accumulation layers may be clearly identifiable in the walls of large crevasses (Figure 3.15). This makes it possible to measure the depth of the uppermost winter layer and estimate the annual balance also for earlier years (using direct measurements or realistic estimates of densification with depth at each location). This approach is easy and fast as it does not require any measurement gear. Nevertheless, results on snow accumulation are less accurate as the attribution of visually detectable horizons to individual periods can be ambiguous. Furthermore, snow depth in the region of large crevasses might not be representative due to wind redistribution effects. Carefully choosing crevasses that have opened after the accumulation season ended partially mitigates the problem of wind redistribution, but ablation rates may be affected as well. Calibration of these factors can be achieved by probing beside a crevasse and then progressively further away from the crevasse.

Figure 3.13. A 117 cm long core drilled through fine-grained winter snow in the upper part of the winter layer (top panel). No specific stratigraphic features are observed in this core. The previous year's *summer surface*, containing visible dust and displaying a change from fine- or medium-grained winter snow to coarse-grained firn from the previous winter (bottom panel). Location: Hofsjökull ice cap, Iceland (1 790 m elevation).

Source: Thorsteinn Thorsteinsson

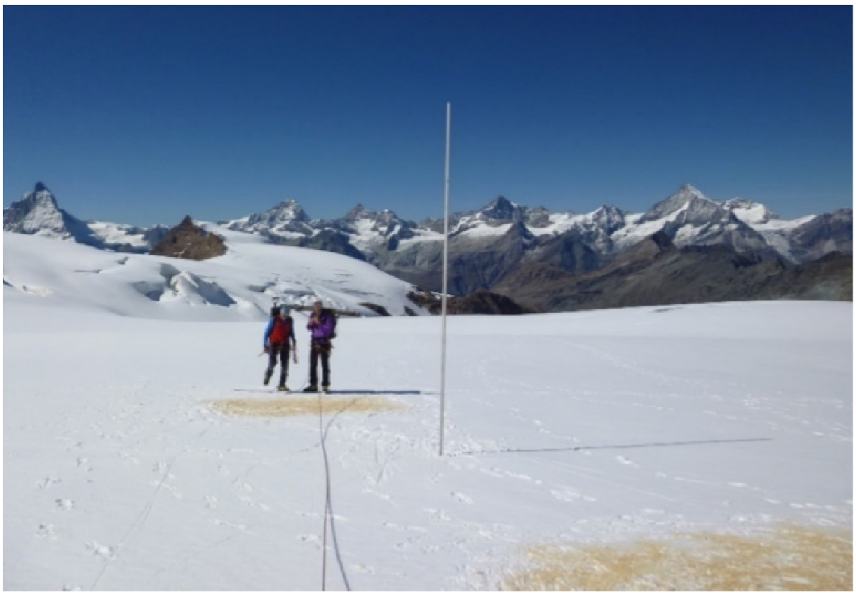

Figure 3.14. Measurement site in the accumulation zone of a Swiss glacier. The late-summer surface is marked by sawdust.

Source: Matthias Huss

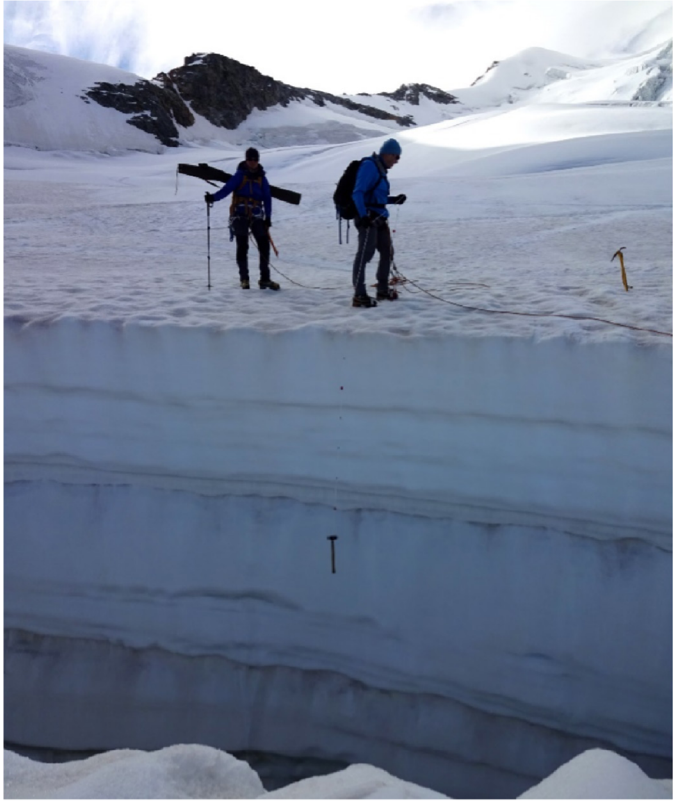

Figure 3.15. Determining accumulation from crevasse stratigraphy

Source: Matthias Huss

Sources of error. In the accumulation zone, determination of the vertical thickness of the winter layer relies on the accurate identification of the previous year's summer surface. However, stratigraphic features characterizing the summer surface (ice layers, windblown dust, transition to coarser and denser firn) are not easily detected in snow cores (or in pit walls) in all years, especially if several meltlayers have been formed during warm autumn spells. When snow depth is measured with a graduated device, visual inspection of the summer surface is not possible and the operator must therefore rely on experience in detecting the difference in hardness at the lower boundary of the winter layer.

During core drilling, sections of the core are sometimes lost if core catchers do not function properly or if drilling is taking place in snow at the melting point. This core loss can be accounted for by measuring the borehole depth at the end of each drilling run and comparing with the accumulated core length. In the density measurements, errors arise from uncertainty in: (i) length of individual core pieces (up to 5% if core breaks are skewed); (ii) diameter of cores (up to 3%) and (iii) mass of cores (normally <1% if precision weights are used, but may become larger if weighing occurs under windy conditions). In most cases, a combination of stratigraphic observations and density measurements allows determination of the water equivalent of the winter layer with an error of less than 10% (Geibel et al., 2022). In the ablation zone, the error is reduced to ~5% because the winter layer is underlain by solid glacier ice, which makes detection of its lower boundary unambiguous.

3.7.2 Snow-depth measurements with ground penetrating radar techniques

The use of GPR to determine snow depth is becoming common practice on glaciers and ice caps. GPR systems can be towed by personnel on skis, by snowmobiles or other vehicles and even airlifted by helicopter (Kohler et al., 1997; Machguth et al., 2006; Sold et al., 2013, 2016; Bauder et al., 2018). The basic principle is the same as for radio-echo sounding (see Section 3.4.1), but a higher frequency must be used (500 MHz–1.2 GHz). The frequency will depend on the snow depth and the expected detail in the internal layering. The sampling frequency will vary with the speed of the instrument, but typically one measurement of snow depth is obtained for every 0.4–2.0 m traversed. The method has the major advantage of producing essentially continuous transects of snow depth as measured perpendicular to the snow surface – 500–2 500 measurements on a 1 000 m transect – whereas only 1–10 measurements are typically obtained with snow coring or probing. Moreover, up to 100 km of GPR profiles can be obtained in a single day under optimum conditions. This will in most cases greatly increase information on the distribution of accumulation on the glacier under investigation. The layout of a measurement grid on a particular glacier or ice-flow basin and the spacing between profiles will depend on the size of the glacier (or ice cap) and on logistical constraints.

Accurate interpretation of GPR data relies on comparison with data on snow depth collected in snow cores and in snow pits. Such a comparison must be made during each measurement campaign, to ensure that the reflector associated with the previous year's summer surface (in the accumulation zone) is correctly interpreted. The in-situ data are also required to calibrate the radar wave velocity (McGrath et al., 2015, 2018).

The electromagnetic wave velocity in snow is typically around 2.1×10^8 m/s (Annan et al., 1994) and may vary between years and campaigns due to variations in snow density, liquid water content and other parameters. Thus it is recommended to calibrate snow depth inferred from GPR data against direct measurements by snow coring or probing. In a plot of the snow depth determined by coring or probing versus the one-way travel time of the electromagnetic wave traveling vertically between the surface and the lower boundary of the winter layer, the velocity equals the slope of the line obtained (Figure 3.16). Data from the entire elevation span of the glacier being investigated should be included.

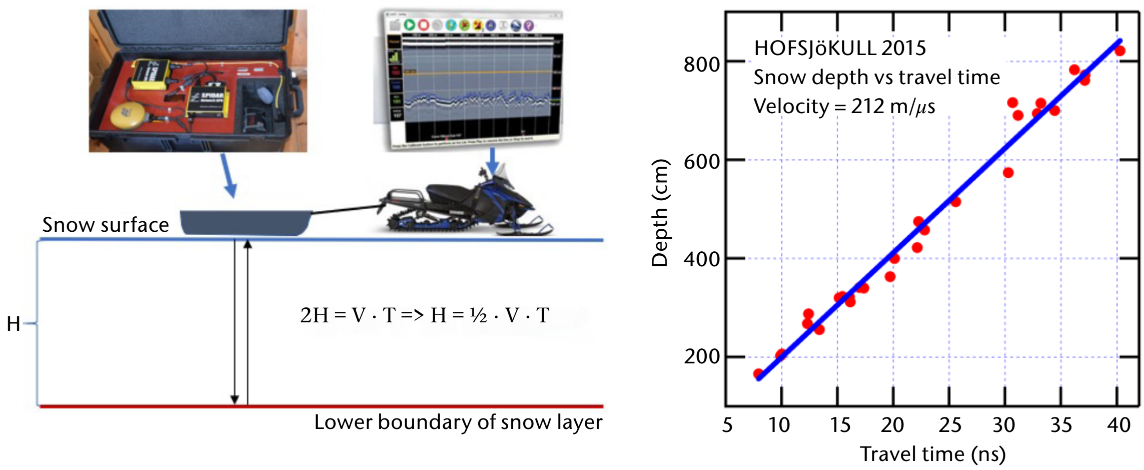

Figure 3.16. (a) A snowmobile towing an IceMap GPR system placed in a toboggan. The transmitter, receiver and GPS are placed in a single unit (upper left corner). The wave travels a relatively short distance and the horizontal component of travel can be ignored. Wireless transmission allows control of the GPR from a laptop placed in front of the driver's seat. (b) Velocity calibration on Hofsjökull during the spring expedition in 2015. Snow depth determined by coring at 28 locations is shown on the y-axis and the measured travel time on the x-axis. The slope of the best-fit line (r^2 = 0.86) is the average velocity in this year's winter layer, 0.212 m/ns = 212 m/μs.

Source: Thorstein Thorsteinsson (2016)

3.8 SURFACE ABLATION MEASUREMENTS

3.8.1 Ablation stakes on glaciers and ice caps

The term *ablation* on a glacier or ice cap refers to the amount of melting that has occurred at a particular point in time. It is measured on stakes or wires placed in snow, firn or ice, and the result at each location is given in m w.e.

Ideally, ablation stakes should be distributed uniformly so that ablation on the entire glacier or ice cap is represented. An ideal distribution pattern is, however, not always possible due to crevassing and other constraints, depending on the size and shape of the glacier/ice cap being measured. For valley glaciers, a central stake profile along the long axis of the glacier is ideal, with transverse stake profiles at regular intervals. On an ice cap, the stake network should be designed to capture the main topographic gradients across the ice cap. The stakes should to the extent possible be placed at regular elevation intervals (Figure 3.17).

Stake types. Aluminium tubes have been extensively used in mass-balance measurements (Figure 3.18). The optimal dimensions are: length 4–6 m, outer diameter 3–4 cm and wall thickness 3–4 mm. The stakes must have sufficient mechanical strength to withstand stresses resulting from riming, strong winds and ice shear. Stakes 2–3 m long can be coupled together with a 30–40 cm aluminium bar sized to fit tightly inside the two stakes. Such couplers can also be used to extend stakes that are intended to stand through the winter. PVC tubes have also been used in ablation areas with good results (Geibel et al., 2022). PVC tubes with a diameter of about 2 cm are used. Bamboo stakes with wire connections between individual 1–2 m segments have been used in mass-balance measurements at high altitudes, where all gear must be carried onto the glaciers (Figure 3.19). Bamboo stakes are easily available, light, strong, weather resistant, inexpensive, and have low thermal conductivity (Kaser et al., 2003).

Stakes should be placed at the same position every year to compensate for ice motion. A GPS device should be used to ensure horizontal position accuracy within ±5 m. In the accumulation area of some glaciers, stakes from the previous year are extended every year by adding a new stake on top. The extension is typically 2 m long.

At stake locations in ablation areas where aluminium stakes with a length of 4–6 m cannot survive the summer due to high melting rates, steel wires may be inserted into boreholes.

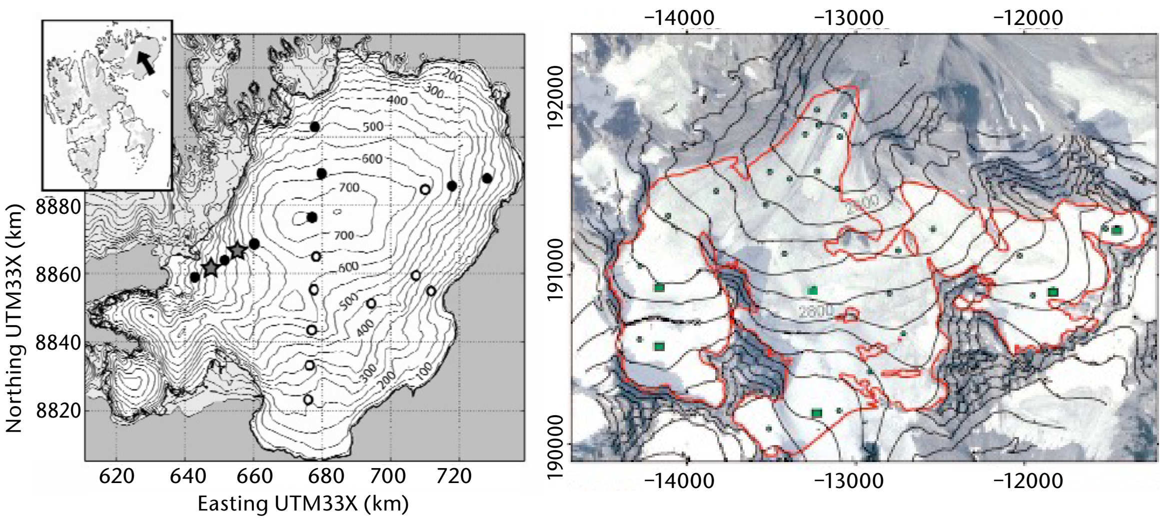

Figure 3.17. (a) Ablation stake network (open and filled circles) on the Austfonna ice cap, Svalbard. The network captures the gradients across the summit (N–S) and along the ice divide trending WSW–ENE. (b) Distribution of stake locations on a mountain glacier, the Jamtal Ferner, Austria.

Source: (a) Schuler et al. (2007); (b) Fischer and Markl (2009)

Figure 3.18. Placing a 6 m aluminium stake in a borehole drilled by a snow corer

Source: Thorstein Thorsteinsson

Figure 3.19. Inserting lightweight bamboo stakes into a borehole at ~5 500 m elevation on Rikha Samba Glacier in Nepal. Short (1–2 m) sections must be connected before deployment in the borehole, using either a rubber tube, a metal sleeve or a wire connection (Kaser et al., 2003).

Source: Photo by T. Gurung, provided by G. Silwal, International Centre for Integrated Mountain Development (ICIMOD)

(a) (b)

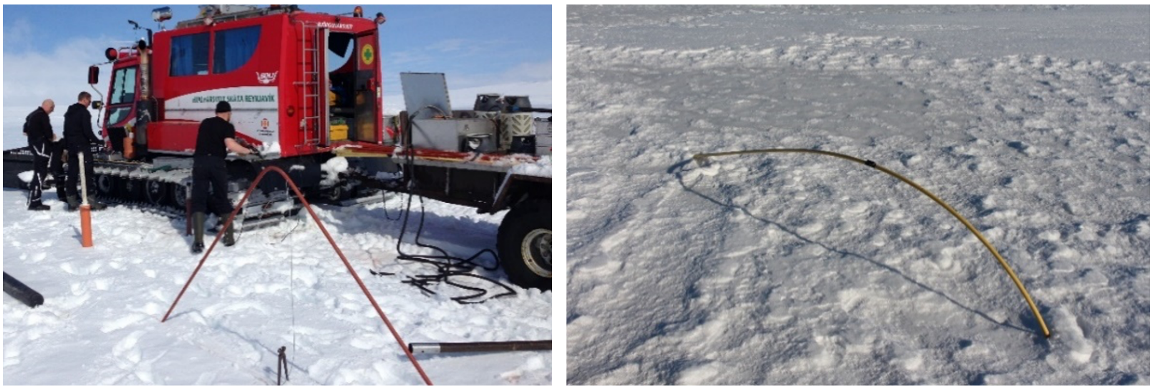

Figure 3.20. (a) A steel wire can be inserted in boreholes where melting rates are very high (8–12 m of ice during the melting season). The wire must be fastened to a structure on the surface, which is visible from a distance. In this photo, the wire is fastened to the top of the inverted V-shaped tube. (b) A PVC tube that has emerged from a borehole due to summer melt.

Source: (a) A. Gunnarsson; (b) Á. Gunnlaugsson

The wire will freeze solid in the ice. The upper end should be tied to a tetrahedron (wood or metal) or some other structure (Figure 3.20). An orange-coloured plastic flag can be fastened onto the structure, making it easier to locate during summer and autumn. Note that readings are unreliable if the cable is not frozen into the ice. Alternatively, systems with flexible stake elements connected with a chain may be used in such cases.

3.8.2 Drilling equipment

Several types of snow coring systems are available from commercial companies. Typically, the drill head has two cutters and during rotation the cuttings are transported upward by the spiral visible in Figure 3.12. The cuttings enter the holes on the core barrel and collect above the core, which can reach a length of 130 cm but is more typically 60–100 cm long (depending on conditions) when a 2 m core barrel is used. A shorter version (1 m) of the core barrel can also be used. Individual extensions are 1–2 m long, and coring to a depth of 15–20 m is possible. The drill is powered with a handheld pipe threader connected to a small (1 kW) generator (Figure 3.12).

For drilling into glacial ice, a steam drill or a handheld power drill is commonly used (Figures 3.21–3.23). Manual drilling is also possible (Østrem and Brugman, 1991). In the steam drill system, up to 10 l of water are poured into a pressure boiler powered by propane gas. The steam enters a 10–15 m rubber hose and then a drill system that is 1.5 m long and 3.5 cm wide. The drill shown in Figure 3.21 (a) can produce a 10 m borehole in less than 1 hour. This type of drill must be transported with a snowmobile or some other vehicle.

A smaller, portable steam drill that can be carried by one person to inaccessible locations is shown in Figure 3.21 (b). Handheld augers, powered with an internal-combustion engine or electric drill (Figure 3.22) provide a faster way to drill into ice. Augers measuring 1 m long and 5 cm in diameter can be connected to each other, allowing drilling to 10 m depth or deeper for placement of stakes or wires. Care should be taken when removing the auger from the hole once it is completed. Instead of taking out several flights at once it is recommended to dismantle them one by one while one operator secures the remaining flights.

3.8.3 Stake placement and readings

In the accumulation area, stakes are sometimes placed in spring in the boreholes produced during drilling of cores through the winter layer (Figures 3.12 and 3.18). The summer balance

(a) (b)

Figure 3.21. (a) A "hot-point drill" using steam produced in a pressure boiler, heated by propane. A 12 m insulated rubber hose delivers steam to the drill stem, which is fitted with an exchangeable nozzle. The narrow, red hose supplies the propane gas to the burner. At a steam pressure of about 6 atmospheres, this drill penetrates 5–10 m of ice per hour. (b) A portable steam drill in operation.

Source: (a) Thorstein Thorsteinsson; (b) Matthias Huss

Figure 3.22. Drilling a hole with a handheld power drill

Source: Matthias Huss

is then obtained from stake readings. Ideally, the stake will be placed with the lower end in the previous year's summer surface. This ensures that readings from the stake reflect thinning of the winter layer during the summer; a stake placed with the lower end higher up than the summer surface will record only a part of the thinning of the winter layer. If the borehole reaches deeper than the summer surface, drilled snow cores can be put back into the hole and compressed and packed thoroughly with the stake until its lower end is level with the summer surface.

Metal stakes without support can sink into the firn; to prevent this, a 15–20 cm wooden plug should be inserted into the lower end. The diameter of the plug should be similar to the stake diameter. A piece cut from a plywood plate with a diameter larger than the stake can also be used for stake support.

It should be kept in mind that autumn snowfall can bury a stake that would otherwise be visible during an autumn visit. To make it easier to find the stake, a RECCO reflector can be fastened onto the stake top, and this can be found with a detector. The active component in the reflector is a small electronic transponder with a copper aerial and a diode.[6] The portable (<1 kg) detector transmits a highly directional radar signal on the 800 MHz frequency band. This signal is received by the transponder, which reflects it toward the detector. A beeping sound from the detector indicates that the reflector has been located. The maximum range of the detector signal is estimated to be 20 m in snow, but this is dependent on snow conditions and may decrease in wet snow (Grasegger et al., 2016). It should be ensured that no metal items are within the search area and other RECCO reflectors (which may be included in personal gear) must be removed beforehand.

In the accumulation area, 6 m stakes drilled during spring are normally left so that the top is 50–150 cm above the snow surface (Figure 3.23). In many settings, thinning of the winter layer during summer typically increases their height above the surface by 1–2 m. The risk of aluminium stakes bending over due to the weight of rime is fairly low if the stake top does not reach more than 2 m above the surface, and in that case they are not likely to disappear below autumn snowfalls prior to the autumn visit.

In other settings stakes are placed during autumn and readings obtained in the following autumn yield annual balance. In such cases it is necessary to place the lower end of an ablation stake deep enough to ensure stability also for potential extreme conditions in the coming year. In addition, the freezing of seasonal snow onto the stake can push the stake downward as the snow compacts. This risk is reduced if stakes are placed with the lower end at 3–4 m depth in older firn. Best practice is to use thickness and density measurements from cores down to a marked horizon for both winter and annual balance, rather than to rely only on measurements from ablation stakes (see Figure 3.24).

Stakes should be labeled each year, to minimize the risk of erroneous readings in case stakes from previous years survive summer melting. This is particularly important near the equilibrium line, where stakes can survive several years. All readings should be given to the nearest cm.

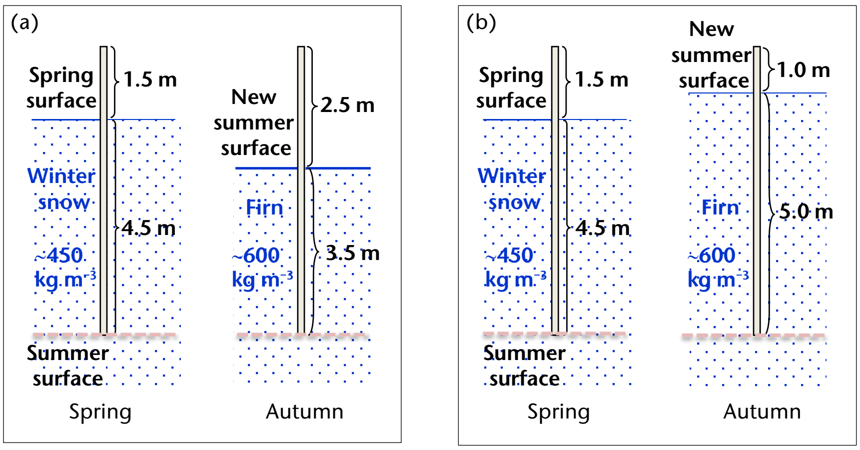

Figure 3.23. Positioning of stakes in the accumulation area during spring. If possible, stakes are placed so that their lowest part is near the base of the winter layer (that is, at the previous year's summer surface). Such placement is assumed here, and typical density values are indicated. (a) A typical change over the summer. The winter layer decreases in thickness due to some melting and a gradual increase in density. As a result, the stake top is 1 m higher above the surface at the end of summer. (b) At the highest locations, very little melting will occur and snowfall will continue throughout the summer, resulting in a net positive summer balance and thus in a reduced stake height above the surface.

[6] More information is available on the manufacturer's website at https://recco.com/technology/.

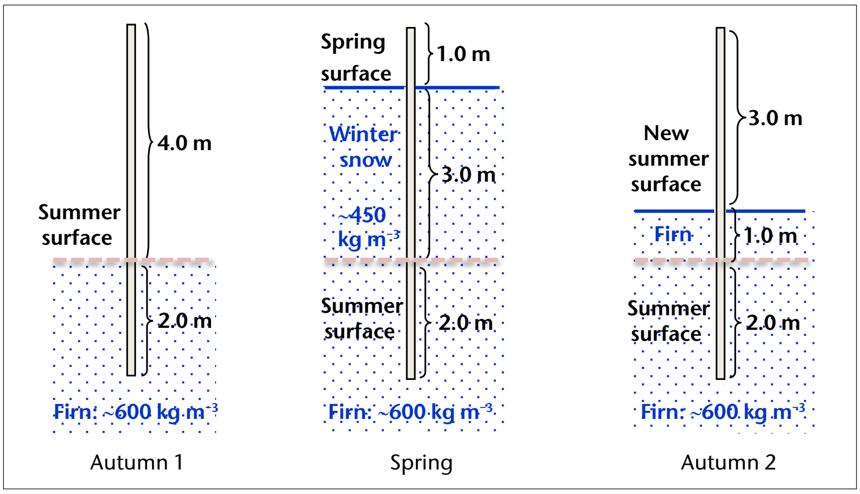

Figure 3.24. Positioning of stakes in the accumulation area during autumn. In this case the lower stake end must be placed ~2 m below the summer surface. The stake top may in some cases be visible above the surface in spring, in other cases not. Autumn readings yield annual balance.

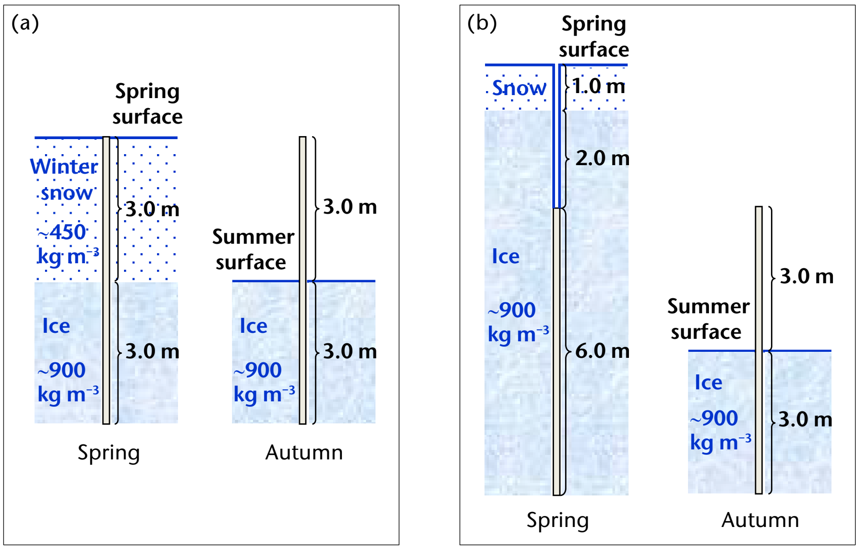

Figure 3.25. Positioning of stakes in the ablation area. (a) At the upper limit of the ablation area, that is, at the equilibrium line. Exactly the amount of snow that fell during the winter melts away during the summer. (b) In the lower part of the ablation area. Because of the high level of melt during summer, the stakes must be placed with the top at a depth of several meters, so it does not melt out completely. Here, 1 m of winter snow and 2 + 3 = 5 m of ice melt during the summer.

In the ablation area stakes may be placed so that the stake top is below the surface at the beginning of summer, because of the relatively high levels of melting. Stakes should be supported with a wooden plug at the lower end. If the drilled hole is deeper than the stake length, another stake must be used to press the stake down to the bottom of the hole. The starting position of the stake top relative to the surface can be measured with a measuring stick, or by lowering another 6 m stake onto the top of the first one to determine its depth (Figure 3.25).

When 6 m stakes are used, high levels of ablation can cause the stake to stand with the top 4–5 m above the surface at the end of summer, making it difficult to reach the top with a measuring stick. This problem is circumvented by placing a tape marker in the middle of the stake during placement in spring. In the autumn, the distance from the ice surface to this marker is measured and 3 m added to obtain the stake height above the surface. If the surface around the stake is uneven, a rod can be placed on the ice surrounding the stake, resting in a direction perpendicular to the ice flow. The lower base of the rod then defines the ice surface.

The difference between spring and autumn readings of the stake top height relative to the ice surface yields the melting that has occurred during the summer. Example: The stake top is 3.2 m below the ice surface in spring and 2.6 m above the ice surface in the autumn. Thus $3.2 + 2.6 = 5.8$ m of glacier ice has melted during the summer, which equals approximately $0.9 \times 5.8 = 5.2$ m w.e. (given a density of ice of 900 kg m^{-3}). Snow on top of the ice during spring must be accounted for separately in the ablation calculations and its depth must be measured with methods outlined above. If the floating-date system is used to calculate mass balance, snow from snowfalls that occurred prior to an autumn expedition should be measured and counted as a positive contribution to the summer balance.

In the accumulation area, part of the winter layer will be lost by ablation. In addition, compaction will occur due to densification. Thus the difference between stake readings during spring and autumn will give information about the thinning of the winter layer due to both ablation and compaction. The ablation (mostly due to melting) can be determined if the mean density of that part of the winter layer that remains in autumn is known. The density can be measured in snow cores or in pits. The range of mean densities at the end of summer is normally not large on a particular glacier, and values between 450 and 600 kg m^{-3} have been reported from different locations on temperate glaciers, depending on altitude and snow thickness (Andreassen et al., 2016a; GLAMOS, 2020; Geibel et al., 2022). When the density has been determined, the water equivalent of the remaining part of the winter layer can be calculated. The summer ablation is found by subtracting that value from the water equivalent of the winter layer at the end of winter.

3.8.4 **Autonomous ablation measurements on glaciers**

Automated weather stations (AWSs) have been used in glacier research for decades, with the main focus on unraveling the components of the surface energy balance (Fausto et al., 2021 and references therein). The individual meteorological fluxes are computed to reproduce the measured surface changes.

On glaciers, both snow accumulation and ablation and ice ablation must be considered when analyzing surface changes. While techniques and methods for automated measurements of snow depth and SWE are covered in general in Chapter 2, 2.3.2 and 2.4.2 of Volume II of the present Guide, we focus in this section on glacier-specific methods for measuring ice ablation. Typically, stand-alone devices that often are connected to AWSs are operated for this purpose.

Glacier movement means that for climatological interpretation, repositioning of the AWS will sometimes be necessary. This is, however, very site specific.

The devices presented in this section allow for ablation over several melt seasons to be recorded automatically without major maintenance efforts; however, the length of operation without major maintenance efforts depends on the drill hole depth and the ablation rate. Complementing the data produced by these devices with measurements of snow depth and determination of SWE is useful in the context of mass-balance studies.

(a) **Pressure transducers.** One way to measure ice ablation directly is to deploy a hose with a pressure transducer in a hole drilled into the ice using a mechanical drill or steam drill. The hose is filled with an antifreeze liquid and connected to an AWS. For measurement to be successful, it is necessary to concurrently measure air pressure to remove the signal of air pressure fluctuations from the actual surface-lowering signal. With surface elevation change due to ablation, the distance between the AWS and the pressure transducer at the bottom of the hole is reduced and the hydrostatic pressure from the vertical liquid column decreases. Figure 3.26 gives a schematic representation of the concept taken from Fausto et al. (2012). After complete meltout of the pressure transducer it can be redeployed at the same site. Pressure transducers are widely used in polar regions and at high-altitude glacier sites (see, for example, Fausto et al., 2021).

(b) **Draw-wire sensors.** A hitherto little used concept is the deployment of a draw-wire sensor. The principle is measuring the linear displacement of a steel wire that has been lowered into a borehole drilled with a steam or power drill (Figure 3.27). When the surface is lowered, the wire winds around a spring-loaded spool. Hulth (2010) proposes an application for glaciers, and currently the concept is being deployed at other sites (see, for example, van Tiggelen et al., 2020).

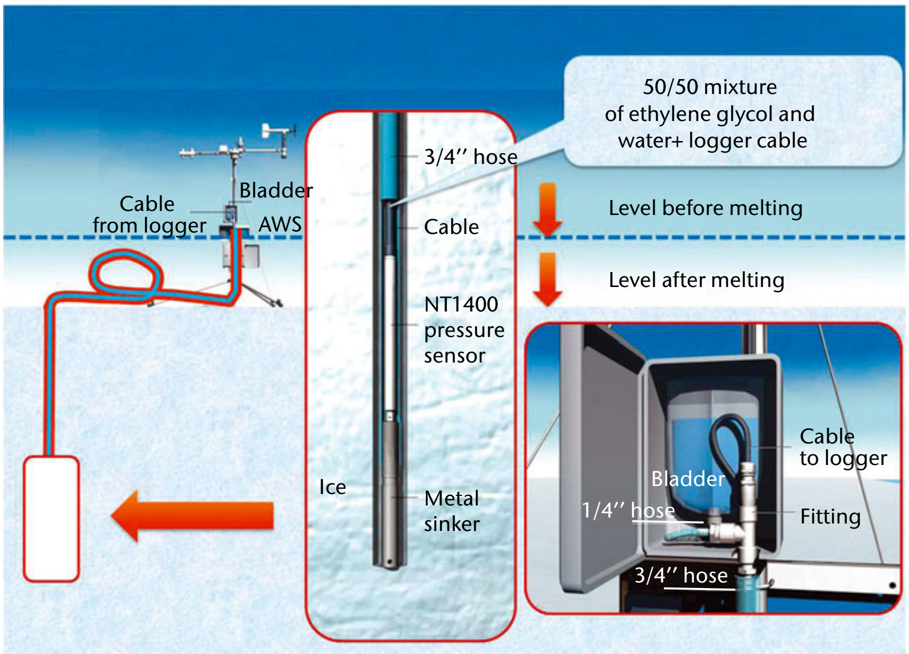

Figure 3.26. Schematic representation of a pressure transducer assembly attached to an AWS

Source: Fausto et al. (2012); reproduced with permission from the Journal of Glaciology

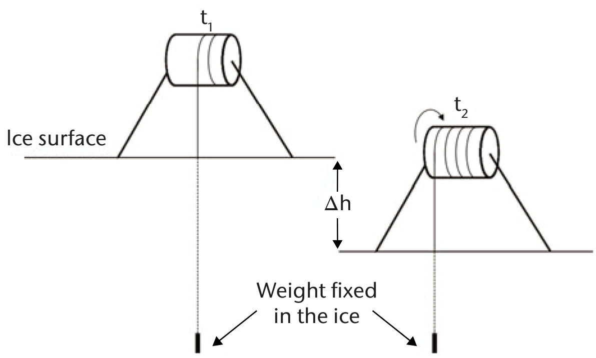

Figure 3.27. Schematic diagram of ablation measurements with a draw-wire sensor. A weight is attached to the end of the wire and fixed in the ice. The instrument registers relative surface elevation change, Δh, in time, t, due to net ablation.

Source: Hulth (2010); reproduced with permission from the Journal of Glaciology

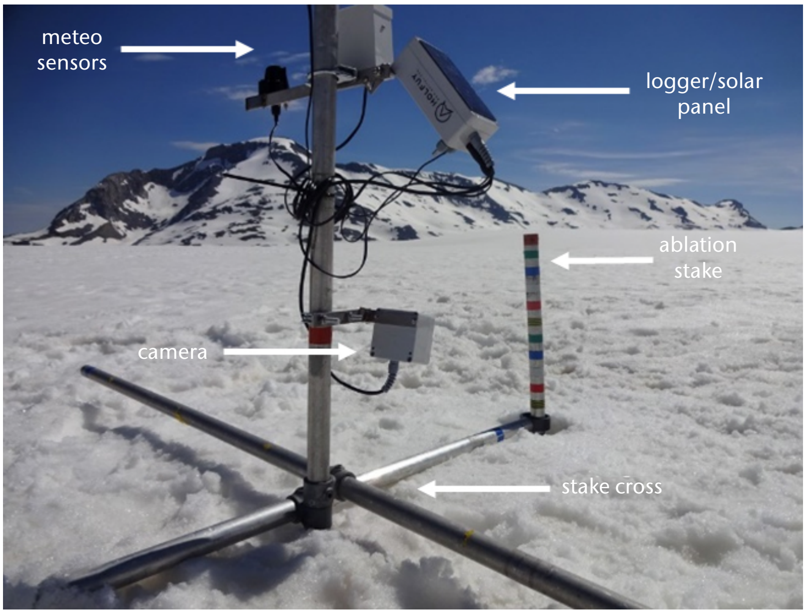

Figure 3.28. System for automated ablation measurements based on a camera observing a mass-balance stake

Source: Landmann et al., 2021

(c) **Camera observing stake.** Another concept to automatically observe ablation in near-real time is the use of an automatic camera observing a mass-balance stake (Landmann et al., 2021). A solar-powered camera is mounted on a tripod sitting on the ice surface, which is loosely attached to a mass-balance stake (Figure 3.28). The system is lightweight (around 2 kg total) and can easily be deployed with conventional mass-balance stakes. If the camera is mounted on a separate, stake fixed about 5 m from the mass-balance stake, the system is also able to observe snow accumulation during the winter season. Readings of the ablation rate based on the pictures are either performed visually or supported by automated tools using image processing (Sold et al., 2021).

3.8.5 Sources of error and uncertainties

Sources of error and misinterpretation can occur with all these methods. For the pressure transducer, the hose has to be filled with sufficient antifreeze to ensure that the membrane of the sensor does not get impacted by brittle failure. Furthermore, a pressure correction with the air pressure has to be performed to derive relative pressure changes due to ice-surface lowering instead of the sum of air pressure changes and ice-surface lowering (Fausto et al., 2012).

For draw-wire sensors, one challenge is the physical set-up and the requirement of a stable structure that can sustain the rather bulky sensor. If the structure moves and the wire does not enter the hole vertically, some artefacts and unrealistic surface changes can occur.

Along the same lines, camera-based measurements require a set-up that prevents significant tilting of the structure, such that the target stake remains visible in the footage.

Fausto et al. (2012) estimate that the accuracy of ablation values obtained with pressure transducers is comparable to the accuracy from sonic ranging, and a temporal drift of 1.6% over a 4-year period is given. For draw-wire sensors, Hulth (2010) estimates an absolute error of around ±10 cm for the measurement range of the sensor. Errors on short timescales (days) are assumed to be at least one order of magnitude smaller. The automated cameras yield uncertainties of ±1.5 cm per day (Landmann et al., 2021).

3.9 CALCULATING MASS BALANCE

3.9.1 Methods to display and calculate mass balance

When winter and summer balances have been calculated at each stake location, the data are used to obtain the mass balance of the entire glacier. The profile and contour methods are commonly used to plot and analyse mass-balance data. Statistical approaches and model-based extrapolation are also used.

Profile method. This method involves plotting the point data on winter, summer and annual balance versus elevation. This is often suitable for individual glaciers or for separate ice-flow basins on ice caps. Mass-balance values representative for each 100 m (or narrower) elevation band are used together with data on the glacier hypsometry – the distribution of area with elevation – to calculate the volume added to or lost from each elevation band. The total volume added to or lost from the entire glacier is then obtained by summation and divided by the total area to yield the average water equivalent accumulation (or ablation) over the entire glacier. The winter, summer and annual balances are then calculated taking into account the specifics of the time system used (Section 3.6).

Figure 3.29 illustrates this method with an example from the Sátujökull basin of the Hofsjökull ice cap, Iceland. The increase of the winter balance with elevation can be approximated with a linear function (Figure 3.29 (b)), and the summer balance with two linear fits with different slopes. For the case shown, the summer balance is positive above 1 550 m elevation but negative below 1 550 m. The change in slope at 1 300 m is due to faster melting of glacier ice exposed in the ablation zone below 1 300 m during the latter part of the ablation season, when the winter layer has melted. The black line shows the net balance, from which the *equilibrium line altitude (ELA)*, where net balance is zero, can be inferred to lie at 1 275 m in 2020. Together with the area-elevation distribution for this part of Hofsjökull (Figure 3.29 (a)), the point data allow calculation of area-averaged winter, summer and annual balances for the entire basin.

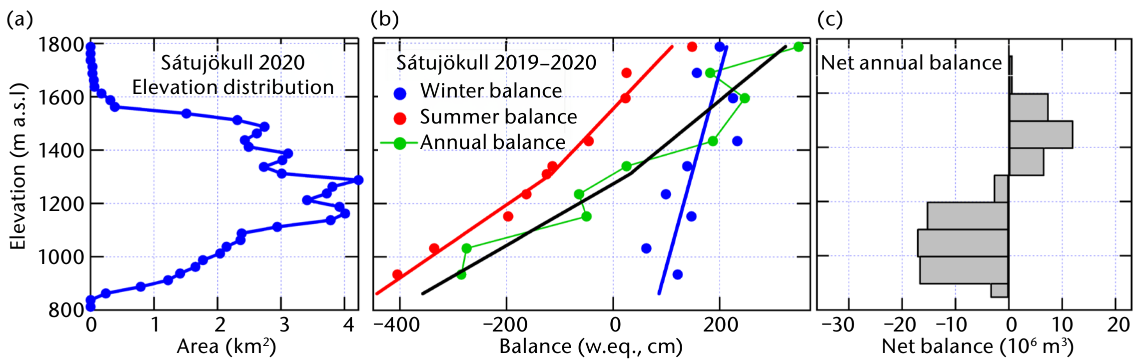

Figure 3.29. (a) The elevation distribution on Sátujökull, a northern transect of the Hofsjökull ice cap, central Iceland. Dots indicate areas of each 25-m elevation band in the altitude interval 800–1 800 m. Total area in 2020: 72.8 km^2. (b) Point values of winter, summer and annual balance on a north–south transect covering Sátujökull, plotted against elevation. (c) The total volume added or lost in each 100-m elevation band during the glaciological year 2019–2020. Results calculated using the *floating date system* (Section 3.6.2).

Source: Data from Icelandic Meteorological Office

Contour method. Another method is based on drawing mass-balance isolines (lines of equal mass balance) onto a map of the glacier, based on the point data. This can be done with GIS software. This method is particularly suitable for ice caps, but can be used for glaciers of all sizes. Separate maps can be made for winter, summer and annual balance. The drawing of isolines requires knowledge of conditions on the glacier, for example, of the effects of surface topography and prevailing winds on the distribution of snow accumulation. The area of each interval between two mass-balance isolines is then multiplied by the value represented by those lines and summation over the entire area yields the mass balance of the glacier. See example in Figure 3.30.

Statistical approaches. Several statistical approaches of varying complexity have been developed to infer glacier-wide mass balance from point measurements. For example, extrapolation to the spatial scale based on Kriging is a powerful approach when there is a relatively dense network of mass-balance stakes (see, for example, Hock and Jensen, 1999). However, simple approaches such as the linear mass-balance model originally proposed by Lliboutry (1974) are also used (see, for example, Thibert et al., 2008). No complete spatial extrapolation of mass balance is attempted in this approach but the spatio-temporal variability in glacier-wide mass balance is directly derived from point measurements. This method is also applicable for networks with relatively few index stakes (Van Beusekom et al., 2010; O'Neel et al., 2019). Terrain-based (or 'topographic') regression approaches can also be used to

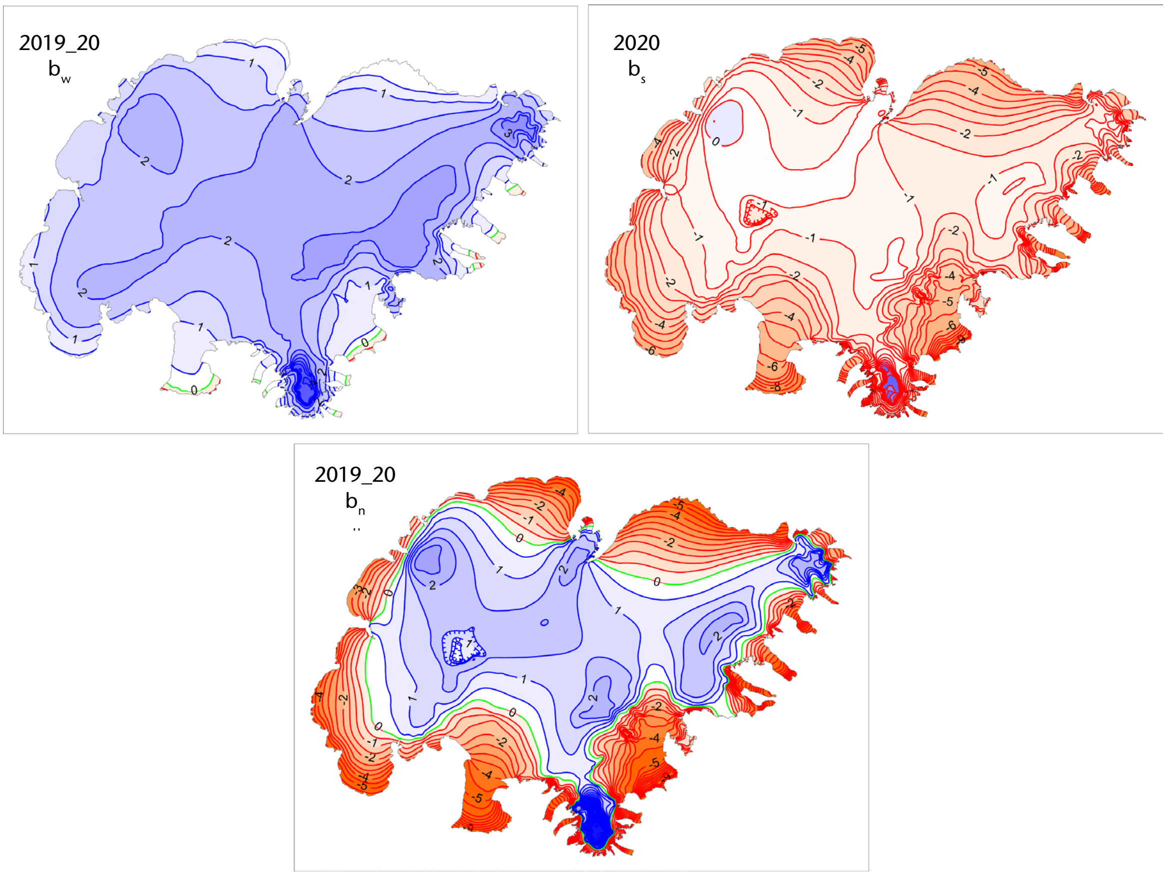

Figure 3.30 Winter, summer and annual surface mass balance of the 7 700 km² Vatnajökull ice cap, Iceland, in the glaciological year 2019–2020, displayed with the *contour method*. Winter balance averages B_w = 1.62 m w.e. for the whole ice cap in this year. Summer balance averages B_s = –2.02 m w.e. and is negative over the entire ice cap except at elevations above 1 900 m. Net annual balance averages B_a = –0.40 m w.e. Climatic regimes on Vatnajökull vary widely, and thus ELA on the main outlets typically ranges between 1 100 m and 1 500 m, displaying significant interannual variability.

Source: Glaciology group, Institute of Earth Sciences, University of Iceland extrapolate winter balances. This approach requires relatively extensive data but reproduces observed patterns of spatial variability. It has been used with GPR data sets (for example, McGrath et al., 2015, 2018; Sold et al., 2016) and traditional snow-pit and probe datasets (for example, Pulwicki et al., 2018, 2019).

Model-based extrapolation. Extending the above approaches, a combination of daily mass-balance modelling constrained with point observations in the field is also used (see, for example, Huss et al., 2009, 2021; Barandun et al., 2015). The basic approach is to use a daily distributed accumulation and temperature-index melt model to infer mass balances in unmeasured regions and to optimize it to agree with all seasonal point measurements that are available (Figure 3.31). The mass-balance model is not regarded as a physical model, but as a statistical tool for obtaining a daily temporal resolution based on seasonal field data and spatial interpolation of point measurements supported by a model. The advantages are, for example, that both winter and annual point data can be incorporated into the same evaluation scheme, allowing consistent analysis for all glaciers of a monitoring network. Furthermore, mass-balance components (accumulation and ablation) can be separated based on the model constrained with seasonal observations, and glacier-wide mass balance can be extracted over arbitrary time periods (for example, the hydrological year), which is important for intercomparing the signals of different glaciers.

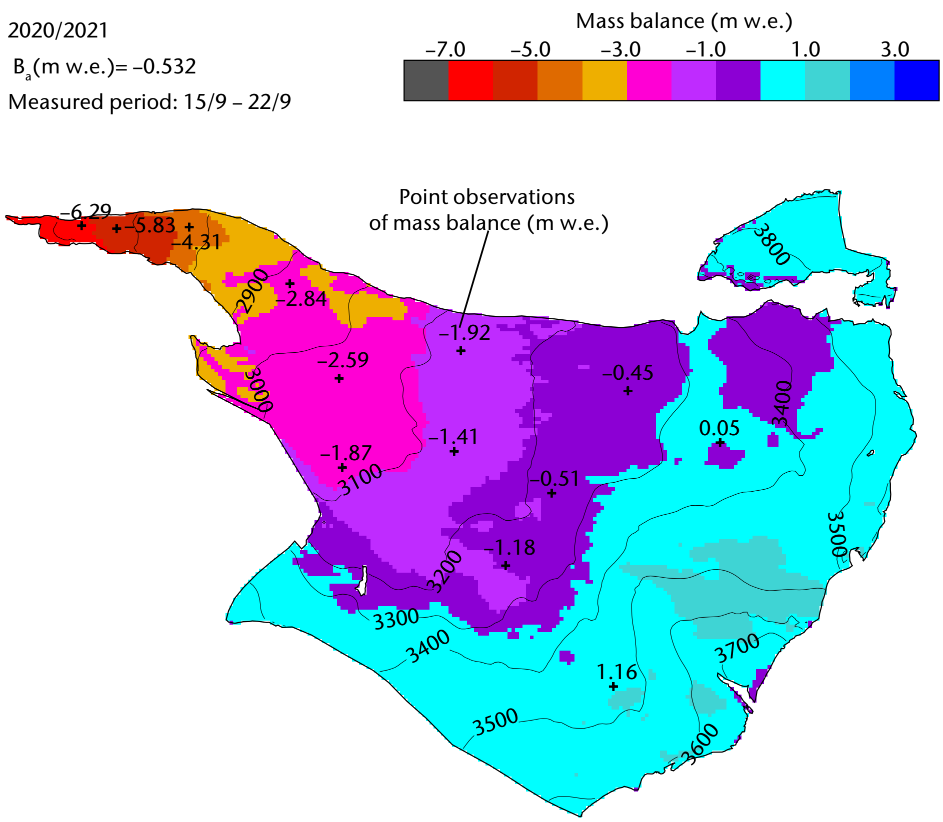

Figure 3.31. Model-based extrapolation of measured point mass balance on Findel Glacier, Switzerland. Annual observations are indicated by crosses and the measured point mass balance is stated in m w.e. The spatial mass balance variability is given by the daily mass-balance model, which includes the observed patterns of winter snow distribution as well as other relevant factors governing the spatial variability in mass balance (such as elevation, solar radiation and surface albedo).

Source: Glacier Monitoring Switzerland (GLAMOS)

3.9.2 Geodetic methods to determine mass balance

The mass balance of a glacier over a specific time interval can be calculated based on repeated measurements of the surface elevation and the derived volume change that has occurred between the two surveys. This is referred to as the *geodetic method*. In general, it is possible to discern between (mainly) airborne geodetic surveys used for validation and calibration of glaciological mass-balance series (see, for example, Zemp et al., 2013) and (mainly) spaceborne geodetic surveys for regional mass-change estimates (see, for example, Brun et al., 2017). Recent developments in satellite processing have made it possible to map surface elevation changes at a high spatio-temporal resolution over all glaciers on the Earth (Hugonnet et al. 2021).

For glaciological mass-balance sites it is recommended to conduct geodetic surveys roughly at 10-year intervals (Zemp et al., 2013). To calculate the geodetic mass balance, the change in surface elevation must be converted to a mass change using a density conversion factor (see below). It is also possible obtain annual and even seasonal signals from the geodetic method (Belart et al., 2017; Klug et al., 2018; Pelto et al., 2019). Recent work on Wolverine Glacier, Alaska, demonstrates the potential of using repeat DEMs from lidar surveys and high-resolution satellite imagery to calculate distributed seasonal balances, taking into account the vertical component of ice flow and firn densification (Zeller et al., 2022).

Many different data sources can be used to map the glacier surface elevation: ground surveys (see, for example, Kapitsa et al., 2020), UAV surveys and aerial photographs (see, for example, Geissler et al., 2021), satellite images (optical and radar) (see, for example, Berthier et al., 2014; Brun et al., 2017) and lidar surveys (see, for example, Barrand et al., 2009; Klug et al., 2018). Surveys can cover the entire glacier or be conducted on transects resulting in elevation profiles, point clouds or regular grids of surface elevations. The data source will depend on the size of the glacier or region and on the instruments/resources available. A very small glacier may be mapped entirely using UAV or terrestrial laser scanning; the mass balance of medium sized glaciers may be mapped using aerial photos or airborne laser scanning, whereas larger regions are most efficiently mapped using satellite images. The optimum timing for carrying out geodetic surveys is the end of the ablation season. Surveying results from the two different points in time are usually converted to DEMs before the two DEMs are differenced applying the same datum and projection using GIS software (Figures 3.31 and 3.32). Misalignment between DEMs should be accounted for by co-registering the DEMs. A common way to do this is to compare stable terrain outside the glacier and check for misalignments (Nuth and Kääb, 2011). Systematic and random errors in the geodetic method can be assessed (see, for example, Zemp et al., 2013), especially when comparing with glaciological observations (see Section 3.9.4).

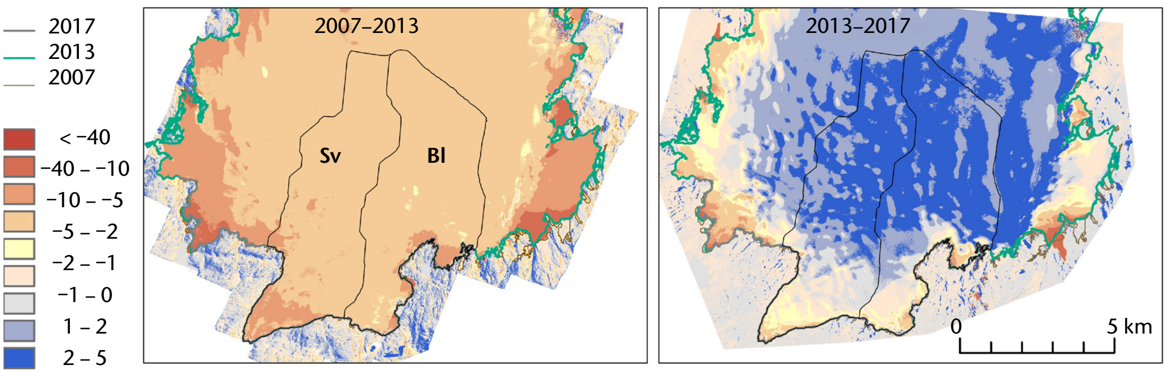

Figure 3.32. Example of elevation changes of the southern part of Søndre (Southern) Folgefonna, Norway, 2007–2013 and 2013–2017 based on differencing of DEMs derived from airborne laser scanning in 2007, 2013 and 2017. The glacier basins of Svelgjabreen (Sv) and Blomstølskardsbreen (Bl) are marked.

Source: Andreassen et al. (2020), reproduced with permission from the Journal of Glaciology

Glacier masks (polygons) are derived from the glacier outlines (Section 3.3.2) for the two periods. When ice divides are used for the delineation of glaciers, the same ice divide should be used for both periods. If profiles are used for one or both surveys, the point datasets (from repeated profile mapping) or point dataset versus DEM dataset are differenced, and the resulting point data differences are interpolated to yield glacier-wide averages.

The geodetic mass balance, B_{geod} (in m w.e. a^{-1}), is calculated by multiplying the volume change, ΔV, by a density conversion factor, $f_{\Delta V}$, and then dividing by the average glacier area of the two surveys (assuming linear area change with time) A_m, and the time interval Δt between the two surveys:

$$B_{geod} = \left(\Delta V \cdot f_{\Delta V}\right) / \left(A_m \cdot \Delta t\right) \tag{3.4}$$

The density conversion factor $f_{\Delta V}$ is often set to 850 ± 60 kg m^{-3} (Huss, 2013), accounting for changes in firn volume and density that occur simultaneously with a reduction or an increase in glacier volume. However, over short time intervals (<5 years) and for small volume changes, values of $f_{\Delta V}$ may strongly deviate from the recommended reference value and can thus represent an important source of uncertainty.

3.9.3 Detecting and correcting bias in glaciological mass-balance records

To ensure the long-term consistency of glaciological mass-balance series, a periodical validation against independent geodetic surveys is important to detect biases (see, for example, Zemp et al., 2013). A bias in glaciological surveys is not uncommon as a glacier-wide assessment of point measurements requires extrapolation. Therefore, the homogenization and reanalysis of mass-balance records is highly relevant and frequently conducted in monitoring programmes (see, for example, Cox and March, 2004; Huss et al., 2009; Zemp et al., 2010; Andreassen et al., 2016b; O'Neel et al., 2019). The basic concept is to compare cumulative mass change from annual glaciological surveys with geodetic mass change over the same period. Whereas the glaciological mass balance provides a high temporal resolution, as well as the spatial distribution of mass-balance components, geodetic surveys more accurately capture the mass change signal of the entire glacier.

Before comparing cumulative annual mass balances to geodetic ice-volume changes, differences in the dates of these independent data acquisition methods need to be taken into account. This can be achieved by adding total mass change as computed by a mass-balance model for the period between the acquisition date of the geodetic survey and the date of field measurements.

In the ideal case, the cumulative direct mass balance coincides with the geodetic mass change. Zemp et al. (2013) provide a detailed framework for deciding whether a misfit between cumulative glaciological mass balance and geodetic mass changes is significant and should be corrected. This mainly depends on the estimated uncertainties in direct point observations and the mass balance extrapolated to the whole glacier, and the uncertainty in geodetic ice-volume change. If there is a significant bias between glaciological and geodetic series, it is suggested that the interpolation of in situ point mass balance to the entire glacier be updated in order to yield a corrected cumulative series better matching the geodetic mass changes.

Figure 3.33 shows the comparison of long-term annual in situ measurements of mass balance (blue) with independent volume changes derived from geodetic surveys (red) on Allalingletscher, Switzerland. In most periods, the agreement between cumulative annual mass balance based on the direct measurements and remotely-sensed elevation change is satisfactory and no adjustment of the glaciological data series was needed (Huss et al., 2015).

3.9.4 Uncertainty in mass changes determined based on the geodetic method

A detailed assessment of the uncertainties is necessary when applying the geodetic method for estimating mass changes. As the approaches to derive DEMs are manifold – ranging from terrestrial and aerial photogrammetry to satellite radar and altimetry – it is beyond the scope of the present chapter to provide a comprehensive description of methodologies to determine

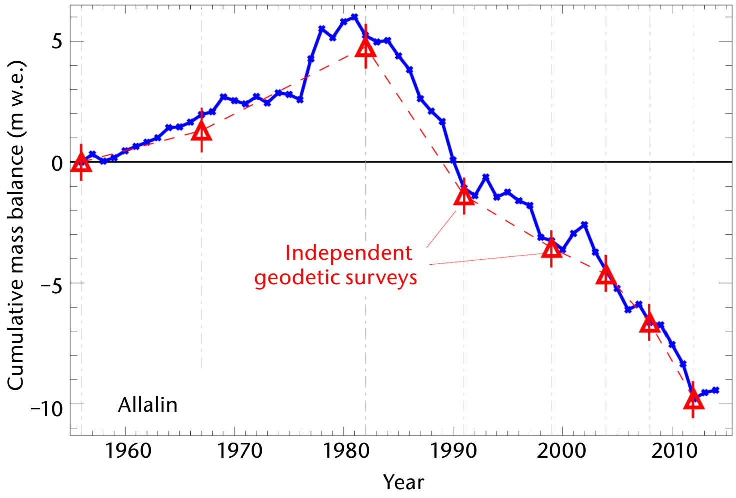

Figure 3.33. Allalingletscher, Switzerland: Comparison of annual mass-balance series derived based on the glaciological method (blue) with independent ice-volume changes (red) based on periodic geodetic surveys

Source: Huss et al. (2015)

uncertainties. Nevertheless, there are some important general aspects that characterize the uncertainties in the geodetic method. It is possible to differentiate between uncertainties due to: (1) random errors in local surface elevation, (2) systematic errors at the scale of entire glaciers or regions, (3) effects of inaccurate glacier outlines, and (4) the conversion from volume to mass change. Whereas for (1) the quality and resolution of the available imagery and the conditions during acquisition are relevant, co-registration of the digital elevation models, as well as potential biases (for example, due to radar wave penetration into snow and firn) need to be considered for (2). For more details regarding the individual processes that define overall uncertainty, as well as their estimation and combination, the reader can consult references such as Rolstad et al. (2009), Nuth and Kääb (2011) and Joerg et al. (2012). Hugonnet et al. (2022) provide a comprehensive overview to reconcile the uncertainties of the geodetic method from the local to the regional scale.

APPENDIX. SAFETY MEASURES DURING FIELDWORK ON GLACIERS

Purpose

Working on and around glaciers presents numerous hazards – crevasses, sudden glacier floods, harsh weather and ice avalanches to name a few. It is therefore essential that personnel conducting glaciological fieldwork have relevant knowledge of conditions on glaciers, receive appropriate training and have full access to safety equipment (Figure 3.34). Training should be offered on a regular basis.

This summary is based on a document made for employees at the Norwegian Water Resources and Energy Directorate (NVE) and includes a short listing of essential equipment, knots and skills required for safe glacier travel. Basic knowledge for employees who perform fieldwork on glaciers is also outlined. Other proven techniques with equivalent or better function can also be used. A full translation is available at: https://www.nve.no/hydrology/glaciers/safety-on-and-near-glaciers/.

Personal safety equipment required for work on glaciers

- 1 rope (30 m × 9 mm). Minimum "rando"-rated (marked 0), preferably rated as a half rope (1/2). Maximum age 10 years.
- 2 progress-capture pulleys
- 1 rope clamp (Tiblock)
- 2 short slings (30 cm) (or small ropes for tying in/friction hitch – 1.2 m × 5 mm). Maximum age 10 years.
- 2 long slings (120 cm) (or rope sling of 9 mm rope adjusted for body length). Maximum age 10 years.
- 6 locking carabiners; 5 screw-lock carabiners and 1 HMS carabiner
- 2 ice screws ~21 cm

Figure 3.34. Walking on a snow-covered glacier in rope, with equipment easily available in harness and ice axe as well as probe in hand. Here two ropes are used, one with knots used to create friction.

Source: Liss M. Andreassen

– 1 harness; maximum age 10 years

– 1 pair of crampons

– 1 snow anchor

– 1 gear bag

Knots

– Loop (roping inn, anchoring), see: https://www.animatedknots.com/figure-8-follow-through-loop-knot

– Double or single fisherman's knot (for joining ropes), see: http://www.animatedknots.com/doublefishermans

– Friction knot (prusik, French prusik) – roping in/self-belay, see: http://www.animatedknots.com/prusik

– Munter hitch (descent, rapell), see: http://www.animatedknots.com/muntermule

– Double half hitch, see: http://www.animatedknots.com/clovehalfhitches

Recommended gear for the harness

– Travel on foot on bare ice: minimum one ice screw and one long sling for self-securing when falling into a crevasse or when stuck

– On skis or foot on snow: minimum one ice screw and one long sling for self-securing when falling into a crevasse

– Helicopter snow/ice: empty harness, with all gear easily available inside the helicopter

– Snow Scooter: empty harness, with all gear easily available on the scooter

Important field techniques

– Setting up anchoring points
– Securing buddies from anchoring points
– Intermediate anchoring
– Hauling systems for crevasse rescue
– Rappelling
– Two-person rope teams for snow
– Rescue in two-person rope team
– Ascending a rope using prusik knots
– Moving in and out of a helicopter on glaciers

Other resources for safety best practice guides

- Safety tips and techniques for glacier travel on skis: https://www.petzl.com/GB/en/Sport

REFERENCES

Andreassen, L. M.; Huss, M.; Melvold, K. et al. Ice Thickness Measurements and Volume Estimates for Glaciers in Norway. *Journal of Glaciology* **2015**, *61* (228), 763–775. https://doi.org/10.3189/2015JoG14J161.

Andreassen, L. M.; Elvehøy, H.; Jackson, M. et al. *Glaciological Investigations in Norway 2011–2015*; Report 88-2016; Kjøllmoen, B., Ed.; Norwegian Water Resources and Energy Directorate: Oslo, 2016a. https://nve.brage.unit.no/nve-xmlui/handle/11250/2634000.

Andreassen, L. M.; Elvehøy, H.; Kjøllmoen, B. et al. Reanalysis of Long-Term Series of Glaciological and Geodetic Mass Balance for 10 Norwegian Glaciers. *The Cryosphere* **2016b**, *10* (2), 535–552. https://doi.org/10.5194/tc-10-535-2016.

Andreassen, L. M.; Elvehøy, H.; Kjøllmoen, B. et al. Glacier Change in Norway since the 1960s – an Overview of Mass Balance, Area, Length and Surface Elevation Changes. *Journal of Glaciology* **2020**, *66* (256), 313–328. https://doi.org/10.1017/jog.2020.10.

Andreassen, L. M.; Nagy, T.; Kjøllmoen, B. et al. An Inventory of Norway's Glaciers and Ice-Marginal Lakes from 2018–19 Sentinel-2 Data. *Journal of Glaciology* **2022**, *68* (272), 1085–1106. https://doi.org/10.1017/jog.2022.20.

Annan, A. P.; Cosway, S. W.; Sigurdsson, T. *GPR for Snow Pack Water Content*; European Association of Geoscientists & Engineers, 1994; cp. https://doi.org/10.3997/2214-4609-pdb.300.33.

Barandun, M.; Huss, M.; Sold, L. et al. Re-Analysis of Seasonal Mass Balance at Abramov Glacier 1968–2014. *Journal of Glaciology* **2015**, *61* (230), 1103–1117. https://doi.org/10.3189/2015JoG14J239.

Barrand, N. E.; Murray, T.; James, T. D. et al. Optimizing Photogrammetric DEMs for Glacier Volume Change Assessment Using Laser-Scanning Derived Ground-Control Points. *Journal of Glaciology* **2009**, *55* (189), 106–116. https://doi.org/10.3189/002214309788609001.

Bauder, A.; Funk, M.; Huss, M. Ice-Volume Changes of Selected Glaciers in the Swiss Alps since the End of the 19th Century. *Annals of Glaciology* **2007**, *46*, 145–149. https://doi.org/10.3189/172756407782871701.

Bauder, A.; Mazzotti, G.; Berger, C. et al. Winter Accumulation Measurements on Alpine Glaciers Using Ground Penetrating Radar. In *2018 17th International Conference on Ground Penetrating Radar (GPR)*; 2018; 1–5. https://doi.org/10.1109/ICGPR.2018.8441559.

Belart, J. M. C.; Berthier, E.; Magnússon, E. et al. Winter Mass Balance of Drangajökull Ice Cap (NW Iceland) Derived from Satellite Sub-Meter Stereo Images. *The Cryosphere* **2017**, *11* (3), 1501–1517. https://doi.org/10.5194/tc-11-1501-2017.

Berthier, E.; Vincent, C.; Magnússon, E. et al. Glacier Topography and Elevation Changes Derived from Pléiades Sub-Meter Stereo Images. *The Cryosphere* **2014**, *8* (6), 2275–2291. https://doi.org/10.5194/tc-8-2275-2014.

Björnsson, H. *Hydrology of Ice Caps in Volcanic Regions*; Rit / Vísindafélag íslendinga ; 45; Societas Scientarium Islandica, University of Iceland: Reykjavík, 1988.

Björnsson, H.; Pálsson, F. Radio-Echo Soundings on Icelandic Temperate Glaciers: History of Techniques and Findings. *Annals of Glaciology* **2020**, *61* (81), 25–34. https://doi.org/10.1017/aog.2020.10.

Brun, F.; Berthier, E.; Wagnon, P. et al. A Spatially Resolved Estimate of High Mountain Asia Glacier Mass Balances from 2000 to 2016. *Nat. Geosci.* **2017**, *10* (9), 668–673. https://doi.org/10.1038/ngeo2999.

Claerbout, J. F. *Imaging the Earth's Interior*; Blackwell Scientific Publications, Ltd.: Oxford, 1985.

Cogley, J. G.; Hock, R.; Rasmussen, L. A. et al. *Glossary of Glacier Mass Balance and Related Terms*; International Hydrological Programme (IHP) of the United Nations Educational, Scientific and Cultural Organization (UNESCO), 2011. https://unesdoc.unesco.org/ark:/48223/pf0000192525.

Cox, L. H.; March, R. S. Comparison of Geodetic and Glaciological Mass-Balance Techniques, Gulkana Glacier, Alaska, U.S.A. *Journal of Glaciology* **2004**, *50* (170), 363–370. https://doi.org/10.3189/172756504781829855.

Eythórsson, J. Variations of Glaciers in Iceland, 1930–47. *Journal of Glaciology* **1949**, *1* (5), 250–252. https://doi.org/10.3189/002214349793702764.

Farinotti, D.; Brinkerhoff, D. J.; Clarke, G. K. C. et al. How Accurate Are Estimates of Glacier Ice Thickness? Results from ITMIX, the Ice Thickness Models Intercomparison eXperiment. *The Cryosphere* **2017**, *11* (2), 949–970. https://doi.org/10.5194/tc-11-949-2017.

Farinotti, D.; Huss, M.; Fürst, J. J. et al. A Consensus Estimate for the Ice Thickness Distribution of All Glaciers on Earth. *Nature Geoscience* **2019**, *12* (3), 168–173. https://doi.org/10.1038/s41561-019-0300-3.

Fausto, R. S.; As, D. V.; Ahlstrøm, A. P. et al. Assessing the Accuracy of Greenland Ice Sheet Ice Ablation Measurements by Pressure Transducer. *Journal of Glaciology* **2012**, *58* (212), 1144–1150. https://doi.org/10.3189/2012JoG12J075.

Fausto, R. S.; van As, D.; Mankoff, K. D. et al. Programme for Monitoring of the Greenland Ice Sheet (PROMICE) Automatic Weather Station Data. *Earth System Science Data* **2021**, *13* (8), 3819–3845. https://doi.org/10.5194/essd-13-3819-2021.

Fierz, C.; Armstrong, R. L.; Durand, Y. et al. *The International Classification for Seasonal Snow on the Ground*; Technical documents in hydrology; 2009; Vol. 83. https://unesdoc.unesco.org/ark:/48223/pf0000186462.

Fischer, A.; Markl, G. Mass Balance Measurements on Hintereisferner, Kesselwandferner, and Jamtalferner 2003 to 2006. *Zeitschrift für Gletscherkunde und Glazialgeologie* **2009**, *42*, 47–83.

Fischer, M.; Huss, M.; Barboux, C. et al. The New Swiss Glacier Inventory SGI2010: Relevance of Using High-Resolution Source Data in Areas Dominated by Very Small Glaciers. *Arctic, Antarctic, and Alpine Research* **2014**, *46* (4), 933–945. https://doi.org/10.1657/1938-4246-46.4.933.

Forel, F.-A. *Les Variations Périodiques des Glaciers*. Extraits des Archives des sciences physiques et naturelles, XXXIV, 209. Commission Internationale des Glaciers: Geneva, 1895.

Gärtner-Roer, I.; Naegeli, K.; Huss, M. et al. A Database of Worldwide Glacier Thickness Observations. *Global and Planetary Change* **2014**, *122*, 330–344. https://doi.org/10.1016/j.gloplacha.2014.09.003.

Gärtner-Roer, I.; Bast, A. (Ground) Ice in the Proglacial Zone. In *Geomorphology of Proglacial Systems: Landform and Sediment Dynamics in Recently Deglaciated Alpine Landscapes*; Heckmann, T., Morche, D., Eds.; Geography of the Physical Environment; Springer International Publishing: Cham, 2019; 85–98. https://doi.org/10.1007/978-3-319-94184-4_6.

Geibel, L.; Huss, M.; Kurzböck, C. et al. Rescue and Homogenisation of 140 Years of Glacier Mass Balance Data in Switzerland. *Glaciology* **2022** [preprint]. https://doi.org/10.5194/essd-2022-56.

Geissler, J.; Mayer, C.; Jubanski, J. et al. Analyzing Glacier Retreat and Mass Balances Using Aerial and UAV Photogrammetry in the Ötztal Alps, Austria. *The Cryosphere* **2021**, *15* (8), 3699–3717. https://doi.org/10.5194/tc-15-3699-2021.

Geist, T.; Elvehøy, H.; Jackson, M. et al. Investigations on Intra-Annual Elevation Changes Using Multi-Temporal Airborne Laser Scanning Data: Case Study Engabreen, Norway. *Annals of Glaciology* **2005**, *42*, 195–201. https://doi.org/10.3189/172756405781812592.

Glacier Monitoring Switzerland (GLAMOS). *Revised Strategy for Monitoring Glacier Length Variation*; Internal Report No 4; GLAMOS: 2020. http://doi.org/10.18752/intrep_4.

Global Land Ice Measurements from Space (GLIMS). *Home* page. http://www.glims.org/.

Grab, M.; Mattea, E.; Bauder, A. et al. Ice Thickness Distribution of All Swiss Glaciers Based on Extended Ground-Penetrating Radar Data and Glaciological Modeling. *Journal of Glaciology* **2021**, *67* (266), 1074–1092. https://doi.org/10.1017/jog.2021.55.

Grasegger, K.; Strapazzon, G.; Procter, E. et al. Avalanche Survival After Rescue with the RECCO Rescue System: A Case Report. *Wilderness & Environmental Medicine* **2016**, *27* (2), 282–286. https://doi.org/10.1016/j.wem.2016.02.004.

Hannesdóttir, H.; Sigurðsson, O.; Þrastarson, R. H. et al. A National Glacier Inventory and Variations in Glacier Extent in Iceland from the Little Ice Age Maximum to 2019. *Jök* **2020**, *70* (1), 1–34. https://doi.org/10.33799/jokull2020.70.001.

Hattersley-Smith, G. The Symposium on Glacier Mapping. *Can. J. Earth Sci.* **1966**, *3* (6), 737–741. https://doi.org/10.1139/e66-055.

Helfricht, K.; Huss, M.; Fischer, A. et al. Calibrated Ice Thickness Estimate for All Glaciers in Austria. *Frontiers in Earth Science* **2019**, *7*, 68. https://doi.org/10.3389/feart.2019.00068.

Hock, R.; Jensen, H. Application of Kriging Interpolation for Glacier Mass Balance Computations. *Geografiska Annaler: Series A, Physical Geography* **1999**, *81* (4), 611–619.

Hock, R.; Bliss, A.; Marzeion, B. et al. GlacierMIP – A Model Intercomparison of Global-Scale Glacier Mass-Balance Models and Projections. *Journal of Glaciology* **2019**, *65* (251), 453–467. https://doi.org/10.1017/jog.2019.22.

Hugonnet, R.; McNabb, R.; Berthier, E. et al. Accelerated Global Glacier Mass Loss in the Early Twenty-First Century. *Nature* **2021**, *592* (7856), 726–731. https://doi.org/10.1038/s41586-021-03436-z.

Hugonnet, R.; Brun, F.; Berthier, E. et al. Uncertainty Analysis of Digital Elevation Models by Spatial Inference From Stable Terrain. IEEE *Journal of Selected Topics in Applied Earth Observations and Remote Sensing* **2022**, *15*, 6456–6472. https://doi.org/10.1109/JSTARS.2022.3188922.

Hulth, J. Using a Draw-Wire Sensor to Continuously Monitor Glacier Melt. *Journal of Glaciology* **2010**, *56* (199), 922–924. https://doi.org/10.3189/002214310794457290.

Huss, M. Density Assumptions for Converting Geodetic Glacier Volume Change to Mass Change. The *Cryosphere* **2013**, *7* (3), 877–887. https://doi.org/10.5194/tc-7-877-2013.
Huss, M.; Bauder, A.; Funk, M. Homogenization of Long-Term Mass-Balance Time Series. Annals of *Glaciology* **2009**, *50* (50), 198–206. https://doi.org/10.3189/172756409787769627.
Huss, M.; Dhulst, L.; Bauder, A. New Long-Term Mass-Balance Series for the Swiss Alps. *Journal of Glaciology* **2015**, *61* (227), 551–562. https://doi.org/10.3189/2015JoG15J015.
Huss, M.; Bauder, A.; Linsbauer, A. et al. More than a Century of Direct Glacier Mass-Balance Observations on Claridenfirn, Switzerland. *Journal of Glaciology* **2021**, *67* (264), 697–713. https://doi.org/10.1017/jog.2021.22.
Intergovernmental Panel on Climate Change (IPCC). *Climate Change 2021 – The Physical Science Basis: Working Group I Contribution to the Sixth Assessment Report of the Intergovernmental Panel on Climate Change*; Masson-Delmotte, V., Zhai P., Pirani A. et al., Eds.; Cambridge University Press: Cambridge, UK, and New York, USA, 2021. https://doi.org/10.1017/9781009157896.
Joerg, P. C.; Morsdorf, F.; Zemp, M. Uncertainty Assessment of Multi-Temporal Airborne Laser Scanning Data: A Case Study on an Alpine Glacier. *Remote Sensing of Environment* **2012**, *127*, 118–129. https://doi.org/10.1016/j.rse.2012.08.012.
Jóhannesson, T.; Björnsson, H.; Magnússon, E. et al. Ice-Volume Changes, Bias Estimation of Mass-Balance Measurements and Changes in Subglacial Lakes Derived by Lidar Mapping of the Surface of Icelandic Glaciers. *Annals of Glaciology* **2013**, *54* (63), 63–74. https://doi.org/10.3189/2013AoG63A422.
Kapitsa, V.; Shahgedanova, M.; Severskiy, I. et al. Assessment of Changes in Mass Balance of the Tuyuksu Group of Glaciers, Northern Tien Shan, Between 1958 and 2016 Using Ground-Based Observations and Pléiades Satellite Imagery. *Frontiers in Earth Science* **2020**, *8*. https://www.frontiersin.org/articles/10.3389/feart.2020.00259.
Kaser, G.; Fountain, A.; Jansson, P. et al. *A Manual for Monitoring the Mass Balance of Mountain Glaciers with Particular Attention to Low Latitude Characteristics*; SC.2003/WS/4; 2003; 137. https://unesdoc.unesco.org/ark:/48223/pf0000129593.
Kienholz, C.; Rich, J. L.; Arendt, A. A. et al. A New Method for Deriving Glacier Centerlines Applied to Glaciers in Alaska and Northwest Canada. *The Cryosphere* **2014**, *8* (2), 503–519. https://doi.org/10.5194/tc-8-503-2014.
Klug, C.; Bollmann, E.; Galos, S. P. et al. Geodetic Reanalysis of Annual Glaciological Mass Balances (2001–2011) of Hintereisferner, Austria. *The Cryosphere* **2018**, *12* (3), 833–849. https://doi.org/10.5194/tc-12-833-2018.
Kohler, J.; Moore, J.; Kennett, M. et al. Using Ground-Penetrating Radar to Image Previous Years' Summer Surfaces for Mass-Balance Measurements. *Annals of Glaciology* **1997**, *24*, 355–360. https://doi.org/10.3189/S0260305500012441.
Kurzböck, C.; Huss, M. *A Best Practice Guide for Long-Term Glacier Monitoring in Switzerland*. **2021**, 60 pp. https://doi.org/10.18752/INTREP_5.
Landmann, J. M.; Künsch, H. R.; Huss, M. et al. Assimilating Near-Real-Time Mass Balance Stake Readings into a Model Ensemble Using a Particle Filter. *The Cryosphere* **2021**, *15* (11), 5017–5040. https://doi.org/10.5194/tc-15-5017-2021.
Lapazaran, J. J.; Otero, J.; Martín-Español, A. et al. On the Errors Involved in Ice-Thickness Estimates I: Ground-Penetrating Radar Measurement Errors. *Journal of Glaciology* **2016**, *62* (236), 1008–1020. https://doi.org/10.1017/jog.2016.93.
Leclercq, P. W.; Oerlemans, J.; Basagic, H. J. et al. A Data Set of Worldwide Glacier Length Fluctuations. *The Cryosphere* **2014**, *8* (2), 659–672. https://doi.org/10.5194/tc-8-659-2014.
Leigh, J. R.; Stokes, C. R.; Carr, R. J. et al. Identifying and Mapping Very Small (<0.5 Km2) Mountain Glaciers on Coarse to High-Resolution Imagery. *Journal of Glaciology* **2019**, *65* (254), 873–888. https://doi.org/10.1017/jog.2019.50.
Lindbäck, K.; Kohler, J.; Pettersson, R. et al. Subglacial Topography, Ice Thickness, and Bathymetry of Kongsfjorden, Northwestern Svalbard. *Earth System Science Data* **2018**, *10* (4), 1769–1781. https://doi.org/10.5194/essd-10-1769-2018.
Linsbauer, A.; Huss, M.; Hodel, E. et al. The New Swiss Glacier Inventory SGI2016: From a Topographical to a Glaciological Dataset. *Frontiers in Earth Science* **2021**, *9*. https://www.frontiersin.org/articles/10.3389/feart.2021.704189.
Lliboutry, L. Multivariate Statistical Analysis of Glacier Annual Balances. *Journal of Glaciology* **1974**, *13* (69), 371–392. https://doi.org/10.3189/S0022143000023169.
Lutz, A. F.; Immerzeel, W. W.; Shrestha, A. B. et al. Consistent Increase in High Asia's Runoff Due to Increasing Glacier Melt and Precipitation. *Nature Climate Change* **2014**, *4* (7), 587–592. https://doi.org/10.1038/nclimate2237.

Machguth, H.; Eisen, O.; Paul, F. et al. Strong Spatial Variability of Snow Accumulation Observed with Helicopter-Borne GPR on Two Adjacent Alpine Glaciers. *Geophysical Research Letters* **2006**, *33* (13). https://doi.org/10.1029/2006GL026576.

Magnússon, E.; Pálsson, F.; Gudmundsson, M. T. et al. Development of a Subglacial Lake Monitored with Radio-Echo Sounding: Case Study from the Eastern Skaftá Cauldron in the Vatnajökull Ice Cap, Iceland. *The Cryosphere* **2021a**, *15* (8), 3731–3749. https://doi.org/10.5194/tc-15-3731-2021.

Magnússon, E.; Pálsson, F.; Jarosch, A. et al. The Bedrock and Tephra Layer Topography within the Glacier-Filled Katla Caldera, Iceland, Deduced from Dense RES-Survey. *Jökull* **2021b**, *71*, 39–70. https://doi.org/10.33799/jokull2021.71.039.

Martín-Español, A.; Lapazaran, J. J.; Otero, J. et al. On the Errors Involved in Ice-Thickness Estimates III: Error in Volume. *Journal of Glaciology* **2016**, *62* (236), 1030–1036. https://doi.org/10.1017/jog.2016.95.

Mass-balance terms. *Journal of Glaciology* 1969, *8* (52), 3–7. https://doi.org/10.3189/S0022143000020736.

Maussion, F.; Hock, R.; Paul, F. et al. *A New Working Group on the Randolph Glacier Inventory (RGI) and Its Role in Future Glacier Monitoring*; Copernicus, 2020. https://doi.org/10.5194/egusphere-egu2020-9888.

Mayo, L. R.; Meier, M. F.; Tangborn, W. V. A System to Combine Stratigraphic and Annual Mass-Balance Systems: A Contribution to the International Hydrological Decade. *Journal of Glaciology* **1972**, *11* (61), 3–14. https://doi.org/10.3189/S0022143000022449.

McGrath, D.; Sass, L.; O'Neel, S. et al. End-of-Winter Snow Depth Variability on Glaciers in Alaska. *Journal of Geophysical Research: Earth Surface* **2015**, *120* (8), 1530–1550. https://doi.org/10.1002/2015JF003539.

McGrath, D.; Sass, L.; O'Neel, S. et al. Interannual Snow Accumulation Variability on Glaciers Derived from Repeat, Spatially Extensive Ground-Penetrating Radar Surveys. *The Cryosphere* **2018**, *12* (11), 3617–3633. https://doi.org/10.5194/tc-12-3617-2018.

McNabb, R. W.; Hock, R. Alaska Tidewater Glacier Terminus Positions, 1948–2012. *Journal of Geophysical Research: Earth Surface* **2014**, *119* (2), 153–167. https://doi.org/10.1002/2013JF002915.

Mingo, L.; Flowers, G. E. An Integrated Lightweight Ice-Penetrating Radar System. *Journal of Glaciology* **2010**, *56* (198), 709–714. https://doi.org/10.3189/002214310793146179.

Moon, T.; Joughin, I. Changes in Ice Front Position on Greenland's Outlet Glaciers from 1992 to 2007. *Journal of Geophysical Research: Earth Surface* **2008**, *113* (F2). https://doi.org/10.1029/2007JF000927.

Müller, F. et al. *Perennial Ice and Snow Masses*; IAHS Technical Papers in Hydrology 1; United Nations Educational, Scientific and Cultural Organization (UNESCO): Paris, 1970.

Müller, F.; Caflisch, T.; Müller, G. *Instructions for Compilation and Assemblage of Data for a World Glacier Inventory: Supplement: Identification/Glacier Number*; Zürich: Federal Institute of Technology, 1978.

Nussbaumer, S. U.; Nesje, A.; Zumbühl, H. J. Historical Glacier Fluctuations of Jostedalsbreen and Folgefonna (Southern Norway) Reassessed by New Pictorial and Written Evidence. *The Holocene* **2011**, *21*, 455–471. https://doi.org/10.1177/0959683610385728.

Nuth, C.; Kääb, A. Co-Registration and Bias Corrections of Satellite Elevation Data Sets for Quantifying Glacier Thickness Change. *The Cryosphere* **2011**, *5* (1), 271–290. https://doi.org/10.5194/tc-5-271-2011.

Oerlemans, J. Extracting a Climate Signal from 169 Glacier Records. *Science* **2005**, *308* (5722), 675–677. https://doi.org/10.1126/science.1107046.

O'Neel, S.; McNeil, C.; Sass, L. C. et al. Reanalysis of the US Geological Survey Benchmark Glaciers: Long-Term Insight into Climate Forcing of Glacier Mass Balance. *Journal of Glaciology* **2019**, *65* (253), 850–866. https://doi.org/10.1017/jog.2019.66.

Østrem, G.; Brugman, M. *Glacier Mass-Balance Measurements: A Manual for Field and Office Work*; NHRI Science Report No. 4; Norwegian Water Resources and Energy Administration: Oslo; National Hydrology Research Institute: Saskatoon, Canada, 1991; 224. https://publications.gc.ca/site/eng/9.608459/publication.html.

Paul, F.; Kääb, A.; Maisch, M. et al. The New Remote-Sensing-Derived Swiss Glacier Inventory: I. Methods. *Annals of Glaciology* **2002**, *34*, 355–361. https://doi.org/10.3189/172756402781817941.

Paul, F.; Barry, R. G.; Cogley, J. G. et al. Recommendations for the Compilation of Glacier Inventory Data from Digital Sources. *Annals of Glaciology* **2009**, *50* (53), 119–126. https://doi.org/10.3189/172756410790595778.

Paul, F.; Barry, R. G.; Cogley, J. G. et al. *Guidelines for the Compilation of Glacier Inventory Data from Digital Sources*; WGMS-GLIMS-GlobGlacier, 2010.

Paul, F.; Andreassen, L. M.; Winsvold, S. H. A New Glacier Inventory for the Jostedalsbreen Region, Norway, from Landsat TM Scenes of 2006 and Changes since 1966. *Annals of Glaciology* **2011**, *52* (59), 153–162. https://doi.org/10.3189/172756411799096169.

Paul, F.; Barrand, N. E.; Baumann, S. et al. On the Accuracy of Glacier Outlines Derived from Remote-Sensing Data. *Annals of Glaciology* **2013**, *54* (63), 171–182. https://doi.org/10.3189/2013AoG63A296.

Paul, F.; Winsvold, S. H.; Kääb, A. et al. Glacier Remote Sensing Using Sentinel-2. Part II: Mapping Glacier Extents and Surface Facies, and Comparison to Landsat 8. *Remote Sensing* **2016**, *8* (7), 575. https://doi.org/10.3390/rs8070575.

Paul, F.; Rastner, P.; Azzoni, R. S. et al. Glacier Shrinkage in the Alps Continues Unabated as Revealed by a New Glacier Inventory from Sentinel-2. *Earth System Science Data* **2020**, *12* (3), 1805–1821. https://doi.org/10.5194/essd-12-1805-2020.

Pelto, B. M.; Menounos, B.; Marshall, S. J. Multi-Year Evaluation of Airborne Geodetic Surveys to Estimate Seasonal Mass Balance, Columbia and Rocky Mountains, Canada. *The Cryosphere* **2019**, *13* (6), 1709–1727. https://doi.org/10.5194/tc-13-1709-2019.

Pfeffer, W. T.; Arendt, A. A.; Bliss, A. et al. The Randolph Glacier Inventory: A Globally Complete Inventory of Glaciers. *Journal of Glaciology* **2014**, *60* (221), 537–552. https://doi.org/10.3189/2014JoG13J176.

Plewes, L. A; Hubbard, B. A Review of the Use of Radio-Echo Sounding in Glaciology. *Progress in Physical Geography* **2001**, *25* (2), 203–236. https://doi.org/10.1177/030913330102500203

Pulwicki, A.; Flowers, G. E.; Bingham, D. Pursuit of Optimal Design for Winter-Balance Surveys of Valley-Glacier Ablation Areas. *Frontiers in Earth Science* **2019**, *7* (199). https://doi.org/10.3389/feart.2019.00199.

Pulwicki, A.; Flowers, G. E.; Radić, V. et al. Estimating Winter Balance and Its Uncertainty from Direct Measurements of Snow Depth and Density on Alpine Glaciers. *Journal of Glaciology* **2018**, *64* (247), 781–795. https://doi.org/10.1017/jog.2018.68.

Purdie, H.; Anderson, B.; Chinn, T. et al. Franz Josef and Fox Glaciers, New Zealand: Historic Length Records. *Global and Planetary Change* **2014**, *121*, 41–52. https://doi.org/10.1016/j.gloplacha.2014.06.008.

Racoviteanu, A. E.; Paul, F.; Raup, B. et al. Challenges and Recommendations in Mapping of Glacier Parameters from Space: Results of the 2008 Global Land Ice Measurements from Space (GLIMS) Workshop, Boulder, Colorado, USA. *Annals of Glaciology* **2009**, *50* (53), 53–69. https://doi.org/10.3189/172756410790595804.

Ramsankaran, R.; Pandit, A.; Azam, M. F. Spatially Distributed Ice-Thickness Modelling for Chhota Shigri Glacier in Western Himalayas, India. *International Journal of Remote Sensing* **2018**, *39* (10), 3320–3343. https://doi.org/10.1080/01431161.2018.1441563.

Rau, F.; Mauz, F.; Vogt, S. et al. *Illustrated GLIMS Glacier Classification Manual*; GLIMS, 2005. http://www.glims.org/MapsAndDocs/assets/GLIMS_Glacier-Classification-Manual_V1_2005-02-10.pdf.

Raup, B.; S. J. S. Khalsa. *GLIMS Analysis Tutorial*; GLIMS, 2010. https://www.glims.org/MapsAndDocs/assets/GLIMS_Analysis_Tutorial_a4.pdf.

Rekstad, J. *Iakttagelser fra bræer i Sogn og Nordfjord*; NGU, 1902. https://openarchive.ngu.no/ngu-xmlui/bitstream/handle/11250/2675062/NGUnr_34_3_Rekstad_s.1-47.pdf.

RGI Consortium. *Randolph Glacier Inventory – A Dataset of Global Glacier Outlines: Version 6.0, GLIMS Technical Report*; Global Land Ice Measurements from Space (GLIMS): Boulder, USA, 2017. https://doi.org/10.7265/N5-RGI-60.

Rolstad, C.; Haug, T.; Denby, B. Spatially Integrated Geodetic Glacier Mass Balance and Its Uncertainty Based on Geostatistical Analysis: Application to the Western Svartisen Ice Cap, Norway. *Journal of Glaciology* **2009**, *55* (192), 666–680. https://doi.org/10.3189/002214309789470950.

Ruddiman, W. F. *Earth's Climate: Past and Future*, Third edition; W. H. Freeman and Company: New York, 2014.

Schuler, T. V.; Loe, E.; Taurisano, A. et al. Calibrating a Surface Mass-Balance Model for Austfonna Ice Cap, Svalbard. *Annals of Glaciology* **2007**, *46*, 241–248. https://doi.org/10.3189/172756407782871783.

Sigurðsson, O. Glacier Variations in Iceland 1930–1995. From the Database of the Iceland Glaciological Society. *Jökull* **1998**, *45*, 3–25. https://doi.org/10.33799/jokull1998.45.003.

Sold, L.; Huss, M.; Hoelzle, M. et al. Methodological Approaches to Infer End-of-Winter Snow Distribution on Alpine Glaciers. *Journal of Glaciology* **2013**, *59* (218), 1047–1059. https://doi.org/10.3189/2013JoG13J015.

Sold, L.; Huss, M.; Machguth, H. et al. Mass Balance Re-Analysis of Findelengletscher, Switzerland; Benefits of Extensive Snow Accumulation Measurements. *Frontiers in Earth Science* **2016**, *4* (18). https://doi.org/10.3389/feart.2016.00018.

Sold, L.; Landmann, J. M.; Borner, J. et al. A*utomated Real-time Ice Ablation Readings Using in Situ Cameras and Computer Vision Techniques*; Copernicus, 2021. https://presentations.copernicus.org/EGU21/EGU21-7663_presentation.pdf.

Talalay, P. G. *Mechanical Ice Drilling Technology*; Springer: Singapore, 2016. https://doi.org/10.1007/978-981-10-0560-2.

Thibert, E.; Blanc, R.; Vincent, C. et al. Glaciological and Volumetric Mass-Balance Measurements: Error Analysis over 51 Years for Glacier de Sarennes, French Alps. *Journal of Glaciology* **2008**, *54* (186), 522–532. https://doi.org/10.3189/002214308785837093.

Thorsteinsson, T. *Distribution of Winter Balance on Hofsjökull Measured with GPR — I*. Report (in Icelandic); Icelandic Meteorological Office, 2016.

van Beusekom, A. E., O'Neel, S. R., March, R. S. et al. *Re-Analysis of Alaskan Benchmark Glacier Mass-Balance Data Using the Index Method*; 2010–5247; US Department of the Interior, US Geological Survey: 2010; 16. https://pubs.usgs.gov/sir/2010/5247/.

van Tiggelen, M.; Smeets, P. C. J. P.; Reijmer, C. H. et al. A Vertical Propeller Eddy-Covariance Method and Its Application to Long-Term Monitoring of Surface Turbulent Fluxes on the Greenland Ice Sheet. *Boundary-Layer Meteorology* **2020**, *176* (3), 441–463. https://doi.org/10.1007/s10546-020-00536-7.

Weber, P.; Boston, C. M.; Lovell, H. et al. Evolution of the Norwegian Plateau Icefield Hardangerjøkulen since the 'Little Ice Age.' *The Holocene* **2019**, *29* (12), 1885–1905. https://doi.org/10.1177/0959683619865601.

Welch, B. C.; Pfeffer, W. T.; Harper, J. T. et al. Mapping Subglacial Surfaces of Temperate Valley Glaciers by Two-Pass Migration of a Radio-Echo Sounding Survey. *Journal of Glaciology* **1998**, *44* (146), 164–170. https://doi.org/10.3189/S0022143000002458.

Welty, E.; Zemp, M.; Navarro, F. et al. Worldwide Version-Controlled Database of Glacier Thickness Observations. *Earth System Science Data* **2020**, *12* (4), 3039–3055. https://doi.org/10.5194/essd-12-3039-2020.

World Glacier Monitoring Service (WGMS). *WGMS Attribute Description*. 2019. https://wgms.ch/.

World Glacier Monitoring Service (WGMS). *Global Glacier Change Bulletin*; No. 4 (2018–2019); Zemp, M.; Nussbaumer, S. U.; Gärtner-Roer, I. et al., Eds.; World Glacier Monitoring Service: Zurich, 2021. https://wgms.ch/downloads/WGMS_GGCB_04.pdf.

Winsvold, S. H.; Andreassen, L. M.; Kienholz, C. Glacier Area and Length Changes in Norway from Repeat Inventories. *The Cryosphere* **2014**, *8* (5), 1885–1903. https://doi.org/10.5194/tc-8-1885-2014.

World Meteorological Organization (WMO). *WIGOS Metadata Standard* (WMO-No. 1192). Geneva, 2019.

Yilmaz, Ö. *Seismic Data Processing*; Society of Exploration Geophysicists: Tulsa, USA, 1987. https://archive.org/details/seismicdataproce0002yilm/page/n547/mode/2up.

Zekollari, H.; Huss, M.; Farinotti, D. On the Imbalance and Response Time of Glaciers in the European Alps. *Geophysical Research Letters* **2020**, *47* (2). https://doi.org/10.1029/2019GL085578.

Zeller, L.; McGrath, D.; Sass, L. et al. Beyond Glacier-Wide Mass Balances: Parsing Seasonal Elevation Change into Spatially Resolved Patterns of Accumulation and Ablation at Wolverine Glacier, Alaska. *Journal of Glaciology* **2022**, *69* (273), 87–102. https://doi.org/10.1017/jog.2022.46.

Zemp, M.; Jansson, P.; Holmlund, P. et al. Reanalysis of Multi-Temporal Aerial Images of Storglaciären, Sweden (1959–99). Part 2: Comparison of Glaciological and Volumetric Mass Balances. *The Cryosphere* **2010**, *4* (3), 345–357. https://doi.org/10.5194/tc-4-345-2010.

Zemp, M.; Nussbaumer, S. U.; Gärtner-Roer, I. et al. *Glacier Mass Balance Bulletin*; No. 11 (2008–2009); World Glacier Monitoring Service (WGMS): Zurich, Switzerland, 2011. https://wgms.ch/downloads/wgms_2011_gmbb11.pdf.

Zemp, M.; Thibert, E.; Huss, M. et al. Reanalysing Glacier Mass Balance Measurement Series. *The Cryosphere* **2013**, *7* (4), 1227–1245. https://doi.org/10.5194/tc-7-1227-2013.

Zemp, M.; Frey, H.; Gärtner-Roer, I. et al. Historically Unprecedented Global Glacier Decline in the Early 21st Century. *Journal of Glaciology* **2015**, *61* (228), 745–762. https://doi.org/10.3189/2015JoG15J017.

Zhang, T.; Wang, W.; Gao, T. et al. Simulation and Assessment of Future Glacial Lake Outburst Floods in the Poiqu River Basin, Central Himalayas. *Water* **2021**, *13* (10), 1376. https://doi.org/10.3390/w13101376.

Zorzut, V.; Ruiz, L.; Rivera, A. et al. Slope Estimation Influences on Ice Thickness Inversion Models: A Case Study for Monte Tronador Glaciers, North Patagonian Andes. *Journal of Glaciology* **2020**, *66* (260), 996–1005. https://doi.org/10.1017/jog.2020.64.

CHAPTER 4. MEASUREMENT OF PERMAFROST

This chapter was authored by:

Anna Irrgang, Alfred Wegener Institute Helmholtz Centre for Polar and Marine Research (Germany)
Ketil Isaksen, Norwegian Meteorological Institute (Norway)
Jeannette Noetzli, WSL Institute for Snow and Avalanche Research SLF; Climate Change, Extremes and Natural Hazards in Alpine Regions Research Center CERC (Switzerland)
Phillippe Schoeneich, Université Grenoble Alpes (France)
Nikolay Shiklomanov, George Washington University (United States of America)
William Cable, Alfred Wegener Institute Helmholtz Centre for Polar and Marine Research (Germany)
Cécile Pellet, University of Fribourg (Switzerland)
Graziano Coppa, National Metrology Institute (Italy)
Andrea Merlone, National Metrology Institute (Italy)
Dongliang Luo, Northwest Institute of Eco-environment and Resources, Chinese Academy of Sciences (China)
Aleksei Portnov, University of Texas Institute for Geophysics (USA)
Lin Zhao, Nanjing University of Information Science and Technology (China)

4.1 GENERAL

4.1.1 Introduction

Permafrost is defined as ground material which remains at or below 0 °C for at least two consecutive years. It typically remains at that temperature for long time periods and reaches considerable depths. It can be found in cold regions in polar and high-elevation areas in both hemispheres. Permafrost warming and thawing can have major consequences for the natural as well as human environment, and can impact ecosystems, hydrological processes and landscape stability (Liljedahl et al., 2016; Walvoord and Kurylyk, 2016; Ward Jones et al., 2019). In the high-latitude permafrost regions, warming and thawing lead to slope instability in ice-rich permafrost (unconsolidated sediments), including active layer detachments and thaw slumps, typically found along stream and river valleys. This has implications for transportation corridors and ecosystems, for example through impacts on water quality. Thaw settlement associated with thawing of ice-rich permafrost is another example of landscape instability. In high-elevation areas, ground instability affects the integrity of infrastructure built on permafrost or on steeper perennially frozen slopes (see, for example, Bommer et al., 2010; Duvillard et al., 2019; Hjort et al., 2022) and increases potential for geohazards such as rock falls or rock avalanches (Haeberli et al., 2017; Hock et al., 2019). In high-latitude permafrost areas, large amounts of carbon are stored in frozen organic matter, which decomposes and releases greenhouse gases upon thawing, with the potential to impact the global climate system (Miner et al., 2022).

As a thermal subsurface phenomenon, permafrost reacts sensitively to changes in climatic conditions and thus was selected as one of the Essential Climate Variables (ECVs) of the Global Climate Observing System (GCOS) (Bojinski et al., 2014; GCOS-200). Decadal changes in the state of permafrost temperature have been used as indicators of climate change (see, for example, Biskaborn et al., 2019; Smith et al., 2022). The Global Terrestrial Network for Permafrost (GTN-P) is the primary international programme concerned with the long-term monitoring of permafrost (Streletskiy et al., 2021). Permafrost monitoring relies on in-situ measurements because permafrost is a subsurface phenomenon. The key indicator variables (Smith and Brown, 2009) observed to monitor long-term changes in permafrost were defined as products of the ECV permafrost (defined in the GCOS Implementation Plan (Zemp et al., 2022)) and measurement of them is implemented within GTN-P (Streletskiy et al., 2021). Standardization and strategic planning of permafrost monitoring are crucial to achieve consistent and comparable long-term records (see, for example, Noetzli et al., 2021).

The methods and corresponding best practices to measure the three products of the ECV permafrost – permafrost temperature, active layer thickness (ALT) and rock glacier velocity – are described in the present chapter (see 4.1.2 for their definition). It focuses on the methods most applied by the scientific community for the long-term monitoring of permafrost in the framework of climate observation:

(1) **The measurement of permafrost temperatures in boreholes** is the direct and quantitative thermal observation of permafrost and the primary method for its long-term climate-related monitoring (see 4.2).

(2) **Measurements of the active layer thickness (ALT)** reflect inter-annual changes in air temperature and snow conditions (see 4.3) in combination with heave and subsidence.

(3) Variations in the viscous creep of perennially frozen ground – termed **rock glacier velocity** (RGV) – have been shown to follow the changes in the thermal conditions and water contents in ice-rich permafrost and are used as an indirect way of observing permafrost evolution, especially in remote mountain areas with difficult access (see 4.4). This variable is the most recent to have been added as a product of the ECV permafrost.

(4) Additional variables are typically observed to characterize permafrost conditions in the framework of a research study, infrastructure planning or a long-term monitoring project. Therefore, a set of **supplementary measurements** and existing guidelines and recommendations are described as well (see 4.5).

The guidelines and best practices for measurements of the key indicator variables of permafrost (that is, the ECV products) were elaborated in coordination and collaboration with global and regional climate-related monitoring programmes, including GTN-P. Detailed local measurements are linked to global process understanding within the framework of the Global Hierarchical Observing Strategy (GHOST), which is linked to GTN-P (see Harris et al. (2001) for its application to permafrost monitoring). The Permafrost and Climate in Europe (PACE) project (Harris et al., 2001) and the Swiss Permafrost Monitoring Network (PERMOS) (Noetzli et al., 2021; PERMOS, 2019) provided valuable details on mountain permafrost measurement approaches and instrumentation. The best practice guidelines on permafrost align with the GCOS Implementation Plan (Zemp et al., 2022) and the GCOS ECV requirements (GCOS-245) as well as with the measurement guidelines and recommendations for GTN-P (Streletskiy et al., 2022).

4.1.2 **Definitions and variables**

Permafrost: Ground material that remains continuously at or below 0 °C for at least two consecutive years.

Permafrost is defined on a thermal and temporal basis as ground that remains at a maximum temperature of 0 °C throughout the year, typically for long time periods (centuries to millennia) and often reaching considerable depths (up to several hundred metres). Permafrost can be found in polar and cold high-elevation regions in both hemispheres. Relict terrestrial permafrost also extends offshore in the Arctic region. It became submerged after the last ice age and is currently degrading beneath the shelf sea above it. Even if permafrost is defined based on its thermal state, its practical relevance and, thus, also the difference with non-permafrost ground, depends primarily on the presence of ice in the ground. With temperatures approaching 0 °C, permafrost can also contain significant amounts of unfrozen water, depending on the properties of the sediment grain size and pore fluid. Permafrost can therefore also be referred to as perennially cryotic ground. The geotechnical and hydrological characteristics of the subsurface can be significantly altered by temperature, as well as by pore ice and excess ice (including ice lenses), ice-filled fractures and unfrozen water.

The layer that is above the top of the permafrost and subject to annual thawing and freezing is termed the “active layer” (Figure 4.1). In contrast to permafrost, the active layer is often defined based on the freezing point of water, which can be lower than 0 °C (see 4.3.1.1 for more information and definitions). The upper boundary of the permafrost below which ground temperatures remain at or below 0 °C is called the “permafrost table”. Due to the different thermal conductivities of thawed and frozen material in the active layer, the mean annual temperature at the permafrost table can be lower than the mean annual ground surface temperature (MAGST). This effect is termed “thermal offset”. The thermal offset means that permafrost can exist even in areas where the MAGST is above 0 °C (see, for example, Smith et al., 2022). Ground temperatures typically increase with depth following the geothermal gradient, which is defined by the geothermal heat flux and the thermal properties of the sediments or bedrock. Permafrost extends down to the permafrost base, below which ground temperatures are above 0 °C. The temperature profile can be influenced by the properties of different soils in the ground (see, for example, Williams and Smith, 1989) as well as by three-dimensional effects of steep topography (Noetzli and Gruber, 2009) and by changes in atmospheric and ground surface temperatures.

Near-surface ground temperatures fluctuate in response to high-frequency variations in air temperature and snow cover regime. The temperature variations experienced at the ground surface are attenuated and delayed with increasing depth. At the depth of zero annual amplitude (DZAA) seasonal changes in temperature remain at or below 0.1 °C (see, for example, French, 2017). Below the DZAA, temperature variations no longer reflect seasonal patterns, but instead reflect long-term thermal changes (that is, the climate signal).

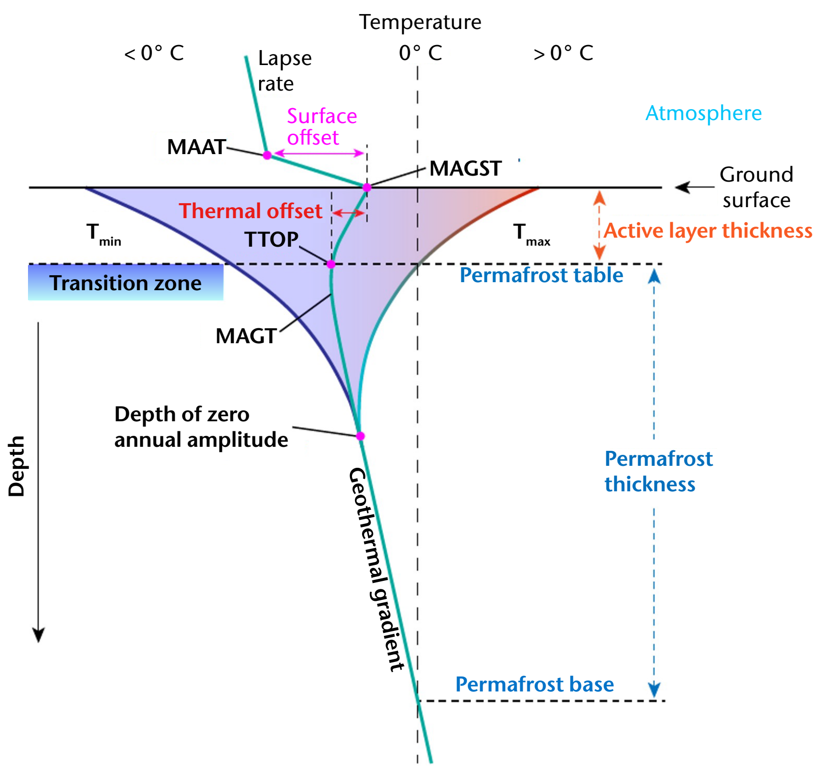

Figure 4.1. Schematic diagram of the equilibrium thermal regime of the ground and near-surface atmosphere in permafrost terrain. The mean annual ground temperature (MAGT) declines toward the temperature at the top of the permafrost (TTOP). The temperature envelope (shaded) between the ground surface and the depth of zero annual amplitude (DZAA) indicates the range of ground temperatures between the minimum (T_{min}) and maximum (T_{max}) during a year. MAAT – mean annual air temperature; MAGST – mean annual ground surface temperature.

Source: Modified from an image produced by Julian Murton

When the active layer no longer freezes down to the permafrost table during winter due to increasing atmospheric and ground surface temperatures, an area develops that is unfrozen but underlain by permafrost, called a “talik”. Taliks also form beneath water bodies.

Characteristic landforms and geomorphic processes in the landscape can be used as indicators of permafrost occurrence, such as rock glaciers, ice wedges, pingos, palsas, peat plateaus, patterned ground and solifluction lobes. A rock glacier (Figure 4.2) is defined as a debris landform generated by the former or current creep of frozen ground (permafrost), detectable in the landscape with the following morphologies: steep front, lateral margins and sometimes ridge-and-furrow surface topography (RGIK, 2023a). Due to high ground ice content, which induces cohesion and reduces internal friction, the material contained in a rock glacier creeps and shows coherent flow fields. Rock glacier kinematics are controlled by a combination of environmental factors (internal structure, landform geometry, topography, geology, lithology and debris loading) and climatic factors (temperature, precipitation and snow) (Arenson et al., 2002).

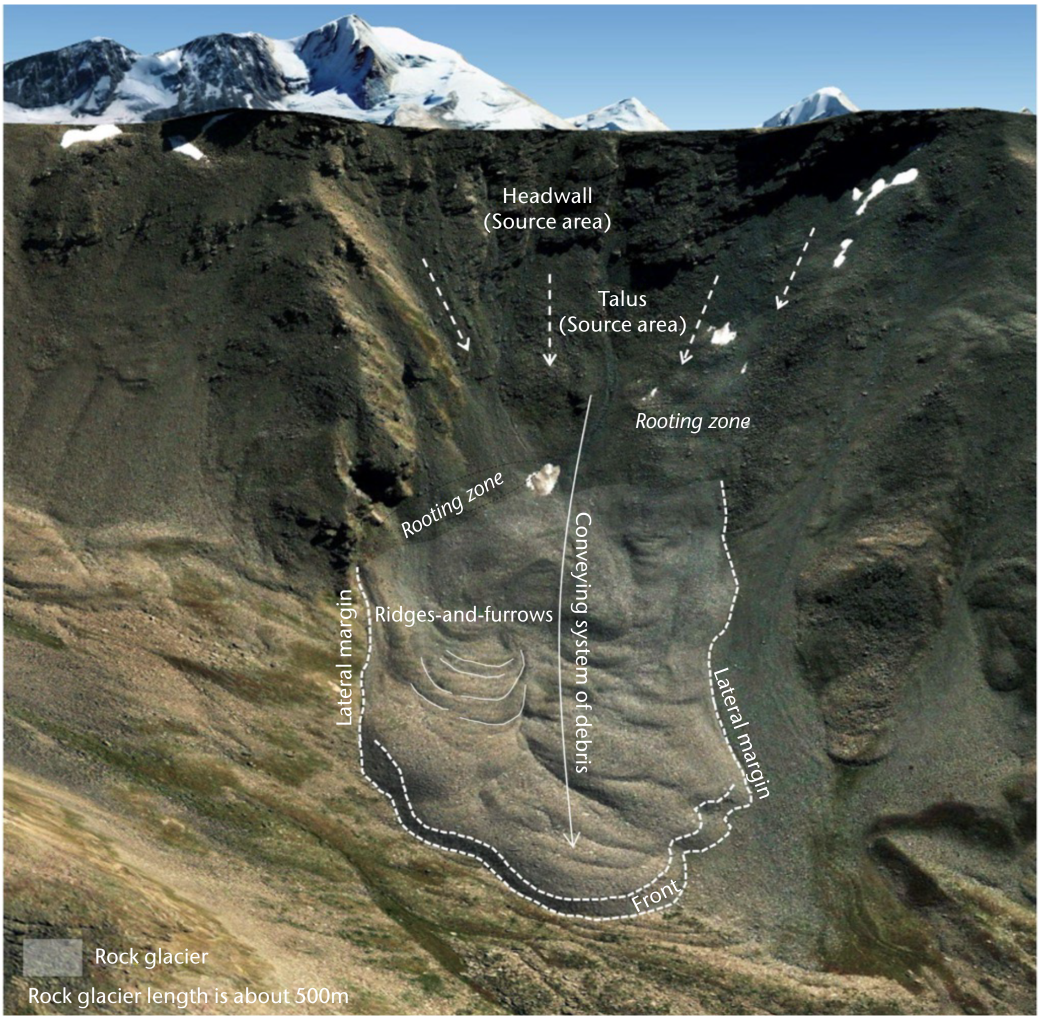

Figure 4.2. Rock glacier in the Vallone di Sort (Italy) identified in the landscape by a front (discernable talus delineating the terminal part of the moving area perpendicular to the main flow direction), lateral margins in continuity of the front and localized ridge-and-furrow surface topography.

Source: Background imagery: Google Earth. Adapted from RGIK (2023a).

4.1.3 Permafrost distribution and characteristics

Permafrost presently underlies ~16–21 × 106 km^2 of Earth's land surface, seafloor and subglacial terrain (Murton, 2021) (Figure 4.3) and is found mainly in the northern hemisphere, but also in southern hemisphere mountain ranges and in Antarctica. Current estimates show that approximately 15% of the northern hemisphere is underlain by permafrost (Obu, 2021).

Permafrost regions are traditionally divided into several zones based on estimated geographic continuity in the landscape. A typical classification (Figure 4.3) recognizes continuous permafrost (underlying 90%–100% of the landscape), discontinuous permafrost (50%–90%), sporadic permafrost (10%–50%), and isolated patches (0%–10%). In the discontinuous and sporadic zones permafrost distribution is complex and patchy, and permafrost-free terrain is common. The thickness of permafrost varies from less than one metre to more than 1600 metres.

Most of the permafrost existing today in polar areas formed during cold glacial periods and has persisted through warmer interglacial periods, including the Holocene (last 10 000 years). Some relatively shallow permafrost (30 to 70 m) formed during the second part of the Holocene (last 6 000 years) and some during the Little Ice Age (from 400 to 150 years ago). In continental interiors permafrost temperatures at the boundaries between continuous and discontinuous are generally about −5 °C, corresponding roughly with the isotherms of the −8 °C mean annual air temperature.

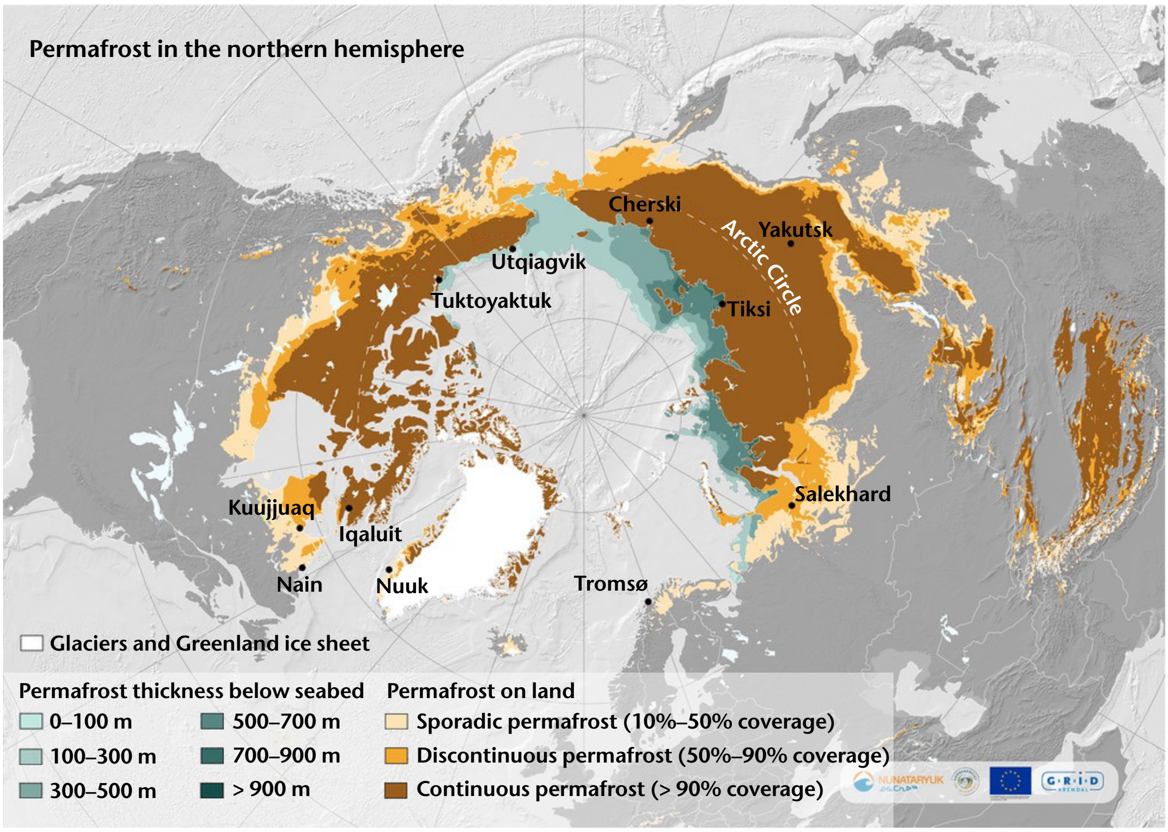

Figure 4.3. Permafrost zonation based on classified modelled permafrost probabilities (Obu et al., 2019). Permafrost exists in steep slopes of mid-latitude high-mountain regions such as the European Alps or the Andes, which is not well represented on this map. The permafrost zonation in the Tibetan Plateau is not well reproduced. In actuality, the plateau consists of extensive regions with discontinuous and sporadic permafrost, rather than continuous permafrost. Isolated patches of permafrost are not shown on this map.

Source: Map by GRID-Arendal/Nunataryuk, https://www.grida.no/resources/13519. Subsea permafrost distribution was modelled with CryoGrid 2 (Overduin et al., 2019).

The distribution of permafrost is primarily a result of the surface energy balance, which is influenced by climatic conditions, topography, and surface and subsurface characteristics. The extreme topography of high-mountain areas leads to extreme horizontal and vertical spatial variability (see, for example, Gruber and Haeberli, 2009; Zhao et al., 2020) in these factors and, hence, to a highly heterogeneous permafrost distribution.

In mountain regions, permafrost is found in bedrock, debris slopes, viscous and ice-rich creeping features (rock glaciers), moraines or glacier forefields, and gravity-driven downslope deformation processes are widespread (Noetzli et al., 2021). Ground ice content varies, ranging from ice-rich terrain, oversaturated with massive ice (tens of metres thick) in loose debris to ice-poor bedrock with permanent ice only present in rock pores and fractures. In mid-latitude mountains, such as the European Alps or the central and southern Andes, widespread permafrost regions have temperatures close to 0 °C, with considerable amounts of unfrozen water present in the soil matrix (Halla et al., 2021; Noetzli et al., 2021). In shady bedrock slopes at high elevations, however, permafrost can be as cold as in the high Arctic (Noetzli et al., 2019).

Subsea permafrost occurs close to 0 °C over large areas of the Arctic continental shelf, where it formed during the last glacial period on the exposed shelf landscapes. Permafrost is geographically continuous beneath the ice-free regions of the Antarctic continent.

In general, the ALT decreases poleward and increases in continental areas in response to changes in the mean annual temperature at the ground surface and its annual amplitude. The thickness will depend on geology (thermal conductivity of material), vegetation and snow cover. The thinnest active layers are commonly located at the highest latitude or at the highest elevation, where permafrost is continuous. In these regions, ALTs are generally about 0.5 m to 1 m. However, some high Arctic maritime locations, especially those under the influence of warm ocean currents, can have considerably warmer permafrost and a thicker active layer than other sites at comparable latitudes. The maritime areas may also receive a larger amount of precipitation compared to more continental locations, resulting in higher accumulation of snow and hence a thicker active layer. For example, observations from the Circumpolar Active Layer Monitoring (CALM) programme (Nelson et al., 2021) indicate that long-term ALT in a continuous permafrost zone of Alaska ranges from 0.3 to 0.7 m (Nyland et al., 2021), while in Svalbard, which is at a higher latitude, it is 1–2 m (Strand et al., 2021). In sub-arctic locations, the active layer can reach 2–3 m in thickness. In areas underlain by discontinuous or sporadic permafrost, an unfrozen layer (talik) can develop between the active layer and the top of permafrost when the layer that thawed in the summer does not completely refreeze in the winter. In alpine environments, the thickness of the active layer can be highly variable as well due to the complex interplay of factors controlling the distribution and characteristics of mountain permafrost.

At local and regional scales, ALT is highly spatially variable. Variations in topography, subsurface properties, soil moisture, and snow and vegetation cover modify the zonal pattern radically, resulting in a high degree of geographic variability. Several conceptual examples of active layer development under similar climatic conditions can be considered (Bonnaventure and Lamoureux, 2013): (1) A thick active layer (ranging from a few metres to ten metres) develops in exposed bedrock due to its high thermal conductivity and low ice/water content. For example, in northern North America ALT of more than 10 m has been observed in bedrock with high thermal conductivity (Smith et al., 2010), and the ALT ranges from about 1 m to more than 10 m in the Swiss Alps and in the Norwegian mountains (Etzelmüller et al., 2023; PERMOS, 2023). Variations in rock structure, surface temperature, and/or snow depth can result in significant thickening or thinning of the active layer in rock material. (2) An active layer of intermediate thickness (up to a few metres) can be found in well-developed mineral soils. In those soils, vegetation, soil texture, soil moisture and ice content of the underlying permafrost, in addition to ground surface temperature and snow depth, control the spatial and temporal variability of the ALT. (3) In permafrost environments with a thick organic mat (>10 cm), the ALT is relatively small (from a few centimetres to a metre) due to the much lower thermal conductivity of mosses and peat in the thawed state than when frozen. As in other permafrost environments, changes in ground surface temperature and/or snow cover can promote changes in the ALT. However, due to the thick protective organic mat, the active layer is slower to respond to these changes. The contrast between mineral- and organic-rich soils is apparent within the high-latitude permafrost regions. For example, in western Siberia ALT in sandy soil is 1.4–1.7 m while in nearby peatlands it is just 0.4–0.5 m (Oblogov et al., 2023).

Rock glaciers are found in all permafrost-affected mountain ranges worldwide. Rock glacier velocity observed at the surface typically ranges from a few centimetres to a few decimetres or metres per year and only occasionally exceeds annual displacements of three metres (Blöthe et al., 2021). At the global scale a multi-decennial trend of accelerating rock glacier velocities has been observed, especially since the 2000s, with regional variability in terms of onset timing and magnitude (Pellet et al., 2023). These can be interrupted by short-term periods of rock glacier stagnation or deceleration, particularly after snow-poor winters with efficient cooling and refreezing of ground water.

4.1.4 Site selection – general considerations

The rationales for measuring permafrost parameters are diverse and can include long-term climate-related observations; detailed process studies of ecosystem, geological or hydrological processes; assessment of permafrost conditions prior to construction; or monitoring climate change impacts on the stability of existing infrastructure constructed on permafrost. The specific objectives of permafrost observation should guide the selection of the location, the selection and spatial arrangement of the instrumentation, and the longevity of the observational site(s). Detailed recommendations for selecting sites for monitoring specific permafrost parameters (for example, permafrost temperature, ALT) are provided in the corresponding sections of the present chapter. Below, following Noetzli et al. (2021), we briefly outline general site selection criteria to be considered for establishing a monitoring network aimed at assessing climate-induced permafrost changes.

The **relevance** of a site is defined by the ability of a new observational site to fill spatial gaps and/or temporal discontinuity in data records provided by existing observational networks. Geographic settings (for example, bioclimatic regions, landscapes, topographic units) underrepresented in existing observational networks should be prioritized for site selection. The socioeconomic relevance of the potential monitoring site(s), for example, to local populations, including Indigenous people, should also be considered.

The **representativeness** of a location refers to how well site conditions (for example, topography, landforms, surficial geology, edaphic properties, vegetation or permafrost properties) represent a specific area and/or object of study. Locations for long-term monitoring of changes in the permafrost should reflect the most common characteristics of the area. Anthropogenic disturbance, artificial surfaces and proximity to infrastructure can greatly alter the ground thermal regime and should be avoided for climate-related monitoring (see, for example, Isaksen et al., 2000).

Feasibility and **longevity** relate to the accessibility of the site as well as to potential hazards or terrain deformation threatening equipment. They can be affected by changing climatic conditions, human activities, hazards and geopolitics (for example, adverse world events that impact international collaboration and field access). The time frame of guaranteed site operation must be assessed, and appropriate resources allocated to ensure the continuity of observations.

It can be valuable to align sites along latitudinal, altitudinal or continentality transects to assess bioclimatic or topoclimatic **gradients** (see ECV permafrost requirements – spatial distribution (GCOS-245)). Existing examples are the latitudinal transects of permafrost temperature (see, for example, Osterkamp and Romanovsky, 1999) and active layer (see, for example, Nyland et al., 2021) monitoring sites along the Dalton Highway/Trans-Alaska Pipeline in Northern Alaska, the network of sites in the Mackenzie Valley in the Northwest Territories of Canada (see, for example, Smith et al., 2010), the European PACE transect from Svalbard to the Sierra Nevada (Harris et al., 2001), the altitudinal transect on Dovrefjell in southern Norway (Sollid et al., 2003), and the transects along the Qinghai–Tibet highway and railway (see, for example, Wu et al., 2010) and along the precipitation gradient from east to west of the Qinghai–Tibet Plateau (Zhao et al., 2021).

For the final selection of an observation site, local permafrost conditions need to be assessed directly: ALT, depth of permafrost base, permafrost temperatures, potential permafrost warming and deformation rates. Information may be derived at the site of interest or from proximate locations, based on permafrost distribution maps, geomorphological and geological maps, meteorological data, ground temperatures, geophysical surveys, ground characteristics, geological or geodetic surveys, and digital image analysis of slope deformation (see, for example, Noetzli et al., 2021).

4.2 MEASUREMENTS OF PERMAFROST TEMPERATURE

4.2.1 General

4.2.1.1 *Definition, units, scales*

Permafrost temperature is the temperature measured in the permafrost at specific depths, typically along a vertical profile (Figure 4.4). The temperature measurement in a borehole is the primary and most direct method to characterize permafrost thermal state and its changes. Permafrost temperature is measured in degrees Celsius (symbol: °C).

Permafrost temperature is commonly measured in a drilled borehole (see 4.2.2), either with a permanently installed sensor chain in the borehole for continuous measurements by a data logger (see 4.2.3), or by temporary lowering of a portable temperature sensor into the borehole to manually measure the temperature at different depths (see 4.2.4). At some sites manual temperature measurements (without data logger) are done using a fixed multisensor cable in the borehole. The depth of the borehole and the measurements depend on the purpose of the measurements, the estimated permafrost temperature and depth, the geology and subsurface materials, the terrain and its accessibility, the available drilling equipment, and financial resources (Noetzli et al., 2021). Typically, permafrost temperature is measured at multiple depths ranging from 1 m to 100 m. Most of the boreholes operational today are 2–30 m deep. The temporal resolution of the measurements along the profile in the borehole typically decrease with depth due to the decreasing temporal variability of the ground temperatures.

Parameters that can be derived from permafrost temperature profiles by interpolation or extrapolation are the ALT (see 4.3), the DZAA, the permafrost base and the presence of taliks (see Figure 4.1). The annual ground temperature envelope, or range, can be derived from the minimum and maximum annual values in continuous temperature time series at each measured depth above the DZAA (Streletskiy et al., 2021). Also, the depth of the 0 °C isotherm can be derived by interpolating temperatures measured at different depths in a borehole. This is often used as a proxy for the ALT, particularly in terrain where other methods are not applicable (for example, debris or bedrock) (see 4.3.6).

4.2.2 Borehole siting and configuration

4.2.2.1 *General principles and siting*

Borehole installation in remote cold regions and in high-mountain areas with steep and complex topography is costly and has challenging logistics. Site selection has therefore historically favoured locations near communities, critical infrastructure and areas of specific research interests (Hock et al., 2019; Smith et al., 2022). Every location poses unique challenges and necessitates specific logistical arrangements. The evaluation and selection of a site should follow the general criteria outlined in 4.1.4. To define the exact drilling location at a selected site (that is, where the drilling rig is placed), the criteria must again be considered for the specific location in view of the heterogeneity of the site characteristics and the rationale for the measurements (in the present chapter the focus is on long-term observation in the context of climate change). The location of the drilling should be narrowed down by starting with coarse methods (like permafrost distribution maps), moving to geophysical site investigation and then to, for example, assessing the ground ice distribution.

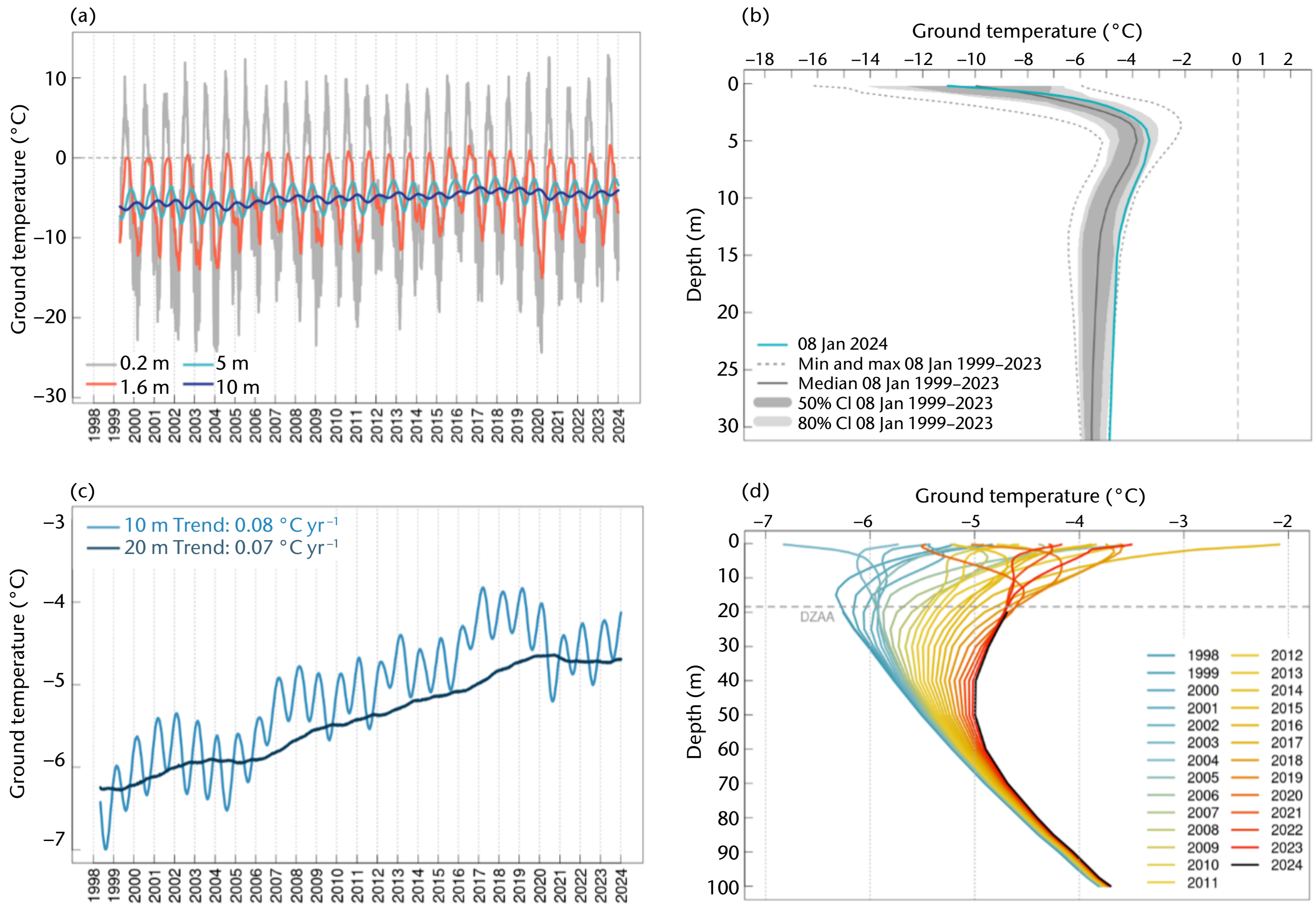

Figure 4.4. Typical permafrost temperature time series and vertical temperature profiles from Janssonhaugen (78.18°N 16.47°E, 275 m above sea level), a permafrost monitoring station in Svalbard. (a) Daily time series of ground temperature at 0.2, 1.6, 5 and 10 m depth. (b) Ground temperature profile on 8 January 2024 (in blue). The past minimum, maximum, median and confidence intervals for the same date during the monitoring period are shown in grey. (c) Long-term changes in daily ground temperature at 10 and 20 m depth, with trends included. At 20 m depth, seasonal variations become negligible (corresponds to DZAA), making the temperature at this depth a suitable indicator of long-term change in permafrost thermal state. (d) Mean annual ground temperature profiles from surface to 100 m depth. Updated operational permafrost monitoring products are available at https://cryo.met.no/en/permafrost (developed based on Isaksen et al., 2022).

The local variations of the permafrost conditions include lateral variations in geothermal properties within the ground due to topography, snow cover, vegetation, surficial geology, ice content and bedrock type and fracturing. Glaciers, rivers and oceans, and human encroachments (such as mines, roads and buildings) close to the chosen drilling site can affect the thermal regime of the ground (Isaksen et al., 2000).

Surface and subsurface properties in cold regions can be heterogeneous, particularly in high-mountain areas. A drilling site should therefore be representative of the general topographic setting (slope angle, solar radiation, snow accumulation). In addition, steep topography-induced lateral heat fluxes affect the subsurface temperature distribution (Noetzli and Gruber, 2009). When installing a borehole on a rock glacier, the annual horizontal surface deformation rate and its spatial distribution and the depth of the shear horizon must be considered before drilling (Noetzli et al., 2021). Often, however, the latter is not known and can only be estimated.

Coastal and lower-elevation areas subject to isostatic uplift have been exposed to colder climate conditions for a shorter period of time. The ground may therefore still be cooling at depth, and permafrost may still be forming, depending on the time since emergence.

4.2.2.2 ***Borehole dimensions***

The minimum **depth** for temperature data to be included in the GTN-P database is generally defined to be the DZAA (Biskaborn et al., 2019), which is around 15–20 m for alpine sites and 5–20 m for sites in tundra areas but may be less than 5 m at warm permafrost sites in the boreal forest. Often, a depth near the DZAA and below is used for reporting long-term changes (see 4.2.3.2) and to determine the temperature gradient with depth (see, for example, Noetzli et al., 2021). However, reaching the DZAA may not be possible due to the composition of the subsurface material, limitations in the available drilling equipment or difficulties of access with heavy equipment (for example, remote areas or steep terrain). Continuous measurements of ground temperatures throughout the year (see 4.2.3) also allow for the determination of long-term changes in temperature in the ground above the DZAA (for example, at 10 m depth). Reaching the DZAA should therefore not be a limiting factor determining the usefulness of a borehole for long-term observations and the assessment of change rates. Deeper boreholes several tens of metres deep – for example the 100 m-deep PACE boreholes – allow inversion modelling to assess the surface temperature evolution for several decades prior to drilling (see, for example, Isaksen et al., 2000; Lachenbruch and Marshall, 1986).

The **diameter** of the borehole should be kept to a minimum to minimize effects of convective heat transfer in the borehole. It needs to be wider for loose debris (approximately 100–140 mm) and can be smaller in solid bedrock and stable ground material (approximately 45–70 mm). In unconsolidated sediments, smaller-diameter holes can also be made with tools such as portable/hand augers and water jet drills (see Figure 4.5). The diameter is determined by the available equipment, the sampling technique and quality, the drill bit and the selected casing. The type of instrumentation to be installed in the borehole is also relevant.

Boreholes can be drilled vertically to the surface or with a documented angular **orientation**. In unconsolidated material, as in loose debris or in sediments, it is recommended to seek a nearly vertical borehole angle, to minimize the risk of sidewall collapse. In steep bedrock terrain, surface normal or oblique boreholes may be installed to measure the permafrost temperature of rock faces (Magnin et al., 2015) or to investigate the complex temperature fields of steep crests and peaks (Gruber et al., 2004; Noetzli et al., 2008). Several boreholes in the European Alps pierce a ridge completely to study thermal regimes and trends on two contrasting mountain sides (see, for example, PERMOS, 2010; Phillips et al., 2016).

4.2.2.3 ***Borehole drilling***

There are a variety of drilling methods for establishing boreholes in permafrost areas (Figure 4.5). The choice of the most appropriate one depends on types of ground material (sediment, soil, bedrock, etc.), topography and access, as well as the desired depth of the borehole, whether sampling will be done and the budget. Drilling and sampling in remote permafrost areas are logistically and technically challenging; budget and accessibility (and sometimes permitting requirements) become the major determining factors. They also require specialized techniques, custom drilling equipment, and knowledge and experience on the part of the drillers and project coordinators (Christiansen et al., 2021; Noetzli et al., 2021). Extreme weather conditions during drilling operations in cold environments often make the process demanding for both personnel and machines.

Drill types include augers (for unconsolidated material), portable water jet drills and a variety of rotary percussion drills (destructive drilling) and rotary core drills. Rotary percussion drilling makes it possible to advance into the ground efficiently, while rotary core drilling is used for retrieving core samples (Christiansen et al., 2021). **Destructive drilling** can be less expensive and faster, and can require less planning, depending on equipment used and if there are accessibility issues and high mobilization/demobilization costs. However, it is only useful when qualitative information exists on stratigraphy, ice content, fractures and water presence. Experienced surveillance is necessary to gain further insights into the material type and properties, as well

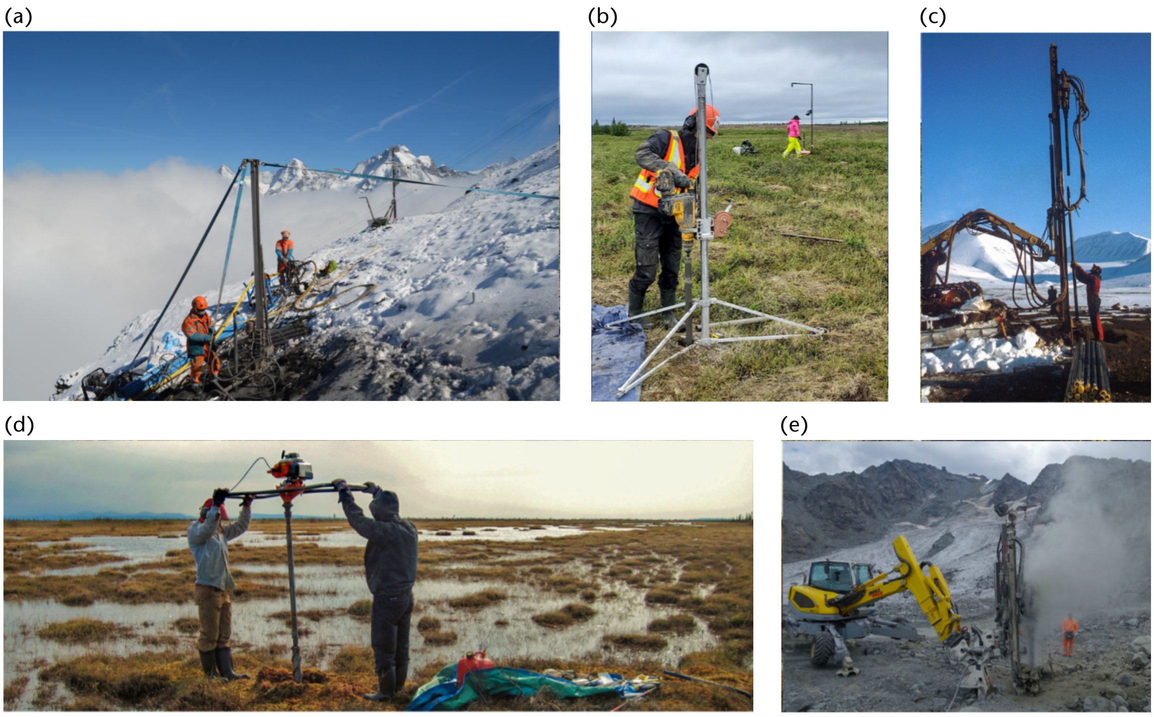

Figure 4.5. Different drilling techniques and settings in typical permafrost environments. (a) Drilling of a new permafrost monitoring borehole on the north slope of the Schilthorn in the Bernese Alps (2950 m above sea level) in Switzerland in September 2018. (b) Drilling with Talon system and adapted AMS frozen soil coring barrel to sample ice-rich morainal deposits, outer Mackenzie Delta, Northwest Territories, Canada in July 2022. (c) Drilling the 102 m deep PACE permafrost borehole on Janssonhaugen, Svalbard, in May 1998. (d) Operating a portable permafrost drilling system (SIPRE model) to retrieve permafrost cores from drained lake basins in Old Crow Flats, northern Yukon, Canada. (e) Drilling of a new borehole in the frozen moraine at Gentianes in Switzerland in Summer 2022 to secure the 20-year permafrost temperature time series. Note that these are examples and the photos do not show all the potential drilling techniques or settings.

Sources: (a) Cécile Pellet, (b) Peter Morse, (c) Johan Ludvig Sollid, (d) Pascale Roy-Léveillée, (e) Christophe Lambiel.

as fissure and water presence (Noetzli et al., 2021; Phillips et al., 2023). For auger drilling, drill cuttings can be sampled and observed in the field. **Core drilling** is more expensive and time-consuming and can also be done for only a part of the borehole profile (and additionally requires a freezer or similar arrangement to store the frozen samples), but it allows quantitative determination of stratigraphy, particle size and ice characteristics (geotechnical tests, dating, ground and ice composition). Duplex or triplex techniques should be used to minimize heat input into the ice core (Arenson et al., 2002; Haeberli, 1988; Vonder Mühll, 1996) by drilling very slowly with compressor-driven air in combination with an air cooling or brine flushing system (no water). The drilling crown used depends on the type of drilling and on the ground material. In inhomogeneous terrain like a rock glacier, where rock and ice layers exist in close proximity, fast adaptation of the drilling technique and crown may be needed (see Noetzli et al. (2021) for more details). Long pauses during the drilling procedure should be avoided because the crown can become stuck due to freezing inside the borehole (after the heat created by the drilling process dissipates) and the borehole could be lost.

In remote Arctic areas, and far away from roads, drilling is typically conducted using heli-portable drills or rigs transported during winter on frozen and snow-covered ground (Christiansen et al., 2021). Drilling during the winter also minimizes the impact of drilling on what will become a new long-term observation site. Even small disturbances to the vegetation and landscape can lead to local deepening of the active layer, subsidence, ponding and increased snow accumulation. In high-mountain regions, drilling is typically conducted in spring or summer. The drill rig and construction site installations must be transported by cable car, truck/bulldozer or helicopter. Road access is typically not possible. Depending on the local regulations, a building permit may be required.

To stabilize the drilling and to enable extraction or replacement of the installed instruments a **casing** is often installed. This is particularly important for unconsolidated material and may not be necessary in bedrock. A borehole in loose debris needs to be supported by a casing immediately after drilling to prevent collapse and blocking (see, for example, Arenson et al., 2002). The casing also protects the sensors and wires from damage and prevents adhesion of the sensors to the borehole walls. A material of low thermal conductivity, such as a round plastic (polyethylene) pipe (in accordance with PACE: see Harris et al. (2001) and Zhang (2005)) is preferred and no metal with high thermal conductivity should be used. However, a steel casing may for example be needed to protect the borehole from damage by animals (for example, bears or moose). The casing should have a diameter that suits the borehole and the inserted instruments. It should be sealed at the base and at all connections to be watertight. To limit potential for convection and improve conductive heat transport between the sensors and the ground, the space between the casing and the borehole wall can be filled with sand, environmentally safe fluid (for example, silicone oil) or special permafrost-grout, and larger cavities can be blocked with geotextiles (or other fabrics, see Noetzli et al. (2021)). In a rock glacier, however, the space will be filled with the deformation of the ground. To allow for additional (geophysical and calibration) measurements to be made in the future, a second tube can be inserted into the borehole (Boike et al., 2019).

A **covering** should be installed at the surface (for example, metal box, plastic pipe or concrete chamber with iron lid) to protect the borehole and to reduce air convection (Streletskiy et al., 2022). The covering should hold space for additional material (for example, sensor chain suspension, data loggers, batteries) and include a water drainage mechanism. Keeping all devices close to the borehole reduces the cable length, which decreases the risk of damage due to lightning, measurement disturbances via heat conduction along the cables (Noetzli et al., 2021), damage by animals (polar bears, foxes, rodents, etc.) and disturbances or damage due to heave and subsidence of the ground surface. Keeping logging equipment inside the casing protects it from the elements as well as from damage by wildlife or people.

4.2.2.4 *Borehole replacement*

In some cases, it is no longer possible to access the sensors in the borehole for servicing or replacement because they cannot be removed from the borehole. Reasons for this can include borehole deformation, ice in the borehole due to water influx, a borehole filling material that stabilizes the instruments in the borehole but prevents their removal, or the absence of a casing. When measurements become inconsistent or erroneous due to problems with the sensors in such a case, a replacement borehole may need to be drilled to continue the time series (see, for example, Noetzli et al., 2021; PERMOS, 2019). Boreholes reaching deeper than the shear horizon of a rock glacier may also need to be redrilled due to shearing off of the cables and casing. The length of time the sensors can operate until cables are sheared off depends on the velocity of the rock glacier at the borehole location and at the depth of the shear horizon. For the homogenization of the time series measured in the old and new boreholes, it is important to guarantee a temporal overlap of the two systems (according to the GCOS Monitoring Principles (https://gcos.wmo.int/en/essential-climate-variables/about/gcos-monitoring-principles)).

4.2.3 Continuous temperature measurements

4.2.3.1 *General principles*

Ground temperature monitoring sites typically consist of boreholes instrumented with permanently installed multisensor cables (called temperature sensor chains) to continuously measure temperature at several depths using a logging system (Biskaborn et al., 2019; Noetzli et al., 2021; Smith et al., 2022) (see 4.2.3.2–4.2.3.4). Periodic retrieval of temperature sensor chains from the boreholes for maintenance (see 4.2.3.7) and recalibration (4.2.3.6) should be considered (Streletskiy, 2022), if possible. However, this may not be possible for practical reasons (for example, when a sensor chain is blocked in the borehole) or, in very remote places, for logistical reasons. In the latter case, inconsistencies such as sensor drift have to be checked for during data processing.

4.2.3.2 *Depth of measurement, sampling and recording interval*

Generally, the spacing of sensors on the temperature sensor chain should increase with depth due to the decreasing temporal variability in the ground temperatures. The requirements for sensor spacing depend on the subsurface characteristics and the thermal regime at the site (depth of the active layer, permafrost base, etc.), as well as the number of sensors available (for example, in the logging equipment). In the past, measurements at the DZAA were typically used for reporting in national and international assessments (see, for example, Biskaborn et al., 2019; Hock et al., 2019)). With continuous recordings of ground temperature, the DZAA is no longer considered a limiting factor for the usefulness of a borehole to determine long-term trends, and, as an example, a depth of 10 m has been used for reporting (see, for example, PERMOS 2023, Noetzli 2021). The recommended depths for permafrost temperature measurements defined by GTN-P are 5, 10 and 20 m below the surface (Streletskiy et al., 2021), with additional sensors placed based on the characteristics of the site, the borehole depth and the instrumentation being used. Where the risk for inaccessible/blocked temperature sensor chains is high (for example, due to ice plugging or borehole shearing), temperature sensor duplication is essential to ensure uninterrupted time series at key depths (Noetzli et al., 2021; Widmer et al., 2023).

A spacing of 0.1–1.0 m is often applied in the uppermost 5–10 m, and below around 10 m depth the spacing increases to 2–5 m down to around 30 m depth. At greater depths, temperature is typically measured every 10 m or more. However, depending on the site characteristics this spacing can vary. Specific depths may be defined to adapt to known local characteristics, account for increasing active layer thickness or monitor other known site-specific zones of interest, such as the DZAA, shear horizons, degrading permafrost, taliks or lateral water and air fluxes (Arenson et al., 2002; Isaksen et al., 2022; Luethi and Phillips, 2016; Luo et al., 2018; Noetzli et al., 2021; Vonder Mühll and Haeberli, 1990; Vonder Mühll and Holub, 1992). Sensors should be duplicated at important depths (for example, using different chains or very close distance) in case one gets damaged or exhibits drift (Noetzli et al., 2021). Closer spacing at the greatest depth may help to validate deep temperatures. As an example, the regional PACE programme has defined the following sensor spacing for a 100 m borehole: 0.2, 0.4, 0.8, 1.2, 1.6, 2.0, 2.5, 3.0, 3.5, 4, 5, 7, 9, 10, 11, 13, 15, 20, 25, 30, 40, 50, 60, 70, 80, 85, 90, 95, 97.5 and 100 m (Harris et al., 2001).

Measurements near the surface can be influenced by a protective borehole casing (for example, a concrete chamber changing the local snow cover and thermal regime), so a dense sensor spacing until 1 m depth may not be advisable. To prevent this effect, an additional shallow borehole for precise temperature measurements can be installed in the proximity of the main borehole (PACE standard: 15–20 m depth) (Harris et al., 2001; Isaksen et al., 2001). Alternatively, miniature temperature data loggers or fixed temperature sensors can be installed near the surface outside the borehole (see, for example, Isaksen et al. 2022; PERMOS, 2019; Pogliotti et al., 2015). Typically, measurement depths for single near-surface temperature sensors are 0.05 m or 0.1 m, following the two standard uppermost depths for soil temperature measurements defined by WMO in the present Guide. On rock glaciers and other coarse blocky ground material, the surface is difficult to define, such that measurements above about 1 m depth may become unreliable. In these cases, the definition of the surface level needs to be well justified and documented (Noetzli et al., 2021).

The sampling and recording interval depend mainly on the depth of the measurement, the purpose of the investigation and the type of instrumentation. Due to the higher temporal variability, the sampling interval in the uppermost metres must be set to a higher frequency, typically between 1 and 6 h (Isaksen et al., 2022; Noetzli et al., 2021). Hourly sampling intervals can resolve variability in the uppermost metres but may be limited by the required energy supply. Below the DZAA, a lower sampling rate with annual temperature measurements captures long-term trends. Below 50 m, measurements can be repeated every two years, or less frequently (every 5 to 10 years). However, at greater depths smaller sampling intervals may be helpful, since they make it possible to assess the measurement stability at depths with small temperature fluctuation as well as to capture potential non-conductive heat transport processes (Noetzli et al., 2021). Recording intervals are typically programmed for the entire sensor chain and are thus based on the minimum interval of interest. In addition, recording with high temporal resolution allows assessment of the stability of the measurements at greater depths with small temperature fluctuations.

In areas with fine-grained soils and/or high ground ice content (including rock glaciers), heave and subsidence of the ground surface can complicate the fixed measurement depths as the level of the ground surface may vary through the year. For some sites long-term ground subsidence due to permafrost thaw requires careful attention regarding measurement depths, and annual adjustments of the measurement depths are essential to avoid misinterpretation of the measured temperature variations. It is advisable to measure the distance between the ground surface and a fixed point, such as the top of the casing, with a measuring tape during field visits, as it will make it possible to detect whether significant ground subsidence has occurred over time.

Especially at locations where the sensor chain cannot be removed from the borehole for servicing (for example, for recalibration, see 4.2.3.6), sensor duplication is a very useful strategy for long-term monitoring to validate the measurements as well as for backup in case of erroneous sensor data (for example, caused by drift (Noetzli, 2021; Widmer, 2023)). Sensor duplication can be achieved by overlapping temperature sensor chains or by placing sensors with a minimal distance on the same sensor chain. It is recommended to duplicate sensors at the key depths of 5, 10, and 20 m. Due to small-scale terrain heterogeneities it can be difficult to compare the data to those from nearby boreholes. The use of two different measurement systems can provide more security, since both systems will not be sensitive to the same perturbations, and this may avoid simultaneous failure (for example, using a thermistor chain and a digital temperature sensor chain (Widmer et al. 2023) together with a sensor chain and a fibre-optic cable for distributed temperature sensing (Schoeneich et al., 2012, 2015)).

4.2.3.3 ***Temperature sensors***

Different types of temperature sensors and measurement systems are available to measure permafrost temperature in a borehole. The choice of the appropriate instrumentation depends on the specific measurement requirements, such as data accuracy and resolution, spatial and temporal resolution and coverage, as well as installation and maintenance costs (see, for example, Lundquist and Lott, 2008). For permafrost observations, the temperature sensors should have the highest absolute accuracy at 0 °C and cover the entire anticipated temperature range (Noetzli et al., 2021). A summary of the most commonly used types of temperature sensors is given below, but for an in-depth tutorial on temperature sensors, see Reverter (2021), for example.

Wires, contacts and casings of the sensor and logging systems (4.2.3.4) should be hermetically sealed to prevent measurement disturbances due to moisture infiltration (Noetzli et al., 2021). To reduce convective heat transport after the installation of the instruments, the borehole can be filled with conducting fluid or, if the sensor chain is to remain permanently in the borehole, with sand. Insulation foam can also be added between the uppermost sensors, where the temperature gradient is the largest.

Resistance temperature sensors

For almost four decades, resistance temperature sensors have been the most commonly used sensors in permafrost temperature studies. They operate based on the principle that the resistance of a material changes with changing temperature. That is, the temperature is calculated based on a well-known relationship between temperature and resistance. Based on the material the sensors are manufactured from, two different categories are generally distinguished, thermistors and resistance temperature detectors (RTDs).

Thermistors are generally manufactured from semiconductors and are characterized by a relatively high sensitivity and medium accuracy (Reverter, 2021). Thermistors can either have a resistance that decreases with increasing temperature, called negative temperature coefficient (NTC), or a resistance that increases with increasing temperature, called positive temperature coefficient. The most commonly used in analogue temperature sensor chains are NTC thermistors, which are most typically manufactured from metal oxides. Measured resistance is converted to temperature, often by the Steinhart–Hart equation, whose coefficients usually are published by thermistor manufacturers. The accuracy of a thermistor depends on the material and processes that were used for its production, the calibration, and its coefficients and age, leading to a drift with time (see, for example, Merlone et al., 2020). The age-dependent drift rate normally corresponds to <0.01 °C per year, depending on the manufacturer (Biskaborn et al., 2019). In addition, the relationship between resistance and temperature is non-linear for thermistors (or is linear only for a small temperature window), leading to different accuracies for different temperature ranges. Typically, NTC thermistors have a higher sensitivity at lower temperatures due to their characteristic line.

Resistance temperature detectors (**RTDs**) are manufactured from pure metals, commonly platinum (PRTDs). RTDs operate on the principle that the resistance of a pure metal increases with increasing temperature (Reverter, 2021). The accuracy of RTDs is higher than that of thermistors; however, their sensitivity is lower, often by several orders of magnitude. The lower sensitivity of RTDs requires more sophisticated equipment to realize their higher accuracy and obtain the required resolution. Due to their high accuracy and linearity, PRTDs are often regarded as the industry standard for temperature sensing. Generally, measurements with thermistors or RTDs are performed by applying an excitation voltage and then measuring the voltage drop across the sensor. Thus, in sensor configurations with long cable lengths of several decametres, the resistance of the wires connecting the sensor to the measurement device can introduce significant errors. Due to their lower sensitivity, RTDs are more susceptible than thermistors to these measurement errors. To compensate for this, rather than deploying the sensor in a common two-wire configuration, a four-wire configuration can be used (Reverter, 2021). However, this can be difficult to produce for long temperature sensor chains of several decametres in length. For analogue thermistor chains it is advisable to place a combination of thermistors on individual wires to prevent a loss of all sensors due to failure of a single wire (Noetzli et al., 2021).

Silicon-based digital temperature sensors

Silicon-based digital temperature sensors are becoming increasingly popular, however, experience with long-term installations is still limited. These sensors can be incorporated into an integrated circuit so that the temperature sensor, and measurement and temperature conversion circuitry are all on a single integrated circuit chip (Reverter, 2021). In this case, signal transmission inaccuracies are reduced by the digitization of the signal directly at the point of measurement. This system is less affected by moisture infiltration and lightning. However, digital sensors are typically mounted on a single cable, which increases the risk of total sensor failure in case of cable damage (Noetzli et al., 2021). Digital temperature sensor chains have been tested in some permafrost boreholes. A first analysis of temperatures measured by two sensor systems (thermistors and digital temperature sensors) under field conditions in mountain permafrost in Switzerland at 15 identical depths in one borehole shows that differences between the temperature sensor types are minimal, with less than 5% of all values outside of a 0.1 °C difference (Widmer et al., 2023). Experience from five to ten years of monitoring with digital chains in Norway and Svalbard is also promising (Isaksen et al., 2022).

Thermocouples

Thermocouples are inexpensive, rugged and flexible temperature sensors (Osterkamp, 1984). Their working mechanism is based on temperature-dependent voltage that is produced at the junction of two dissimilar metals, known as the Seebeck effect (Reverter, 2021). They offer good resistance to weathering and corrosion. Since a thermocouple junction is also created at the point of connection to a measurement instrument, only the difference between the two junctions is measured. Thus, an accurate reference temperature (thermistor or PRTD) is required. Their sensitivity and accuracy lie in between those of resistance thermometers and mechanical thermometers (Culik et al., 1982). Due to their relatively low accuracy, they are no longer recommended for permafrost temperature monitoring applications.

4.2.3.4 ***System configuration***

Permanent installation of a temperature sensor chain connected to a data logger allows for a continuous record of ground temperatures at specific depths. Data loggers make it possible to preset the measurement routine and to define the data format, and provide information on calibration as well as conversion and data storage. When site visits are infrequent, and depending on the sampling size and interval, loggers can save data for 1–2 years or more, assuming sufficient power is available. Remote access through a mobile network or through satellite or radio communication allows for near-real-time data transmission as well as rapid intervention in case of technical problems (Isaksen et al., 2022, Noetzli et al., 2021). Logging systems can be placed inside the protective cover of the borehole or they can be fixed to a mast of a co-located weather station or solar panel.

The logging systems often use some combination of battery, solar and/or wind power, but many use batteries alone. In Arctic areas special care must be taken regarding the dark season, during which solar power is not available for several months. In mountain areas and lowland areas with thick snow cover, solar panels and wind turbines can be installed above the snow surface in avalanche-free locations to operate all year (wind turbines may be affected by freezing of their blades). In avalanche-affected terrain, safety is more important than solar-radiation reception (for example, solar power can be reduced by temporary snow coverage). Mounting the logging system on a mast may protect it from smaller avalanches. In this case, the exposed box should be well ventilated to prevent inner condensation. Logging systems located at exposed high-mountain sites need robust lightning protection that covers the entire observation installation (Noetzli et al., 2021). To facilitate this, the station should only be connected to the ground at a single point, and surface cable layout needs to be kept to a minimum. Cables can additionally be shielded, susceptible components insulated and surge protection installed at the connection outlet of the logging box (Noetzli et al., 2021).

4.2.3.5 *Uncertainty and sources of error*

According to the International Vocabulary of Metrology (BIPM, 2012), **measurement accuracy** is defined as "closeness of agreement between a measured quantity value and a true quantity value of a measurand." The definition notes that: "The concept 'measurement accuracy' is not a quantity and is not given a numerical quantity value." The **uncertainty of a measurement**, on the other hand, must be associated with a non-negative number "characterizing the dispersion of the quantity values being attributed to a measurand, based on the information used" and must be always evaluated when measurements are performed.

It is desired that the measurement uncertainty of the entire measurement system remain at ±0.1 °C or less according to the GTN-P measurement guidelines (Streletskiy et al., 2022). Breakthrough uncertainty is reached at ≤0.05 °C. The ideal measurement uncertainty is ≤0.02 °C (see, for example, the GCOS ECV requirements (GCOS-245)), since the system uncertainty should be lower than the measured changes. Over one decade the permafrost temperature change below the DZAA can be on the order of a few tenths of a degree Celsius (see, for example, Biskaborn et al., 2019; Etzelmüller et al., 2020, Smith et al., 2022).

Not all sensors easily fulfill the measurement uncertainty requirements over a larger temperature range, for example, an uncertainty of ±0.1 °C from –30 °C to +10 °C (see, for example, Biskaborn et al., 2019, Noetzli et al., 2021, Streletskiy et al., 2022). Depending on sensor type, the largest contributors to uncertainty are typically potential drift, hysteresis (ability to measure the same temperature starting from lower or higher temperature environments) and sensitivity (see 4.2.3.3). In addition, measurements can be influenced by the configuration of the measurement system, which includes, for example, long cables and multiplexers.

The environment in which the sensors work can often be the largest source of uncertainty in measurements. Several associated quantities of influence can affect both the measurand and, more importantly, the sensors themselves. A further contributor to the measurement uncertainty in a permafrost setting, particularly for a shallow borehole, is the degree of thermal contact between the sensor and soil: when a permafrost sensor chain is put inside a borehole in direct contact with the air inside the hole but not the soil around it, the largest uncertainties arise given the low thermal conductivity of air itself and associated convective phenomena. Due to the low temperature gradient at great depth (<0.1 °C m–1), a mm-level positioning error has no effect on measurement accuracy (Biskaborn et al., 2019).

In boreholes subject to borehole deformation, cable stretching may induce drift in recorded temperatures or breakage and destruction of the cable. In thermistors, the direction of drift depends on the influencing factor. They drift downwards (producing falsely low temperature values) if the wires are stretched (Luethi and Phillips, 2016). Moisture infiltration into the logging system, sensors or connections can induce an upward drift or (producing falsely high values, Luethi and Phillips, 2016).

Ice often develops in the borehole tube at the level of the permafrost table, probably due to condensation of air moisture or damage to the tube. In some cases, it can evolve to form an ice plug that blocks melt water above it. This can affect measured temperatures, inducing a zero curtain in the measurements which is not present in the surrounding ground. Ice plugs can be removed by melting them either with a heating device (electric resistance) or by blowing warm air on them (blow dryer). Little is known about the effect of water infiltration and refreezing in the borehole on temperature measurements. Also, water may enter the borehole due to problems with the seal between casing sections (for example, deterioration of the cement or improper application of cement).

Long-term permafrost monitoring in warm and/or saline permafrost will benefit from deeper boreholes to avoid the possibility of upward vertical displacement (frost jacking) of the casing.

Casing pipes embedded insufficiently deeply in permafrost may not have sufficient resistance to counteract heaving forces that develop in the active layer (see, for example, Gruber, 2020; Ladanyi and Foriero, 1998).

4.2.3.6 *Calibration*

Traceability, that is, the "property of a measurement result whereby the result can be related to a reference through a documented unbroken chain of calibrations, each contributing to the measurement uncertainty" (BIPM, 2012), is crucial to achieving comparable measurement results at different sites, with different systems, and at different times.

Sensor calibration may not be possible in all regions or settings or for all types of equipment. In most such cases, sensors are either frozen in or are blocked due to borehole deformation, or the borehole was filled from the beginning. In remote Arctic locations it may not be possible logistically. On a rock glacier with borehole shearing, thermistors cannot be removed from the borehole after a few months or years, depending on the deformation rate and shearing of the borehole (see, for example, Noetzli et al., 2021). In addition, pulling out a sensor chain for recalibration incurs the risk that it will not be possible to install it again at the same depths or down to the bottom of the borehole.

Sensors should be provided with a calibration certificate from an accredited laboratory. For long-term monitoring, the sensor drift of the temperature probe – for example, for NTC thermistors – can lie in the range of the permafrost temperature trend to be captured. To ensure accurate measurements, instrument calibration is essential. Calibration is a documented comparison of the measurement system to be tested against a traceable reference standard. Calibration is typically performed in a laboratory prior to permanent field installation. Calibration of the sensors should be performed using the same instrument setup (that is, temperature sensor chain, logging device, cables, etc.) as is used at the measurement site. In the laboratory, sensors should be calibrated in a shaved ice bath or snow–water bath checked with an accurate reference thermometer (Wise, 1988). If the ice bath is prepared properly and regularly stirred, it will be at 0 °C with an accuracy of at least 0.005 K. Also, a double bath (that is, a bath in a bath) is sometimes used for better insulation against the outside temperatures. Further calibration at other temperatures can also be performed using a liquid calibration bath and reference thermometer (Merlone et al., 2020).

Temperature calibration should involve at least three setpoints around 0 °C, to be able to interpolate (usually by means of a simple square polynomial) the behaviour of the devices under test. To do this, an alcohol bath is required in which three temperatures can be set. The temperature range of the calibration should be larger than the actual temperature range experienced by the sensors during normal operation, because extrapolation introduces larger uncertainties than interpolation.

To achieve and maintain the prescribed system uncertainty, sensor **recalibration** should be performed every 5–10 years of station operation to identify sensor drift or after changes in the measurement setup. At reference sites or when low uncertainties are required (for example, 0.01 °C), recalibration should be performed every 2–5 years, to correct for potential drift of sensors and systems. Ideally, sensor chains should be removed from the borehole for recalibration in the laboratory. However, the remoteness of some boreholes does not allow for that. In such cases, calibration should be performed in the field. If a second access tube is installed in the borehole, it can provide an opportunity to check the plausibility of the data registered by the long-term sensors. One way to calibrate the sensors is to insert a high-precision, calibrated PT1000 (a PRTD with a nominal resistance of 1 000 ohms at 0 °C) next to the long-term sensor. It is important to note that several hours of equilibration might be needed before the measurement can be performed. There are systems, such as those described in Merlone et al. (2020), that can be brought to the measurement site and used for calibrating permafrost temperature sensors without the need for a complete disassembly of the system. These systems also have the advantage of allowing calibration in the environmental conditions that the sensors and data logger system encounter during normal operation (temperature, wind, solar radiation, humidity, atmospheric pressure).

If the borehole setup is properly designed and established in a stable environment (for example, in an air-filled casing without deformation of the borehole by permafrost creep), it may be possible to set up a second newly calibrated system in the same borehole and compare the measurements, ideally for a year (but as a minimum for one day), to be sure that all sensors are allowed to come to equilibrium with the adjacent ground temperature.

4.2.3.7 *Maintenance*

Regular maintenance of the instruments is essential for successful collection of continuous high-quality data, to repair or replace broken parts and to prolong the service life of the equipment (Noetzli et al., 2021). Maintenance typically includes one field visit per year, however this may not be possible due to logistical or budget constraints (remoteness of the sites, number of boreholes to maintain). The maintenance should include a visual check of all parts of the measurement system (that is, logger box, batteries, modem and antenna, cables at the surface and their connections and protection) and checks for possible subsidence or frost jacking of the borehole casing. It is also important to consider the replacement of certain components on a regular basis.

Regular field visits are particularly important if there is no remote access. In areas with many animals (mice, foxes, reindeer, bears, etc.) or that are prone to thunderstorms or natural hazards (avalanches, rock fall) that can potentially damage the installation, it is particularly important to look for damage and repair it. If possible, measures must be taken to prevent further damage in the future. Taking photographs of each part of the measurement system and the conditions at the site during each visit in order to document the current state (and hence any changes) has proven helpful for future reference. A standardized field visit protocol helps with the full documentation of the station history including the work completed and changes or updates made to the instruments or logger programme (Noetzli et al., 2021). Without such crucial information, later data processing, correction or homogenization is extremely difficult and time-consuming, or even impossible.

4.2.4 Manual temperature reading

4.2.4.1 *General principles*

Logging of temperatures in boreholes by lowering a single sensor probe (Figure 4.6) into the borehole is still common, especially for boreholes deeper than 40 m in Arctic areas (Osterkamp, 2003; Smith et al., 2010, 2022). To allow for permafrost temperature data comparison, repeated measurements should be taken in the same spatial and temporal frame when possible (same measurement depth and time of the year). Further, the time stamp should be shared along with the data, indicating if the measurement has been taken at one single time, or if it reflects the average value of a time period (as specified by GTN-P: https://gtnp.arcticportal.org/data/data-handling/19-data/mining/80-protocols-good-work-practices).

While it is generally undesirable to take measurements only once per year from a borehole, one advantage of this approach is that the same, well calibrated sensor is used at all depths and in all boreholes. Thus, quality and confidence in the measurements can be higher than for measurements from temperature sensor chains. Therefore, boreholes allowing manual measurements are an excellent way to check an installed temperature sensor chain for drift (see 4.2.3.6). In addition, annual measurements at depths below the DZAA are considered sufficient to capture the long-term changes of the permafrost temperature driven by a conductive thermal regime.

4.2.4.2 *Depth of measurement, sampling and recording interval*

Generally, the depth of manual measurements is the same as with measurements using temperature sensor chains (4.2.3). Sampling of the borehole temperature profile is performed by lowering a temperature sensor stepwise into the borehole, pausing at each depth of interest to allow the sensor to adequately equilibrate. It is helpful if the depths are marked on the sensor cable is marked to allow accurate placement of the sensor.

Typically, the upper 10 to 15 m are measured at 1 m intervals and the deeper depths at 2 or 5 m intervals, depending on the time available and if the borehole is filled with liquid or air. The borehole filling (liquid or air), the temperature gradient between measurements and the thermal mass of the sensor determine the amount of time required for the sensor to equilibrate (Widmer et al., 2023). For example, in a liquid-filled borehole this time may be as short as 2 or 3 minutes, whereas in an air-filled borehole equilibration may take as long as an hour or more. Thus, it is important to test a sensor's equilibration time in the borehole medium before use. The recording interval should be set so that it can be clearly observed when and if the sensor has equilibrated.

4.2.4.3 *Temperature sensors*

The measurement systems currently in use generally provide an accuracy and precision of 0.1 °C or better and are either based on resistance temperature or digital temperature techniques (see 4.2.3.3).

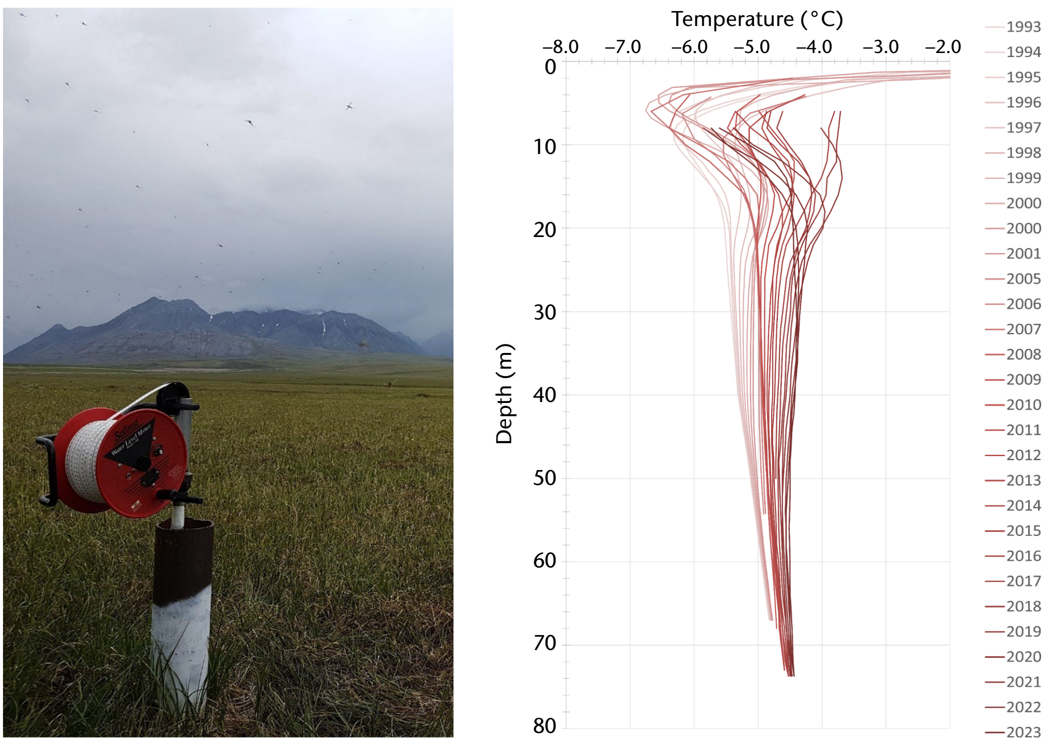

Figure 4.6. Left: borehole at Galbraith Lake, Alaska with manual measurement system in place. The system consists of a measurement tape on a reel with a self-contained temperature logger mounted at the end. Right: thirty years of annually measured borehole temperature data from Galbraith Lake. The borehole was drilled in 1985 and is 75 m deep.

Sources: William Cable (left); Romanovsky et al., 2022 and Osterkamp, 2003 (right)

4.2.4.4 *System configuration*

A typical manual temperature system consists of the temperature sensor and measuring device. Often this is a temperature sensor (for example, thermistor), attached by a long cable to either a data logger or resistance meter (Osterkamp, 2003). Care should be taken with long cable lengths as the resistance of the cable itself starts to become a factor and needs to be compensated for (for example, with a 3- or 4-wire bridge). The use of a digital temperature sensor eliminates this problem because the temperature conversion is performed at the sensor and transmitted as a digital signal. With the measuring device at the surface the temperature or resistance can be monitored until the sensor value is no longer changing, indicating that the sensor is in equilibrium.

Another possible system configuration is to have the sensor and data logger combined into one device that is lowered into the borehole. While this is a simple and effective measurement technique, the user is "flying blind" and will have to wait at each depth a predetermined amount of time for the sensor to equilibrate.

Sometimes, permanently installed multisensor temperature cables are not connected to a continuous logging system for logistical or other reasons. In this case, measurement of these cables requires a high-accuracy digital multimeter.

4.2.4.5 *Uncertainty and sources of error*

The sources of error and uncertainty for manual temperature readings are generally the same as with temperature sensor chains (see 4.2.3.5), with the exception of sensor drift, as the sensor can be calibrated before and after every use.

4.2.4.6 *Calibration*

Generally, sensor calibration for manual temperature readings is the same as with temperature sensor chains (see 4.2.3.6). Before each measurement campaign, the sensor and measurement system should be calibrated or, at a minimum, checked in an ice bath.

4.2.4.7 *Maintenance*

Temperature sensors and measurement systems should be kept in good working order to ensure the quality of the data. Temperature sensors should be replaced when drift becomes excessive and can no longer be compensated for through calibration.

4.2.5 **Fibre optic (distributed temperature sensing)**

Distributed temperature sensing (DTS) uses optoelectronic devices that can measure temperature via optical fibres. In contrast to conventional point-sensor methods, DTS sensors provide high spatial and temporal resolution by recording continuous temperature measurements along a cable that defines the profile (Tyler et al., 2009). Measurements are based on the detection of backscattered light pulses. For high temperature precision, Raman backscattering is used. Modern instruments allow a spatial resolution of 0.5 or even 0.25 cm along the fibre optic cable, on cable lengths up to several km (Ukil et al., 2012). This new technology has been applied to some sites in polar (see, for example, Roger et al., 2015) and mountain permafrost (see, for example, Harrington and Hayashi, 2019; Schoeneich et al., 2015) environments. It has been used in boreholes as well as for spatial monitoring of subsurface evolution (Roger et al., 2015) and has proven effective in capturing thermal transfer processes. Technical specifications as well as an example of a borehole installation can be found in Schoeneich et al. (2012). Further studies need to evaluate if long-term implementation of fibre-optic cables is feasible in the dynamic environment of permafrost, where frost processes cause ground perturbation and cracking (Roger et al., 2015).

4.2.5.1 *System configuration*

DTS measures temperatures along a fixed fibre-optic cable (coated quartz fibre) that can be either laid down in a subsurface trench (Roger et al., 2015) or installed in a borehole (Schoeneich et al., 2012). The cable must be longer than the measurement section, with the remaining length at the beginning and the end of the cable being used for calibration. The cable should be accessible from both ends, in order to allow double-ended measurement.

DTS can either be measured periodically or monitored continuously. The measurement instrument is, however, very expensive, and in the very harsh conditions common in permafrost areas, the instrument must be protected for continuous measurements.

4.2.5.2 *Calibration*

DTS measurement gives relative values that need to be calibrated. Modern instruments include an internal calibration, but for periodic measurements it is necessary to calibrate the device every time in an ice/water bath.

4.2.5.3 *Uncertainty and sources of error*

The theoretical accuracy of DTS measurements is within 0.1 °C, or even 0.01 °C. However, this accuracy can be reached only with long measurement times. In the case of periodic measurements with short measurement times (1–2 h), the observed uncertainty is in the range of 0.1 °C. This can be reduced by calculating average values on double-ended or replicated fibre sections or measurements. The calibrated uncertainty has to be added to the measurement uncertainty, so that the total uncertainty can be estimated. Uncertainty on the order of ±0.1 °C is achievable (Schoeneich et al., 2015).

4.2.6 Subsea permafrost temperature measurements

Measurements of subsea permafrost can be available from borehole logs acquired in offshore wells (for example, for oil and gas exploration). The borehole measurement locations often depend on the locations of hydrocarbon fields. Further, hydrocarbon boreholes are typically designed for depths significantly exceeding permafrost thickness, which requires a larger borehole casing diameter in the uppermost sediment section, which can affect the quality of temperature measurements. Underwater drilling is very challenging and expensive. If possible, alternative drilling sites may be placed at or near offshore islands (Ruppel et al., 2016). With distance from the shore, subsea permafrost evolves from continuous to discontinuous permafrost.

Currently subsea permafrost temperature determination relies mainly on bottom water temperature measurements and sediment temperature probes that can constrain the upper boundary conditions for heat flux modelling in subsea sediments (Frederick and Buffett, 2015; Gavrilov et al., 2020; Nicolsky et al., 2012). In this case, borehole temperature measurements may be used. However, these are typically compromised by seawater, drilling fluids and hole conditions and have to be analyzed with extra caution. In shallow water, to prevent seawater from entering the borehole, a metal casing can be drilled into the seafloor sediments through the sea ice water column. For example, an approach has been described by Overduin et al. (2016) using a portable rotary drill rig and a dry drilling technique.

4.3 MEASUREMENTS OF ACTIVE LAYER THICKNESS

4.3.1 General

This section describes the most common methods of direct in situ thaw depth measurements used for assessing the active layer thickness (ALT) in permafrost-affected environments, its spatial variability, and temporal dynamics. The information provided is for direct active layer measurements using end-of-season manual probing and a visual interpretation of the ALT using a thaw depth indicator gauge (frost/thaw tube). The ALT can also be estimated using a vertical profile of temperature sensors extending through the active layer and upper permafrost.
The measurement strategy as well as the pros and cons will be presented for each technique.

4.3.1.1 *Definitions*

The term "active layer thickness" (ALT) in permafrost-affected regions refers to the thickness of the thawed layer (measured relative to the ground surface) that is reached at the end of the warm season (van Everdingen, 1998). The term "thawed" can indicate either melting of ice or warming above 0 °C. The distinction between temperature-based and phase transition-based definitions is relevant as the ice-nucleation temperature in soils can be depressed due to salinity, capillary effects and pressure, causing the ground to remain unfrozen at temperatures below 0 °C. As a result, the bottom portion of the active layer as defined on the basis of phase changes in water can be considered to be part of the permafrost layer. The ALT is distinct from the term "thaw depth", which refers to the thickness of the thawed layer at any time during its development. In permafrost environments, the maximum annual thaw depth is indicative of the annual thickness of the active layer. In other words, thaw depth is essentially an instantaneous value that is always less than or equal to the thickness of the fully developed active layer. The thickness of the active layer is inferred from the thaw depth measurements at the end of the thawing season.

Unless otherwise specified, a thaw depth measurement refers to a measurement at a single location at a given time, and a thaw depth survey is a series of measurements at a single site following a predetermined spatial pattern. Thaw depth is typically measured in cm.

4.3.1.2 *Spatial and temporal variability of the active layer thickness*

Factors influencing thaw depth and thickness of the active layer and their spatial and temporal distribution include: (i) mean annual ground surface temperature (MAGST); (ii) the amplitude of the annual temperature cycle at the ground surface; (iii) the composition and thermal properties of the surface cover and subsurface material; and (iv) the ground moisture regime. Zonal trends in ALT are discernable if similar soils and surface cover are considered at all sample locations (Luo et al., 2016). In general, ALT decreases poleward and with elevation, and it increases in continental areas as the elevation decreases. At local and regional scales, however, both thaw depth and ALT are highly variable over space in response to variations in subsurface properties, soil moisture, topographic position, and snow and surface cover (vegetation, debris, etc.). The spatial variability of thaw depth tends to increase over the course of a single warm season due to variable rates of thaw propagation through surface and subsurface materials with highly heterogeneous properties (Hinkel and Nelson, 2003). Due to the high variability of ALT over short lateral distances, thaw depth surveys are preferable for generating samples statistically representative of local conditions (compare 4.4.1.3).

ALT can vary substantially on an inter-annual basis in response to variability in atmospheric climate (for example, air temperature, precipitation).

4.3.2 Active layer thickness observations

Observations of the ALT involve direct measurements of the end-of-season thaw depth during one or more years. There are two primary ways in which this is accomplished:

(1) Measurements aimed at identifying the maximum annual depth to frozen (ice-bonded) Earth material by manual probing (4.3.4). Manual probing observations may consist of a measurement at a single point or thaw depth surveys with multiple measurements in a predetermined spatial pattern (for example, transects, grids). Unlike a point measurement, thaw depth surveys enable the observer to assess the spatial variability at the observation site (Brown et al., 2000) (Figure 4.7). Manual thaw depth probing at the end of the thawing season is the most frequently used method for monitoring active layer changes at the Circumpolar Active Layer Monitoring (CALM) network of observational sites (see, for example, Nelson et al., 2021). The results have been used in numerous long-term studies (for example, Abramov et al., 2021; Kaverin et al., 2021; Nyland et al., 2021; Oblogov et al., 2023; Strand et al., 2021).

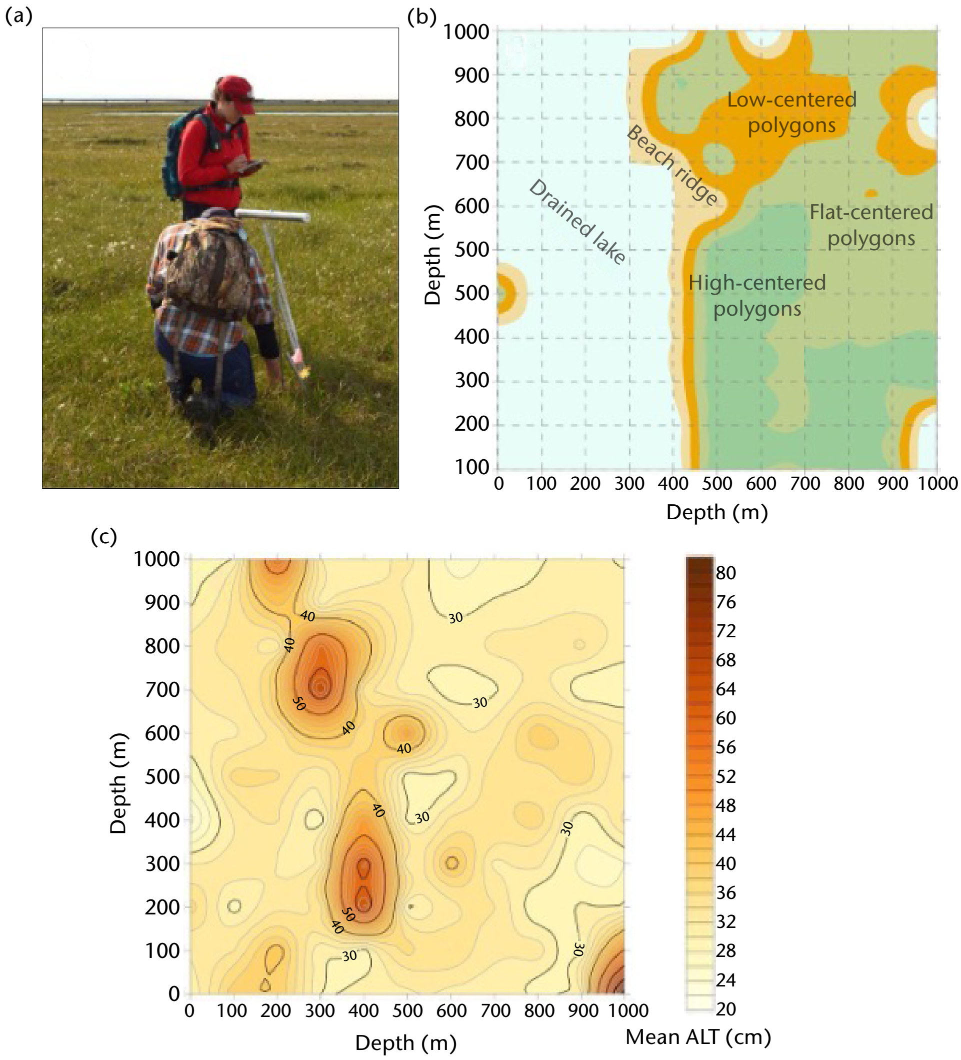

Figure 4.7. (a) Thaw depth measurements by mechanical probing conducted at the Circumpolar Active Layer Monitoring (CALM) site in Arctic Alaska. (b) A landform map of CALM U1 (Utqiagvik) 1 km × 1 km site. The site encompasses major landforms characteristic of the North Slope of Alaska. Locations of 121 annual thaw depth measurements are indicated by intersections of dashed grid lines. (c) Spatial representation of 1995–2023 mean of the annual end-of-thaw season (third week of August) thaw depth measurements from the CALM U1 (Utqiagvik) 1 km × 1 km site.

(2) Visual interpretation of the maximum annual depth of the 0 °C isotherm using a thaw depth indicator gauge (frost/thaw tube) (Bonnaventure and Lamoureux, 2013; Mackay, 1973) (4.3.5). Frost/thaw tubes are devices that extend from above the ground surface through the active layer and are anchored in the underlying permafrost (Figure 4.8). They are used to derive ALT value for the preceding summer independent of the vertical position of the ground surface and corrected to a standard height above the ground established during installation (that is, a fixed datum). Examples of frost tube applications for active layer monitoring can be found in Christiansen (2004), Garibaldi et al. (2022), Mackay (1973), O'Neill et al. (2023, 2019), Smith and Brown (2009), and Vieira et al. (2010).

As previously noted, these two measurement strategies may yield different results, representing an example of the problems arising from differing definitions of the active layer.

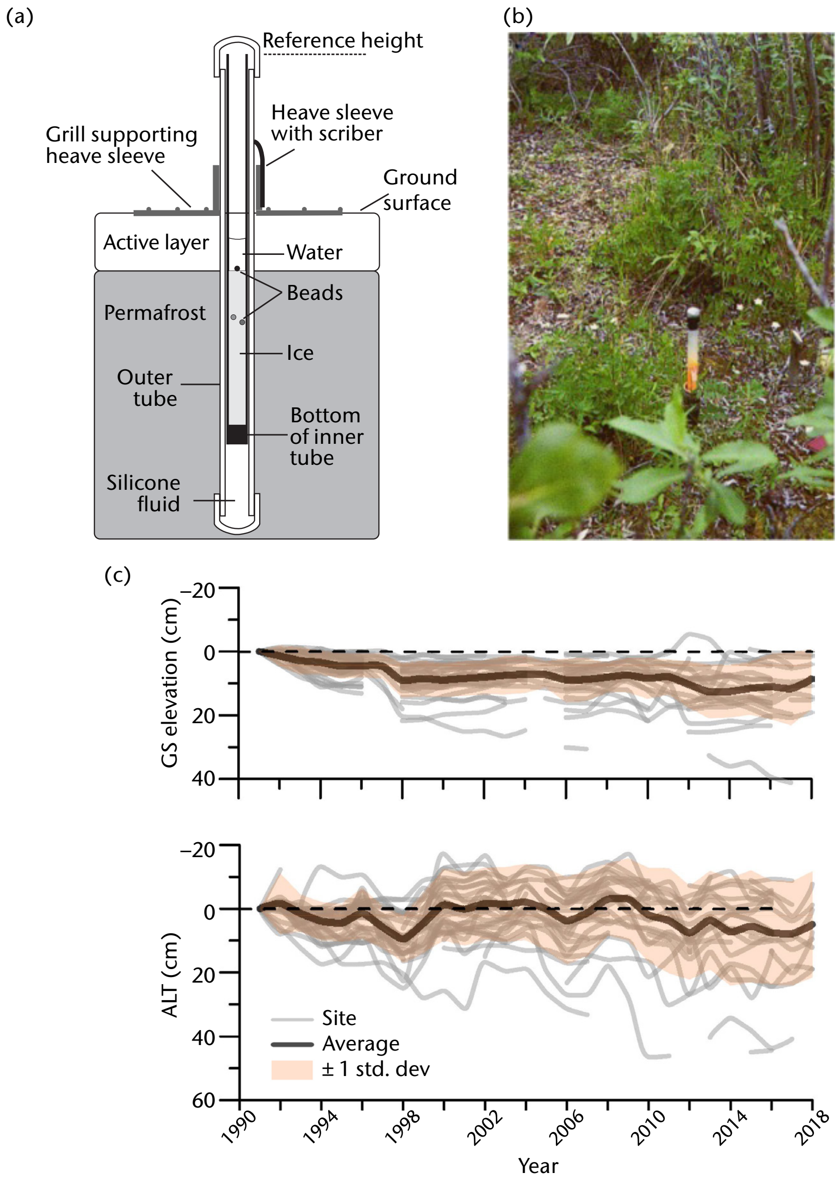

Figure 4.8. (a) Schematic diagram of the typical frost/thaw tube used to measure the active layer thickness (ALT) and ground surface (GS) elevation (after Mackay, 1973). (b) Frost/thaw tube installed at the Reindeer Depot (C07) Circumpolar Active Layer Monitoring (CALM) site in the Northwest Territories, Canada. (c) A long-term ground surface elevation and ALT record from 28 frost/thaw tube sites in north-west Canada. The values are plotted relative to the first year's value in the record for each site (after O'Neill et al., 2023).

Source: Reproduced with permission from Natural Resources Canada

4.3.3 Site selection

Prior knowledge of the surface and subsurface conditions of the area should guide the selection of an appropriate site (see also 4.1.4). Specifically, it should be considered that manual probing works best in organic and fine-grained subsurface materials that are ice-bonded when frozen. However, probing is not a useful method for determining thaw depths in areas with very thick active layers (more than approximately 2 m as typically measured in mid-latitude mountain areas), areas containing consolidated Earth material (bedrock) or areas where the surface is covered in coarse debris (rock glaciers, talus). Well-drained sands and gravels may contain too little interstitial ice for adequate resistance to probing to develop. Accurate readings may be very difficult to obtain in stony substrates such as glacial till. As a result, simple probing may not be suitable in mountainous areas or areas with a complex topography and surface/subsurface conditions where ALTs can vary considerably, or permafrost can go from being present to absent over short horizontal or vertical distances. For these areas, the ALT can only be determined based on the 0 °C isotherm (see 4.3.6).

Because in many cases measurements can be made rapidly and with little effort, probing is well-suited for implementing thaw depth surveys to obtain a statistical sample of ALT values representative of local surface and subsurface conditions. The ideal site for a probing survey should be representative of the surrounding landscapes based on topography (for example, slope, exposition, concavity/convexity) and ground surface cover (for example, vegetation, surface water) (see 4.1.4). Ideally, each site should encompass the local-scale variability in microtopographic features of the landscape. Examples of typical microtopographic variability within permafrost-affected landscapes may include tundra polygons, hummocks or tussocks, frost mounds/palsas, water-filled depressions and small water tracks (Boike et al., 2022).

The typical site for a thaw depth survey consists of a series of regularly spaced observational nodes arranged along one or more transects or in a grid pattern across/within the representative landscape (Brown et al., 2000). The size of the grid and the length of the transects can vary depending on site geometry, the scale of the active layer's local variability, and monitoring objectives. Transects are typically 10 to 100 m in length, with sampling nodes spaced 1 to 10 m apart. Grids are typically 10, 100 or 1 000 m on a side, with nodes distributed evenly at 1, 10 or 100 m spacing, respectively (Figure 4.7). Exploratory sampling may be necessary to establish transects or grids of dimensions appropriate to the local conditions and the scientific goals. In many instances, it is more advantageous to establish a site consisting of several shorter/smaller transects/grids representing major relatively homogeneous landscape units characteristic of the area than to try to capture all local variability with one long/large transect/grid. To facilitate inter-annual comparison, sampling node locations along a transect or within a grid are identified using stakes or other semi-permanent markers, and replicate measurements are made at approximately the same location each year.

Frost/thaw tubes can be installed in areas where thaw propagation is too deep to monitor by probing, and in stony, fine-textured or saline substrates in which probing is not feasible. An important advantage of frost/thaw tubes over probing is the ability to capture the maximum thaw depth. However, unlike with manual probing, each frost/thaw tube record consists of only a single-point measurement which might not be representative of the surrounding landscape. As a result, the exact location of a single frost tube should be determined based on an extensive thaw depth probing survey at the end of the first summer of measurements. The installation point should be representative of the mean end-of-season thaw depth for the entire landscape. If logistically possible, periodic probing surveys timed to coincide with maximum thaw depth are recommended to assess the spatial representativeness of the point measurement (Tarnocai et al., 2004).

Manual probing does not produce any negative environmental impact other than that caused by walking. For sites intended for long-term monitoring, the issue of surface disturbance must be considered. Periodic walking along the same path can in some instances disturb the natural vegetation cover, altering the ground thermal regime and affecting thaw depth. Logistical constraints such as accessibility should also be considered when establishing long-term monitoring sites. Frost/thaw tube installation typically involves drilling, which might result in significant disturbance of the surface and subsurface materials.

The characteristics of the observational site should be captured in the site metadata. Important details to be listed in the metadata for thaw depth measurement sites include, but may not be limited to, location (GPS coordinates), general climate and permafrost characteristics, slope, aspect, surface and subsurface parameters (vegetation type/height, surface hydrology, organic and/or subsurface layers, ground ice, etc.) of the location, site layout and sampling strategy.

4.3.4 Manual thaw depth probing

4.3.4.1 *Probing equipment*

The standard tool to measure thaw depth by manual probing is a metal rod with a handle called a probe. Other common names include "frost probe", "ALT probe", "tile probe" and "active layer probe". The typical probe is a 1 to 1.3 m long metallic rod with a tapered point and is 1 cm in diameter (Figure 4.7 (a)). The simplest probe is a sharpened metallic rod welded to a pipe. Because the probe will be continually exposed to water in the saturated soils, a stainless steel rod should be used to prevent rusting. Graduated probes have lengths in cm engraved onto the rod to simplify measuring. Breakdown probes come apart for easy shipping, with the pieces stored in the handle. At sites where the thaw depth is large (for example, 1–3 m) longer probes should be used. The diameter of long probes must also be greater to withstand the bending stress generated by insertion. However, it can be very difficult to extract a probe in deeply thawed soils if the probe's surface area is very large.

4.3.4.2 *Timing*

Timing of the thaw depth probing is essential for determining the thickness of the active layer. Ideally, measurements should be collected at the time of maximum thaw penetration, which can vary from year to year and with location. Ground temperature monitoring within the active layer and near-surface permafrost can also be used to estimate the timing of the maximum depth of thaw penetration. However, the exact date when the thaw depth reaches its annual maximum at a specific site is impossible to predict. Moreover, field measurements are often constrained by logistical or weather-related considerations. It is therefore unlikely that the measurement of thaw depth will coincide perfectly with the actual maximum ALT. The CALM programme addresses this problem by conducting annual thaw depth measurements during the same calendar week at the end of the thawing season (mid-August to mid-September in the northern hemisphere) (Luo et al., 2014; Nelson et al., 2021; Nyland et al., 2021). While this approach provides only the approximate thickness of the active layer in any given year, it ensures consistency of the thaw depth record for discerning long-term trends.

4.3.4.3 *Measurement procedure*

Manual probing to measure thaw depth is a simple procedure. The observer pushes the probe into the ground normally to the surface until it encounters a resistance by the ice-bonded layer, which is also indicated by a distinct "thump" sound. Once the frozen layer is reached, the observer places the thumb at the surface and pulls the probe out of the ground. The penetration depth of the rod is then measured from the pointed end of the rod to the observer's thumb using a measuring tape, or from graduated marks on the rod. Observations are conducted in cm and are rounded to the nearest centimetre.

Probes typically cannot penetrate the rocky ground or tree roots and make a "ping" or scraping sound when encountering stones or roots, rather than the "thump" that can be heard when hitting frozen ground. If a stone is encountered the measurement should be tried in a different spot nearby. If it is impossible to find a spot without rocks at a specific sampling node, this is noted in the data log.

When observations are conducted in barrens or areas covered with grass or woody shrubs, the observer's thumb is pushed down to the soil surface. When probing in moss- or lichen-covered areas where the vegetation–soil boundary is hard to define, the observer's thumb is pushed down to depress vegetation until resistance. When probing in standing water, both thaw depth and water depth are recorded. On inclined surfaces, the probe should be inserted perpendicular to the ground.

During a thaw depth survey, two measurements are typically performed within one metre of the node marker and each other at each sampling node, and the average of the two measurements is reported.

4.3.4.4 *Uncertainty and sources of error*

The major sources of error associated with manual thaw depth probing include the observer's errors when reading or recording the measurement, or in interpreting the location of the ice-bonded frozen layer relative to the surface.

Errors in manual measurements may result from misinterpretation of a thaw depth reading or incorrect entry in a log book. These errors should be minimized by following measurement procedures. Errors in measurements of this type can usually be removed through data quality control processes.

Significant uncertainty can result from determining the location of the ground surface in vegetated or water-covered areas. For example, vegetation like moss or lichen has spatially varying levels of compression during thumb placement, or it might be difficult to correctly locate the ground surface in standing water. This can be especially relevant for hummocky/tussocky terrain where the observed thaw depth can be significantly different depending on whether the measurement is taken on top or at the base of the hummock/tussock. Similarly, the observer can misinterpret the location of the ice-bonded frozen layer in areas underlain by a stony substrate. These errors can be avoided by having prior knowledge of the surface and subsurface conditions and through the observer's experience. Depending on vegetation and edaphic properties, the magnitude of such errors could range from a few centimetres to tens of centimetres. The accuracy of a single thaw depth measurement by manual probing in moss-covered tundra underlain by fine-grained subsurface material with a well-defined thawed/frozen interface is estimated at ±2 cm. Rounding off to the nearest centimetre introduces an uncertainty of about ±0.5 cm.

A primary concern for the accuracy of long-term ALT assessments using thaw depth observations is the potential inconsistency of the probing measurements from year to year. A discrepancy in annual end-of-season thaw depth value may result from inconsistent timing of the observations and inconsistent selection of probing location(s) in sites with complex microtopography. In addition, if measurements are conducted by different observers, the amount of pressure exerted by each individual during probing might not be consistent. Another concern is related to the potential for site disturbance and year-to-year ground surface subsidence, which is possible in environments with high ground ice content (see, for example, Shiklomanov et al., 2013). Subsidence is a phenomenon that occurs when the ground surface sinks or settles due to the removal of underlying material, such as the melting of subsurface ice in permafrost areas. Surface subsidence is important because even if measurements are taken by the same observer(s) in successive years, changes in thaw depth derived from manual probing might not be detected or might be underestimated, as lowering of the permafrost table is accompanied by subsidence of the ground surface (O'Neill et al., 2019). As a result, thaw depth observations collected to detect inter-annual variability of the ALT should be as consistent as possible. The use of secondary measurements (for example, frost/thaw tubes, ground temperature monitoring) can potentially minimize the uncertainty related to year-to-year inconsistency in manual thaw depth probing (Bonnaventure and Lamoureux, 2013). In some situations, long-term changes in ALT obtained by mechanical probing without consideration for surface movement can underestimate the total response of ice-rich permafrost to climatic forcing (O'Neill et al., 2023; Shiklomanov et al., 2013; Smith et al., 2022).

4.3.5 Frost/thaw tubes gauges

4.3.5.1 *Measurement device*

A frost/thaw tube is a gauge that allows an observer to evaluate the ALT by visually determining the maximum depth of the 0 °C isotherm in any given year. Several variants of frost/thaw tubes which differ by construction material and design are available (see, for example, Christiansen, 2004; Mackay, 1973; O'Neill et al., 2023; Rickard and Brown, 1972; Sharratt and McCool, 2005; Smith and Brown, 2009; Tarnocai et al., 2004; Vieira et al., 2010). The typical gauge consists of nested plastic tubes. A rigid outer tube is made of plastic (PVC) with a watertight plug at the bottom and a removable watertight screw cap on top. It is anchored into the permafrost to a depth well below the active layer. A flexible transparent inner tube extends below the potential maximum thaw depth for the area and contains liquid water (Figure 4.8). Once placed in the ground, the water will freeze at the 0 °C isotherm, indicating the position of the frost table. In order to determine the ALT, indicated by maximum thaw propagation in a given season, a small marker is dropped into the inner tube and rests on the top of the water–ice interface. As thawing propagates downward the marker follows the water–ice interface until the maximum depth is reached. On refreezing, it is incorporated into the ice and records the maximum annual thaw depth or ALT for that year. If sufficiently anchored in the permafrost, frost/thaw tubes can also be used to measure ground surface heave and/or subsidence by installing a scriber that is allowed to move vertically, positioned level with the ground surface, and encircling the immobile outer tube (Tarnocai et al., 2004). The position of the scriber will provide information on the vertical position of the ground surface by recording maximum (frost heave) and minimum (thaw subsidence) surface elevations achieved during the year. To provide the total thaw penetration, ALT values can be corrected to account for net ground surface deformation.

4.3.5.2 *Installation and measurement procedure*

The initial installation of frost/thaw tubes should be done in the winter or at the beginning of the thaw season in order to ensure that the marker rests on top of the water–ice interface before maximum thaw penetration. The outer tube is installed into a predrilled hole filled with slurry and allowed to freeze in place. To prevent frost heave, the outer tube should be long enough to be anchored in permafrost. Anti-heave rings can be firmly attached to the outer tube to prevent frost heaving. The uppermost ring should be located well below the potential active layer. Within the active layer, the space around the outer tube should be filled with sand to minimize soil adhesion to the tube and to provide better thermal contact between the tube and the ground. The diameter of the outer tube should be relatively small to prevent unnecessary site disturbance (Mackay, 1973; Nixon and Taylor, 1994; Sharratt and McCool, 2005; Tarnocai et al., 2004).

The removable, water-filled, clear plastic observation tube should withstand expansion when water freezes. The inner tube should be long enough to extend well below the potential active layer of the area and have a diameter that allows ample play between two tubes to prevent binding when frozen. An inner tube 2.5 m long and 2 cm in diameter placed inside an outer tube 2.5 cm in diameter and 4 m long should work well for most permafrost-affected landscapes.

The thaw depth marker should be placed in the inner tube after the water in the tube freezes to the frost table of adjacent ground. The marker should be placed before the thaw depth reaches its annual maximum (winter or early summer). Freezing is rapid if installation is done in winter. In summer the ice surface in the inner tube can lie below the ground frost line since a large amount of heat needs to be removed to freeze the water. The size and density of the marker should be such that it resists vertical movement with the freezing front. Field and laboratory experiments indicate that a coloured glass bead 3 mm in diameter works very well (Nixon et al., 1995).

If the frost/thaw tube is equipped with a heave/subsidence gauge, the scriber of the gauge is placed level with the ground surface and a reference mark is made on the outer tube to indicate the position of the scriber. Maximum frost heave and subsidence are recorded by a scriber scratching a painted surface of the outer tube on either side of a reference mark (Nixon and Taylor, 1994; O'Neill et al., 2023; Tarnocai et al., 2004).

The ALT observations are conducted after the thaw depth for the year of interest has reached its annual maximum, and usually before the maximum thaw of the following summer. At that time, the inner tube is raised and the vertical position (depth) of the bead is measured in cm relative to the stable reference point represented by the outer tube. To ensure that the expansion of the water column during freezing is only upward, the bottom of the inner tube is examined. The maximum surface heave and subsidence are observed by measuring the length of scratches above (for heave) and below (for subsidence) the reference mark on the outer tube which represents a fixed datum.

The maximum thaw penetration, which is assumed to occur at the time of maximum ALT, is calculated as the depth of the bead minus the height of the ground surface at maximum surface subsidence (Nixon et al., 1995; Tarnocai et al., 2004). The values of ALT, heave/subsidence and thaw penetration are reported in cm and are rounded to the nearest centimetre.

After observations are complete, a bead of a different colour is introduced to the inner tube, and the paint and a surface reference mark on the outer tube are renewed.

4.3.5.3 ***Uncertainty and sources of error***

Since the active layer observations using frost/thaw tubes involve manual measuring of distance/length, the observer's mistakes can result in erroneous observations. As with any manual measurements, this type of error can be minimized by the diligence and experience of the observer.

The principal errors in frost/thaw tube measurements come from heat conduction down the tube during the summer resulting in an overestimation of the observed thaw depth and ALT. This error tends to be larger at the beginning of the thawing season and then decreases along with the increase in thaw depth. Field research conducted in continuous permafrost regions of Canada indicates that the overall accuracy of measurements using frost/thaw tubes is within 5% of the thaw depth (Mackay, 1973). To minimize the error, the outer tube should be made of light-coloured low heat conductive material and protrude only slightly above the ground surface. If possible, installation should be done in shaded areas.

The inner tube with an ice column containing a bead can experience expansion and contraction due to extremes of near-surface ground temperature. In properly constructed and installed gauges this error is less than 0.01 cm (Nixon et al., 1995). However, a detailed study conducted in the seasonal frost areas of Japan indicated that the accuracy of frost/thaw tubes in determining the depth of frost/thaw penetration is ±0.035 m (Iwata et al., 2012).

The largest errors can potentially result from improper installation of the frost/thaw tube. For example, not adequately anchoring the outer tube in permafrost can result in it moving vertically due to frost heave and/or thaw subsidence, resulting in erroneous or inconsistent thaw depth and ALT values. However, measuring the height of the outer pipe above the ground surface periodically (yearly) allows this error to be accounted for.

To evaluate frost/thaw tube performance it is recommended to conduct thaw depth probing in multiple locations in close proximity to the gauge during each site visit. For a properly working gauge, the depth of the ice–water interface in the inner tube should be within the range of thaw depth values obtained by probing.

The overall accuracy of a properly installed and maintained frost/thaw tube is ~2 cm (Smith and Brown, 2009).

4.3.6 Inferring active layer thickness from the ground temperature measurements

The ALT can be inferred from the maximum annual propagation of the 0 °C isotherm into the ground estimated from the temperature records obtained by a vertical array of temperature sensors inserted or installed in a borehole or a soil profile (see, for example, Haberkorn et al., 2021; Hrbáček et al., 2021; Isaksen et al., 2022; Noetzli et al., 2021) (see 4.2.3). Usually, the thickness of the active layer is estimated by locating the maximum annual depth of the 0 °C isotherm by linearly interpolating between the lowermost thermistor in the active layer (where the maximum annual temperature is positive) and the uppermost thermistor in the permafrost (where the maximum annual temperature is negative). The exponential best-fit interpolation can also be employed if there are several thermistors. The installation procedure, monitoring equipment, calibration and accuracy are similar to those described in sections related to measurements of permafrost temperature using thermistor chains (see 4.2.3). However, to achieve higher accuracy in the active layer estimates the sensor spacing should be reduced to 2–20 cm depending on the equipment, the thickness of the active layer and the desired accuracy of the interpolation process. The length of the sensor chain should be sufficient to extend at least a metre into the permafrost to account for variations in ALT due to climate variability and change. In mountain regions of mid-latitude permafrost, several metres of extension into the permafrost may be required, as a doubling of ALT (increasing it by several metres) has been recorded at some sites in recent decades (see, for example, PERMOS, 2023). Overall, the thermistor spacing, data collection interval, sensor calibration and interpolation method are crucial parameters in assessing the accuracy and precision of the active layer estimates (Riseborough, 2008).

Since the near-surface ground thermal regime is highly sensitive to surface disturbance, the disturbance should be minimized during the installation of equipment. As with frost/thaw tubes, the estimation of the ALT from temperature measurements is effectively based on only a single point measurement (Smith and Brown, 2009). As a result, the exact location of a thermistor chain installation should be determined based on an extensive end-of-season thaw depth survey by mechanical probing if possible, and the installation point should be representative of the mean end-of-season thaw depth for the entire landscape. If logistically possible, periodic probing surveys timed to coincide with maximum thaw depth are recommended to assess the spatial representativeness of the point measurement. Freeze–thaw processes can result in the vertical movement of the thermistors due to frost heave and/or thaw subsidence, resulting in erroneous or inconsistent estimates of the ALT. Measuring the vertical position of the ground surface relative to a stable benchmark, such as thermistor casings embedded in permafrost, can minimize this error.

4.4 MEASUREMENTS OF ROCK GLACIER VELOCITY

4.4.1 General

Since the early 2000s, an increasing number of studies have been quantifying and/or monitoring the kinematic behaviour of rock glaciers, contributing to a better understanding of their motion mechanisms and reaction to climate change (Kellerer-Pirklbauer et al., 2018; PERMOS, 2023). In particular, observations show that many rock glaciers within a specific region have similar inter-annual to longer-term evolution of surface displacement rates, which strongly depends on ground temperature changes (Delaloye et al., 2008; Kääb et al., 2021; Monnier and Kinnard, 2017). The monitoring of changes in rock glacier velocity (RGV) thus provides information about the impact of climate change on creeping mountain permafrost and, indirectly, on its thermal state (Frauenfelder et al., 2003; Staub et al., 2016).

This section presents the necessary concepts and definitions for the standardized production of RGV time series. It provides practical recommendations for setting up long-term RGV monitoring sites as well as a general procedure for producing consistent RGV products from collected kinematic data. The content of this section was compiled by the International Permafrost Association (IPA) Action Group on Rock Glacier Inventories and Kinematics (RGIK, 2023a, 2023b, 2023c, 2023d).

Here two important clarifications of the terminology adopted in the present Guide:

- **Kinematics** describes the general mechanical behaviour/processes of rock glaciers in the form of surface and/or internal deformation, and **velocity** refers to the quantifiable variable.

- **Creep** or **rock glacier creep** is a generic term referring to the variable combination of both internal deformation within the crystalline structure of the frozen ground (creep in the literal sense) and shearing in one or several discrete layers at depth (shear horizon).

4.4.1.1 *Definition, units, scales*

Rock glaciers are defined as debris landforms generated by the former or current creep of permafrost, detectable in the landscape with the following morphologies: steep front and lateral margins, and optionally, ridge-and-furrow surface topography (RGIK, 2023a).

Rock glacier velocity (RGV) is defined as a time series of annualized surface velocity values expressed in m/a and measured/computed on a rock glacier unit or a part of it. RGV refers to surface velocities related to permafrost creep. The annual surface velocity values, which build up RGV, are called RGV values (RGIK, 2023c).

The RGV values are measured/computed from **velocity data** of any dimension (1D–3D), which are spatially and/or temporally aggregated following a methodology that must be precisely documented and remain consistent over time (RGIK, 2023c).

The velocity data are surface velocity values measured/computed based on **initial data** and expressed in m/a (RGIK, 2023d).

The initial data are surface velocity, displacement or position data obtained with a specific technique. Depending on the selected technique, initial data may have different geometric references (Lagrangian or Eulerian), units, dimensions (1D–3D) as well as spatial and temporal resolutions (RGIK, 2023d).

4.4.1.2 *Temporal variability of rock glacier velocity*

The velocity of a rock glacier primarily depends on driving factors such as internal structure, landform geometry, topography, geology, lithology and debris loading, which often are constant or change very slowly (excluding rock glaciers affected by glacial processes or rock avalanches). The temporal evolution of RGV depends in particular on shifts in ground temperature between the permafrost table and the main shearing horizon, which are constrained by the evolution of the ground surface temperature and impact the rheological and hydrological properties of the frozen ground (see, for example, Kääb et al., 2007). The closer to 0 °C that the permafrost temperature rises, the faster the rock glacier moves. Hydrological processes related to water infiltration (for example, changing water content and pore pressure during melt or rain periods), which interact with the internal structure of the rock glacier, can also play a significant role in rock glacier kinematic behaviour (see, for example, Cicoira et al., 2019).

Three superimposed types of temporal variability in RGV have been identified:
(i) multi-decennial trends, (ii) inter-annual variation and (iii) seasonal rhythm.

The multi-decennial behaviour (change over several decades) of RGVs reflects the impact of climate change and responds regionally almost synchronously to changes in permafrost temperatures. Increases in velocity by a factor of 2 to 10 have been reported for recent decades from various rock glaciers in different regions on Earth (see, for example, Pellet et al., 2023). Rock glaciers connected to glaciers appear to have a specific evolution that differs from that of other types of rock glacier. At the inter-annual scale, velocity variations are likely controlled by changes in ground temperature, which are mainly driven by annually fluctuating snow cover insulation as well as air temperature. Such inter-annual variations can be comparatively large, even exceeding ±50% of the value of the previous year. However, they appear to occur simultaneously and proportionally for many rock glaciers within a region, independent of the activity rate and morphological characteristics (see, for example, PERMOS, 2023). At a seasonal scale rock glaciers usually exhibit a repetitive landform-specific intra-annual behaviour (annual cyclic pattern). The highest velocities are most often reached after the warm season or in some cases during the snow ablation period, whereas a decreasing trend occurs throughout the cold season. The amplitude (minimum-to-maximum ratio) of the seasonal variations is extremely diverse, ranging almost from 1:1.1 to 1:10 (see, for example, Wirz et al., 2016). In comparison to the annual mean velocity, both the landform-specific pattern and relative amplitude have been shown to remain almost constant at a decennial time scale in most documented cases.

Behaviours falling outside of the three types of identified temporal variabilities can occur and are typically associated with site-specific conditions not connected to climate forcing. RGVs deviating from the common multi-decennial regional trend can be observed. This particularly results from significant changes in the rheology and internal structure of the rock glacier (including ice and water content), in its geometry and interaction with subjacent topography, or in debris loading (including any possible interaction with or connection to a glacier or rock avalanches). Such temporal evolution typically suggests that the rock glacier is degrading (that is, continuously decelerating) or destabilizing (that is, accelerating excessively). Short-term acceleration (over several hours to several weeks) can sometimes be observed at the surface of a rock glacier. This reflects either an actual motion related to permafrost creep (daily variation) or specific movements in the active layer (that is, block sliding/tilting, etc.). This behaviour usually results from a significant input of water into the ground from melting snow or rain.

Given the relation between changes in climate and the multi-decennial and inter-annual variations in RGV, the optimal frequency of observation for climate-oriented time series is yearly. Computing annual velocity time series minimizes the contribution of seasonally-dependent processes and short-term variations to the velocity changes, while the repetitiveness of the intra-annual behaviour over time allows the exploitation of sub-annual observations. For intra-annual observations, the period considered must remain approximately the same every year and must be long enough (minimum 1 month) to prevent short-term (that is, non-repetitive) variations from influencing the velocity changes.

4.4.1.3 ***Spatial variability of rock glacier velocity***

The displacements observed at the surface of a rock glacier unit build up a spatially coherent flow field due to the motion mechanism of permafrost creep, which primarily takes place at depth, in the shear horizon (see, for example, Haeberli et al., 2006). This flow field often displays a certain degree of spatial heterogeneity, depending on landform-related (for example, internal structure) and topographical settings. For instance, the movement of the terminal part (front), the lateral margins and the rooting zone are often slower than that of the central part of the rock glacier. The relative velocity changes (that is, acceleration/deceleration rates in relation to a reference period), however, are usually much more spatially homogeneous. Various processes not related to permafrost creep can alter the spatial homogeneity of the flow field (for example, subsidence induced by ice melt, movement of isolated boulders) (Figure 4.9).

Rock glacier velocity time series must refer to a consistent flow field representing the downslope movement of a rock glacier unit or a part of it. The surface displacements considered should represent the downslope movement of the rock glacier related to permafrost creep and should not be significantly altered by local movement processes (for example, movement of isolated boulders, subsidence induced by ice melt). Areas affected by such local processes should be avoided for the measurement/computation of the time series. Moreover, rock glacier monitoring strategies must account for the spatially heterogeneous kinematic behaviour within a unit and be adapted accordingly.

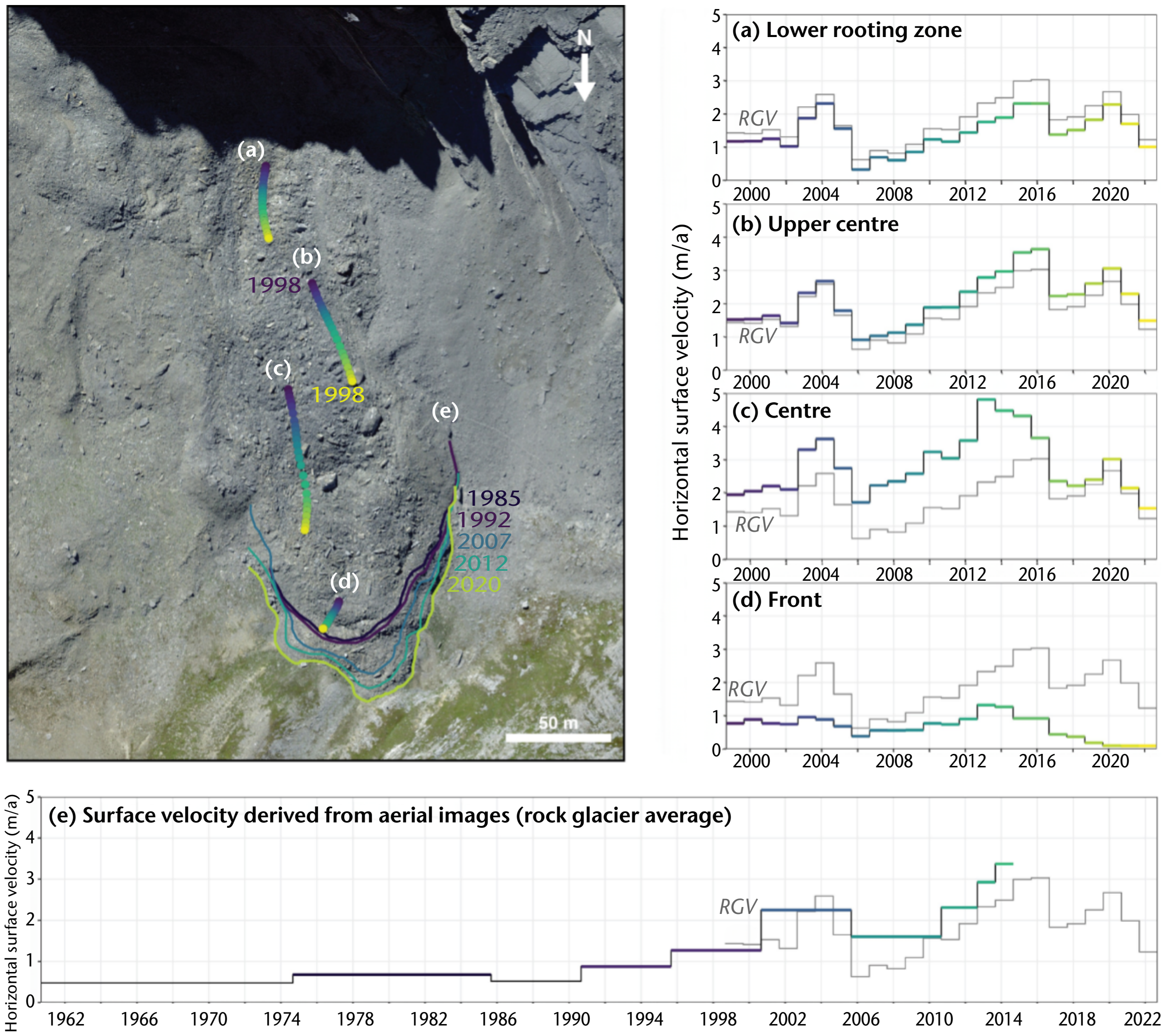

Figure 4.9. Overview of the spatial and temporal variability of the surface velocity of the Gemmi rock glacier in the Swiss Alps. Annual positions and velocity of four selected boulders are shown for the period 1998–2022 (panels (a)–(d)). Advance of the front of the rock glacier is shown based on orthorectified aerial images that were also used to compute the rock glacier average surface velocity starting in 1960 (panel (e)). The Gemmi RGV time series shown on all velocity plots as reference (gray line) is based on in-situ measurement (aggregation of 5 points located in the upper centre and lower rooting zone areas).

Sources: Data from Swiss Permafrost Monitoring Network (PERMOS); image background: Swisstopo

4.4.2 General principles and requirements

4.4.2.1 *Site selection*

The motivations for monitoring RGVs are diverse. In the context of the ECV products, the goal is the generation of long-term time series with a climate-oriented perspective. Therefore, to select suitable sites, the following selection criteria (see also RGIK, 2023d) should be assessed based on available data, and they should also be regularly evaluated using newly collected data:

- RGV monitoring must be performed on active or transitional rock glacier units whose deformation mechanism is dominantly related to permafrost creep.
- Rock glaciers with surface movement dominantly caused by processes other than permafrost creep (for example, ice melt-induced subsidence, landform destabilization) must be avoided.
- Multi-decennial monitoring must appear to be feasible at the selected site.

Over a decadal to multi-decadal time scale, RGV production can be limited by various constraints hindering the feasibility of consistent monitoring:

- **Landform constraints** such as development of large scarps (onset of a rock glacier destabilization phase), occurrence of rock falls, instability of surface boulders (rotation, tilt, fall), onset of subsidence induced by ice melt.
- **Technical constraints** such as data availability (for example, satellite revisit period), data quality (for example, sensor shift, drift or failure), feasibility of measurements (for example, lack of coverage, or partial coverage by aerial/satellite images), technological development.
- **Practical constraints** such as site accessibility, safety of people and of equipment, permit for instrumentation and/or field visits.
- **Resource constraints** such as funding, expertise.
- **Processing constraints** such as availability of processing tools, computing power, data property.

A landform should only be selected if decadal to multi-decadal RGV consistency is considered achievable after evaluating the constraints. The constraints listed above may change over time. They may lead to necessary adaptations of the RGV monitoring strategy and thus must be regularly assessed.

4.4.2.2 *Technique selection*

Rock glacier surface velocities can be measured/computed using a wide range of different "techniques". The term "technique" here refers to available technologies able to provide velocity measurements over rock glaciers and includes the specificities of the sensor, platform and algorithm used for data processing.

Existing techniques range from in-situ surveys (for example, repeated global satellite navigation system (GNSS) field campaigns, permanent GNSS stations) to remote sensing-based approaches (for example, synthetic aperture radar interferometry (InSAR), satellite-/air-/UAV-borne photogrammetry, terrestrial laser scanning). Each technique has its own characteristics that affect the temporal and spatial resolution, dimensionality, accuracy and geometric reference frame of the data obtained. In addition, the spatial and temporal resolution of the data also depends on practical and resource constraints (for example, cost, workforce). Depending on the site-specific constraints (for example, topography, location, vegetation, velocity range) not all techniques are suitable for RGV monitoring. Careful evaluation must be performed to determine the most appropriate technique for RGV monitoring on the chosen landforms.

The basic principles and limitations of the most widely used techniques are described in 4.4.3.

4.4.2.3 *Processing steps to produce rock glacier velocity*

Following the site and technique selection, several steps are necessary to acquire data and transform it into RGV time series, namely:

(i) **Design of the monitoring setup:** Definition of the survey design controlling the initial data acquisition and its spatial and temporal resolution.

(ii) **Acquisition of initial data:** Implementation of the survey design and acquisition of initial data.

(iii) **Preparation of initial data:** Pre-processing, calibrating and quality control of initial data.

(iv) **Processing of velocity data:** Conversion of initial data into surface velocity values and quality control of velocity data.

(v) **Processing of RGV:** Spatial and temporal aggregation of velocity data to produce RGV. Spatial and temporal aggregation procedures both include the following stages: velocity data gap-filling, velocity data selection and velocity data aggregation.

(vi) **Evaluation of RGV consistency:** Evaluation of the consistency throughout all above-mentioned steps and qualitative assessment of the overall RGV consistency.

4.4.3 Widely used techniques

4.4.3.1 *Terrestrial geodetic survey*

Terrestrial geodetic survey (TGS) is the most widely used technique for in-situ measurements of surface RGVs. TGS is mostly performed using high-precision differential GNSS (see, for example, Berthling et al., 1998; Lambiel and Delaloye, 2004) or theodolites/total stations (see, for example, Wahrhaftig and Cox, 1959). Both techniques follow the same measurement principle: the positions of a number of observation points spatially distributed over the rock glacier and stable areas next to it are surveyed regularly, and the surface velocity is computed from the observed displacements (Figure 4.10).

Observation points are divided into two categories: survey points located on the rock glacier surface within the moving terrain and control points located on stable areas outside the rock glacier. The survey points, used to measure the surface velocity, must be set on large blocks well embedded within the active layer matrix to avoid measuring individual movements of the blocks instead of the general displacement of the creeping body (Lambiel and Delaloye, 2004). The control points, used to calibrate and adjust the measured coordinates of the survey points, are set in stable terrain outside of the observed landform. Depending on the size and characteristics of the surveyed landform (that is, spatial consistency of the flow field, surface characteristics, absolute velocity range), between 10 and 100 points are selected (see, for example, PERMOS, 2023). The different morphological areas of the rock glacier (front, lateral margins, rooting zone, central part) should be accounted for as well as any features specific to the selected landform (secondary front, subsidence areas, levees, distinct velocity areas). To make it possible to precisely re-survey the same points, measurement locations are chiseled into the rocks and marked with coloured place markers (differential GNSS), or permanent prisms are fixed into the boulders (total station). The typical accuracy of differential GNSS and/or total station measurements is around 1–3 cm (Lambiel and Delaloye, 2004).

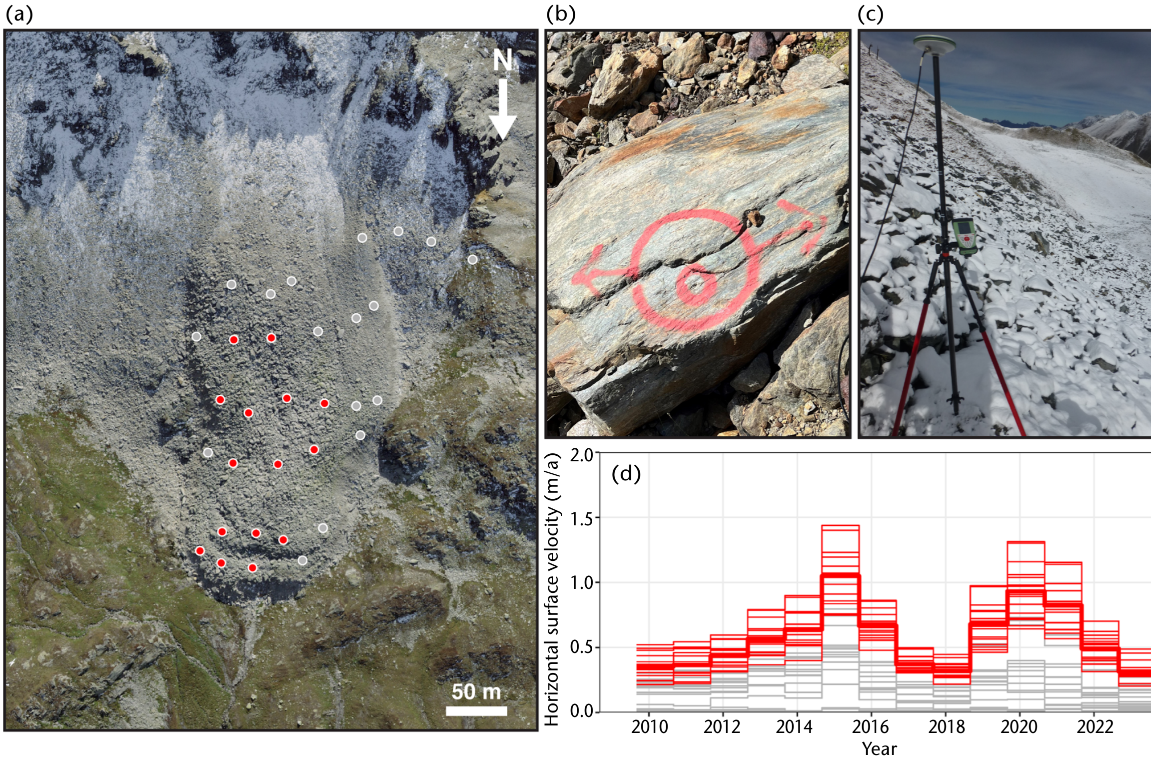

Figure 4.10. Network of points (a, b) measured using terrestrial geodetic survey (c) on the Monte Prosa rock glacier (Switzerland). The resulting annual velocities (d) are shown for all the survey points (in grey) and for the points selected for RGV computation (red). The bold red line represents the RGV time series.

Sources: Data from Swiss Permafrost Monitoring Network (PERMOS); image background from Swisstopo; photos by Lea Schmid (b) and Reynald Delaloye (c)

TGS is performed at least once a year to obtain annual displacement values (RGIK, 2023c, 2023d). Surveys are performed on approximately the same date each year (±15 days is recommended). Surface velocity can be retrieved for each time step in between measurements.

4.4.3.2 *Synthetic aperture radar interferometry*

Synthetic aperture radar interferometry (InSAR) is a remote sensing technique that compares satellite radar images acquired at different times to measure ground surface displacements (Figure 4.11). The procedure starts with the acquisition of complex SAR images. InSAR exploits the phase component of the radar images, related to the sensor-to-ground distance. The user must pay attention to the chosen SAR orbit depending on the slope orientation of the study area. The displacement measurements are along the line of sight of the sensor. To avoid underestimating the velocity, viewing geometry aligned with the expected rock glacier creep direction is preferred (Barboux et al., 2014; RGIK, 2023b).

As snow disturbs the interferometric signal, only measurements made in summer seasons can effectively be used in cold areas. Depending on the rock glacier of interest, a consistent snow-free observation window has to be chosen. Image pairs (interferograms) are generated with a minimal time interval depending on the revisit time of the satellite (weekly to monthly for most sensors) and a maximal time interval depending on the RGV in relation to the detection capability (half the radar wavelength). Absolute displacements (converted to annual velocity) are then retrieved using an unwrapping procedure (see, for example, Chen and Zebker, 2002) relative to a stable area outside the landform.

Velocity data can be retrieved for each documented InSAR pixel and each unwrapped image pair. Several 10–100 time series can typically be generated. The number depends on the landform size, the data resolution (10–100 m depending on the sensor) and the extent of areas that are masked by typical InSAR limitations (for example, shadow, vegetation). Depending on the rock glacier characteristics, advanced multitemporal InSAR methods, such as the small baseline subset (SBAS) technique (Berardino et al., 2002) or persistent scatterer interferometry (PSI) (Ferretti et al., 2001) can also be applied to provide similar velocity time series.

Each initial image pair provides an initial velocity information that may indicate seasonal variability (Strozzi et al., 2020). To document inter-annual RGV, the results are averaged for each season using a consistent observation window (a maximum of ±15 days of variation is recommended).

4.4.3.3 *Optical imagery*

Feature tracking image correlation is a set of numerical/computer-based techniques that essentially seek to detect and locate similarity patterns between two different images (Scambos et al., 1992). The images used for this purpose are usually acquired by optical sensors (for example, Landsat), but could also be radar images (4.4.3.2). Optical sensors can be mounted on different platforms, including terrestrial (ground-based photogrammetry), airborne (UAV or planes) and spaceborne ones (satellites), or can even be collected manually (Bodin et al., 2018).

The aim of image correlation is to measure the displacement of objects between two images taken at different times that are days, months, years or even decades apart (Cusicanqui et al., 2021). To do this, the images must have a common grid reference (same number of rows and columns), the same spatial resolution and the same coordinate system. The classical

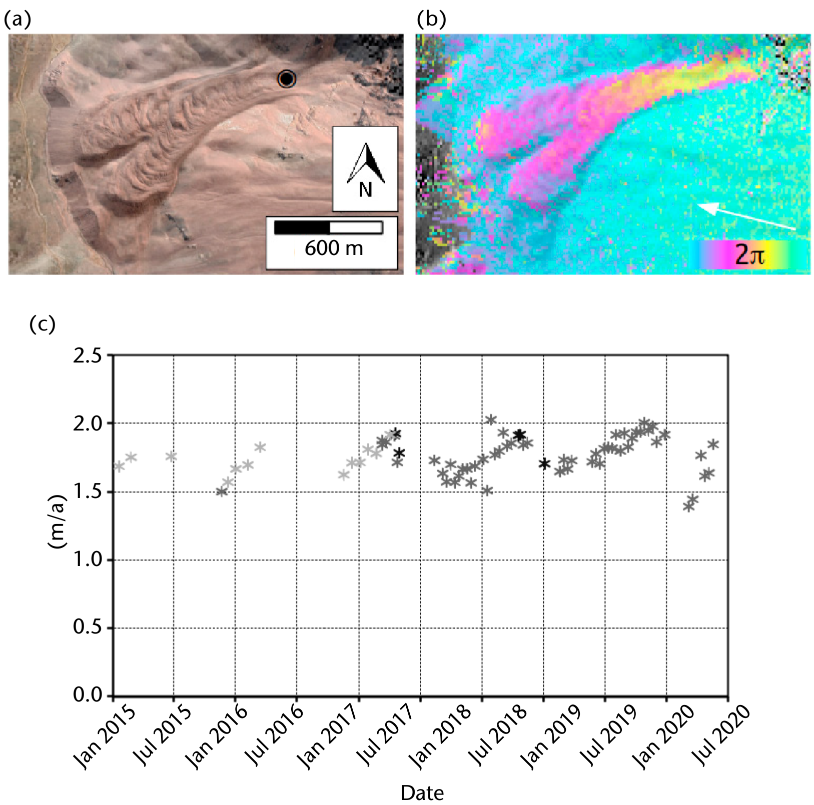

Figure 4.11. Dos Lenguas rock glacier (Argentinian Andes) (a), Sentinel-1 interferogram for 21 April 2017–27 April 2017 (b) (2π <=> 2.8 cm), and Sentinel-1 InSAR time series (c)

Sources: Background image from Google, DigitalGlobe; figure adapted from Strozzi et al. (2020)

approach is to find the displacement between two images by optimizing their similarity (Fitch et al., 2002). This is usually done using small windows that allow the displacement to be estimated at different parts of the image.

The quality of image correlation using optical images depends mainly on the choice of image correlation parameters, reference and correlation window size (Debella-Gilo and Kääb, 2011) (Figure 4.12). These parameters should preferably be chosen with prior knowledge of the maximum displacement magnitude of the rock glacier and the pixel size. A signal-to-noise ratio (SNR) between the maximum similarity value and the average similarity value in the search window serves to evaluate the quality of the correlation (Kääb et al., 2021). In addition, other factors related to the image quality, such as resolution and contrast, affect the quality of the results. The presence of snow, shadows and orthorectification artifacts could cause some errors during the correlation process. Therefore, images should be carefully selected, preferably during the same period of the year (a maximum of ±30 days of variation is recommended) to avoid strong surface changes.

The accuracy of the image correlation process has been estimated to be approximately 1/10 of the pixel size (Debella-Gilo and Kääb, 2011). Rock glacier surface velocity fields can be validated using in-situ measurement (Vivero et al., 2021). As in-situ datasets are not always available, having a significant number of stable areas (between 20% and 40% of the image) helps to provide confidence in the uncertainty of the image correlation (Cusicanqui et al., 2023). Velocity data can be retrieved for each pixel of the surface velocity field for the selected image pair. The documented velocity is an average over the entire period. Depending on the image availability and rock glacier characteristics, advanced multitemporal inversion methods such as time-series inversion can also be applied to provide velocity time series (Bontemps et al., 2018).

The use of image archives allows for reconstruction of past velocity values and changes. The spatial accuracy may be limited by the image quality and size. This can be compensated for by using a longer time interval. Larger uncertainties are accepted for reconstructions based on image archives (see ECV requirements (GCOS-245)).

4.5 SUPPLEMENTARY MEASUREMENTS

Additional measurements may be recommended or desirable at or in the vicinity of permafrost monitoring sites. They are used for indirect monitoring of permafrost conditions, for the interpretation of the permafrost measurements, for modelling of the climate/permafrost relationship, or for site characterization. The following list is not complete and will be extended in the future.

4.5.1 Meteorological variables

Permafrost is mainly a temperature-dependent phenomenon, and the climate is its main driver. Measuring meteorological variables is therefore necessary to assess the surface energy balance, and to interpret the permafrost temperature, active layer and creep velocity measurements.

The key variables driving the permafrost thermal regime are air temperature, solar radiation and snow cover. Air temperature and solar radiation are the main drivers of the subsurface thermal regime in snow-free periods. The timing of the snow cover during winter defines the period during which the subsurface is thermally insulated from atmospheric processes.

- **Air temperature and solar radiation:** For measurement and processing methods refer to the present Guide, Volume I. If air temperature and/or solar radiation are not measured directly on the site, data can be extrapolated from nearby stations. However, microclimate, local variability and inversion effects must be carefully addressed for the extrapolation of air temperature time series to a permafrost observation site.

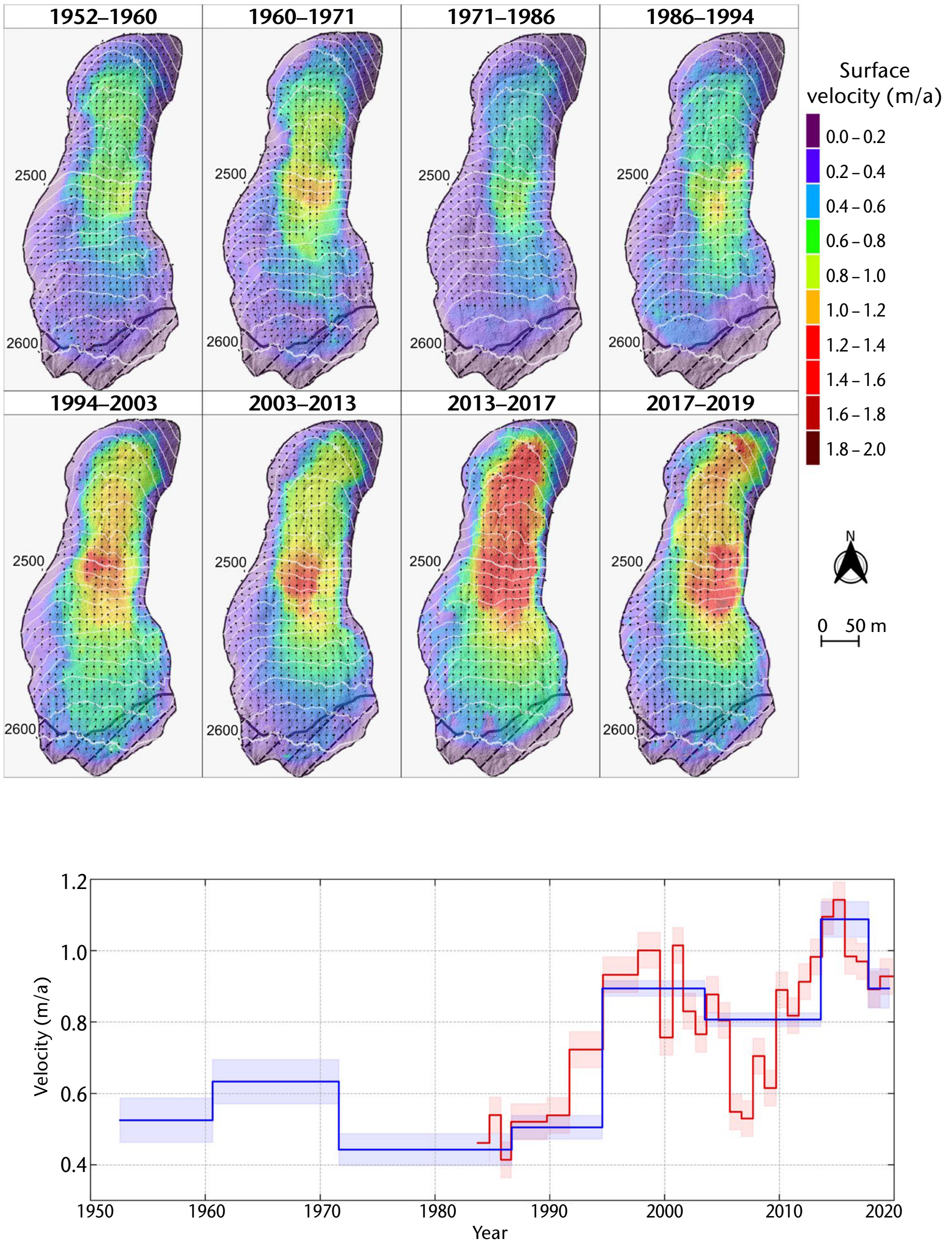

Figure 4.12. Surface velocity of the Laurichard rock glacier from image aerial optical correlation. The left panel shows the horizontal velocity fields obtained for each time interval. The right panel shows the mean velocities computed for each time interval (blue line) compared to the mean values measured by terrestrial geodetic survey.

Source: Image from Cusicanqui et al. (2021) with licence CC BY-NC 4.0

- **Snow depth** is an additional driver of permafrost thermal state changes owing to the snow cover's insulating effect, which limits winter heat loss from the ground and modulates the influence of air temperature changes on the ground thermal regime. It should be measured in situ, because of its large spatial variability. For methods, refer to Chapter 2.

To allow the calculation of the surface energy balance, wind speed and direction, relative humidity as well as a full radiation balance (incoming and outgoing long- and short-wave radiation) also need to be measured (compare Hoelzle et al., 2022).

The colocated measurement of both cryospheric and meteorological variables (see, for example, Boike et al., 2018; Isaksen et al., 2022; Noetzli et al., 2021) is the key approach promoted by the Global Cryosphere Watch (GCW) CryoNet network.

4.5.2 Ground surface variables

Many studies reveal an offset between near-surface air temperature and ground surface temperature (see Figure 4.1), called "surface offset", due to ground surface characteristics, topography or snow cover. The ground surface temperature integrates the surface energy balance and directly drives temperature change in the subsurface thermal regime. It is used as an input variable for ground temperature modelling.

- **Ground surface temperature (GST)** is typically measured about one decimetre below the ground surface (Noetzli et al., 2021) with autonomous miniature data loggers or individual temperature sensors connected to a remote data logger. For methods and strategies, see PermaNET Guidelines.

- **Soil moisture** in the active layer can be an explanatory factor for the thermal offset. It should be measured together with ground temperatures in the active layer. For methods, refer to the present Guide, Volume I, Chapter 11.

For the measurement of soil temperature with single near-surface measurements at depths of 0.05 m and 0.1 m, refer to the present Guide, Volume I, Chapter 2.

On rock glaciers and other coarse blocky ground material, the surface can be difficult to define, such that measurements deeper than about 1 m depth may become unreliable. In these cases, the definition of the surface level needs to be clear and documented (Noetzli et al., 2021).

4.5.3 Geophysical measurements

Making use of the different physical properties of the ground materials, geophysical measurements enable the indirect and non-invasive detection and monitoring of subsurface characteristics from the surface. In permafrost studies, they are commonly used to provide evidence of the presence of ground ice and identify the composition of the subsurface as well as its thermal state (that is, frozen or unfrozen). Typically, geophysical measurements yield 1- to 3-dimensional information that reaches down to tens of metres depth and covers horizontal distances ranging from several metres up to thousands of metres. A large range of methods and instruments can be applied either for site characterization, or when repeated at regular intervals, to assess the temporal evolution of site characteristics and permafrost conditions (see, for example, Hauck and Kneisel, 2008).

Four main geophysical methods are commonly used in permafrost research, namely electric, electromagnetic, seismic and radar methods (Hauck, 2013). These methods are often combined to improve the assessment of the subsurface characteristics (Wagner and Uhlemann, 2021) as well as to quantify the water and ice content of the ground through the application of petrophysical models (see, for example, Hauck et al., 2011; Wagner et al., 2019).

- **Electrical resistivity tomography (ERT)** is the geophysical method most commonly applied in permafrost monitoring (see, for example, PERMOS, 2019) and research. It uses the exponential increase in electrical resistivity at the freezing point of water to detect and characterize ice bodies and ice-bonded sediment within the subsurface. ERT has been used for decades in the field of permafrost research, and detailed methods and strategies can be found in the literature (see, for example, Farzamian et al., 2020; Hauck and Kneisel, 2008; Mollaret et al., 2019; Supper et al., 2014). The IPA-supported Action Group "Towards an International Database of Geoelectrical Surveys on Permafrost (IDGSP)" created an international database for ERT data (see IDGSP website) as well as guidelines for measurement repetition and processing (Herring et al., 2023). ERT can be associated with **induced polarization (IP)** (see, for example, Duvillard et al., 2021) or **frequency or time domain electro-magnetometry (FDEM and TDEM)** (see, for example, Boaga et al., 2020) to improve the differentiation of frozen and unfrozen terrain.

- **Seismic refraction tomography (SRT) and ground penetrating radar (GPR)** are often used in combination with ERT, as both the seismic P-wave velocity and the transmission of electromagnetic waves are strongly affected by contrasts between frozen and unfrozen substrates. Typical applications include the mapping of the active layer–permafrost interface, internal discontinuities and/or the bedrock profile (see, for example, Monnier and Kinnard, 2015), as well as the monitoring of ground ice evolution (see, for example, Hilbich, 2010).

4.5.4 Environmental parameters

For arctic active layer sites, environmental parameters such as vegetation type and soil are surveyed on CALM grids in order to serve both for site characterization and as interpretation parameters for explaining the spatial variability of ALT measurements. Guidelines are provided by the CALM protocol.

ACKNOWLEDGEMENTS

WMO would like to acknowledge the European Union (EU) project Arctic PASSION, a WMO-endorsed project that provided support for the leader of the team, Anna Irrgang, to develop this chapter, and the contributions of the following experts as reviewers:

Wilfried Haeberli, Geography Department, University of Zurich (Switzerland);
Antoni Lewkowicz, University of Ottawa (Canada);
Daniel Vonder Mühll, Swiss Commission for Cryosphere Observation; PHRT ETH Zurich, (Switzerland);
Marcia Phillips, WSL Institute for Snow and Avalanche Research SLF; Climate Change, Extremes and Natural Hazards in Alpine Regions Research Center CERC (Switzerland);
Sharon Smith, Geological Survey of Canada, Natural Resources Canada, (Canada);
Dario Trombotto, CCT CONICET Mendoza, National Scientific and Technical Research Council (CONICET) (Argentina);
Qingbai Wu, Northwest Institute of Eco-environment and Resources, Chinese Academy of Sciences (China);
Julia Boike, Alfred Wegener Institute Helmholtz Centre for Polar and Marine Research, Humboldt-University (Germany).

REFERENCES

Abramov, A.; Davydov, S.; Ivashchenko, A. et al. Two Decades of Active Layer Thickness Monitoring in Northeastern Asia. *Polar Geography* **2021**, *44* (3), 186–202. https://doi.org/10.1080/1088937X.2019.1648581.

Arenson, L.; Hoelzle, M.; Springman, S. Borehole Deformation Measurements and Internal Structure of Some Rock Glaciers in Switzerland. *Permafrost and Periglacial Processes* **2002**, *13* (2), 117–135. https://doi.org/10.1002/ppp.414.

Barboux, C.; Delaloye, R.; Lambiel, C. Inventorying Slope Movements in an Alpine Environment Using DInSAR. *Earth Surface Processes and Landforms* **2014**, *39* (15), 2087–2099. https://doi.org/10.1002/esp.3603.

Berardino, P.; Fornaro, G.; Lanari, R. et al. A New Algorithm for Surface Deformation Monitoring Based on Small Baseline Differential SAR Interferograms. *IEEE Transactions on Geoscience and Remote Sensing* **2002**, *40* (11), 2375–2383. https://doi.org/10.1109/TGRS.2002.803792.

Berthling, I.; Etzelmüller, B.; Eiken, T. et al. Rock Glaciers on Prins Karls Forland, Svalbard. I: Internal Structure, Flow Velocity and Morphology. *Permafrost and Periglacial Processes* **1998**, *9* (2), 135–145. https://doi.org/10.1002/(SICI)1099-1530(199804/06)9:2<135::AID-PPP284>3.0.CO;2-R.

Biskaborn, B. K.; Smith, S. L.; Noetzli, J. et al. Permafrost Is Warming at a Global Scale. *Nature Communications* **2019**, *10* (1), 264. https://doi.org/10.1038/s41467-018-08240-4.

Blöthe, J. H.; Halla, C.; Schwalbe, E. et al. Surface Velocity Fields of Active Rock Glaciers and Ice-Debris Complexes in the Central Andes of Argentina. *Earth Surface Processes and Landforms* **2021**, *46* (2), 504–522. https://doi.org/10.1002/esp.5042.

Boaga, J.; Phillips, M.; Noetzli, J. et al. A Comparison of Frequency Domain Electro-Magnetometry, Electrical Resistivity Tomography and Borehole Temperatures to Assess the Presence of Ice in a Rock Glacier. *Frontiers in Earth Science* **2020**, *8*. https://doi.org/10.3389/feart.2020.586430.

Bodin, X.; Thibert, E.; Sanchez, O. et al. Multi-Annual Kinematics of an Active Rock Glacier Quantified from Very High-Resolution DEMs: An Application-Case in the French Alps. *Remote Sensing* **2018**, *10* (4), 547. https://doi.org/10.3390/rs10040547.

Boike, J.; Chadburn, S.; Martin, J. et al. Standardized Monitoring of Permafrost Thaw: A User-Friendly, Multiparameter Protocol. *Arctic Science* **2022**, *8* (1), 153–182. https://doi.org/10.1139/as-2021-0007.

Boike, J.; Juszak, I.; Lange, S. et al. A 20-Year Record (1998–2017) of Permafrost, Active Layer and Meteorological Conditions at a High Arctic Permafrost Research Site (Bayelva, Spitsbergen). *Earth System Science Data* **2018**, *10* (1), 355–390. https://doi.org/10.5194/essd-10-355-2018.

Boike, J.; Nitzbon, J.; Anders, K. et al. A 16-Year Record (2002–2017) of Permafrost, Active-Layer, and Meteorological Conditions at the Samoylov Island Arctic Permafrost Research Site, Lena River Delta, Northern Siberia: An Opportunity to Validate Remote-Sensing Data and Land Surface, Snow, and Permafrost Models. *Earth System Science Data* **2019**, *11* (1), 261–299. https://doi.org/10.5194/essd-11-261-2019.

Bojinski, S.; Verstraete, M.; Peterson, T. C. et al. The Concept of Essential Climate Variables in Support of Climate Research, Applications, and Policy. *Bulletin of the American Meteorological Society* **2014**, *95* (9), 1431–1443. https://doi.org/10.1175/BAMS-D-13-00047.1.

Bommer, C.; Phillips, M.; Arenson, L. U. Practical Recommendations for Planning, Constructing and Maintaining Infrastructure in Mountain Permafrost. *Permafrost and Periglacial Processes* **2010**, *21* (1), 97–104. https://doi.org/10.1002/ppp.679.

Bonnaventure, P. P.; Lamoureux, S. F. The Active Layer: A Conceptual Review of Monitoring, Modelling Techniques and Changes in a Warming Climate. *Progress in Physical Geography: Earth and Environment* **2013**, *37* (3), 352–376. https://doi.org/10.1177/0309133313478314.

Bontemps, N.; Lacroix, P.; Doin, M.-P. Inversion of Deformation Fields Time-Series from Optical Images, and Application to the Long Term Kinematics of Slow-Moving Landslides in Peru. *Remote Sensing of Environment* **2018**, *210*, 144–158. https://doi.org/10.1016/j.rse.2018.02.023.

Brown, J.; Hinkel, K. M.; Nelson, F. E. The Circumpolar Active Layer Monitoring (Calm) Program: Research Designs and Initial Results 1. *Polar Geography* **2000**, *24* (3), 166–258. https://doi.org/10.1080/10889370009377698.

Bureau International des Poids et Mesures (BIPM). *International Vocabulary of Metrology – Basic and General Concepts and Associated Terms (VIM)*. BIPM: Geneva, 2012. https://www.bipm.org/en/committees/jc/jcgm/publications.

Chen, C. W.; Zebker, H. A. Phase Unwrapping for Large SAR Interferograms: Statistical Segmentation and Generalized Network Models. *IEEE Transactions on Geoscience and Remote Sensing* **2002**, *40* (8), 1709–1719. https://doi.org/10.1109/TGRS.2002.802453.

Christiansen, H. H. Meteorological Control on Interannual Spatial and Temporal Variations in Snow Cover and Ground Thawing in Two Northeast Greenlandic Circumpolar-Active-Layer-Monitoring (CALM) Sites. *Permafrost and Periglacial Processes* **2004**, *15* (2), 155–169. https://doi.org/10.1002/ppp.489.

Christiansen, H. H.; Gilbert, G. L.; Neumann, U. et al. *Ground Ice Content, Drilling Methods and Equipment and Permafrost Dynamics in Svalbard 2016–2019 (PermaSval)*; Svalbard Integrated Arctic Earth Observing System: Longyearbyen, 2021. https://doi.org/10.5281/zenodo.4294095.

Cicoira, A.; Beutel, J.; Faillettaz, J. et al. Water Controls the Seasonal Rhythm of Rock Glacier Flow. *Earth and Planetary Science Letters* **2019**, *528*, 115844. https://doi.org/10.1016/j.epsl.2019.115844.

Culik, M. N.; Doran, J. W.; Richards, K. A. Construction of Soil Thermocouples for the Novice. *Soil Science Society of America Journal* **1982**, *46* (4), 882–884. https://doi.org/10.2136/sssaj1982.03615995004600040044x.

Cusicanqui, D.; Bodin, X.; Duvillard, P.-A. et al. Glacier, Permafrost and Thermokarst Interactions in Alpine Terrain: Insights from Seven Decades of Reconstructed Dynamics of the Chauvet Glacial and Periglacial System (Southern French Alps). *Earth Surface Processes and Landforms* **2023**, *48* (13), 2595–2612. https://doi.org/10.1002/esp.5650.

Cusicanqui, D.; Rabatel, A.; Vincent, C. et al. Interpretation of Volume and Flux Changes of the Laurichard Rock Glacier Between 1952 and 2019, French Alps. *Journal of Geophysical Research: Earth Surface* **2021**, *126* (9), e2021JF006161. https://doi.org/10.1029/2021JF006161.

Debella-Gilo, M.; Kääb, A. Sub-Pixel Precision Image Matching for Measuring Surface Displacements on Mass Movements Using Normalized Cross-Correlation. *Remote Sensing of Environment* **2011**, *115* (1), 130–142. https://doi.org/10.1016/j.rse.2010.08.012.

Delaloye, R.; Perruchoud, E.; Avian, M., et al. Recent Interannual Variations of Rock Glacier Creep in the European Alps. In *Proceedings of the 9th International Conference on Permafrost*, Fairbanks, Alaska, 29 June–3 July 2008; 2008; 343–348.

Duvillard, P.-A.; Magnin, F.; Revil, A. et al. Temperature Distribution in a Permafrost-Affected Rock Ridge from Conductivity and Induced Polarization Tomography. *Geophysical Journal International* **2021**, *225* (2), 1207–1221. https://doi.org/10.1093/gji/ggaa597.

Duvillard, P.-A.; Ravanel, L.; Marcer, M. et al. Recent Evolution of Damage to Infrastructure on Permafrost in the French Alps. *Regional Environmental Change* **2019**, *19* (5), 1281–1293. https://doi.org/10.1007/s10113-019-01465-z.

Etzelmüller, B.; Guglielmin, M.; Hauck, C. et al. Twenty Years of European Mountain Permafrost Dynamics—the PACE Legacy. *Environmental Research Letters* **2020**, *15* (10), 104070. https://doi.org/10.1088/1748-9326/abae9d.

Etzelmüller, B.; Isaksen, K.; Czekirda, J. et al. Rapid Warming and Degradation of Mountain Permafrost in Norway and Iceland. *The Cryosphere* **2023**, *17* (12), 5477–5497. https://doi.org/10.5194/tc-17-5477-2023.

Farzamian, M.; Vieira, G.; Monteiro Santos, F. A. et al. Detailed Detection of Active Layer Freeze–Thaw Dynamics Using Quasi-Continuous Electrical Resistivity Tomography (Deception Island, Antarctica). *The Cryosphere* **2020**, *14* (3), 1105–1120. https://doi.org/10.5194/tc-14-1105-2020.

Ferretti, A.; Prati, C.; Rocca, F. Permanent Scatterers in SAR Interferometry. *IEEE Transactions on Geoscience and Remote Sensing* **2001**, *39* (1), 8–20. https://doi.org/10.1109/36.898661.

Fitch, A. J.; Kadyrov, A.; Christmas, W. J. et al. Orientation Correlation. In *Proceedings of the 13th British Machine Vision Conference*, Cardiff, UK, 2–5 September 2002; Marshall, D.; Rosin, P. L., Eds.; British Machine Vision Association, 2002; 133–142. https://citeseerx.ist.psu.edu/document?repid=rep1&type=pdf&doi=f8bf0bf36d1eaf711d0451305cfa9fdec43b6eea

Frauenfelder, R.; Haeberli, W.; Hoelzle, M. Rockglacier Occurrence and Related Terrain Parameters in a Study Area of the Eastern Swiss Alps. In *Permafrost, Proceedings of the 8th International Conference on Permafrost*, Zurich, Switzerland, 21–25 July 2003; 2003; 253–258.

Frederick, J. M.; Buffett, B. A. Effects of Submarine Groundwater Discharge on the Present-Day Extent of Relict Submarine Permafrost and Gas Hydrate Stability on the Beaufort Sea Continental Shelf. *Journal of Geophysical Research: Earth Surface* **2015**, *120* (3), 417–432. https://doi.org/10.1002/2014JF003349.

French, H. M. *The Periglacial Environment*; John Wiley & Sons, 2017.

Garibaldi, M. C.; Bonnaventure, P. P.; Smith, S. L. et al. Active Layer Variability and Change in the Mackenzie Valley, Northwest Territories between 1991-2014: An Ecoregional Assessment. *Arctic, Antarctic, and Alpine Research* **2022**, *54* (1), 274–293. https://doi.org/10.1080/15230430.2022.2097156.

Gavrilov, A.; Pavlov, V.; Fridenberg, A. et al. The Current State and 125 Kyr History of Permafrost on the Kara Sea Shelf: Modeling Constraints. *The Cryosphere* **2020**, *14* (6), 1857–1873. https://doi.org/10.5194/tc-14-1857-2020.

Global Climate Observing System (GCOS). *The Global Observing System for Climate: Implementation Needs Technical Report* (GCOS-200); World Meteorological Organization (WMO): Geneva, 2016.

Global Climate Observing System (GCOS). *The 2022 GCOS ECVs Requirements* (GCOS-245); World Meteorological Organization (WMO): Geneva, 2022.

Global Climate Observing System (GCOS). *The 2022 GCOS Implementation Plan* (GCOS-244); World Meteorological Organization (WMO): Geneva, 2022.

Gruber, S. Ground Subsidence and Heave over Permafrost: Hourly Time Series Reveal Interannual, Seasonal and Shorter-Term Movement Caused by Freezing, Thawing and Water Movement. *The Cryosphere* **2020**, *14* (4), 1437–1447. https://doi.org/10.5194/tc-14-1437-2020.

Gruber, S.; Haeberli, W. Mountain Permafrost. In *Permafrost Soils*; Margesin, R., Ed.; Springer: Berlin, Heidelberg, 2009; 33–44. https://doi.org/10.1007/978-3-540-69371-0_3.

Gruber, S.; King, L.; Kohl, T. et al. Interpretation of Geothermal Profiles Perturbed by Topography: The Alpine Permafrost Boreholes at Stockhorn Plateau, Switzerland. *Permafrost and Periglacial Processes* **2004**, *15* (4), 349–357. https://doi.org/10.1002/ppp.503.

Haberkorn, A.; Kenner, R.; Noetzli, J. et al. Changes in Ground Temperature and Dynamics in Mountain Permafrost in the Swiss Alps. *Frontiers in Earth Science* **2021**, *9*. https://doi.org/10.3389/feart.2021.626686.

Haeberli, W.; Hallet, B.; Arenson, L. et al. Permafrost Creep and Rock Glacier Dynamics. *Permafrost and Periglacial Processes* **2006**, *17* (3), 189–214. https://doi.org/10.1002/ppp.561.

Haeberli, W.; Huder, J.; Keusen, H.-R. et al. Core Drilling through Rock Glacier-permafrost. In *Proceedings on the 5th International Conference on Permafrost*, Trondheim, Norway, 2–5 August 1988; 1988; 937–942.

Haeberli, W.; Schaub, Y.; Huggel, C. Increasing Risks Related to Landslides from Degrading Permafrost into New Lakes in De-Glaciating Mountain Ranges. *Geomorphology* **2017**, *293*, 405–417. https://doi.org/10.1016/j.geomorph.2016.02.009.

Halla, C.; Blöthe, J. H.; Tapia Baldis, C. et al. Ice Content and Interannual Water Storage Changes of an Active Rock Glacier in the Dry Andes of Argentina. *The Cryosphere* **2021**, *15* (2), 1187–1213. https://doi.org/10.5194/tc-15-1187-2021.

Harrington, J. S.; Hayashi, M. Application of Distributed Temperature Sensing for Mountain Permafrost Mapping. *Permafrost and Periglacial Processes* **2019**, *30* (2), 113–120. https://doi.org/10.1002/ppp.1997.

Harris, C.; Haeberli, W.; Vonder Mühll, D. et al. Permafrost monitoring in the high mountains of Europe: the PACE Project in its global context. *Permafrost and Periglacial Processes* **2001**, *12* (1), 3–11. https://doi.org/10.1002/ppp.377.

Hauck, C. New Concepts in Geophysical Surveying and Data Interpretation for Permafrost Terrain. *Permafrost and Periglacial Processes* **2013**, *24* (2), 131–137. https://doi.org/10.1002/ppp.1774.

Hauck, C.; Böttcher, M.; Maurer, H. A New Model for Estimating Subsurface Ice Content Based on Combined Electrical and Seismic Data Sets. *The Cryosphere* **2011**, *5* (2), 453–468. https://doi.org/10.5194/tc-5-453-2011.

Hauck, C.; Kneisel, C., Eds. *Applied Geophysics in Periglacial Environments*; Cambridge University Press: Cambridge, UK, 2008. https://doi.org/10.1017/CBO9780511535628.

Herring, T.; Lewkowicz, A. G.; Hauck, C. et al. Best Practices for Using Electrical Resistivity Tomography to Investigate Permafrost. *Permafrost and Periglacial Processes* **2023**, *34* (4), 494–512. https://doi.org/10.1002/ppp.2207.

Hilbich, C. Time-Lapse Refraction Seismic Tomography for the Detection of Ground Ice Degradation. *The Cryosphere* **2010**, *4* (3), 243–259. https://doi.org/10.5194/tc-4-243-2010.

Hinkel, K. M.; Nelson, F. E. Spatial and Temporal Patterns of Active Layer Thickness at Circumpolar Active Layer Monitoring (CALM) Sites in Northern Alaska, 1995–2000. *Journal of Geophysical Research: Atmospheres* **2003**, *108* (D2). https://doi.org/10.1029/2001JD000927.

Hjort, J.; Streletskiy, D.; Doré, G. et al. Impacts of Permafrost Degradation on Infrastructure. *Nature Reviews Earth & Environment* **2022**, *3* (1), 24–38. https://doi.org/10.1038/s43017-021-00247-8.

Hock, R.; Rasul, G, Adler, C. et al. High Mountain Areas. In *IPCC Special Report on the Ocean and Cryosphere in a Changing Climate*. Pörtner, H.-O.; Roberts, D. C.; Masson-Delmotte, V. et al., Eds.; Cambridge University Press: Cambridge, United Kingdom and New York, USA, 2019. https://www.ipcc.ch/site/assets/uploads/sites/3/2022/03/04_SROCC_Ch02_FINAL.pdf.

Hoelzle, M.; Hauck, C.; Mathys, T. et al. Long-Term Energy Balance Measurements at Three Different Mountain Permafrost Sites in the Swiss Alps. *Earth System Science Data* **2022**, *14* (4), 1531–1547. https://doi.org/10.5194/essd-14-1531-2022.

Hrbáček, F.; Vieira, G.; Oliva, M. et al. Active Layer Monitoring in Antarctica: An Overview of Results from 2006 to 2015. *Polar Geography* **2021**, *44* (3), 217–231. https://doi.org/10.1080/1088937X.2017.1420105.

International Permafrost Association Action Group Rock Glacier Inventories and Kinematics (RGIK). *Guidelines for Inventorying Rock Glaciers: Baseline and Practical Concepts*; Version 1.0; RGIK, 2023a. https://doi.org/10.51363/unifr.srr.2023.002.

International Permafrost Association Action Group Rock Glacier Inventories and Kinematics (RGIK). *InSAR-based Kinematic Attribute in Rock Glacier Inventories: Practical InSAR Guidelines*; Version 4.0; RGIK, 2023b. https://bigweb.unifr.ch/Science/Geosciences/Geomorphology/Pub/Website/CCI/CurrentVersion/Current_InSAR-based_Guidelines.pdf.

International Permafrost Association Action Group Rock Glacier Inventories and Kinematics (RGIK). *Rock Glacier Velocity as an Associated Parameter of ECV Permafrost: Baseline Concepts*; Version 3.2; RGIK, 2023c. https://bigweb.unifr.ch/Science/Geosciences/Geomorphology/Pub/Website/IPA/CurrentVersion/Current_RockGlacierVelocity.pdf.

International Permafrost Association Action Group Rock Glacier Inventories and Kinematics (RGIK). *Rock Glacier Velocity as Associated Product of ECV Permafrost: Practical Concept*; Version 1.2; RGIK, 2023d. https://bigweb.unifr.ch/Science/Geosciences/Geomorphology/Pub/Website/IPA/CurrentVersion/Current_RGV_PC.pdf.

Isaksen, K.; Holmlund, P.; Sollid, J. L. et al. Three deep Alpine-permafrost boreholes in Svalbard and Scandinavia. *Permafrost and Periglacial Processes* **2001**, *12* (1), 13–25. https://doi.org/10.1002/ppp.380.

Isaksen, K.; Lutz, J.; Sørensen, A. M. et al. Advances in Operational Permafrost Monitoring on Svalbard and in Norway. *Environmental Research Letters* **2022**, *17* (9), 095012. https://doi.org/10.1088/1748-9326/ac8e1c.

Isaksen, K.; Mühll, D. V.; Gubler, H. et al. Ground Surface-Temperature Reconstruction Based on Data from a Deep Borehole in Permafrost at Janssonhaugen, Svalbard. *Annals of Glaciology* **2000**, *31*, 287–294. https://doi.org/10.3189/172756400781820291.

Iwata, Y.; Hirota, T.; Suzuki, T. et al. Comparison of Soil Frost and Thaw Depths Measured Using Frost Tubes and Other Methods. *Cold Regions Science and Technology* **2012**, *71*, 111–117. https://doi.org/10.1016/j.coldregions.2011.10.010.

Kääb, A.; Frauenfelder, R.; Roer, I. On the Response of Rockglacier Creep to Surface Temperature Increase. *Global and Planetary Change* **2007**, *56* (1), 172–187. https://doi.org/10.1016/j.gloplacha.2006.07.005.

Kääb, A.; Strozzi, T.; Bolch, T. et al. Inventory and Changes of Rock Glacier Creep Speeds in Ile Alatau and Kungöy Ala-Too, Northern Tien Shan, since the 1950s. *The Cryosphere* **2021**, *15* (2), 927–949. https://doi.org/10.5194/tc-15-927-2021.

Kaverin, D.; Malkova, G.; Zamolodchikov, D. et al. Long-Term Active Layer Monitoring at CALM Sites in the Russian European North. *Polar Geography* **2021**, *44* (3), 203–216. https://doi.org/10.1080/1088937X.2021.1981476.

Kellerer-Pirklbauer, A.; Delaloye, R.; Lambiel, C. et al. Interannual Variability of Rock Glacier Flow Velocities in the European Alps. In *Book of Abstracts: 5th European Conference on Permafrost*, Chamonix, France, 23 June–1 July 2018; 2018; 396–397.

Lachenbruch, A. H.; Marshall, B. V. Changing Climate: Geothermal Evidence from Permafrost in the Alaskan Arctic. *Science* **1986**, *234* (4777), 689–696. https://doi.org/10.1126/science.234.4777.689.

Ladanyi, B.; Foriero, A. Evolution of Frost Heaving Stresses Acting on a Pile. In *Proceedings of the 7th International Conference on Permafrost*, Yellowknife, Canada, 23–27 June 1998; 1998; 623–633.

Lambiel, C.; Delaloye, R. Contribution of Real-Time Kinematic GPS in the Study of Creeping Mountain Permafrost: Examples from the Western Swiss Alps. *Permafrost and Periglacial Processes* **2004**, *15* (3), 229–241. https://doi.org/10.1002/ppp.496.

Liljedahl, A. K.; Boike, J.; Daanen, R. P. et al. Pan-Arctic Ice-Wedge Degradation in Warming Permafrost and Its Influence on Tundra Hydrology. *Nature Geoscience* **2016**, *9* (4), 312–318. https://doi.org/10.1038/ngeo2674.

Luethi, R.; Phillips, M. Challenges and Solutions for Long-Term Permafrost Borehole Temperature Monitoring and Data Interpretation. *Geographica Helvetica* **2016**, *71* (2), 121–131. https://doi.org/10.5194/gh-71-121-2016.

Lundquist, J. D.; Lott, F. Using Inexpensive Temperature Sensors to Monitor the Duration and Heterogeneity of Snow-Covered Areas. *Water Resources Research* **2008**, *44* (4). https://doi.org/10.1029/2008WR007035.

Luo, D.; Jin, H.; Jin, X. et al. Elevation-Dependent Thermal Regime and Dynamics of Frozen Ground in the Bayan Har Mountains, Northeastern Qinghai-Tibet Plateau, Southwest China. *Permafrost and Periglacial Processes* **2018**, *29* (4), 257–270. https://doi.org/10.1002/ppp.1988.

Luo, D.; Jin, H.; Lü, L. et al. Spatiotemporal Characteristics of Freezing and Thawing of the Active Layer in the Source Areas of the Yellow River (SAYR). *Chinese Science Bulletin* **2014**, *59* (24), 3034–3045. https://doi.org/10.1007/s11434-014-0189-6.

Luo, D.; Wu, Q.; Jin, H. et al. Recent Changes in the Active Layer Thickness across the Northern Hemisphere. *Environmental Earth Sciences* **2016**, *75* (7), 555. https://doi.org/10.1007/s12665-015-5229-2.

Mackay, J. R. A Frost Tube for the Determination of Freezing in the Active Layer above Permafrost. *Canadian Geotechnical Journal* **1973**, *10* (3), 392–396. https://doi.org/10.1139/t73-033.

Magnin, F.; Deline, P.; Ravanel, L. et al. Thermal Characteristics of Permafrost in the Steep Alpine Rock Walls of the Aiguille Du Midi (Mont Blanc Massif, 3842 m a.s.l). *The Cryosphere* **2015**, *9* (1), 109–121. https://doi.org/10.5194/tc-9-109-2015.

Merlone, A.; Al-Dashti, H.; Faisal, N. et al. Temperature Extreme Records: World Meteorological Organization Metrological and Meteorological Evaluation of the 54.0°C Observations in Mitribah, Kuwait and Turbat, Pakistan in 2016/2017. *International Journal of Climatology* **2019**, *39* (13), 5154–5169. https://doi.org/10.1002/joc.6132.

Merlone, A.; Sanna, F.; Coppa, G. et al. Transportable System for On-Site Calibration of Permafrost Temperature Sensors. *Permafrost and Periglacial Processes* **2020**, *31* (4), 610–620. https://doi.org/10.1002/ppp.2063.

Miner, K. R.; Turetsky, M. R.; Malina, E. et al. Permafrost Carbon Emissions in a Changing Arctic. *Nature Reviews Earth & Environment* **2022**, *3* (1), 55–67. https://doi.org/10.1038/s43017-021-00230-3.

Mollaret, C.; Hilbich, C.; Pellet, C. et al. Mountain Permafrost Degradation Documented through a Network of Permanent Electrical Resistivity Tomography Sites. *The Cryosphere* **2019**, *13* (10), 2557–2578. https://doi.org/10.5194/tc-13-2557-2019.

Monnier, S.; Kinnard, C. Internal Structure and Composition of a Rock Glacier in the Dry Andes, Inferred from Ground-Penetrating Radar Data and Its Artefacts. *Permafrost and Periglacial Processes* **2015**, *26* (4), 335–346. https://doi.org/10.1002/ppp.1846.

Monnier, S.; Kinnard, C. Pluri-Decadal (1955–2014) Evolution of Glacier–Rock Glacier Transitional Landforms in the Central Andes of Chile (30–33° S). *Earth Surface Dynamics* **2017**, *5* (3), 493–509. https://doi.org/10.5194/esurf-5-493-2017.

Murton, J. B. Permafrost and Climate Change. In *Climate Change (Third Edition)*; Letcher, T. M., Ed.; Elsevier, 2021; 281–326. https://doi.org/10.1016/B978-0-12-821575-3.00014-1.

Nelson, F. E.; Shiklomanov, N. I.; Nyland, K. E. Cool, CALM, Collected: The Circumpolar Active Layer Monitoring Program and Network. *Polar Geography* **2021**, *44* (3), 155–166. https://doi.org/10.1080/1088937X.2021.1988001.

Nicolsky, D. J.; Romanovsky, V. E.; Romanovskii, N. N. et al. Modeling Sub-Sea Permafrost in the East Siberian Arctic Shelf: The Laptev Sea Region. *Journal of Geophysical Research: Earth Surface* **2012**, *117* (F3). https://doi.org/10.1029/2012JF002358.

Nixon, F. M.; Taylor, A. E. Active Layer Monitoring in Natural Environments, Mackenzie Valley, Northwest Territories. In *Current Research 1994-B, Interior Plains and Arctic Canada*; Geological Survey of Canada: Ottawa, 1994; 27–34. https://ostrnrcan-dostrncan.canada.ca/entities/publication/9d0636bd-5bc9-4fe4-96b0-ecee11626fc4.

Nixon, F. M.; Taylor, A. E.; Allen, V. S. et al. Active Layer Monitoring in Natural Environments, Lower Mackenzie Valley, Northwest Territories. In *Current Research 1995-B, Interior Plains and Arctic Canada*; Geological Survey of Canada: Ottawa, 1995 99–108. https://ostrnrcan-dostrncan.canada.ca/entities/publication/bc0f5e77-be01-4149-a6b9-1c71b46b7994.

Noetzli, J.; Arenson, L. U.; Bast, A. et al. Best Practice for Measuring Permafrost Temperature in Boreholes Based on the Experience in the Swiss Alps. *Frontiers in Earth Science* **2021**, *9*. https://doi.org/10.3389/feart.2021.607875.

Noetzli, J.; Biskaborn, B. K.; Christiansen, H. H. et al. Permafrost Thermal State. *Bulletin of the American Meteorological Society* **2019**, *100* (9) [special issue: "State of the Climate 2018"], 21–22. https://doi.org/10.1175/2019BAMSStateoftheClimate.1.

Noetzli, J.; Gruber, S. Transient Thermal Effects in Alpine Permafrost. *The Cryosphere* **2009**, *3* (1), 85–99. https://doi.org/10.5194/tc-3-85-2009.

Noetzli, J.; Hilbich, C.; Hauck, C. et al. Comparison of Simulated 2D Temperature Profiles with Time-lapse Electrical Resistivity Data at the Schilthorn Crest. In *Proceedings of the 9th International Conference on Permafrost*, Fairbanks, Alaska, 29 June–3 July 2008; 2008; *1293–1298*.

Nyland, K. E.; Shiklomanov, N. I.; Streletskiy, D. A. et al. Long-Term Circumpolar Active Layer Monitoring (CALM) Program Observations in Northern Alaskan Tundra. *Polar Geography* **2021**, *44* (3), 167–185. https://doi.org/10.1080/1088937X.2021.1988000.

Oblogov, G. E.; Vasiliev, A. A.; Streletskiy, D. A. et al. Localized Vegetation, Soil Moisture, and Ice Content Offset Permafrost Degradation under Climate Warming. *Geosciences* **2023**, *13* (5), 129. https://doi.org/10.3390/geosciences13050129.

Obu, J. How Much of the Earth's Surface Is Underlain by Permafrost? *Journal of Geophysical Research: Earth Surface* **2021**, *126* (5), e2021JF006123. https://doi.org/10.1029/2021JF006123.

Obu, J.; Westermann, S.; Bartsch, A. et al. Northern Hemisphere Permafrost Map Based on TTOP Modelling for 2000–2016 at 1 km2 Scale. *Earth-Science Reviews* **2019**, *193*, 299–316. https://doi.org/10.1016/j.earscirev.2019.04.023.

O'Neill, H. B.; Smith, S. L.; Burn, C. R. et al. Widespread Permafrost Degradation and Thaw Subsidence in Northwest Canada. *Journal of Geophysical Research: Earth Surface* **2023**, *128* (8), e2023JF007262. https://doi.org/10.1029/2023JF007262.

O'Neill, H. B.; Smith, S. L.; Duchesne, C. Long-Term Permafrost Degradation and Thermokarst Subsidence in the Mackenzie Delta Area Indicated by Thaw Tube Measurements. In *Cold Regions Engineering 2019: Proceedings of the 18th International Conference on Cold Regions Engineering and the 8th Canadian Permafrost Conference*, Quebec City, Canada, 18–22 August 2019; 2019, 643–651. https://doi.org/10.1061/9780784482599.074.

Osterkamp, T. E. *Temperature Measurements in Permafrost*; Report No. FHWA-AK-RD-85-11; Alaska Department of Transportation and Public Facilities: Juneau, USA, 1984.

Osterkamp, T. E. Establishing Long-Term Permafrost Observatories for Active-Layer and Permafrost Investigations in Alaska: 1977–2002. *Permafrost and Periglacial Processes* **2003**, *14* (4), 331–342. https://doi.org/10.1002/ppp.464.

Osterkamp, T. E.; Romanovsky, V. E. Evidence for Warming and Thawing of Discontinuous Permafrost in Alaska. *Permafrost and Periglacial Processes* **1999**, *10* (1), 17–37. https://doi.org/10.1002/(SICI)1099-1530(199901/03)10:1<17::AID-PPP303>3.0.CO;2-4.

Overduin, P. P.; Schneider von Deimling, T.; Miesner, F. et al. Submarine Permafrost Map in the Arctic Modeled Using 1-D Transient Heat Flux (SuPerMAP). *Journal of Geophysical Research: Oceans* **2019**, *124* (6), 3490–3507. https://doi.org/10.1029/2018JC014675.

Overduin, P. P.; Wetterich, S.; Günther, F. et al. Coastal Dynamics and Submarine Permafrost in Shallow Water of the Central Laptev Sea, East Siberia. *The Cryosphere* **2016**, *10* (4), 1449–1462. https://doi.org/10.5194/tc-10-1449-2016.

Pellet, C.; Bodin, X.; Cusicanqui, D. et al. Rock Glacier Kinematics. *Bulletin of the American Meteorological Society* **2022**, *104* [special issue: "State of the Climate 2023"], 41–42. https://doi.org/10.1175/2023BAMSStateoftheClimate.1.

Phillips, M.; Buchli, C.; Weber, S. et al. Brief Communication: Combining Borehole Temperature, Borehole Piezometer and Cross-Borehole Electrical Resistivity Tomography Measurements to Investigate Seasonal Changes in Ice-Rich Mountain Permafrost. *The Cryosphere* **2023**, *17* (2), 753–760. https://doi.org/10.5194/tc-17-753-2023.

Phillips, M.; Haberkorn, A.; Draebing, D. et al. Seasonally Intermittent Water Flow through Deep Fractures in an Alpine Rock Ridge: Gemsstock, Central Swiss Alps. *Cold Regions Science and Technology* **2016**, *125*, 117–127. https://doi.org/10.1016/j.coldregions.2016.02.010.

Pogliotti, P.; Guglielmin, M.; Cremonese, E. et al. Warming Permafrost and Active Layer Variability at Cime Bianche, Western European Alps. *The Cryosphere* **2015**, *9* (2), 647–661. https://doi.org/10.5194/tc-9-647-2015.

Reverter, F. A Tutorial on Thermal Sensors in the 200th Anniversary of the Seebeck Effect. *IEEE Sensors Journal* **2021**, *21* (20), 22122–22132. https://doi.org/10.1109/JSEN.2021.3105546.

Rickard, W.; Brown, J. The Performance of a Frost-tube for the Determination of Soil Freezing and Thawing Depths. *Soil Science* **1972**, *113* (2), 149.

Riseborough, D. W.; Kane, D. L.; Hinkel, K. M. Estimating Active Layer and Talik Thickness from Temperature Data: Implications from Modeling Results. In *Proceedings of the 9th International Conference on Permafrost,* Fairbanks, Alaska, 29 June–3 July 2008; 2008; 1487–1492.

Roger, J.; Allard, M.; Sarrazin, D. et al. Evaluating the Use of Distributed Temperature Sensing for Permafrost Monitoring in Salluit, Nunavik. In *Proceedings of the 7th Canadian Permafrost Conference*, Quebec City, Canada, 21–23 September 2015; 2015. https://doi.org/10.13140/RG.2.1.4273.7365.

Romanovsky, V.; Kholodov, A.; Nicolsky, D. et al. *Thermal State of Permafrost in North America – Annually Observed Ground Temperatures, 2022*. Arctic Data Center, 2022.

Ruppel, C. D.; Herman, B. M.; Brothers, L. L. et al. Subsea Ice-Bearing Permafrost on the U.S. Beaufort Margin: 2. Borehole Constraints. *Geochemistry, Geophysics, Geosystems* **2016**, *17* (11), 4333–4353. https://doi.org/10.1002/2016GC006582.

Scambos, T. A.; Dutkiewicz, M. J.; Wilson, J. C. et al. Application of Image Cross-Correlation to the Measurement of Glacier Velocity Using Satellite Image Data. *Remote Sensing of Environment* **1992**, *42* (3), 177–186. https://doi.org/10.1016/0034-4257(92)90101-O.

Schoeneich, P.; Echelard, T.; Krysiecki, J. M. et al. The Borehole 2Alpes-3065 – A Pilot Installation for Fiber Optic DTS Measurements in Permafrost. In *Proceedings of the 10th International Conference on Permafrost*, Salekhard, Russian Federation, 25–29 June 2012; 2012; 20–27.

Schoeneich, P.; Krysiecki, J. M.; Mingrat, L. et al. DTS Ground Temperature Measurements in Mountain Permafrost – The 2Alpes-3065 Borehole (French Alps). In *Proceedings of the 7th Canadian Permafrost Conference*, Quebec City, Canada, 21–23 September 2015; 2015.

Sharratt, B.; McCool, D. Frost Depth. *United States Department of Agriculture-Agricultural Research Service/ University of Nebraska-Lincoln: Faculty Publications* **2005**. https://digitalcommons.unl.edu/usdaarsfacpub/1405.

Shiklomanov, N. I.; Streletskiy, D. A.; Little, J. D. et al. Isotropic Thaw Subsidence in Undisturbed Permafrost Landscapes. *Geophysical Research Letters* **2013**, *40* (24), 6356–6361. https://doi.org/10.1002/2013GL058295.

Smith, S.; Brown, J. *Permafrost: Permafrost and Seasonally Frozen Ground*; Assessment of the Status of the Development of the Standards for the Terrestrial Essential Climate Variables – T7; Global Terrestrial Observing System: Rome, 2009. https://library.arcticportal.org/668/1/T07.pdf.

Smith, S. L.; O'Neill, H. B.; Isaksen, K. et al. The Changing Thermal State of Permafrost. *Nature Reviews Earth & Environment* **2022**, *3* (1), 10–23. https://doi.org/10.1038/s43017-021-00240-1.

Smith, S. L.; Romanovsky, V. E.; Lewkowicz, A. G. et al. Thermal State of Permafrost in North America: A Contribution to the International Polar Year. *Permafrost and Periglacial Processes* **2010**, *21* (2), 117–135. https://doi.org/10.1002/ppp.690.

Sollid, J. L.; Isaksen, K.; Eiken, T. et al. The Transition Zone of Mountain Permafrost on Dovrefjell, Southern Norway. In *Proceedings of the 8th International Conference on Permafrost*, Zurich, Switzerland, 21–25 July 2003; Phillips, M.; Springman, S. M.; Arenson, L. U., Eds.; Volume 2, 2003; 1085–1090.

Staub, B.; Lambiel, C.; Delaloye, R. Rock Glacier Creep as a Thermally-driven Phenomenon: A Decade of Inter-annual Observation from the Swiss Alps. In *Book of Abstracts: 11th International Conference on Permafrost*, Potsdam, Germany, 20–24 June 2016; 2016, 96–97. https://doi.org/10.2312/GFZ.LIS.2016.001.

Strand, S. M.; Christiansen, H. H.; Johansson, M. et al. Active Layer Thickening and Controls on Interannual Variability in the Nordic Arctic Compared to the Circum-Arctic. *Permafrost and Periglacial Processes* **2021**, *32* (1), 47–58. https://doi.org/10.1002/ppp.2088.

Streletskiy, D.; Noetzli, J.; Smith, S. L. et al. *Strategy and Implementation Plan for the Global Terrestrial Network for Permafrost (GTN-P) 2021–2024*; Zenodo, 2021. https://doi.org/10.5281/zenodo.6075468.

Streletskiy, D.; Noetzli, J.; Smith, S. L. et al. *Measurement Recommendations and Guidelines for the Global Terrestrial Network for Permafrost (GTN-P)*; Zenodo, 2022. https://doi.org/10.5281/zenodo.5973079.

Strozzi, T.; Caduff, R.; Jones, N. et al. Monitoring Rock Glacier Kinematics with Satellite Synthetic Aperture Radar. *Remote Sensing* **2020**, *12* (3), 559. https://doi.org/10.3390/rs12030559.

Supper, R.; Ottowitz, D.; Jochum, B. et al. Geoelectrical Monitoring of Frozen Ground and Permafrost in Alpine Areas: Field Studies and Considerations towards an Improved Measuring Technology. *Near Surface Geophysics* **2014**, *12* (1), 93–115. https://doi.org/10.3997/1873-0604.2013057.

Swiss Permafrost Monitoring Network (PERMOS). *Permafrost in Switzerland 2006/2007 to 2007/2008*; Glaciological Report Permafrost No. 8/9; Cryospheric Commission of the Swiss Academy of Sciences: 2010. http://doi.org/10.13093/permos-rep-2010-8-9.

Swiss Permafrost Monitoring Network (PERMOS). *Permafrost in Switzerland 2014/2015 to 2017/2018*; Glaciological Report Permafrost No. 16–19; Cryospheric Commission of the Swiss Academy of Sciences: 2019. https://doi.org/10.13093/permos-rep-2019-16-19.

Swiss Permafrost Monitoring Network (PERMOS). *Swiss Permafrost Bulletin 2022*; Number 4; PERMOS: 2023.

Tarnocai, C.; Mark Nixon, F.; Kutny, L. Circumpolar-Active-Layer-Monitoring (CALM) Sites in the Mackenzie Valley, Northwestern Canada. *Permafrost and Periglacial Processes* **2004**, *15* (2), 141–153. https://doi.org/10.1002/ppp.490.

Tyler, S. W.; Selker, J. S.; Hausner, M. B. et al. Environmental Temperature Sensing Using Raman Spectra DTS Fiber-Optic Methods. *Water Resources Research* **2009**, *45* (4). https://doi.org/10.1029/2008WR007052.

Ukil, A.; Braendle, H.; Krippner, P. Distributed Temperature Sensing: Review of Technology and Applications. *IEEE Sensors Journal* **2012**, *12* (5), 885–892. https://doi.org/10.1109/JSEN.2011.2162060.

Van Everdingen, R. O. *Multi-language Glossary of Permafrost and Related Ground-ice Terms: in Chinese, English, French, German, Icelandic, Italian, Norwegian, Polish, Romanian, Russian, Spanish, and Swedish*. Arctic Institute of North America: Calgary, Canada, 1998.

Vieira, G.; Bockheim, J.; Guglielmin, M. et al. Thermal State of Permafrost and Active-Layer Monitoring in the Antarctic: Advances during the International Polar Year 2007–2009. *Permafrost and Periglacial Processes* **2010**, *21* (2), 182–197. https://doi.org/10.1002/ppp.685.

Vivero, S.; Bodin, X.; Farías-Barahona, D. et al. Combination of Aerial, Satellite, and UAV Photogrammetry for Quantifying Rock Glacier Kinematics in the Dry Andes of Chile (30°S) Since the 1950s. *Frontiers in Remote Sensing* **2021**, *2*. https://doi.org/10.3389/frsen.2021.784015.

Vonder Mühll, D. S. Drilling in Alpine Permafrost. *Norsk Geografisk Tidsskrift – Norwegian Journal of Geography* **1996**, *50* (1), 17–24. https://doi.org/10.1080/00291959608552348.

Vonder Mühll, D.; Haeberli, W. Thermal Characteristics of the Permafrost within an Active Rock Glacier (Murtèl/Corvatsch, Grisons, Swiss Alps). *Journal of Glaciology* **1990**, *36* (123), 151–158. https://doi.org/10.3189/S0022143000009382.

Vonder Mühll, D. S.; Holub, P. Borehole Logging in Alpine Permafrost, Upper Engadin, Swiss Alps. *Permafrost and Periglacial Processes* **1992**, *3* (2), 125–132. https://doi.org/10.1002/ppp.3430030209.

Wagner, F. M.; Mollaret, C.; Günther, T. et al. Quantitative Imaging of Water, Ice and Air in Permafrost Systems through Petrophysical Joint Inversion of Seismic Refraction and Electrical Resistivity Data. *Geophysical Journal International* **2019**, *219* (3), 1866–1875. https://doi.org/10.1093/gji/ggz402.

Wagner, F. M.; Uhlemann, S. Chapter One - An Overview of Multimethod Imaging Approaches in Environmental Geophysics. In *Advances in Geophysics*; Schmelzbach, C., Ed.; Inversion of Geophysical Data; Elsevier, 2021; Vol. 62, 1–72. https://doi.org/10.1016/bs.agph.2021.06.001.

Wahrhaftig, C.; Cox, A. Rock Glaciers in the Alaska Range. *GSA Bulletin* **1959**, *70* (4), 383–436. https://doi.org/10.1130/0016-7606(1959)70[383:RGITAR]2.0.CO;2.

Walvoord, M. A.; Kurylyk, B. L. Hydrologic Impacts of Thawing Permafrost—A Review. *Vadose Zone Journal* **2016**, *15* (6), vzj2016.01.0010. https://doi.org/10.2136/vzj2016.01.0010.

Ward Jones, M. K.; Pollard, W. H.; Jones, B. M. Rapid Initialization of Retrogressive Thaw Slumps in the Canadian High Arctic and Their Response to Climate and Terrain Factors. *Environmental Research Letters* **2019**, *14* (5), 055006. https://doi.org/10.1088/1748-9326/ab12fd.

Widmer, L.; Phillips, M.; Buchli, C. Brief Communication: Comparison of the Performance of Thermistors and Digital Temperature Sensors in a Mountain Permafrost Borehole. *The Cryosphere* **2023**, *17* (10), 4289–4295. https://doi.org/10.5194/tc-17-4289-2023.

Williams, P. J.; Smith, M. W. *The Frozen Earth: Fundamentals of Geocryology*; Studies in Polar Research; Cambridge University Press: Cambridge, 1989. https://doi.org/10.1017/CBO9780511564437.

Wirz, V.; Gruber, S.; Purves, R. S. et al. Short-Term Velocity Variations at Three Rock Glaciers and Their Relationship with Meteorological Conditions. *Earth Surface Dynamics* **2016**, *4* (1), 103–123. https://doi.org/10.5194/esurf-4-103-2016.

Wise, J. A. *Liquid-in-glass Thermometer Calibration Service*; NIST Special Publication 250-23; National Institute of Standards and Technology: Washington, DC, USA, 1988.

Wu, Q.; Zhang, T.; Liu, Y. Permafrost Temperatures and Thickness on the Qinghai-Tibet Plateau. *Global and Planetary Change* **2010**, *72* (1), 32–38. https://doi.org/10.1016/j.gloplacha.2010.03.001.

Zhang, T. Influence of the Seasonal Snow Cover on the Ground Thermal Regime: An Overview. *Reviews of Geophysics* **2005**, *43* (4). https://doi.org/10.1029/2004RG000157.

Zhao, L.; Zou, D.; Hu, G. et al. Changing Climate and the Permafrost Environment on the Qinghai–Tibet (Xizang) Plateau. *Permafrost and Periglacial Processes* **2020**, *31* (3), 396–405. https://doi.org/10.1002/ppp.2056.

Zhao, L.; Zou, D.; Hu, G. et al. A Synthesis Dataset of Permafrost Thermal State for the Qinghai–Tibet (Xizang) Plateau, China. *Earth System Science Data* **2021**, *13* (8), 4207–4218. https://doi.org/10.5194/essd-13-4207-2021.

For more information, please contact:

World Meteorological Organization

7 bis, avenue de la Paix – P.O. Box 2300 – CH 1211 Geneva 2 – Switzerland

Strategic Communications Office

Tel.: +41 (0) 22 730 83 14

Email: cpa@wmo.int

wmo.int

JN 24604